

Microphysiological Models for Predictive Pre-Clinical Assessment of Pulmonary Drug Exposure

**Microphysiological Models for Predictive
Pre-Clinical Assessment of Pulmonary Drug Exposure**

By

Adeel Ahmed

Submitted to the University of Hertfordshire in partial fulfilment
of the requirements of the degree of
Doctor of Philosophy with Industry Experience

University of Hertfordshire

School of Life and Medical Sciences

Department of Pharmacy, Pharmacology and Postgraduate Medicine

July 2024

Acknowledgements

I would like to thank Professor Darragh Murnane for his supervision, support, and guidance during this project. His unwavering support helped me throughout all the challenges of this project. I am also immensely to Dr Emily Richardson, her help and support with the complex cell culture techniques gave me the confidence needed to carry out my research. Her insightful advice deepened my understanding of the intricate world of the lungs, and I am truly thankful for all the knowledge and wisdom she has shared over the years. I would also like to thank Dr Daniel Baker for his invaluable help and patience. His expertise and extensive knowledge in analytical methods have been crucial in this project and I am truly appreciative of his guidance.

I would like to express my appreciation to Dr Tomasz Kostrzewski and the incredible team at CN Bio Innovations for their support and allowing me to use the cell culture facilities for the research in this project. I am also very grateful to Kim Lachani for her patience and guidance through the many laboratory hiccups I encountered over the years.

To all the amazing research students at the University of Hertfordshire past and present, I would like to extend a massive thank you for all the laughs and tears we shared through our PhD journey. I would like to thank: Altin Kocinaj, Victoria Legh-Land, Niamh Haslett, Caterina Fantuzzi, Jed Kellaway, Harry Jones, Mohammed Ahmad, Denis Mustafov and Nathan Mistry for making every day brighter with your friendship.

I want to extend a special thank you to Dr Jesus Calvo-Castro, Dr Mehrnoosh Ostovar and Dr Ute Gerhard who have served as my role models, helping me grow both personally and professionally. In particular, I would like to extend my deepest gratitude to for believing in me and exemplifying the highest standards scientific research.

To Professor Stewart Kirton and Dr Michelle Botha I would like to extend my deepest gratitude for being the guiding lights in my lift, steering me in the right direction throughout my academic journey. Your help and advice have been invaluable in making this PhD possible.

A heartfelt thank you to Saima Shofique for your patience throughout the years and for celebrating every success, big and small. Your love and encouragement have been my driving force in completing this thesis. I look forward to spending the rest of my life with you and celebrating many more successes together.

I dedicate this thesis to my family, friends and to those no longer with us. Your unwavering support and love have been my strength throughout my life. I love you all deeply and will cherish the time I have with you all.

Abstract

The communication between the epithelial cells and smooth muscle cells in the airways is a vital characteristic of physiology and pathophysiology, specifically the response of airway smooth muscle to stimulants in the environment and inhaled therapeutics, in both healthy and diseased tissues. However, models currently used to evaluate drugs and environmental stimuli lack the physiological features present *in vivo*. The lack of respiratory *in vitro* models that are representative of the human *in vivo* anatomy, physiology and pathophysiology has resulted in the reliance on models that possess poor predictive power for the assessment of drugs, resulting in a high attrition rate of new drug candidates in clinical trials due to lack of efficacy or unforeseen adverse events. This highlights the need for a more *in vivo*-like respiratory model. Microphysiological system (MPS) -based *in vitro* models of the respiratory tissues have the potential to enhance the understanding of disease states and improve drug candidate research through their ability to mimic biomechanical stimuli experienced *in vivo*.

This thesis investigates the morphological and functional effect of perfusion on a human bronchial epithelium cell line, Calu-3, and primary human bronchial smooth muscle cells in a direct coculture, cultured in the Barrier-12 plate PhysioMimix® Organ-on-a-Chip (OOC) Microphysiological System. Perfusion enhanced the Calu-3 epithelial model's barrier function and phenotype, whilst decreasing the time needed for differentiation that achieves minimal apparent permeability (P_{app}) of the paracellular markers lucifer yellow (LY) and sodium fluorescein (NaFL) by up to 7 days compared to the non-perfused comparator.

The coculture of the Calu-3 epithelial cells with primary bronchial smooth muscle cells in combination with the perfused condition controlled by the PhysioMimix system further enhanced the barrier functionality of the epithelium, reducing the P_{app} of NaFL compared to both the non-perfused coculture and both perfused and non-perfused Calu-3 monoculture. Utilising the liquid chromatography tandem mass spectrometry (LC-MS) method that was validated in this thesis, terbutaline transport across the perfused coculture barrier was assessed and the resultant relaxation of the bronchial smooth muscle cells was shown to be more sensitive to the dose-normalized effect of terbutaline than the non-perfused co-culture. This thesis highlighted the benefits of an MPS model for the development and assessment of inhaled therapeutics in a model more representative of the pulmonary *in vivo* microenvironment.

Contents

1. GENERAL INTRODUCTION.....	2
1.1. RESPIRATORY DISEASES.....	2
1.1.1. INCIDENCE AND IMPORTANCE OF RESPIRATORY DISEASES.....	2
1.1.2. CHALLENGES OF DEVELOPING NOVEL RESPIRATORY THERAPIES.....	3
1.2. DRUG DELIVERY AND RESPIRATORY PHYSIOLOGY	5
1.2.1. TARGETS FOR RESPIRATORY THERAPIES: LUNG STRUCTURE AND TISSUE SUBTYPES.....	5
1.2.2. PULMONARY DRUG DELIVERY.....	8
1.3. MODELLING OF RESPIRATORY PHYSIOLOGY AND DISEASE	9
1.3.1. RESPIRATORY IN VIVO MODELS	9
1.3.2. RESPIRATORY EX VIVO MODELS.....	10
1.3.3. RESPIRATORY IN VITRO MODELS.....	10
1.4. IN VITRO MODELS OF THE HUMAN LUNG	11
1.4.1. TYPES OF IN VITRO CELL SOURCES	11
1.4.2. BRIDGING THE GAP BETWEEN 2D AND 3D CELL CULTURE APPROACHES.....	14
1.4.3. MICROPHYSIOLOGICAL SYSTEMS (MPS)/ORGAN-ON-A-CHIP (OOC) MODELS.....	24
1.4.4. CHARACTERISATION APPROACHES FOR TISSUE CULTURE MODELS	31
1.5. AIMS AND OBJECTIVES	38
2. METHODS AND MATERIALS	42
2.1. INTRODUCTION	42
2.2. CHAPTER AIMS.....	45
2.3. MATERIALS	45
2.3.1. GENERAL CHEMICALS	45
2.3.2. TRANSWELLS® COLLAGEN COATING REAGENTS.....	45
2.3.3. CELL CULTURE REAGENTS	45
2.3.4. PHYSIOMIMIX® ORGAN-ON-A-CHIP (OOC) MICROPHYSIOLOGICAL SYSTEMS (MPS) INSTRUMENTS	46
2.3.5. LUNG MUCUS QUANTIFICATION REAGENTS	46

2.3.6. APPARENT PERMEABILITY REAGENTS	46
2.3.7. QUANTITATIVE POLYMERASE CHAIN REACTION (QPCR) REAGENTS	46
2.3.8. FIXATION AND IMMUNOFUORESCENCE (IF) REAGENTS	46
2.3.9. HISTOLOGY REAGENTS.....	47
2.3.10. LIQUID CHROMATOGRAPHY-MASS SPECTROMETRY (LC-MS) REAGENTS	47
2.4. EQUIPMENT	47
2.5. METHODS	48
2.5.1. CELL THAWING METHOD	48
2.5.2. CALU-3 CELL CULTURE METHOD.....	48
2.5.3. HUMAN BRONCHIAL SMOOTH MUSCLE CELL (BSMC) CULTURE METHOD	48
2.5.4. CRYOSTORAGE OF CELLS	49
2.5.5. TRANSWELLS® COLLAGEN COATING METHOD.....	49
2.5.6. PHYSIOMIMIX® ORGAN-ON-A-CHIP (OOC) MICROPHYSIOLOGICAL SYSTEMS (MPS) METHOD	49
2.5.7. CULTURE OF CELLS IN THE PHYSIOMIMIX OOC SYSTEM.....	50
2.5.8. AIR-LIQUID INTERFACE (ALI) CULTURE METHOD	51
2.5.9. TRANSEPITHELIAL ELECTRICAL RESISTANCE (TEER) METHOD	51
2.5.10. LUNG MUCUS QUANTIFICATION METHOD	51
2.5.11. APPARENT PERMEABILITY (P_{APP}) METHOD	52
2.5.12. QUANTITATIVE POLYMERASE CHAIN REACTION (QPCR) METHOD.....	53
2.5.13. FIXATION AND IMMUNOFUORESCENCE (IF) METHOD	53
2.5.14. HISTOLOGY METHOD	54
2.5.15. STATISTICAL TESTING METHODS	56
2.6. LC-MS MATERIALS AND METHODS.....	56
2.7. CHAPTER CONCLUSIONS	58
3. DEVELOPMENT OF THE PERFUSED CALU-3 BRONCHIAL EPITHELIUM MODEL	60
3.1. INTRODUCTION	60
3.1.1. LUNG EPITHELIUM FEATURES	60
3.1.2. LUNG EPITHELIUM CELL SOURCES.....	60

3.1.3. LUNG BRONCHIAL EPITHELIUM CELL LINES	61
3.1.4. CALU-3 IN VITRO BRONCHIAL MODELS	64
3.2. CHAPTER AIMS.....	69
3.3. METHODS	70
3.3.1. OPTIMIZING THE SEEDING DENSITY OF CALU-3 BRONCHIAL EPITHELIAL CELLS ON A TRANSWELL INSERT	70
3.3.2. PERFUSION ACCELERATED THE FORMATION OF A FUNCTIONAL CALU-3 EPITHELIAL BARRIER MODEL BY 7 DAYS.....	70
3.3.3. LONG TERM CHARACTERISATION OF THE ALI PERFUSED CALU-3 MPS BRONCHIAL EPITHELIAL MODEL.....	71
3.4. RESULTS AND DISCUSSION.....	72
3.4.1. OPTIMISING THE SEEDING DENSITY OF CALU-3 BRONCHIAL EPITHELIAL CELLS ON A TRANSWELL INSERT	72
3.4.2. PERFUSION ACCELERATES THE FORMATION OF A FUNCTIONAL CALU-3 EPITHELIAL BARRIER MODEL BY 7 DAYS.....	77
3.4.3. LONG-TERM MAINTENANCE OF THE ALI PERFUSED CALU-3 BRONCHIAL EPITHELIAL TRANSWELL MODEL FOR 28 DAYS	87
3.5. CHAPTER CONCLUSIONS	92
4. DEVELOPMENT OF THE PERFUSED BRONCHIAL COCULTURE MODEL	94
4.1. INTRODUCTION	94
4.1.1. CONTRACTION AND RELAXATION IN SMOOTH MUSCLE CELLS.....	96
4.1.2. BRONCHIAL SMOOTH MUSCLE IN DISEASE STATES	96
4.1.3. PRIMARY BRONCHIAL EPITHELIUM AND PRIMARY SMOOTH MUSCLE COCULTURE CELL MODELS	97
4.1.4. CELL LINE AIRWAY EPITHELIUM AND PRIMARY SMOOTH MUSCLE COCULTURE MODELS.....	99
4.2. CHAPTER AIMS.....	101
4.3. METHODS AND MATERIALS	102
4.3.1. BRONCHIAL SMOOTH MUSCLE SEEDING DENSITY AND PLACEMENT OPTIMISATION	102

4.3.2. ESTABLISHING THE COCULTURE MODEL IN STATIC CONDITIONS AND MEDIUM OPTIMISATION	104
4.3.3. EVALUATING THE EFFECTS OF PERFUSION ON THE COCULTURE MODEL	104
4.4. RESULTS AND DISCUSSION	106
4.4.1. BRONCHIAL SMOOTH MUSCLE SEEDING DENSITY AND PLACEMENT OPTIMISATION	106
4.4.2. ESTABLISHING THE COCULTURE MODEL IN STATIC CONDITIONS AND MEDIUM OPTIMISATION	111
4.4.3. EVALUATING THE EFFECTS OF PERFUSION ON THE CALU-3/BSMC COCULTURE MODEL	117
4.5. CHAPTER CONCLUSIONS	127
5. EVALUATION OF THE PERFUSED BRONCHIAL COCULTURE MODEL	129
5.1. INTRODUCTION	129
5.1.1. INHALED TREATMENTS FOR ASTHMA AND COPD	130
5.1.2. MECHANISM OF CONTRACTION AND RELAXATION IN SMOOTH MUSCLE CELLS	130
5.1.3. <i>IN VITRO</i> COCULTURE MODELS FOR ASSESSING BRONCHODILATOR ACTION	134
5.2. CHAPTER AIMS	135
5.3. METHODS	136
5.3.1. OPTIMISING EXTRACTION SOLVENTS FOR BIOANALYSIS METHOD	136
5.3.2. OPTIMISING VOLUME OF EXTRACTION SOLVENT FOR BIOANALYSIS METHOD	136
5.3.3. OPTIMISING THE VOLUME OF EXTRACTED MEDIA SAMPLES FOR BIOANALYSIS METHOD	136
5.3.4. ASSESSING EXTRACTION RECOVERY AND MATRIX EFFECT METHOD ...	136
5.3.5. VALIDATION OF THE LC-MS METHOD FOR TERBUTALINE HEMI-SULPHATE SALT IN CELL CULTURE MEDIUM METHOD	137
5.3.6. ANALYSIS OF SAMPLE INTEGRITY WHEN DILUTED WITHIN THE CALIBRATION RANGE	137

5.3.7. INVESTIGATION OF TOTAL RECOVERY OF TERBUTALINE FROM THE BARRIER-12 PLATES AND TRANSWELL INSERTS WITH NO CELLS PRESENT...	137
5.3.8. TERBUTALINE TRANSPORT ACROSS A DIFFERENTIATED CALU-3 MPS MODEL.....	138
5.3.9. OPTIMISATION OF THE CAMP QUANTIFICATION ASSAY	139
5.3.10. EVALUATION OF THE BRONCHIAL COCULTURE MPS MODEL'S RESPONSE TO A BETA-2 (B ₂) ADRENERGIC RECEPTOR AGONIST	140
5.4. RESULTS AND DISCUSSION.....	142
5.4.1. OPTIMISING EXTRACTION SOLVENTS FOR BIOANALYSIS	142
5.4.2. OPTIMISING THE VOLUME OF EXTRACTION SOLVENT FOR BIOANALYSIS	143
5.4.3. OPTIMISING THE VOLUME OF EXTRACTED MEDIUM SAMPLES.....	143
5.4.4. ASSESSING EXTRACTION RECOVERY AND MATRIX EFFECT	145
5.4.5. VALIDATION OF THE LC-MS METHOD FOR TERBUTALINE HEMI-SULPHATE IN CELL CULTURE MEDIUM.....	149
5.4.6. ANALYSING SAMPLE INTEGRITY WHEN DILUTED WITHIN THE CALIBRATION RANGE.....	151
5.4.7. TERBUTALINE CAN BE EFFECTIVELY EXTRACTED FROM CELL CULTURE MEDIUM IN THE TRANSWELL INSERTS AND THE MPS BARRIER-12 PLATES WITH NO CELLS PRESENT	152
5.4.8. THE TRANSPORT RATE OF TERBUTALINE IS HIGHER IN THE APICAL-TO-BASOLATERAL DIRECTION IN THE CALU-3 MPS MODEL THAN THE BASOLATERAL-TO-APICAL.....	157
5.4.9. THE PRESENCE OF 3-ISOBUTYL-1-METHYLXANTHINE (IBMX) OPTIMISES HITHUNTER® CAMP ASSAY FOR SMALL MOLECULES FOR THE QUANTIFICATION OF INTRACELLULAR CAMP.....	162
5.4.10. THE PERFUSED CALU-3/BSMC COCULTURE MPS MODEL ELICITS A MORE SENSITIVE RESPONSE TO B ₂ -AR AGONISTS THAN THE STATIC MODEL	164
5.5. CHAPTER CONCLUSIONS	172
6. GENERAL DISCUSSION.....	174
6.1. OVERVIEW OF THE SCOPE OF THIS THESIS	174
6.2. OVERCOMING CURRENT LIMITATIONS OF <i>IN VITRO</i> CELL MODELS	174

6.3. MICROPHYSIOLOGICAL SYSTEMS AND RECAPITULATING RESPIRATORY BIOMECHANICAL STIMULI	175
6.4. ENHANCEMENT OF THE CALU-3 BRONCHIAL EPITHELIUM MODEL	175
6.5. OPTIMISATION OF THE CALU-3 BRONCHIAL EPITHELIUM MODEL.....	177
6.5.1. ASSESSMENT OF BARRIER FUNCTIONS AND THEIR LIMITATIONS	178
6.5.2. TIGHT JUNCTION EXPRESSION AND LIMITATIONS OF THE ASSAYS	180
6.5.3. TRANSPORTER EXPRESSION ANALYSIS	182
6.5.4. DETECTION OF MUCINS PRESENT AND METHOD LIMITATIONS	183
6.5.5. MUCUS QUANTIFICATION AND METHOD LIMITATIONS	183
6.6. LIMITATIONS OF THE CURRENT BRONCHIAL COCULTURE MODELS	184
6.7. ADDRESSING THE NEED FOR A PHYSIOLOGICALLY RELEVANT BRONCHIAL COCULTURE MODEL.....	185
6.8. RECAPITULATING BRONCHIAL SMOOTH MUSCLE CELLULAR RESPONSE TO BRONCHODIALATORS	187
6.9. FUTURE WORK.....	188
6.10. CONCLUSIONS	190

List of tables

Table 1.1: Advantages and disadvantages of the three major sources for human cells for the development of human relevant cell models.	13
Table 1.2: A summary table of the different types of advanced cell culture models/techniques and their associated advantages and disadvantages.	18
Table 2.1: MRM setting for positive ion MS/MS analysis of terbutaline and D3-salbutamol.	57
Table 3.1: Calu-3 models observed under both static and dynamic conditions, culture details on seeding density, TEER, ALI culture duration, and morphological characteristics. The permeability coefficients (P_{app}) of these models were determined for the molecules Lucifer Yellow (LY), FITC-Dextran (Dex), and Fluorescein Sodium (NaFL).....	65
Table 4.1: Summary of all coculture models discussed. Normal Human Bronchial Epithelium (NHBE), Bronchial Smooth Muscle Cells (BSMCs), air-liquid interface (ALI), BEAS-2B (human epithelial cell line).	100
Table 4.2: Supplements in the Lonza Smooth Muscle Cell Growth Medium (SmGM). Components in the SmGM medium with the final concentrations and their purposes in <i>in vitro</i> cell culture.....	103
Table 5.1: Spiked media samples for determination of recovery.	137
Table 5.2: Reagents in the HitHunter® cAMP Assay kit.	139
Table 5.3: Working cAMP Detection Solution reagent composition with ratio and volumes.	139
Table 5.4: Nominal concentration of each standard level calculated from the calibration curve using Equation 5.1 (N=3)	145
Table 5.5: Recovery of terbutaline from cell culture medium. expressed as a percentage of the ratio of the RRF of terbutaline extracted from media samples to the RRF of terbutaline at that concentration spiked into blank media samples extracted in the same method and performed at seven concentration levels (N=3).	148
Table 5.6: Matrix effect of cell culture medium on terbutaline response. Expressed as a percentage of the ratio of the RRF of terbutaline extracted from media samples to the RRF of terbutaline at that concentration extracted from solvent samples extracted in the same method and performed at seven concentration levels (N=3).	148
Table 5.7: Summary table of all calculated values of from the calibration curves in Figure 5.9 (N=3)	150
Table 5.8: Quality control (QC) standards summary table for all QC samples in the validation runs (N=5).	151

Table 5.9: Summary table of all LC-MS validation data with the validation criteria from the EMA ICH M10 Bioanalytical Validation (EMA, 2022).	151
Table 5.10: Concentration of the diluted samples. Nominal concentration calculated using Equation 5.1 with standard deviation (N=5).....	152
Table 5.11: Average amount of terbutaline in each chamber relative to the total dosed amount. Percentage of the total amount and standard deviation in each compartment of the Calu-3 epithelial Transwell model in static and perfused in the apical to basolateral direction and the basolateral to apical direction	154
Table 5.12: Average amount of terbutaline in each chamber relative to the total amount dosed after 180 mins. Percentage (%) of the total amount of terbutaline and standard deviation (STDEV) in each compartment of the Calu-3 epithelial Transwell model in static and perfused in the apical to basolateral direction and the basolateral to apical direction. The associated TEER values for each condition is indicated (N=3).....	160
Table 5.13: Average amount of terbutaline in each compartment of each model after 180 minutes. Percentage of the total dosed amount with the standard deviation of the replicates (N=3).....	167

List of Figures

Figure 1.1: Pathway of drug development and approval. Figure adapted from (Purandare, 2021).	5
Figure 1.2: Anatomical features of the respiratory and conducting zones of the airways. Indication of the size and biological components of each structure within the respiratory tract. 0 indicates not present, + indicates sparse, ++ indicates present and +++ indicates abundant. The figure was obtained from (Stanfield, 2016).	6
Figure 1.3: Cross-section schematic of the bronchus, bronchioles and alveoli and the resident cells present in each section. CC: Ciliated Cell, GC: Goblet Cell, MU: Mucus, CIL: Cilia, TJ: Tight Junction, BM: Basement Membrane, SM: Smooth Muscle Cell, BG: Bronchial Gland, CR: Cartilage Ring, ECM: Extracellular Matrix, T1: Type 1 Alveolar Cell, T2: Type 2 Alveolar Cell and AM: Alveolar Macrophage. Airflow and blood flow labelled on the respective sides of the diagram. Figure adapted from (Weibel, 2011).	7
Figure 1.4: Diagram of a Transwell® insert within a standard cell culture well plate, illustrating the apical and basolateral compartment sides of the Transwell®	23
Figure 1.5: (A) AX12 lung chip based on a 96-well plate format, consisting of two chips supported by a plate, each of which comprise six independent units. The ultrathin membrane (blue) is deflected by negative pressure inside the basal chip chamber through an integrated micro-diaphragm (gray). Images from (AlveoliX, 2024) (B) The Human Emulation system from Emulate Inc. comprising organ chips which fit into the Pod™ carrier. The Zoë™ culture module controls the rate of flow and stretch for up to 12 chips. The Orb™ provides the precise mixture of gas, power, and vacuum stretch required by the Zoë™ culture module. Images from (Emulate, 2024) (C) The Barrier-12 plate allows the culture of cells on commercial inserts such as Transwell® inserts, with circulating flow in the basolateral chamber pumped through microchannels at a customisable flow rate.	30
Figure 1.6: Diagram highlighting the main structure of an LC system. Figure obtained from (Rasmussen <i>et al.</i> , 2011).	34
Figure 1.7: Diagrams of the two common ionisation techniques for mass spectrometry. (A) Chemical ionisation and (B) Electrospray ionisation. Figures obtained from (Rasmussen <i>et al.</i> , 2011).	35
Figure 1.8: Diagram of a (A) quadrupole and a (B) triple quadrupole found in mass spectrometry detectors. Diagrams obtained from (Rasmussen <i>et al.</i> , 2011).	36
Figure 2.1: Labelled diagram of the PhysioMimix OOC system components and set up.	50
Figure 3.1: Seeding density 1×10^5 cells/cm² (33,000 cells/well) required up to 7 days of ALI culture to reach confluency. Brightfield images of Calu-3 cell growth in static and	

perfused conditions seeded at a density of 1×10^5 cells/cm² (33,000 cells/well), on days 0, 4 and 7 of ALI culture. Scale bar = 100 μ m. 73

Figure 3.2: Seeding density 3×10^5 cells/cm² (100,000 cells/well) required up to 4 days of ALI culture to reach confluency. Brightfield images of Calu-3 cell growth in static and perfused conditions seeded at a density of 3×10^5 cells/cm² (100,000 cells/well), on days 0, 4 and 7 of ALI culture. Scale bar = 100 μ m. 73

Figure 3.3: Seeding density 5×10^5 cells/cm² (165,000 cells/well) reached confluency at day 0 ALI. Brightfield images of Calu-3 cell growth in static and perfused conditions seeded at a density of 5×10^5 cells/cm² (165,000 cells/well), on days 0, 4 and 7 of ALI culture. Scale bar = 100 μ m. 74

Figure 3.4: Perfused cells had a lower TEER profile than their static equivalent, whilst 100K and 165K cells/well had similar TEER profiles. Transepithelial Electrical Resistance (TEER) measurements reported as Ohms (Ω)/cm² for the static (A) and perfused (B) conditions with all three densities in each graph. 33K = 1×10^5 cells/cm², 100K = 3×10^5 cells/cm², 165K = 5×10^5 cells/cm² (N \leq 3). 75

Figure 3.5: The P_{app} of LY is variable across seeding densities and culture conditions. P_{app} of LY across the Calu-3 monolayer at Day 7 of ALI culture in the (A) static and (B) perfused conditions. Both graphs show the P_{app} of all three densities (ANOVA * = $P < 0.05$) (N=3). 76

Figure 3.6: P_{app} of LY was lowest in the 3×10^5 cells/cm² (100,000 cells/well) density in both conditions. Comparison of the P_{app} of LY in the static and perfused conditions across the Calu-3 monolayer at Day 7 in the three densities: (A) 1×10^5 cells/cm² (33,000 cells/well), (B) 3×10^5 cells/cm² (100,000 cells/well) and (C) 5×10^5 cells/cm² (165,000 cells/well) (Unpaired T-test * = $P < 0.05$, **** = $P < 0.0001$) (N=3). 77

Figure 3.7: Perfusion did not affect cell viability but reduced the TEER profile of Calu-3 epithelium. Cell viability determined by number of viable cells present at Day 7 and Day 14 of ALI culture in the static and perfused condition determined by using the (A) Cell Titer-Glo[®] luminescence assay which was not significantly different between the samples (ANOVA ns = $P > 0.05$). (B) Transepithelial Electrical Resistance (TEER) measurements of the static and perfused Calu-3 models performed every 2/3 days with from day 0 ALI till day 14 ALI (N \leq 4). 79

Figure 3.8: Perfusion resulted in a significantly lower P_{app} value than the static model at day 7 ALI. Comparison of the apparent permeability (P_{app}) of Lucifer Yellow (LY) across the Calu-3 epithelial Transwell model in the static and perfused conditions at (A) Day 7 ALI and (B) day 14 ALI culture (Unpaired T-test ns = $P > 0.05$, ** = $P < 0.005$) (N=3). 80

Figure 3.9: There was an increase in variability in P_{app} between Day 7 and Day 14 of the Calu-3 epithelial barrier in both conditions but no significant difference in permeability. Comparison of the apparent permeability (P_{app}) of Lucifer Yellow (LY) across the Calu-3

epithelial Transwell model at day 7 and day 14 of air-liquid interface (ALI) culture in the (A) static and (B) perfused conditions (Unpaired T-test ns = $P > 0.05$) (N=3).....	81
Figure 3.10: Perfused Calu-3 Transwell model established a more uniform monolayer than the static model at Day 7. Calu-3 cells cultured in static or perfused conditions were cultured for 7 days before being fixed and stained with antibodies against ZO1 (green), MUC5AC (magenta) and Hoechst for DNA (blue). Scale bar = 100 μm	82
Figure 3.11: At Day 14, the perfused Calu-3 Transwell model exhibited a more uniform monolayer than the static model. Calu-3 cells cultured in static or perfused conditions were cultured for 7 days before being fixed and stained with antibodies against ZO1 (green), MUC5AC (magenta) and Hoechst for DNA (blue). Scale bar = 100 μm	83
Figure 3.12: Perfusion causes increased ZO1 expression and maintains mucus expression. DNA fluorescence intensity of the greyscale image showing (A) Hoechst 33342. (B) ZO1 intensity of the greyscale image showing only ZO1 scaled to the DNA intensity of the same image shown in (A). (C) MUC5AC intensity of the greyscale image showing only MUC5AC scaled to the DNA intensity of the same image shown in (A) (ANOVA * = < 0.05 , ** = < 0.005 , **** = < 0.0001) (N=4).	84
Figure 3.13: Perfusion increased the expression of the cation transporter OCTN2 in Calu-3 epithelium at Day 7. qPCR expression of three different transport proteins that are present in the Calu-3 epithelial cells in the static and perfused model at Days 7 and 14 when cultured at ALI. (A) SLC22A1/OCT1, (B) SLC22A5/OCTN2 and (C) ABCC1/MRP1. (ANOVA * = $P < 0.05$, ** = $P < 0.005$, *** = $P < 0.0005$, **** = $P < 0.0001$) (N=4).	86
Figure 3.14: Static and perfused conditions resulted in a similar expression of tight junction proteins. qPCR expression of two tight junction proteins that are present in the Calu-3 epithelial cells in the static and perfused models at Days 7 and 14 of ALI culture. (A) TJP1/ZO1 and (B) CLDN1/Claudin-1. (ANOVA * = $P < 0.05$, ** = $P < 0.005$, *** = $P < 0.0005$, **** = $P < 0.0001$) (N=4).	86
Figure 3.15: Perfusion resulted in a lower TEER profile than the static Calu-3 model. (A) TEER measurements of the Calu-3 Transwell model across 28-days at ALI in the static and perfused conditions with the (B) statistical P-values of the Two-Way ANOVA showing the significant differences between the two conditions (Static vs Perfused) on each timepoint (N=12).....	88
Figure 3.16: P_{app} was significantly lower in the perfused model than the static at Days 7 and 21. P_{app} values of NaFL across the Calu-3 monolayer in the static and perfused conditions on Days (A) 7, (B) 14, (C) 21 and (D) 28. (Unpaired T-test * = $P < 0.05$, ** = $P < 0.002$). (N=6)	89

- Figure 3.17: Perfusion resulted in a consistent Calu-3 barrier for up to 21 days.** P_{app} of NaFL across the 28-day ALI culture for the (A) static and (B) perfused Calu-3 Transwell and MPS models. (ANOVA * = $P < 0.05$, ** = $P < 0.001$, *** = $P < 0.0002$, **** = $P < 0.0001$) (N=6)... 90
- Figure 3.18: Maximum mucus expression was reached at Day 14 for both the perfused model and static model.** Mucus quantification of the PBS wash post-TEER measurements on Days 2, 7, 14, 21 and 28 for the (A) static and (B) perfused Calu-3 Transwell models with the tables showing the statistical differences between the days within the condition as evaluated using an ANOVA statistical test. (ANOVA * = $P < 0.05$, ** = $P < 0.001$) (N=6) 91
- Figure 4.1: Comparison of the histology cross-section images and diagrams of the (A) structure of skeletal muscle cells and the (B) structure of smooth muscle.** Figure taken from (Stanfield, 2016)..... 95
- Figure 4.2: Histology cross-section image of the human bronchiole wall highlighting the proximity of the epithelium and smooth muscle tissue layers.** Image obtained from (Sheffield, 2017)..... 95
- Figure 4.3: Transwell- or baseplate-seeded BSMCs showed little significant difference in cell number or cellular stress after 7 days of culture.** BSMCs were seeded at three densities (3,000, 15,000 or 30,000 cells/well) on either the baseplate of the well (BP) or on the underside of the Transwell (TI). (A) Total cell number and (B) LDH release were assessed after 7 days of culture (ANOVA ns = $P > 0.05$, * = $P < 0.05$) (N≤3) 108
- Figure 4.4: Baseplate and Transwell-seeded BSMCs at 3,000 cells/well were morphologically similar.** 3,000 BSMCs were seeded on either the baseplate or the underside of a Transwell insert for 7 days, before being fixed and stained using antibodies against anti- α -SMA (green), Phalloidin (actin- red) and Hoechst-3332 (DNA – blue). Scale bar = 100 μ m. 109
- Figure 4.5: Baseplate and Transwell-seeded BSMCs at 15,000 cells/well were morphologically similar.** 15,000 BSMCs were seeded on either the baseplate or the underside of a Transwell insert for 7 days, before being fixed and stained using antibodies against anti- α -SMA (green), Phalloidin (actin- red) and Hoechst-3332 (DNA – blue). Scale bar = 100 μ m..... 109
- Figure 4.6: Baseplate and Transwell-seeded BSMCs at 15,000 cells/well were morphologically similar.** 15,000 BSMCs were seeded on either the baseplate or the underside of a Transwell insert for 7 days, before being fixed and stained using antibodies against anti- α -SMA (green), Phalloidin (actin- red) and Hoechst-3332 (DNA – blue). Scale bar = 100 μ m..... 110
- Figure 4.7: 3,000 cells/well had the highest expression of α -SMA when grown on the Transwell inserts.** (A) The intensity of α -SMA is reported as a ratio of the Hoechst 33342

intensity in the same image with all densities in both seeding locations, with the (B) intensity for the Transwell insert (ANOVA ** = $P < 0.01$, **** = $P < 0.0001$) (N=3)	110
Figure 4.8: No significant increase of LDH release from culture in 50/50 SmGM medium: Calu-3 medium or 100% SmGM medium. LDH was monitored on days (A) 0, (B) 2, (C) 7 and (D) 14 of air-liquid interface (ALI) and are presented with the Two-way ANOVA results alongside the graph. (Two-Way ANOVA * = $P < 0.05$, ** = $P < 0.01$, *** = $P < 0.001$, **** = $P < 0.0001$) (N≤3).	113
Figure 4.9: Transepithelial Electrical Resistance (TEER) of the 100% SmGM media was higher than the 50:50 composition. (A) Calu-3 epithelial barrier integrity of the Calu-3 monoculture in both medium types and the (B) coculture epithelium in both medium types. (C) Comparison of the barrier integrity of the Calu-3 monoculture against the coculture epithelium in the 50/50 medium and the (D) 100 media (Two-Way ANOVA * = $P < 0.05$) (N=6)	114
Figure 4.10: Apparent permeability (P_{app}) of sodium fluorescein (NaFL) through the Calu-3 epithelium barrier was lowest in the coculture 100% SmGM media. P_{app} in either monoculture or coculture with BSMCs in the 50/50 or 100 media at (A) Day 7 and (B) Day 14 (ANOVA * = $P < 0.05$, ** = $P < 0.01$, *** = $P < 0.001$, **** = $P < 0.0001$) (N=3).....	115
Figure 4.11: Mucus produced by the Calu-3 epithelium in the 100% SmGM was higher than the 50/50 media in the monoculture and coculture. Calu-3 cells were grown at ALI and mucus removed using a PBS wash and then analysed using the alcian blue mucus quantification assay. Mucus (μg) was analysed at (A) Day 7 and (B) Day 14 and (C) percentage increase of mucus from day 7 to 14 (ANOVA * = $P < 0.05$, ** = $P < 0.01$, *** = $P < 0.001$, **** = $P < 0.0001$) (N≤3).....	116
Figure 4.12: Transepithelial electrical resistance (TEER) profiles of the static and perfused conditions of both cultures was similar across seven days. (A) Calu-3 monoculture and the (B) Calu-3/BSMC coculture (Two-Way ANOVA *** = $P < 0.001$) (N=6).....	117
Figure 4.13: Transepithelial electrical resistance (TEER) profiles of the coculture were lower than the Calu-3 monoculture. (A) Static and the (B) perfused conditions of the Calu-3 monoculture and Calu-3/BSMC coculture (Two-Way ANOVA ** = $P < 0.01$, *** = $P < 0.001$, **** = $P < 0.0001$) (N=6)	118
Figure 4.14: Apparent permeability (P_{app}) of sodium fluorescein (NaFL) across the barrier model was lower in coculture perfused than Calu-3 perfused. Transwell insert with no cells (Blank), Bronchial Smooth Muscle Cell Monoculture (BSMC), Calu-3 monoculture, or Calu-3/BSMC coculture grown on the membrane. The P_{app} is expressed in cm/s in the (A) static and (B) perfused conditions. (ANOVA * = $P < 0.05$, *** = $P < 0.0002$, **** = $P < 0.0001$) (N≤3).	119

- Figure 4.15: Apparent permeability (P_{app}) of the static Calu-3 monoculture was similar to the Calu-3 perfused monoculture which in turn was significantly higher than the perfused coculture model (ANOVA * = $P < 0.05$) (N=6)..... 120**
- Figure 4.16: Significantly higher mucus expression from the Calu-3 epithelium in the perfused coculture model compared to the static equivalent and perfused monoculture.** Calu-3 cells were grown at ALI and mucus removed using a PBS wash and then analysed using the alcian blue mucus quantification assay. Mucus (μg) was analysed at **(A)** Day 3 and **(B)** day 7 air-liquid interface (ALI) measured using the alcian blue mucus quantification assay (ANOVA * = $P < 0.05$, *** = $P < 0.0002$) (N=6). 121
- Figure 4.17: Quantitative polymerase chain reaction (qPCR) analysis of the Calu-3 epithelium showed the coculture perfused model to express MUC5AC, FOXJ1 and SLCC22A1 genes by one-fold higher than the static equivalent.** Cells quantified for the genes **(A)** MUC5AC, **(B)** FOXJ1, and **(C)** SLC22A1. The gene expression is expressed as fold change difference from Calu-3 static cells after difference in expression from undifferentiated cells was calculated to give rise to $2^{-\Delta\Delta Ct}$ (ANOVA * = $P < 0.05$, ** = $P < 0.01$) (N=3). 122
- Figure 4.18: Quantitative polymerase chain reaction (qPCR) analysis of the Bronchial Smooth Muscle Cells (BSMCs) showed the coculture perfused model to have the highest contractile phenotype expressed.** BSMCs quantified for the genes **(A)** ACTA2 and **(B)** SM22. The gene expression is expressed as fold change difference from monoculture BSMC static cells after difference in expression from undifferentiated cells was calculated to give rise to $2^{-\Delta\Delta Ct}$ (ANOVA ** = $P < 0.01$, *** = $P < 0.001$, **** = $P < 0.0001$) (N=3). 123
- Figure 4.19: Static and perfused BSMCs were morphologically similar.** BSMCs were maintained on the underside of a Transwell insert in static and perfused conditions for 7 days, before being fixed and stained using antibodies against anti- α -SMA (green), Phalloidin (actin- red) and Hoescht-3332 (DNA – blue). Scale = 50 μm 124
- Figure 4.20: Static Calu-3 had more ‘patches’ of cells than the perfused Calu-3 barrier.** Calu-3 cells were maintained at ALI on a Transwell insert in static and perfused mono-culture conditions for 7 days, before being fixed and stained using antibodies against anti- ZO1 (green), Phalloidin (actin- red) and Hoescht-3332 (DNA – blue). Scale = 50 μm 124
- Figure 4.21: Perfused coculture epithelium had a more uniform cell barrier cells than the static coculture barrier.** Calu-3 cells were maintained at ALI on a Transwell insert in coculture with BSMC cells in static and perfused conditions for 7 days, before being fixed and stained using antibodies against anti- ZO1 (green), Phalloidin (actin- red) and Hoescht-3332 (DNA – blue). Scale = 50 μm 125
- Figure 4.22: Histological samples of the different culture conditions showed differences in morphology between the conditions and cultures. (A)** Static coculture, **(B)** Static monoculture, **(C)** Perfused coculture, and **(D)** Perfused monoculture. Cells are stained for

cytoplasm (light pink/red), nucleus (dark purple/pink), and acidic mucins (blue), as stained by alcian blue. Scale = 20 μm .	126
Figure 5.1: Smooth muscle contraction and the resultant muscle fibre shortening from the myosin proteins pulling the actin filaments. Figure from (Gunst & Zhang, 2008)...	131
Figure 5.2: Terbutaline and salbutamol have similar molecular structure which could account for their clinical similarities. Molecular structures of the β_2 -adrenoceptor agonists (A) terbutaline and (B) salbutamol.	134
Figure 5.3: Peak area response was highest in 95:5 v/v MeCN: H₂O. Peak area response of terbutaline at 100 ng/mL with the different extraction solvent ratio with statistical significance of 95:5 solvent shown (ANOVA **** = $P < 0.0001$) (N=3).	142
Figure 5.4: 250 μL extraction volume resulted in the highest peak area response. Peak area response of terbutaline at 100 and 1000 ng/mL at the two extraction solvent volumes 150 and 250 μL with statistically significant shown (unpaired T-test 100 ng/mL $P = 0.000518$ 1000 ng/mL $P = 0.000015$) (N=3).	143
Figure 5.5: 50 μL sample resulted in a higher gradient and y-intercept than the 25 μL sample. Linear regression analysis of terbutaline relative response factor (RRF) extracted from cell culture medium across a range from 10 ng/mL to 1000 ng/mL with the equation of the lines (N \leq 3).	144
Figure 5.6: The medium sample extracts had a higher signal intensity at each concentration than the solvent equivalent. Chromatograms of terbutaline at 100 ng/mL and 600 ng/mL in extracted medium samples and extracted solvent (95:5 Acetonitrile: Water).	146
Figure 5.7: The signal intensity of D3-Salbutamol was similar regardless of terbutaline concentration and only a slight increase in signal intensity in medium extracts compared to the solvent extracts. Chromatograms of D3 Salbutamol at 10 ng/mL in medium and solvent (95:5 Acetonitrile: Water) samples of terbutaline at 100 ng/mL and 600 ng/mL after extraction.	147
Figure 5.8: All three calibration curves were similar in gradient and y-intercept. Calibration curves generated from the validation calibration runs across the full concentration range with the linear regression and equation of the lines with the linearity (R^2).	150
Figure 5.9: Marginal difference in terbutaline permeation and adsorption were observed in perfused and static conditions. Proportion of terbutaline (% total dosed amount) in the compartments in both the static and perfused conditions in the (A) apical to basolateral direction and the (B) basolateral to apical direction (Two-Way ANOVA ns = $P > 0.05$, *** = $P < 0.001$) (N \leq 2).	154
Figure 5.10: There is a significant difference in the amount of drug in each chamber between the two directions in static and perfused conditions. Proportion of terbutaline (% of total dosed amount) in the compartments in the (A) static condition and the (B) perfused	

condition, comparing the apical to basolateral direction against the basolateral to apical direction. (Two-Way ANOVA **** = $P < 0.0001$) ($N \leq 2$)	155
Figure 5.11: The rate of permeability was not different for either transport direction, regardless of condition. Apparent permeability (P_{app}) of terbutaline hemisulphate across the blank Transwell insert in the static and perfused conditions in the two directions (apical to basolateral and basolateral to apical) (ANOVA ns = $P > 0.05$, **** = $P < 0.0001$) ($N \leq 2$).	156
Figure 5.12: The static Calu-3 barrier model had a higher TEER profile than the perfused Calu-3 barrier model. TEER measurements of the Calu-3 Transwell models in the static and perfused conditions from days 3 to 12 post ALI (Two-Way ANOVA ns = $P > 0.05$, * = $P < 0.05$, ** = $P < 0.01$) ($N = 6$).	157
Figure 5.13: There was no significant difference in the amount of drug in each chamber of the cell models, regardless of condition after 180 mins. Proportion of terbutaline (% of total dosed amount) in the compartments in both the static and perfused conditions in the (A) apical to basolateral direction and the (B) basolateral to apical direction (Two-Way ANOVA ns = $P > 0.05$) ($N = 3$).	158
Figure 5.14: More drug was transported in the A-B direction than the B-A direction after 180 mins. Proportion of terbutaline (% of total dosed amount) in the compartments in the (A) static condition and the (B) perfused condition, comparing the two transport directions (Two-Way ANOVA ns = $P > 0.05$, * = $P < 0.05$, ** = $P < 0.01$, *** = $p < 0.001$, **** = $P < 0.0001$) ($N = 3$).	159
Figure 5.15: Rate of permeability was higher in the A-B direction in both conditions. Apparent permeability (P_{app}) of terbutaline hemisulfate across the Calu-3 epithelial barrier in the static and perfused conditions in the two directions (apical to basolateral and basolateral to apical) (ANOVA ns = $P > 0.05$, ** = $P < 0.01$) ($N = 3$).	161
Figure 5.16: 3-isobutyl-1-methylxanthine (IBMX) resulted in more sensitive measurements of cyclic adenosine monophosphate (cAMP). The cAMP response of Bronchial Smooth Muscle Cells (BSMCs) across a range of densities was measured using the HitHunter® cAMP Assay for Small Molecules on (A) control cells in the presence and absence of IBMX, (B) cells dosed with isoprenaline (10 μ M) in the presence and absence of IBMX, (C) control and dosed cells without IBMX and (D) control and dosed cells with IBMX present. (Two-Way ANOVA * = $P < 0.05$, ** = $P < 0.01$, *** = $P < 0.001$ and **** = $P < 0.001$) ($N = 3$).	163
Figure 5.17: Transepithelial Electrical Resistance (TEER) profile of the perfused coculture model was lower than the static equivalent. TEER measurements of the (A) Calu-3 monoculture and the (B) Calu-3/BSMC coculture Transwell models in the static and perfused conditions (Two-Way ANOVA ** = $P < 0.01$, *** = $P < 0.001$, **** = $P < 0.0001$) ($N \leq 6$).	164

- Figure 5.18: Transepithelial Electrical Resistance (TEER) profile of the coculture models was higher than the monoculture models at day 7.** Comparison of the TEER measurements of the Calu-3 monoculture and the Calu-3/BSMC coculture Transwell models in the **(A)** static and **(B)** perfused conditions (Two-Way ANOVA ns = $P > 0.05$, ** = $P < 0.01$, **** = $P < 0.0001$) (N=6). 165
- Figure 5.19: More mucus is produced by the coculture epithelium than the monoculture epithelium.** Mucus (μg) produced by the Calu-3 epithelium in the monoculture and coculture models in the static and perfused conditions, quantified on **(A)** day 2 of air-liquid interface (ALI) culture and **(B)** day 7 ALI culture (ANOVA ns = $P > 0.05$, ** = $P < 0.01$, *** = $P < 0.001$, **** = $P < 0.0001$) (N=6). 166
- Figure 5.20: The amount of drug in each compartment was similar between the coculture and the Calu-3 monoculture models.** Amount of terbutaline (%) in the apical to basolateral direction in both the static and perfused conditions of the different models: BSMC monoculture, Calu-3 monoculture, and the Calu-3/BSMC coculture. **(A)** Percentage of the terbutaline (%) dose in the basolateral chamber after 180 min, **(B)** Percentage of the terbutaline (%) dose in the Calu-3 epithelial cells after 180 min, **(C)** Percentage of the terbutaline (%) dose in the apical chamber after 180 min (ANOVA *** = $P < 0.001$, **** = $P < 0.0001$) (N=3). 168
- Figure 5.21: The presence of Calu-3 cells significantly reduced the transport of terbutaline.** Apparent permeability (P_{app}) of terbutaline across the cell model after 180 minutes (ANOVA ns = $P > 0.05$, * = $P < 0.05$, **** = $P < 0.0001$) (N=3). 169
- Figure 5.22: The coculture models exhibited a similar cAMP response to terbutaline with less terbutaline reaching the BSMCs in the coculture than the monoculture.** **(A)** Amount of terbutaline (ng) that reaches the BSMCs in the monoculture and coculture model and the resultant **(B)** cAMP response as determined by the HitHunter® cAMP Assay (RLU) (N=3). 170
- Figure 5.23: The coculture models resulted in a more sensitive cAMP response to terbutaline after 180 mins.** cAMP response per ng (RLU/ng) of available terbutaline in the receiver chamber (N=3). 171

List of Abbreviations

3-Isobutyl-1-Methylxanthine (IBMX)

4-(2-Hydroxyethyl)-1-Piperazine-Ethanesulfonic Acid (HEPES)

Absorption, Distribution, Metabolism and Excretion (ADME)

Acetonitrile (MeCN)

Adenosine Triphosphate (ATP)

Adenylyl Cyclase (AC)

Air-Liquid Interface (ALI)

Airway Smooth Muscle (ASM)

Alpha Smooth Muscle Actin (α -SMA)

American Type Culture Collection (ATCC)

Analysis of Variance (ANOVA)

Apical to Basolateral (A-B)

Apparent Permeability (Papp)

Applied Biological Materials Incorporated (ABM)

Atmospheric Pressure Chemical Ionisation (APCI)

ATP-Binding Cassette (ABC)

Basolateral to Apical (B-A)

Biosafety Level 1 (BSL-1)

Biosafety Level 2 (BSL-2)

Bovine Serum Albumin (BSA)

Calcium ions (Ca^{2+})

Carbon Dioxide (CO_2)

Chronic Obstructive Pulmonary Disorder (COPD)

Collision-Induced Dissociation (CID)

Cyclic Adenosine Monophosphate (cAMP)

Cyclic Olefin Copolymer (COC)

Deionised Water (H₂O)

Deoxynucleic Acid (DNA)

Dimethyl Sulfoxide (DMSO)

Double-Distilled Water (ddH₂O)

Eagle's Minimum Essential Medium (EMEM)

Electrospray Ionisation (ESI)

Enzyme-Linked Immunosorbent Assay (ELISA)

European Medicines Agency (EMA)

Extracellular Matrix (ECM)

FITC-Dextran (Dex)

Fluorescein isothiocyanate (FITC)

Fluorescein Sodium Salt (NaFL)

Foetal Bovine Serum (FBS)

Food and Drug Administration (FDA)

Gas Chromatography (GC)

Gas Chromatography-Mass Spectrometry (GC-MS)

Gentamicin Sulphate and Amphotericin (GA-1000)

Global Initiative for Asthma (GINA)

Haematoxylin and Eosin (H&E)

Hank's Balance Salt Solution (HBSS)

High Performance Liquid Chromatography (HPLC)

Human Bronchial Smooth Muscle Cells (BSMC)

Human Epidermal Growth Factor (hEGF)

Human Fibroblastic Growth Factor (hFGF)

Human Trachea Bronchial Epithelial Cells (NH(T)BEC)

Immunofluorescence Imaging (IF)

Histology Imaging (HISTOLOGY)

Induce Pluripotent Stem Cells (iPSC)

Inhaled corticosteroids (ICS)

International Council for Harmonisation (ICH)

Interstitial lung disease (ILD)

Lactate Dehydrogenase (LDH)

Liquid Chromatography (LC)

Liquid Chromatography-Mass Spectrometry (LC-MS)

Liquid Chromatography-Tandem Mass Spectrometry (LC-MS/MS)

Liquid-Liquid Extraction (LLE)

Liquid-Liquid Interface (LLI)

Long-Acting Beta-2 (β 2) Agonists (LABA)

Long-Acting Muscarinic Antagonist (LAMA)

Lower Limit of Quantification (LLOQ)

Lucifer Yellow (LY)

Matrix Metalloproteinase (MMP-9)

Microbiological Safety Cabinets (MBSC)

Microphysiological System (MPS)

Multiple Reaction Monitoring (MRM)

Myosin Heavy Chain (MYH11)

Myosin Light Chain Kinase (MLCK)

Myosin Light Chain Phosphatase (MLCP)

New Approach Methodologies (NAMs)

Non-Essential Amino Acids (NEAA)

Normal Human Bronchial Epithelial Cells (NHBE)

Organic Cation Transporters (OCT)

Organ-on-Chip (OOC)

Paraformaldehyde (PFA)

Phalloidin-Tetramethyl rhodamine B Isothiocyanate (TRITC)

Pharmacodynamics (PD)

Pharmacokinetics (PK)

Phosphate-Buffered Saline (PBS)

Phosphate-Buffered Solution with 0.1% Tween-20 (PBST)

Polydimethylsiloxane (PDMS)

Polymerase Chain Reaction (PCR)

Polytetrafluoroethylene (PTFE)

Quality Control (QC)

Quantitative Polymerase Chain Reaction (qPCR)

Relative Luminescence Unit (RLU)

Relative Response Factor (RRF)

Ribonucleic Acid (RNA)

Short Acting Beta-2 (β 2) Agonists (SABA)

Short-Acting Muscarinic Antagonists (SAMA)

Signal-to-Noise (S/N)

Smooth Muscle Cell Growth Medium (SmGM)

Sodium Dodecyl Sulphate (SDS)

Solid Phase Extraction (SPE)

Standard Deviation (STDEV)

Tandem Mass Spectrometry (MS/MS)

transepithelial Electrical Resistance (TEER)

Transgelin (TAGLN or SM22)

Ultraviolet/Visual Spectroscopy (UV/Vis)

Upper Limit of Quantification (ULOQ)

World Health Organisation (WHO)

Zonular Occludens (ZO1)

β_2 -adrenoceptor (β_2 -AR)

Chapter One

General Introduction

1. GENERAL INTRODUCTION

Drug discovery and development can take 10-15 years for a therapy to be approved for clinical use, with the development of a single drug estimated to cost on average \$2.6-2.8 billion (DiMasi *et al.*, 2016; Schlander *et al.*, 2021; D. Sun *et al.*, 2022). The costs of developing drugs have doubled every 10 years for the past 40 years (PhRMA, 2014). This rapid increase in the cost of research and development (R&D) of novel drugs has a knock-on effect through the industry, with patients and healthcare systems ultimately taking the burden with the increase in drug prices (Tefferi *et al.*, 2015).

The largest contributor to the increase in drug R&D cost is the high failure rate in the clinical trial phases, which is the most expensive stage of the drug development process (Mullard, 2016). Approximately 90% of drugs fail during the clinical stages due to lack of clinical efficacy, unmanageable toxicity, poor drug-like properties, and lack of commercial need and poor strategic planning (Kola & Landis, 2004; Mullard, 2016; D. Sun *et al.*, 2022). Between 2010-2017, 40-50% of clinical failures were due to lack of clinical efficacy and a further 30% failed due to unmanageable toxicity (Dowden & Munro, 2019; Harrison, 2016).

A major area of significant interest is the development of new treatments for respiratory diseases as these diseases contribute to almost 20% of all deaths in the UK (Sugawara & Nikaido, 2014). The recent COVID-19 pandemic has highlighted these issues, with data suggesting individuals who suffered SARS-CoV-2 infection have an increased risk of developing asthma, chronic obstructive pulmonary disease (COPD), interstitial lung disease (ILD), and lung cancer diseases (Meng *et al.*, 2024).

1.1. RESPIRATORY DISEASES

1.1.1. INCIDENCE AND IMPORTANCE OF RESPIRATORY DISEASES

The World Health Organisation (WHO) reported respiratory disease as a major cause of death and disability, with COPD and lower respiratory infections among the top 5 leading causes of death worldwide (Forum of International Respiratory Societies, The Global Impact of Respiratory Disease, 2012; WHO, 2020). Chronic respiratory diseases such as asthma and COPD are major contributors to the rising burden of non-communicable diseases (diseases that are not directly transmitted) globally (The Lancet, 2018). Asthma affects between 5-16% of people globally and affects 10-15% of the UK population (Akinbami *et al.*, 2001; Sugawara & Nikaido, 2014). Asthma and COPD are further explored in Chapter Five of this thesis. Pneumonia is another significant respiratory disease that is the largest infectious cause of death in children worldwide. The mortality rate of lower respiratory tract infection (such as

pneumonia and acute bronchitis) exceeds 4 million people/year (Forum of International Respiratory Societies The Global Impact of Respiratory Disease, 2012).

Lung diseases vary across the world, ranging from acute infectious and genetic diseases to social/environmental and working-related diseases. The main causes of lung disease are acute infections (30.5%), progressive non-malignant disease (30.6%) and lung cancer (29.6%) (Sugawara & Nikaido, 2014). Smoking-related diseases are the single greatest cause of preventable illnesses and death, accounting for 5 million deaths/year across the world with 114,000 deaths attributed to the UK (Sugawara & Nikaido, 2014). The second major factor group is environmental and social factors such as air pollution (including passive smoking), poor living conditions, poor sanitation and occupational exposure. These factors all increase susceptibility to acute infectious diseases, asthma and hypersensitivity pneumonitis (Sugawara & Nikaido, 2014).

Lung cancer is a leading cause of cancer death worldwide with over 1.8 million deaths each year and is the most common cause of cancer death in men and women in the USA and Europe, with cigarette smoking accounting for most cases of cancer worldwide (S. Sun *et al.*, 2007; World Cancer Research Fund International, 2022). Other risk factors include exposure to radon, asbestos, and cancer-causing agents such as radiation and coal products (J. Huang *et al.*, 2022).

The burden of respiratory disease is high in the UK and indeed the global population. This is a result of the lack of available treatments that adequately address the disease pathology. As a result, current treatments for COPD and asthma cannot be limited to the typical inhaled bronchodilators, muscarinic antagonist and corticosteroids which do not achieve complete relief of symptoms for patients severely affected by the diseases (Cazzola & Matera, 2021). Although some new drugs are in development, it is difficult to predict which will be effective and approved for clinical use due to the challenge of translating from animal models to human disease outcomes (Cazzola & Matera, 2021). The drug treatments for respiratory disease is further explored in Chapter Five of this thesis. The lack of predictive pre-clinical models has led to the lack of novel therapeutics treatment or novel drug classes, resulting in heavy reliance on drug therapies that do not adequately treat the disease.

1.1.2. CHALLENGES OF DEVELOPING NOVEL RESPIRATORY THERAPIES

The global respiratory drug market is currently growing at a 4-6% rate annually (Technavio, 2023). However, respiratory drug development suffers an overall failure rate of around 70%, with a calculated cumulative probability to reach the clinical market equal to 3%, compared to the 6-14% probability for drugs used to treat other diseases (Barnes *et al.*, 2015). The drug development problem for respiratory drug development is multi-factorial and has several

causes that contribute to this overall failure rate (Mestre-Ferrandiz *et al.*, 2012). During the drug development pipeline, refer to Figure 1.1, drugs undergo extensive research and development before pre-clinical testing, typically in animals, to determine toxicity, dosing and efficacy. Once proven safe and effective, the drugs are then taken through three rounds of human clinical trials, each phase increasing in patient number to determine safety and efficacy in human patients before their approval to market (Pognan *et al.*, 2023). Pulmonary drugs tend to fail in the clinical trial phase 1 or 2 due to lack of efficacy and/or safety concerns (Barnes *et al.*, 2015; Vogelmeier *et al.*, 2012).

The primary source of clinical trial failure is the inability to demonstrate efficacy (Hwang *et al.*, 2016). Poor understanding of the underlying complex mechanisms of respiratory diseases can lead to the poor drug performance and leads to significant impact on the success rates of drugs in clinical trials (Mestre-Ferrandiz *et al.*, 2012; Movia & Prina-Mello, 2020). For example, despite being considered as one of the leading causes of death worldwide, COPD treatments have only had one new drug class (phosphodiesterase (PDE4) inhibitors) approved in the last decade (Haarst *et al.*, 2019). Current therapies manage the disease, but there is significant work to be done before the disease can be considered cured or even controlled in patients. There are several examples of COPD treatments failing in clinical trials (e.g. AZD9668 neutrophil elastase inhibitor for management of acute lung injury/acute respiratory distress syndrome), which has led some to question whether the best therapeutic or preclinical approaches are currently employed for COPD (Vogelmeier *et al.*, 2012).

A possible approach to decrease attrition rates of pharmaceutical R&D is the increased focus on validation of drug targets in preclinical research to understand the drug targets' role in the disease mechanism and how the drug therapies can affect the target to reduce the symptoms of disease (Pammolli *et al.*, 2020). Novel compounds undergo preclinical assessment before going to human clinical trials, utilising representative models of the organ/organ system the drugs are intended to work on. For example, induced animal models of respiratory disease (such as COPD, pneumonia, pulmonary fibrosis, and asthma) are used to provide key information on *in vivo* drug response such as efficacy and toxicity (Y. I. Wang *et al.*, 2018; Williams & Roman, 2016). However, despite the effort to humanise animal models, the issue of translation and therefore high drug attrition remains (B. Jiang *et al.*, 2014; Moeller *et al.*, 2008; Mullard, 2016; van der Worp *et al.*, 2010).

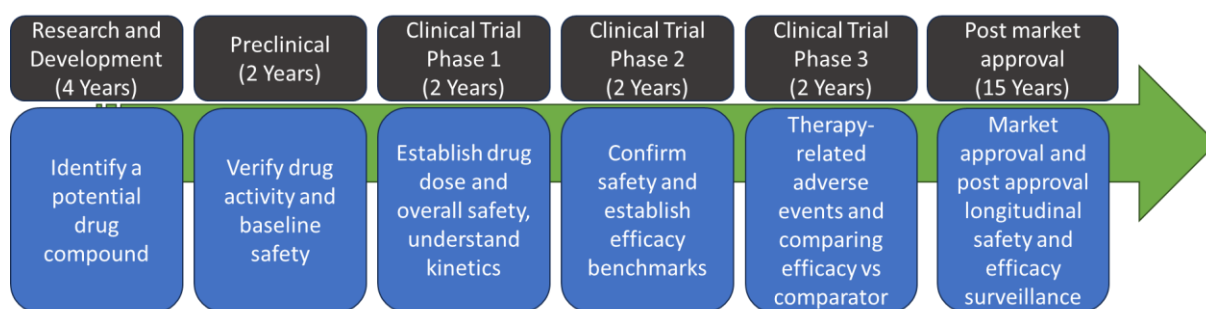


Figure 1.1: Pathway of drug development and approval. Figure adapted from (Purandare, 2021).

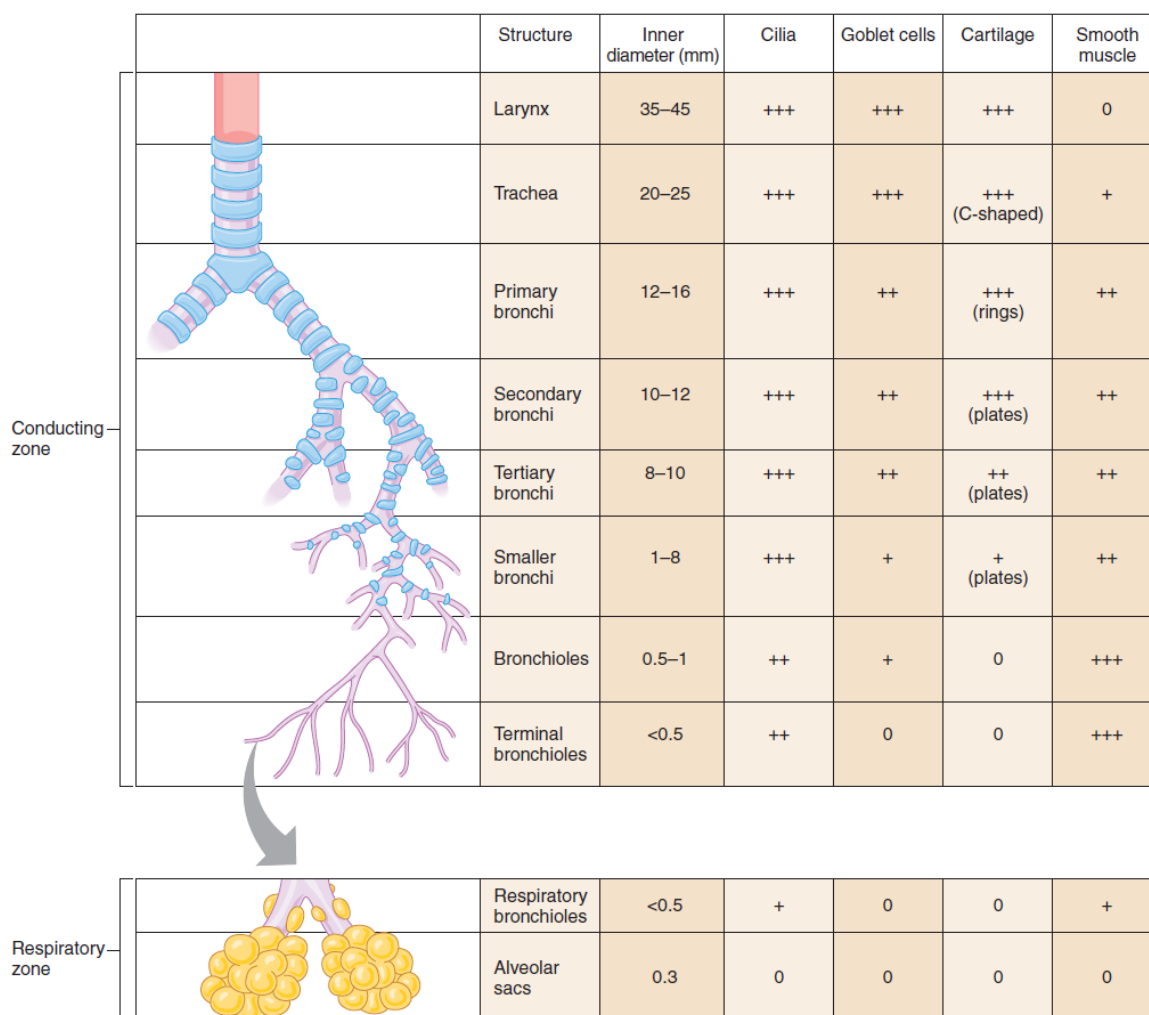
Current drug development processes would greatly benefit from better approaches that allow investigation and interrogation of a healthy or disease state lungs as well as the ability to test novel drug compounds on a human relevant model (Hoeng, 2019). Tissue models that effectively replicate the human pathophysiology are desperately needed to bridge the gap between the animal studies and human clinical trials to reduce the attrition rate of drugs in the clinic and improve screening hits to increase the probability of success in the clinic (Franzen *et al.*, 2019). There is an overwhelming need to engineer robust *in vitro* models to reduce the attrition rate of drugs as the current models are not representative of the human *in vivo* situation which leads to poor predictive power of any adverse effects of a drug candidate (Forbes *et al.*, 2014; Hacker & Rafat, 2020; Hoeng, 2019). This thesis will explore the potential to improve the initial selection criteria for novel drug molecules by developing and utilising novel human relevant *in vitro* models.

1.2. DRUG DELIVERY AND RESPIRATORY PHYSIOLOGY

1.2.1. TARGETS FOR RESPIRATORY THERAPIES: LUNG STRUCTURE AND TISSUE SUBTYPES

Models of the lung must be representative of the lung structures and the complex tissue substructures. To gain insight into tackling this challenge, understanding the lung structure is paramount to developing a representative model. During respiration, air is inhaled through the nose or mouth, passes through the glottis and larynx to enter the tracheobronchial tree. This is called the conducting zone and is made up of the trachea, which leads to the bronchi branches which then further branches into the bronchioles (Figure 1.2). There can be up to 23 branches before reaching the respiratory zone (Levitzy, 2018). The respiratory zone is made up with respiratory bronchioles, alveolar ducts and alveolar sacs, the structures are responsible for gaseous exchange (Levitzy, 2018). The trachea is surrounded by rings of cartilage for support and as the bronchi branch away from the trachea, there is a reduction in cartilage and an increase in smooth muscle tissue surrounding the branches, and by the bronchiolar generations, there is no cartilage (Figure 1.2). As the branches reach the alveolar

region, the smooth muscle becomes thinner and the outermost layer of the bronchial wall is surrounded by dense connective tissue with elastic fibres (Levitzky, 2018; Stanfield, 2016).



	Structure	Inner diameter (mm)	Cilia	Goblet cells	Cartilage	Smooth muscle
Conducting zone	Larynx	35–45	+++	+++	+++	0
	Trachea	20–25	+++	+++	+++ (C-shaped)	+
	Primary bronchi	12–16	+++	++	+++ (rings)	++
	Secondary bronchi	10–12	+++	++	+++ (plates)	++
	Tertiary bronchi	8–10	+++	++	++ (plates)	++
	Smaller bronchi	1–8	+++	+	+ (plates)	++
	Bronchioles	0.5–1	++	+	0	+++
	Terminal bronchioles	<0.5	++	0	0	+++
Respiratory zone	Respiratory bronchioles	<0.5	+	0	0	+
	Alveolar sacs	0.3	0	0	0	0

Figure 1.2: Anatomical features of the respiratory and conducting zones of the airways. Indication of the size and biological components of each structure within the respiratory tract. 0 indicates not present, + indicates sparse, ++ indicates present and +++ indicates abundant. The figure was obtained from (Stanfield, 2016).

The lining of the respiratory tract from the trachea to the bronchiolar region is predominately lined with ciliated cells, mucus-secreting goblet cells and club cells. Ciliated cells are pseudostratified columnar cells in the larger airways and are cuboidal in the bronchioles. Goblet cells are less abundant in the bronchioles and are replaced by Club cells, which secrete lipids, glycoproteins and inflammatory cytokines (Figure 1.3) (Breeze & Turk, 1984; Franks *et al.*, 2008; Levitzky, 2018; Stanfield, 2016). Although the main cell types outlined here are well characterised, interestingly there are still cell types in the lung that are being identified (Travaglini *et al.*, 2020). The lung epithelium is further explored in Chapter Three of this thesis.

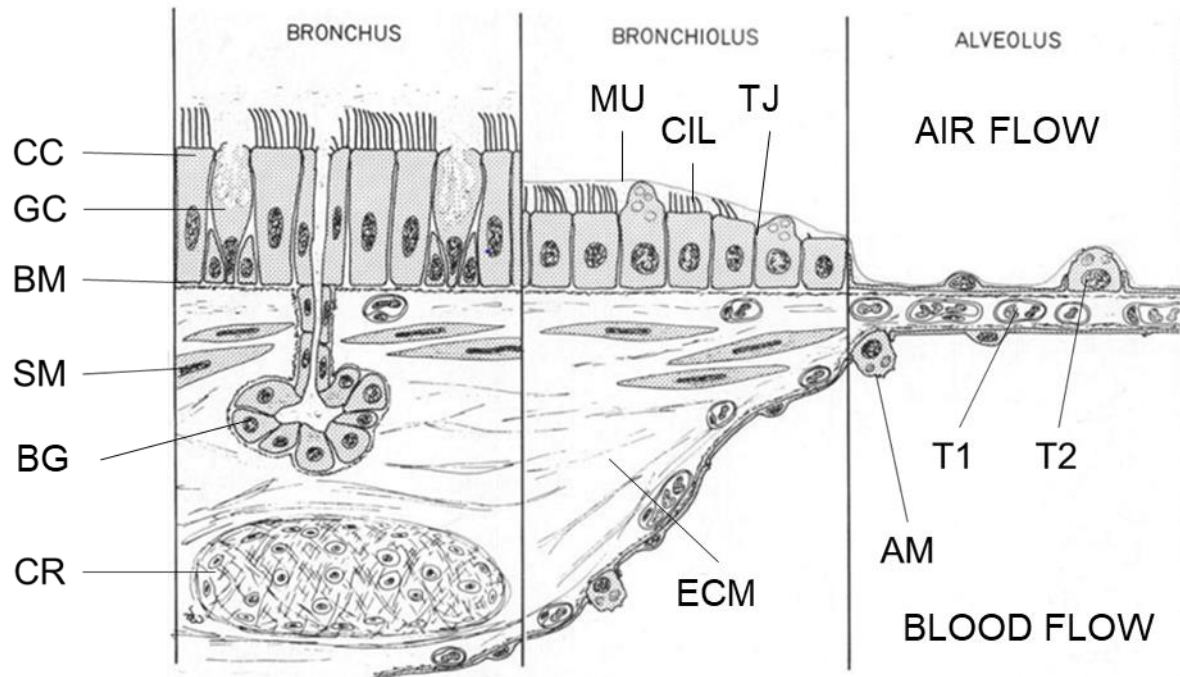


Figure 1.3: Cross-section schematic of the bronchus, bronchioles and alveoli and the resident cells present in each section. CC: Ciliated Cell, GC: Goblet Cell, MU: Mucus, CIL: Cilia, TJ: Tight Junction, BM: Basement Membrane, SM: Smooth Muscle Cell, BG: Bronchial Gland, CR: Cartilage Ring, ECM: Extracellular Matrix, T1: Type 1 Alveolar Cell, T2: Type 2 Alveolar Cell and AM: Alveolar Macrophage. Airflow and blood flow labelled on the respective sides of the diagram. Figure adapted from (Weibel, 2011).

The terminal bronchioles lead into the respiratory zone structures: the respiratory bronchioles and alveolar ducts which lead to the alveoli, where gaseous exchange occurs (Stanfield, 2016). The alveoli walls consist of a single layer of epithelial cells called type I alveolar cells interspersed with type II alveolar cells and alveolar macrophages on a basement membrane in close proximity to pulmonary capillaries to allow efficient gas exchange to occur (Levitzky, 2018; Stanfield, 2016). Smooth muscle surrounds the branches in the conducting zone and are responsible for the diameter of the lumen of the branches: under contraction they reduce the lumen in size and when relaxed the size of the lumen is increased (Stanfield, 2016). Smooth muscle and its functions are further explored in Chapter Four of this thesis. Muscles such as the diaphragm and intercostal muscles are responsible for changing the pressure in the thoracic cavity to facilitate inspiration and expiration of air into and out of the lungs (Levitzky, 2018; Stanfield, 2016).

Changes in the structural features of the airways are a result of illness/disease, such as increased mucus production and smooth muscle density in asthma, loss of elastic fibres in emphysema, and inflammation leading to thickening and scarring of connective tissue in pulmonary fibrosis. Together, all of these changes contribute to the development of COPD in patients (Stanfield, 2016).

1.2.2. PULMONARY DRUG DELIVERY

Respiratory treatments mainly rely on drug delivery to the site of action in the lungs which is preferably achieved by inhaling medication (Borghardt *et al.*, 2018). This is achieved using inhalers (nebulizers, dry powder inhalers or metered-dose inhalers) which aim to propel drug particles to the non-ciliated regions of the lungs (Dolovich *et al.*, 1987). The drug particles that reach the respiratory tract land on the epithelial membrane where they can most effectively dissolve in lung fluids (Davies & Feddah, 2003; Dolovich *et al.*, 1987). The dissolved fraction of the drug is then available for absorption across the epithelial membrane, where they can proceed to their intended targets (Davies & Feddah, 2003; Dolovich *et al.*, 1987).

Major advantages of inhaled drug therapy of respiratory conditions include: rapid therapeutic onset with lower drug doses as the drug is delivered to the site of action; painless and minimally invasive so increasing patient's compliance; and, significantly less local metabolism compared to the oral route and bypassing first-pass metabolism, which provides optimal pharmacokinetic conditions and reduction of systemic side effects (Labiris & Dolovich, 2003; Pilcer & Amighi, 2010; Sécher, Dalonneau, *et al.*, 2019; Sécher, Mayor, *et al.*, 2019; L. J. Zhang *et al.*, 2008). Inhalation therapy may also be applied for the treatment of systemic conditions, in which case avoidance of first-pass metabolism and a potential rapid systemic absorption are major benefits (Labiris & Dolovich, 2003).

However, a major disadvantage is that typically less than 20% of the drug dose reaches the respiratory tract after administration from an inhaler as some particles impact the mouth and back of the throat due to the propulsion from the device (Lipworth, 1996; Newman, 2017; Wood & Barnes, 1995). Furthermore, in a process called "mucociliary clearance", mucus produced by goblet cells in the epithelium traps inhaled matter (drugs, pathogens, pollutants, allergens and xenobiotics) and the ciliated cells push this mucus up the airways to the oesophagus to be disposed of in the digestive tract (Breeze & Turk, 1984; Franks *et al.*, 2008; Levitzky, 2018; Stanfield, 2016). Mucociliary clearance is designed to protect the lungs and the body, however, this biological mechanism can hinder drug action. A key example is the absorption and subsequent mechanism of action of inhaled bronchodilators, which dissolve on the epithelium before being absorbed and transported across the membrane to reach the receptors on airway smooth muscle (Horvath *et al.*, 2007). The efficacy of such drugs can be negatively affected if the drug is cleared prior to reaching the intended target.

Current treatments for COPD and asthma include bronchodilators (such as short acting beta-2 (β_2) adrenergic receptor agonists (SABA)) and anti-inflammatory drugs (such as corticosteroids) (Stanfield, 2016). Beclomethasone dipropionate (corticosteroid), formoterol fumarate (long-acting beta-2 (β_2) agonist/LABA), salbutamol sulphate (SABA) and salmeterol

xinafoate (LABA) are all inhaled drugs that manage asthma and COPD symptoms (Joint Formulary Committee, 2024). Other treatments that are inhaled include: conventional antipsychotics (e.g. loxapine), influenza treatments (e.g. Zanamivir) and diabetes (e.g. Insulin Human) (Joint Formulary Committee, 2024). These treatments and mechanism of action are further explored in Chapter Five of this thesis.

1.3. MODELLING OF RESPIRATORY PHYSIOLOGY AND DISEASE

1.3.1. RESPIRATORY IN VIVO MODELS

Development of novel *in vitro* models and improvement of the current preclinical models to develop more physiologically relevant drug that accurately predict human response to drug compounds is necessary to improve and streamline the drug development process, particularly the translation of data from the pre-clinical stage to the clinical trial phases. Current preclinical drug screening processes for toxicity, efficacy, and metabolism are heavily reliant on simple *in vitro* cell culture models and animal models (Y. I. Wang *et al.*, 2018).

Induced animal models of respiratory disease (such as COPD, pneumonia, pulmonary fibrosis and asthma) are used to observe and investigate disease pathogenesis to unveil potential targets for drugs as well as provide key information on *in vivo* drug response (Y. I. Wang *et al.*, 2018; Williams & Roman, 2016). Typically, rodent models are used however there is significant lack of disease features in rodents, such as the loss of fibroblastic foci in the mouse model of idiopathic pulmonary fibrosis. Moreover, as rodents are obligate nose breathers the deposition of inhaled compounds is greatly different compared to human oral inhalation (Movia *et al.*, 2020; Ogi & Aruga, 2013; Yaddanapudi *et al.*, 2013). Dogs have also been used due to their respiratory frequency and tidal volume being closer to human respiratory parameters, with development of aerosol exposure methods mimicking human devices (S. Sellers *et al.*, 2015). Sheep have been utilised for their respiratory tract features such as nasal cavity size being similar to humans (Scheerlinck *et al.*, 2008). Pig models are used to investigate drug deposition in the lungs and inhaled drug absorption, distribution, metabolism and excretion (ADME) due to the similarities to human respiratory parameters and membrane enzymes and transporters (Sood *et al.*, 2008; Underwood & Raeburn, 1996). A major limitation of pigs is their nose and mouth anatomy which renders aerosol administration poorly feasible and intratracheal procedures difficult (Wemyss-Holden *et al.*, 1999). Non-human primates are considered the gold standard model by the Food and Drug Administration (FDA) however, they require extensive handling with specialised equipment and techniques with increased housing costs compared to the previous models and ethical concerns (Sécher *et al.*, 2020). However, non-human primates and dogs have been found to result in highly inconsistent results in predicting toxicity responses in humans (Bailey *et al.*, 2015).

Animal studies have major ethical concerns surrounding them as well as being expensive and taking a significant amount of time to study (Wright *et al.*, 2008). Cross species differences between preclinical animal models can result in confounding findings and as well as not effectively predicting the outcome in humans (B. Jiang *et al.*, 2014; Moeller *et al.*, 2008; Mullard, 2016; van der Worp *et al.*, 2010). This can increase the difficulties faced by drug developers to progress drug candidates through the drug pipeline. The development of methods to accurately predict the human response to drugs has become increasingly more valuable in recent years.

1.3.2. RESPIRATORY EX VIVO MODELS

Ex vivo lung models are where the whole organ is removed from an organism (animal/human) and then perfused via the pulmonary circulation and ventilated by the trachea, opening up possibilities to measure drug transfer from the lung into the perfusate and back across (Ehrhardt *et al.*, 2017). These models have been used to study transport of inhaled drugs examining the link between pharmacokinetics and lung mechanics (Gnadt *et al.*, 2012). *Ex vivo* models retain the complex 3D arrangements of cell-cell and cell-matrix of the organ and are the closest to the *in vivo* situation. They have been used for many applications, including to aid the investigation of lung oedema, oxygenation capacity, vascular reactivity and bacterial infection (Ainslie *et al.*, 2019; J. W. Lee *et al.*, 2013; McAuley *et al.*, 2014; Medeiros *et al.*, 2012; Sadaria *et al.*, 2011). However, these models have a very limited availability and require complex handling procedures, coupled with the short term culture results in an expensive and low throughput model of the lung (Ainslie *et al.*, 2019; J. W. Lee *et al.*, 2013; McAuley *et al.*, 2014; Medeiros *et al.*, 2012; Sadaria *et al.*, 2011).

Slices of the lung can be taken to be used in drug testing such as tissue binding (E. Cooper *et al.*, 2012). The slices keep the 3D arrangement seen *in vivo* and can maintain tissue specific functions for longer than other *ex vivo* models however, they still maintain similar drawbacks to the whole lung explants due to their low throughput and restricted access. Although the viability is longer than whole lung explants (up to a week), it is still a significant drawback to developing a model for long term studies (Ainslie *et al.*, 2019; Alsafadi *et al.*, 2017; Bai *et al.*, 2016; Bérubé *et al.*, 2009; Mazzoleni *et al.*, 2009; Uhl *et al.*, 2015).

1.3.3. RESPIRATORY IN VITRO MODELS

In vitro model is an umbrella term for a complex range of representations of the human body from simple 2D monolayers and more complex cocultures, to tissue engineering, 3D spheroids and Organ-on-a-Chip (OOC) devices. Current *in vitro* models mostly comprise of simple, single cell-type monolayers (such as epithelium, endothelium, smooth muscle etc.) typically grown in a flat 2D culture system where cells are grown submerged in cell culture medium

adhered to glass or plastic (Artzy-Schnirman *et al.*, 2020; Breslin & O'driscoll, 2012; Hickey & da Rocha, 2019; Ryan, 2008). 2D cell culture has been established in drug toxicity and metabolism screening as it is easy to automate, low cost to maintain and can be high throughput due to their simplicity (Kapałczyńska *et al.*, 2016; Sanyal & Kosovsky, 2017).

However, there is still significant critique of their inability to reproduce an accurate representation of complex interactions between several human cells types and tissues seen *in vivo* as they do not reproduce the natural structures of tissues or tumours, and both cell-cell, and cell-extracellular environment interactions are not represented (de Souza Carvalho *et al.*, 2014; Kapałczyńska *et al.*, 2016). These interactions are responsible for cell proliferation, differentiation, vitality, gene expression and other cellular functions such as drug metabolism, and so are crucial for biological relevance of the *in vitro* model (Baker & Chen, 2012; Bissell *et al.*, 2003; Hickman *et al.*, 2014; Pampaloni *et al.*, 2007).

In December 2022, the FDA Modernisation Act 2.0 detailed the adoption of new approach methodologies (NAMs) for the submission of preclinical safety and efficacy data to regulatory bodies to progress a novel drug compound to human testing. This replaced the exclusivity of animal testing to 'nonclinical tests' including human-biology-based test methods and *in silico* (Stresser *et al.*, 2023). This highlights the advancement of *in vitro* modelling has made a significant impact on the drug development pipeline with pre-clinical *in vitro* modelling playing a powerful role in the submission of new drug therapies. To create these *in vitro* cell culture models, several different types of cells can be used from different sources.

1.4. IN VITRO MODELS OF THE HUMAN LUNG

1.4.1. TYPES OF IN VITRO CELL SOURCES

There are several types of human cell sources that can be employed to create a more representative *in vitro* model of the human lung (summarised in Table 1.1). A key source of cells are primary cells, which are cultured directly from their organ source from a patient donor such as human (trachea) bronchial epithelial cells (NH(T)BEC) (Y. W. Chen *et al.*, 2017; McCauley *et al.*, 2017). Primary cultures of human lung epithelial cells serve as the most representative models of normal lung epithelial cells (Sato *et al.*, 2020). However, primary cells have the potential to lose their phenotype or differentiate into an undesirable cell type (e.g. Type-2 alveolar epithelial cells lose surfactant expression and differentiate into type-1 alveolar epithelial cells) as well as having significant variation between donors, limited availability and cost (Ainslie *et al.*, 2019). This restricts their experimental utility and their ability to be widely distributed to the research community (Sato *et al.*, 2020).

Stem cells are another source that have the potential to differentiate into several cell types. There are three main source of stem cells: Embryonic stem cells, adult stem cells and induced pluripotent stem cells (iPSC) (Y. W. Chen *et al.*, 2017; McCauley *et al.*, 2017; Nawroth *et al.*, 2019; Van Der Sanden *et al.*, 2010). Embryonic stem cells are pluripotent and are derived from the inner cell mass of an embryo, they can self-renew, however they may develop abnormalities during passage in culture (Van Der Sanden *et al.*, 2010). The main restriction of their use is the ethical concerns of destroying an embryo to harvest the stem cells which is considered by some as ethically questionable (Evans & Kaufman, 1981; University of Nebraska: Medical Center, 2020). Adult stem cells are tissue-specific (e.g. bone marrow) and are multipotent cells. They have limited self-renewal and culture conditions significantly influence stem cell survival which is a significant drawback (Van Der Sanden *et al.*, 2010). iPSCs are somatic cells which are reprogramed to a pluripotent stem cell state that can be taken from patients to reproduce the disease characteristics *in vitro*, this has been seen in iPSC-derived lung epithelial cells (McCauley *et al.*, 2017; Van Der Sanden *et al.*, 2010). This cell source is accessible and has a non-carcinoma origin however, there are ethical concerns in gene editing human cells as there is potential to grow embryos from iPSCs (Sedláková *et al.*, 2019; University of Nebraska: Medical Center, 2020).

Cell lines are another widely used source for cell culture models. The main advantages over other cell sources is that they are almost an unlimited mammalian cell source, cost effective and bypass many ethical concerns that are typically associated with animal and human tissue (Hickey & da Rocha, 2019; Kaur & Dufour, 2012). Cell lines have been used in many applications (e.g. vaccine production, drug testing for metabolism and toxicity, gene function and therapeutic proteins) and have greatly furthered scientific research as they provide a pure population of cells (Foster *et al.*, 1998; Gao *et al.*, 2013; Garg & Zhang, 2016). Common lung epithelial cell lines used in research are: Calu-3, H441, 16HBE14o- and A549 (Braakhuis *et al.*, 2015). There is a more in-depth review of these cell lines explored in Chapter Three of this thesis. However, most cell lines are cancer-derived cells which have a high proliferation rate and can lead to misleading results compared to the *in vivo* situation (Courcot *et al.*, 2012; Hogan *et al.*, 2014). They can also have major differences in gene and protein expression, such as lacking tight junctions (A549) or mucus production (16HBE14o-) (Braakhuis *et al.*, 2015; Hickey & da Rocha, 2019). These differences reduce the ability of the cell lines to model healthy lung response, however they are still a valuable asset to pre-clinical data acquisition as previously reported (Foster *et al.*, 1998; Gao *et al.*, 2013; Garg & Zhang, 2016).

Table 1.1: Advantages and disadvantages of the three major sources for human cells for the development of human relevant cell models.

Cell Source	Primary Cells	Stem Cells	Cell Lines
Examples	<ul style="list-style-type: none"> • human (trachea) bronchial epithelial cells (NH(T)BEC) (Y. W. Chen <i>et al.</i>, 2017; McCauley <i>et al.</i>, 2017). 	<ul style="list-style-type: none"> • iPSC derived Lung Epithelial cells 	<ul style="list-style-type: none"> • Calu-3, H441, 16HBE14o- and A549 (Braakhuis <i>et al.</i>, 2015).
Advantages	<ul style="list-style-type: none"> • Directly from their organ source/patient (Y. W. Chen <i>et al.</i>, 2017; McCauley <i>et al.</i>, 2017). • Most representative of normal lung cells (Sato <i>et al.</i>, 2020). 	<ul style="list-style-type: none"> • Embryonic stem cells are pluripotent and self-renew (Van Der Sanden <i>et al.</i>, 2010). • Adult stem cells are multi-potent/tissue specific (Van Der Sanden <i>et al.</i>, 2010). • iPSCs can become pluripotent (Van Der Sanden <i>et al.</i>, 2010). 	<ul style="list-style-type: none"> • Unlimited mammalian cell source, cost effective and bypass many ethical concerns (Hickey & da Rocha, 2019; Kaur & Dufour, 2012). • Used in many applications (e.g. vaccine production, drug testing for metabolism and toxicity, gene function and therapeutic proteins) (Foster <i>et al.</i>, 1998; Gao <i>et al.</i>, 2013; Garg & Zhang, 2016). • Ability to create a tumour model for use in drug screening (Ekert <i>et al.</i>, 2014). • Most cost effective and least ethically concerning source of cells
Disadvantages	<ul style="list-style-type: none"> • Potential to lose their phenotype (Ainslie <i>et al.</i>, 2019). • Significant variation between donors and limited availability (Ainslie <i>et al.</i>, 2019). • Restricted ability to be widely distributed (Sato <i>et al.</i>, 2020). 	<ul style="list-style-type: none"> • Stem cells can develop abnormalities (Van Der Sanden <i>et al.</i>, 2010). • Adult stem cells have limited self-renewal (Van Der Sanden <i>et al.</i>, 2010). • Ethical concerns from embryonic and iPSC sources (Evans & Kaufman, 1981; Sedláková <i>et al.</i>, 2019). 	<ul style="list-style-type: none"> • Cancer-derived cells which have a high proliferation rate and can lead to misleading results compared to <i>in vivo</i> organs (Courcot <i>et al.</i>, 2012; Hogan <i>et al.</i>, 2014) • Major differences. in gene and protein expression such as lacking tight junctions (A549) or mucus production (16HBE14o-)(Braakhuis <i>et al.</i>, 2015; Hickey & da Rocha, 2019)

1.4.2. BRIDGING THE GAP BETWEEN 2D AND 3D CELL CULTURE APPROACHES

Simple 2D models cannot capture the *in vivo* 3D cell environment with the complex multi-tissue and organ interactions, which can be important in order to understand dynamic drug processes *in vivo* (Y. I. Wang *et al.*, 2018). Particularly when comparing the cells grown in 2D culture with those within a native 3D tissue structure, the dissimilarity in morphology is apparent (Baker & Chen, 2012). Cells grown in a monolayer are flat and can adhere and spread freely but have no support in the vertical dimension. This can have a direct impact on cell function which has resulted in the adoption of cell lines in many 2D lung models as primary/iPSC lines cannot be maintained in these non-physiological conditions (Baker & Chen, 2012).

Lung cells grown submerged in media have been considered a 'gold standard' to mimic *in vitro* key events known to occur *in vivo*. However, the major drawback to the submerged culture of lung epithelium is the lack of realism in replicating *in situ* inhaled drug delivery and the *in vivo* situation where epithelial cells are subject to the air (Artzy-Schnirman *et al.*, 2019). The cells are then not a true representation of the *in vivo* epithelium and lacking key epithelial characteristics such as mucus production, cilia and pseudostratified cell layers (D. Cozens *et al.*, 2018; Pezzulo *et al.*, 2011; Whitcutt *et al.*, 1988). This has led to the development of scaffold structures which allow air-liquid interface culture (detailed in Section 1.5.2.4).

In 3D tissue culture systems, cells can develop into tissue-like structures which are more representative of tissues in living organisms (Bissell *et al.*, 2002; Griffith & Swartz, 2006; O'Brien *et al.*, 2002; Stoker *et al.*, 1990). As they mimic anatomical structures, the responses produced are more similar to the responses seen *in vivo* (Birgersdotter *et al.*, 2005; Green & Yamada, 2007; Schmeichel & Bissell, 2003). However, they are not without their limitations. Some examples of using 3D culture systems show the potential for over/underestimating drug response, sensitivity, resistance as well as its dosage (Cawkill & Eaglestone, 2007; Griffith & Swartz, 2006) due to the differences between the culture type and the *in vivo* situation such as the absence of an extracellular matrix (ECM), or the cell type being used to model a healthy lung actually being a cancerous cell line. As well as being more expensive and technically complex, some systems can only maintain cell viability for a few hours. On the other hand, they are more representative and can be used in dynamic/perfused systems, and some systems such as scaffolds or gel/matrix-based cultures can keep cells viable for several days (Ainslie *et al.*, 2019; Artzy-Schnirman *et al.*, 2020; A. J. Booth *et al.*, 2012; Gilpin *et al.*, 2014; Mazzoleni *et al.*, 2009; Nichols *et al.*, 2013; O'Neill *et al.*, 2013; H. Sun *et al.*, 2016; Wagner, Bonenfant, Parsons, *et al.*, 2014; Wagner, Bonenfant, Sokocevic, *et al.*, 2014). Many types of 3D cell culture have been employed in various fields of research. The different types of 3D culture models have been summarised in Table 1.2.

1.4.2.1. LUNG COCULTURES

In the culture methods explored in this chapter (summarised in Table 1.2), the culture of multiple cell types is possible. These multi-cell cultures are called cocultures and are highly relevant for drug research as they can provide a model of human *in vivo*-like tissues, that is more representative than animal models whilst allowing for high-throughput testing and detailed monitoring of drug effects on cell-cell interactions. The multiple cell types create a micro-scale model of a region of intact tissue as the cells develop tissue-like structures which are more representative of tissues in living organisms (Bissell *et al.*, 2002; Griffith & Swartz, 2006; O'Brien *et al.*, 2002; Stoker *et al.*, 1990).

Cell coculture techniques are a crucial tool to create a more representative *in vivo*-like cell culture models for drug development research and functional organs contain multiple cell types that perform specific physiological roles collaboratively (Wu *et al.*, 2010). However, they can be very complicated to culture and optimise in practice and as a result become more labour intensive. With the employment of various bioengineering technologies, there is a diverse range of tissue-tissue interfaces with 3D multicellular structures that resemble functional human organs (Bhatia & Ingber, 2014a). Co-culturing requires a highly specific environment to meet the potentially disparate requirements of the different cell types and, therefore, requires optimisation. This can achieve the goal of developing more complex, reproducible, *in vitro* tissue models (Vis *et al.*, 2020).

1.4.2.2. ORGANOID AND SPHEROIDS

Spheroids and organoids are an *in vitro* 3D cell structure that are formed with one or more cell types differentiating, and self-organizing within close proximity to one another, forming complex and organised cell structures that recapitulate some structural and functional features of *in vivo* organs or tissues (Clevers, 2016). The generation of spheroids and organoids require cells to be suspended or embedded in a 3D matrix whilst maintaining cell-cell interactions for the cells to form a structure that is not generated from external inputs (Yin *et al.*, 2016). Organoids are generated from pluripotent stem cells and adult stem cells by mimicking the biochemical and physical cues of tissue development and homeostasis in a 3D scaffold, allowing the cells to differentiate and self-organise to form tissue-specific organoids (Lancaster & Knoblich, 2014; Yin *et al.*, 2016).

The culture of spheroids can be accomplished by culturing cell lines and/or primary cells in low attachment conditions (e.g. hanging droplet), or in a naturally derived hydrogel scaffold such as decellularized ECM (Turner *et al.*, 2016; Woei Ng *et al.*, 2007). Naturally derived ECM is often used as a supporting scaffold with components such as laminin and fibronectin to maintain cell function during the formation of organoids. A widely used example is the

Engelbreth-Holm-Swarm matrix, also known as Matrigel[®], which is a gelatinous protein mixture harvested from mouse sarcoma cells (Jo *et al.*, 2016; J. Lee *et al.*, 2018; Sampaziotis *et al.*, 2017). However, animal-derived matrices suffer from batch-to-batch variability and cannot be easily tailored to obtain unique organoids for specific organs (Kleinman & Martin, 2005). They also often contain signalling factors and proteins which are unsuitable for normal human cell cultures. Several pulmonary spheroids have been derived from human primary lung tissues, embryonic stem cells (ESCs) or iPSCs, and have been referred to as tracheopheres, bronchospheres or alveolospheres. These models have been successfully employed to study lung development and pathophysiology (Barkauskas *et al.*, 2013; Y. W. Chen *et al.*, 2017; Rock *et al.*, 2009; Tata *et al.*, 2013).

Organoids are simple and allow for coculture of cells, however, their cultures can be limited to hours-to-days depending on the bioreactor used (Amann *et al.*, 2014; Ekert *et al.*, 2014; Zanoni *et al.*, 2016). The inner cells are difficult to expose to air and the limited diffusion can lead to a necrotic core in larger spheres and issues with uniformity around the spheroid (Ainslie *et al.*, 2019). Although organoids are able to capture cellular heterogeneity, which grants an advantage over 2D cell-based assays in screening drugs and diseases, the lack of complete structural and functional features of *in vivo* tissues or organs reduces their ability to be employed as a representative model of the lung (Clevers, 2016; Nguyen *et al.*, 2018). Structurally, spheroids do not effectively recapitulate respiratory structures as the spheroids do not recapitulate the *in vivo* architecture as airway epithelium is not organised in sphere/masses or embedded in ECM. Spheroids are also not able to be effectively grown at an air-liquid interface (ALI) (Amann *et al.*, 2014; Ekert *et al.*, 2014; Zanoni *et al.*, 2016).

1.4.2.3. MATRIX EMBEDDED CULTURES

In vivo, some cell types are embedded within a complex 3D microenvironment composed of ECM components, biological factors and neighbouring cells e.g. fibroblasts (Benders *et al.*, 2013; G. Huang *et al.*, 2017). To mimic the ECM, hydrogels are fabricated for the culture of cells *in vitro*. Hydrogels formed from synthetic polymers can produce similar and reproducible mechanical properties as the native tissues, whereas hydrogels fabricated from natural biopolymers can present bioactive ECM components to cells (Antman-Passig & Shefi, 2016; S.-H. Kim *et al.*, 2018; Mohammed & Murphy, 2009; Sahiner, 2013; Y. Yu *et al.*, 2019).

The pulmonary ECM has been found to be a bioactive environment that regulates cell viability, phenotype and function with roles in the maintenance of tissue homeostasis and injury-repair responses (Burgess *et al.*, 2016; White, 2015). Changes in the lung ECM composition, architecture, and viscoelasticity are associated with the pathology of many chronic respiratory diseases, including asthma, COPD and idiopathic pulmonary fibrosis (Herrera *et al.*, 2018; Y.

Zhou *et al.*, 2018). Polyacrylamide hydrogel has been used to embed lung fibroblasts promoting alpha-smooth muscle actin (α -SMA) expression when treated with TGF- β 1 (Marinković *et al.*, 2012). Polyacrylamide has also been used to grow primary alveolar type 2 cells with RLE-6TN epithelial cells, which expressed a rounded epithelial morphology whereas on stiffer matrices cells were more elongated (Brown *et al.*, 2013). Collagen gels have been used to embed fibroblasts from COPD/emphysema patients and were observed to be unable to effectively contract the collagen hydrogel and repair fibrillar collagen (Campbell *et al.*, 2012). The properties of engineered biomaterials could have impacts on the formation of cell microstructures such as organoids due to characteristics such as cell-adhesive ligands, mechanical properties e.g. stiffness, stress relaxation and stiffening, matrix geometry and degradation (Kratochvil *et al.*, 2019). The cells are kept viable with polarity and function sustained when embedded, however there is heavy variation between matrix preparation, and harvesting the cells from the matrix needs to be optimised (Mazzoleni *et al.*, 2009).

Table 1.2: A summary table of the different types of advanced cell culture models/techniques and their associated advantages and disadvantages.

Model	Description	Advantages	Disadvantages	References
Gel/matrix-based cultures	<ul style="list-style-type: none"> ➤ Hydrogels (ECM like): ➤ Natural products such as collagen and Matrigel ➤ Synthetic self-assembling peptide hydrogels 	<ul style="list-style-type: none"> ➤ Situation like ECM seen <i>in vivo</i>. ➤ Sustain cell viability, polarity, and function 	<ul style="list-style-type: none"> ➤ Harvesting cells to be optimised ➤ Problems of mass transfer if not coupled to a perfused system. ➤ Matrices vary between preparations so standardised protocols needed 	(Mazzoleni <i>et al.</i> , 2009)
3D Spheroids and Organoids	<ul style="list-style-type: none"> ➤ Multicellular spheroids 	<ul style="list-style-type: none"> ➤ Simple ➤ Allows coculture with different cell types. ➤ Recapitulates a tissue-like organisation (polarity, function, viability) ➤ Scaffolds can be avoided. ➤ Primary or iPSC-derived cells ➤ Self-renewal and self-organizing, recapitulating ➤ Produce multiple differentiated cell types from the same donor 	<ul style="list-style-type: none"> ➤ Short term cultures (hours-days) Low to medium throughput ➤ Lack of immune system and cells are typically immature. ➤ Limited size of spheroids due to necrotic cores ➤ Limited recapitulation of respiratory organisation as respiratory structures are not spheres 	(Ainslie <i>et al.</i> , 2019; Amann <i>et al.</i> , 2014; Ekert <i>et al.</i> , 2014; Han <i>et al.</i> , 2014; Mazzoleni <i>et al.</i> , 2009; Zanoni <i>et al.</i> , 2016)

<p>Scaffold and insert based models</p>	<ul style="list-style-type: none"> ➤ Cells cultured on an insert membrane or scaffold with basolateral compartment. ➤ Produced using naturally, derived materials (e.g. collagen or fibrin) or synthetic polymers (e.g. PDMS). 	<ul style="list-style-type: none"> ➤ Long-term cultivation (weeks-months) ➤ Perfusion/flow is possible (used with OOC/MPS devices) ➤ Direct application of substances ➤ Can mimic various pathologies using cell lines, primary or stem cells. ➤ Apical side can be exposed to air with media in a basolateral compartment (ALI culture) ➤ Maintains the characteristics of various disease pathologies. ➤ Cells can be seeded on vascular or airway compartments. ➤ Reproduce heterogenetic of human disease. ➤ Provides physical, structural, and biochemical support. ➤ Sustain cell viability and tissue-like functions. ➤ Can be used in dynamic/perfused culture systems. ➤ Use of cell lines, primary or stem cells 	<ul style="list-style-type: none"> ➤ Cells are seeded in two or three dimensions. ➤ Initial seeding is stochastic. ➤ Limited nutrients and oxygen to the inner portion of the scaffold ➤ Lack of complexity and modifiability ➤ Usually only a single cell type 	<p>(Ainslie <i>et al.</i>, 2019; Bérubé <i>et al.</i>, 2009; A. J. Booth <i>et al.</i>, 2012; Brandenberger <i>et al.</i>, 2010; Choe <i>et al.</i>, 2006; Ehrhardt <i>et al.</i>, 2017; Gilpin <i>et al.</i>, 2014; Marrazzo <i>et al.</i>, 2016; Mazzoleni <i>et al.</i>, 2009; Nichols <i>et al.</i>, 2013; O'Neill <i>et al.</i>, 2013; Papritz <i>et al.</i>, 2010; H. Sun <i>et al.</i>, 2016; Wagner, Bonenfant, Parsons, <i>et al.</i>, 2014; Wagner, Bonenfant, Sokocevic, <i>et al.</i>, 2014)</p>
--	--	--	--	--

<p>3D Micro-physiological System (MPS)/ Organ-on-a-Chip (OOCs)</p>	<p>➤ Biometric devices that can capture the natural physiology of human/animal tissues in a micro-environment</p>	<p>➤ Precise dynamic control over microenvironment</p> <p>➤ Microfluidics increase duration of viability by providing oxygen/nutrients and waste removal.</p> <p>➤ Fluid flow provides shear stress.</p> <p>➤ Perfusate analysis for secreted factors with mechanical stretch possible</p> <p>➤ Full cellular complexity of epithelium, ciliated and non-ciliated cells, apical mucous secretions, expression of ion channels, tight junctions</p> <p>➤ Can mimic blood and air barriers through the culture of alveolar epithelium in air and endothelial cells in media.</p> <p>➤ Use of cell lines, primary or stem cells</p>	<p>➤ Highly variable manufacturing protocols</p> <p>➤ Usually lack cellular components of the immune system (e.g., lymphocytes, macrophages, and dendritic cells)</p> <p>➤ Low to medium throughput</p> <p>➤ Relatively labour-intensive</p>	<p>(Ainslie <i>et al.</i>, 2019; Artzy-Schnirman <i>et al.</i>, 2020)</p>
---	---	--	--	---

1.4.2.4. AIR-LIQUID INTERFACE (ALI) CULTURE

It can be challenging to recapitulate essential features of the target tissue in 2D, such as cell polarity (Barrila *et al.*, 2018). Various scaffolds and insert-based platforms have been employed to create an extra layer of complexity to the more established 2D *in vitro* models. Insert-based systems harbour a suspended membrane which compartmentalises the culture, allowing cells to be grown on the insert and/or below the insert on the bottom of a well. The particular interest in insert-based cultures for pulmonary cells is the ability to create an air-liquid-interface (ALI) (Adler *et al.*, 1990; Ainslie *et al.*, 2019; Bérubé *et al.*, 2010; Brandenberger *et al.*, 2010; Choe *et al.*, 2006; Chowdhury *et al.*, 2010; Ehrhardt *et al.*, 2017; Klein *et al.*, 2011; Marrazzo *et al.*, 2016; Papritz *et al.*, 2010; Sakagami, 2006). ALI culture of lung epithelial cells is an essential feature of a representative lung model, since in the *in vivo* situation epithelial cells are exposed to air (Adler *et al.*, 1990). Under ALI conditions, bronchial epithelial cells can produce a 3D, multicellular pseudostratified lung epithelium with basal cells and ciliated and goblet cells (Sakagami, 2006). Cells cultured in a liquid-liquid-interface (LLI) (submerged cultures) are not representative of the *in vivo* environment and so do not develop into representative phenotypes (Lacroix *et al.*, 2018). ALI methods represent a simple, alternative, and more physiologically representative option to standard 2D cultures. The use of ALI cultures also allows for a direct application of drugs to the cell surface using aerosols to further represent the *in vivo* situation (Bérubé *et al.*, 2010).

ALI culture has been employed using several sources of cells including primary cells, cell lines, and cocultures (Klein *et al.*, 2011; Neilson *et al.*, 2015; Secondo *et al.*, 2017). It has previously been reported that submerged culture may reduce the level of differentiated morphology expressed by Calu-3 cells and the influences of submerged vs ALI appears to be a major factor on transepithelial electrical resistance (TEER) and permeability to common permeability markers in 16HBE14o- cells (Florea *et al.*, 2003; Forbes & Ehrhardt, 2005). Reduction in cilia and robustness to media manipulation in Calu-3 and 16HBE14o- cells may be due to submerged culture, with Calu-3 cells reported to have reduced mucus production in submerged culture (Fiegel *et al.*, 2003). The importance of ALI culture is more significant for promoting cellular differentiation in primary cultures (de Jong *et al.*, 1994; Yamaya *et al.*, 1992). Primary tracheal and bronchial epithelial cells cultured at the ALI show differentiation that recapitulates the *in vivo* characteristics of upper airway epithelium such as pseudostratified cell layers with tight junctions, cilia and mucin production.(D. Cozens *et al.*, 2018; Pezzulo *et al.*, 2011; Whitcutt *et al.*, 1988) So, whilst simple 2D culture has been established as an effective high-throughput screening tool for early in the drug discovery pipeline, models that are more human physiologically relevant by ALI culture allows drug developers to more closely mimic and predict human response.

1.4.2.4.1. SCAFFOLD/INSERT-BASED CULTURE

Aiding the culture at an ALI, scaffold-based cultures have been established to generate a model that is more representative of the *in vivo* environment. The scaffolds themselves can be made from materials such as collagen/fibrin or synthetic polymers such as polydimethylsiloxane (PDMS) (Mazzoleni *et al.*, 2009). Alongside utilisation in ALI culture, scaffolds are advantageous in their use to enable coculture of different cell types on either side of the scaffold membrane. This can allow for more physiologically relevant cultures as well as recapitulating the heterogenous aspects of lung tissue and disease states (A. J. Booth *et al.*, 2012; Gilpin *et al.*, 2014; Mazzoleni *et al.*, 2009; Nichols *et al.*, 2013; O'Neill *et al.*, 2013; H. Sun *et al.*, 2016; Wagner, Bonenfant, Parsons, *et al.*, 2014; Wagner, Bonenfant, Sokocevic, *et al.*, 2014).

However, initial seeding is stochastic which can result in highly variable results. The inserts can also require expensive manufacture and optimisation alongside the controversial use of PDMS due to its drug adsorption properties. Scaffolds also have limited access to oxygen and nutrients to their inner portions potentially affecting cell behaviour, however this may be overcome by incorporating scaffolds in microphysiological systems (MPS)/organ-on-chip (OOC) devices (A. J. Booth *et al.*, 2012; Gilpin *et al.*, 2014; Mazzoleni *et al.*, 2009; Nichols *et al.*, 2013; O'Neill *et al.*, 2013; H. Sun *et al.*, 2016; Wagner, Bonenfant, Parsons, *et al.*, 2014; Wagner, Bonenfant, Sokocevic, *et al.*, 2014).

Commercially available cell culture plate inserts such as Corning's Transwell® inserts have been employed to develop lung *in vitro* models that enable lung epithelium cells to be cultured at an ALI. Transwell inserts have been shown to exhibit elevated levels of pro-inflammatory markers compared to submerged cell cultures when exposed to aerosolised toxic compounds like zinc oxide nanoparticles (Lenz *et al.*, 2013). ALI culture can also be achieved by culturing epithelial cells on the apical side of a Transwell insert and removing the tissue culture medium from the apical side once a monolayer has been established, leaving medium present only in the basolateral chamber (illustrated in Figure 1.3). The implementation of ALI culture on Transwells generates a more complex and physiologically relevant model of the lung epithelium, generating a differentiated respiratory epithelium with the formation of tight junctions with apical and basolateral polarity, mucin production and multicellular complexity (e.g. ciliated cells, goblet cells, club cells etc) (Bukowy-Bieryłło, 2021). Cell polarity refers to the orientation of the apical cell surface to the lumen and the basolateral surface away from the lumen, this aids in the transport of ions and solvents and to the localisation of proteins and lipids at one of the cell surfaces (Tapia *et al.*, 2017).

Transwell models have successfully been used to study inhaled drugs such as fluticasone propionate and salbutamol for their deposition profile and transport across the ALI-cultured epithelium (Cingolani *et al.*, 2019; Haghi *et al.*, 2012a, 2013; V. Kumar *et al.*, 2022, 2022). Other avenues of research have been on the evaluation of inhaled toxicants, such as tobacco flavouring extracts and nanoparticles (zinc oxide and titanium dioxide), as well as the investigation of various pathogens (Ji *et al.*, 2022; D. Kim *et al.*, 2021; Mösbauer *et al.*, 2021; Sims *et al.*, 2008; Stuetz *et al.*, 2023). This is further explored in Chapter Three and Chapter Five of this thesis.

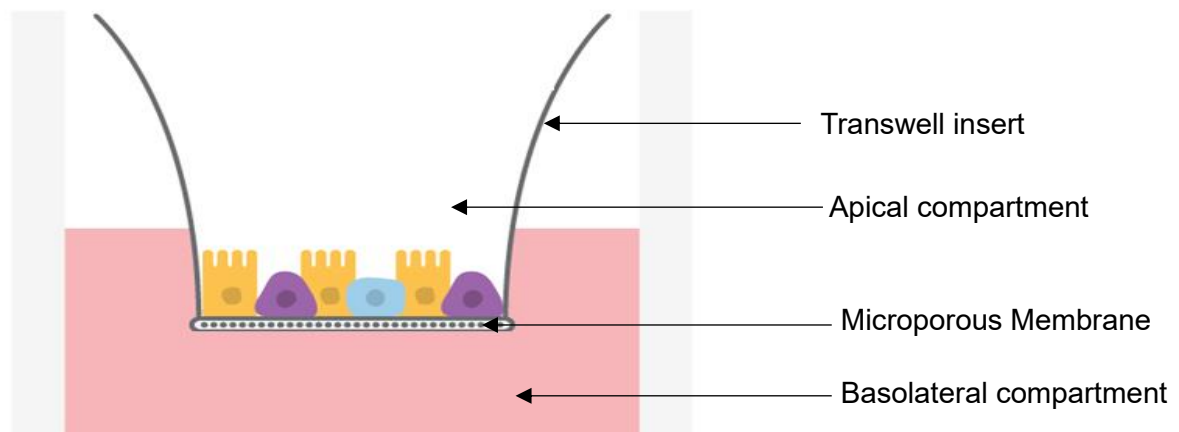


Figure 1.4: Diagram of a Transwell® insert within a standard cell culture well plate, illustrating the apical and basolateral compartment sides of the Transwell®

1.4.2.4.2. COMMERCIAL ALI CULTURE MODELS

A few commercial examples of insert-based ALI lung models are the EpiAirway™ and EpiAlveolar™ models from MatTek® and the MucilAir™, SmallAir™ and AlveolAir™ models from Epithelix® (EpiAirway 3D in Vitro Microtissues, 2015; Epithelix, 2024). These models utilise primary cells from the human respiratory tract and boast a long lifespan of multi-layered and differentiated epithelial cells that form cilia, tight junctions and secrete mucus (BéruBé *et al.*, 2010). The models have been developed to model diseases such as COPD and asthma and have been utilised in applications such as acute and chronic toxicity test, drug delivery, immune responses and bacterial/viral infections (S. Huang *et al.*, 2009). However, these models are not immortalised so cannot be expanded for new cultures as is the case with cell line models. New cultures require purchasing the model kit again which incurs a higher cost per experiment than using cell line models (BéruBé *et al.*, 2010).

1.4.3. MICROPHYSIOLOGICAL SYSTEMS (MPS)/ORGAN-ON-A-CHIP (OOC) MODELS

1.4.3.1. GENERAL FEATURES OF MPS AND OOC MODELS AND SYSTEM DESIGN

Organ-on-a-chip (OOC) or microphysiological systems (MPS) are microfluidic devices for growing cells in micrometre-sized chambers in order to model physiological functions of tissues or organs, such as perfusion and stretch (Polini *et al.*, 2014). Human cells are cultured in these devices from the three sources of cells discussed previously in Section 1.5.1 to increase the human relevancy of the culture model. One of the popular, novel culture aspect of the MPS/OOC devices is to incorporate perfusion/fluid flow through the microchannels to replicate the *in vivo* blood/interstitial fluid flow experienced by the organs/tissues (Ainslie *et al.*, 2019; D. Huh, Matthews, Mammoto, Montoya-Zavala, Hsin, *et al.*, 2010). MPS/OOC devices allow the study of cells under physiologically relevant fluid flow environments that can regulate physiological stress, chemical signalling, transport processes and cell-to-cell interaction (Atencia & Beebe, 2005; Ayliffe *et al.*, 1999; Duan *et al.*, 2008; Walker *et al.*, 2004).

MPS/OOC devices also involve other physical forces such as fluid shear stress, cyclic strain and mechanical compression at a physiologically relevant level to mimic the human microenvironment to effectively develop a representative *in vitro* model (R. Booth & Kim, 2012). Passive stimuli is also considered, including but not limited to substrate stiffness and geometric confinement (Thompson *et al.*, 2020a). These devices influence cell phenotypes such as polarity, gene expression and differentiation similar to that seen *in vivo*, capturing the natural physiology of human/animal tissues induced by the mechanical features of the MPS/OOC devices (Ainslie *et al.*, 2019). Alongside these physiologically relevant mechanical features, these devices can be fabricated to contain sensors that can provide real-time feedback of the tissue health and function such as oxygen sensors and transepithelial electrical resistance measurements (Srinivasan *et al.*, 2015). For simplicity, all OOC and MPS devices will be referred to as MPS devices within this thesis.

Using MPS to simulate *in vivo* environments has great potential to characterise the relationship between biomarkers and clinical outcomes due to the enhanced physiological relevance of tissues cultured in the devices (Bhatia & Ingber, 2014a; Ewart *et al.*, 2018). Reliable MPS models have great potential to enhance the understanding of disease states and improve drug candidate selection efficiency, thereby decreasing the reliance on animal models and decreasing drug attrition, all of which will ultimately provide patients with new and alternative therapeutic options (Ainslie *et al.*, 2019).

In the simplest MPS models, there is a single micro-chamber with a single cell type, however there are more complex designs with two or more micro-chambers connected by porous membranes, lined with different types of cells to recreate interfaces between tissues (Bhatia

& Ingber, 2014b; Polini *et al.*, 2014). These devices are versatile with the types of organs and tissues they can model. Other MPS developers have taken to produce more organ-specific models to further increase the physical relevance of the model such as microcurved wells to mimic the alveolus (AlveoliX, 2024). Whilst others have developed more versatile and adoptable MPS devices that can incorporate established complex cell models such as scaffold/insert based cultures (CN Bio, 2019).

The design of MPS differs according to the tissue/organ modelled and the biomechanical stimuli investigated. There are multiple commercial single organ systems with fluid flow through (Alveolix, CNBio, Emulate, Kirkstall) (AlveoliX, 2024; CN Bio, 2019; *Emulate*, 2024; Kirkstall, 2024). However, there is massive potential to connect several MPS models to create a multi-organ platform system and be able to study the effect of compounds from one organ to another e.g. lung to liver (Sedláková *et al.*, 2019). MPS devices that concentrate on the fluid flow between two or more organ types have been developed and commercialised; CN Bio: Liver/Intestine, Kirkstall: Pancreas/Liver, TissUse: Intestine-Liver-Brain-Kidney, Intestine-Liver-Skin-Kidney, Liver-Lung (W. L. K. Chen *et al.*, 2017; Faure *et al.*, 2016; Maschmeyer, Lorenz, *et al.*, 2015; Ramme *et al.*, 2019; Schimek *et al.*, 2020).

All of these MPS devices could be used to study human lung development, pathophysiology and study the responses to inhaled compounds to study pharmacodynamics (PD) and pharmacokinetics (PK) and toxicity to ultimately discover new diagnostics and therapeutics (Artzy-Schnirman *et al.*, 2020; Nawroth *et al.*, 2019). The FDA Modernisation Act 2.0 highlights the openness of regulators to accept data from NAMs, such as MPS. However, whilst many drug developers are already using MPS, stronger and more robust use-case evidence and standardisation from regulators is required for drug developers to fully integrate NAMs into their preclinical pipelines (Pognan *et al.*, 2023; Stresser *et al.*, 2023).

1.4.3.2. LIMITATIONS OF MPS MODELS

Many MPS manufacturers use synthetic polymers such as polydimethylsiloxane (PDMS) to develop the consumable plates, which is popular due to its transparency and reduced cytotoxicity (Danku *et al.*, 2022; Schimek *et al.*, 2020). However, the use of PDMS is controversial because of its ability to adsorb hydrophobic substances (Nianzhen Li *et al.*, 2009; Toepke & Beebe, 2006; J. D. Wang *et al.*, 2012). Compounds with a log P > 2.6, the quantitative measure of the hydrophobicity of a compound, get extensively adsorbed into the PDMS channels of the MPS devices (J. D. Wang *et al.*, 2012). When conducting experiments with drug molecules using devices containing PDMS, the log P of the molecule needs to be considered and potentially leading to adsorption preventative coating of the channels, decreasing the ease of use (J. D. Wang *et al.*, 2012). PDMS lacks the ECM simulations cells

require to exhibit phenotypes similar to that seen *in vivo* and requires culture surfaces to be coated with hydrogels such as Matrigel/collagen to mimic the ECM (Sedláková *et al.*, 2019).

Another major issue of MPS devices is the labour intensity, as they can take more time to develop and analyse than typical 2D culture systems (Ainslie *et al.*, 2019). Furthermore, as a newer technology, the absence of standardisation in the production of MPS devices hinders the reproducibility of experiments but also acts as a bottleneck for large-scale, cost-effective production (Srivastava *et al.*, 2024). Analysis of some MPS is another significant issue as the small sizes and lower fluid volumes require highly sensitive biochemical methods such as ELISA and quantitative polymerase chain reaction (qPCR). This limits the high throughput capability of the systems (Sedláková *et al.*, 2019). However, the lower volume is advantageous for reducing the costs for drug development processes as it allows smaller amounts of compound. The latter reduction of compound requirements have been exploited in various physiological studies including ADME and toxicity (Ahadian *et al.*, 2018; Ishida, 2018; S. H. Lee & Sung, 2018). A significant drawback of MPS models is the translatability of the model to *in vivo* response as the surface-volume ratio of the cells in the microchannels/wells limits the scalability of dose response to the whole tissue/organ in the body, this is especially prevalent when the endpoint assays used are not representative of the *in vivo* human response (Wikswa *et al.*, 2013). The analysis of MPS models is explored in Chapter Two of this thesis.

1.4.3.3. MPS AND OOC MODELS OF THE RESPIRATORY SYSTEM

MPS have immense potential to be the most representative *in vitro* lung models as they have the potential to incorporate ALI culture with air and/or media flow as well as cyclical stretch. Air flow and cyclical stretch recapitulate the stretching motions in cyclic breathing and the subsequent cellular strains. Perfusion with medium mimics the blood flow cells would experience *in vivo* which not only provides enhanced nutrient and oxygen availability, but also shear stress (Artzy-Schnirman *et al.*, 2020; Sedláková *et al.*, 2019). Ainslie *et al.* (2019) detailed key practical features that should be considered in a lung MPS model for the airways (Ainslie *et al.*, 2019):

- User friendly interface/culture.
- Reasonable throughput, incorporating replicates and positive/negative controls.
- Reproducible with low inter- and intra-lab variability on a stable platform system.
- Automated sampling from air and/or fluid compartments.
- Materials with little to no drug binding.
- Ability to modulate cells to mimic disease or reflect natural population variances.
- Physiologically relevant metabolic and gene expression profile.

- Ability to image cells without interference from MPS device materials.
- Pseudostratified epithelium with metabolically active club cells and goblet cells producing mucus.
- Amenable to coculture.
- Applicable to small molecules, biologics, gene editing, cell therapy modalities.
- Extended *in vitro* culture times (2–4 weeks).

These considerations of MPS devices should be adopted by developers of MPS devices for the culture of lung MPS models.

There are many commercially available MPS devices with multiple tissue models, a few have been used to model the human lung. Emulate commercialised the lung model developed by the Wyss institute at Harvard University (*Emulate*, 2024). The OOC device, Chip-S1, mimics a breathing stretch motion seen *in vivo* on a porous membrane. The Orb™ provides the precise mixture of gas, power, and vacuum stretch required by the Zoë™ culture module, which then controls the rate of flow and stretch for up to 12 chips (*Emulate*, 2024). Emulate have developed a coculture model of the human lung, utilising primary human lung airway basal stem cells cultured under ALI and primary human pulmonary microvascular endothelial cells on opposing sides of the membrane replicate the alveolar-capillary barrier of the human lung (D. Huh, Matthews, Mammoto, Montoya-Zavala, Hsin, *et al.*, 2010; Jain *et al.*, 2018). The vascular channel is exposed to continuous fluid flow at a rate of 60 $\mu\text{L/h}$ with a shear stress of 0.0017 Pa (D. Huh, Matthews, Mammoto, Montoya-Zavala, Hsin, *et al.*, 2010; Jain *et al.*, 2018). Emulate's chip has been used to replicate the SARS-CoV-2 and influenza viral infection, observe drug toxicity-induced pulmonary oedema and how mechanical breathing forces influence disease development (D. Huh, Matthews, Mammoto, Montoya-Zavala, Hsin, *et al.*, 2010; Si *et al.*, 2020).

Similarly, AlveoliX have commercialised the 'breathing' ^{AX}Lung-on-Chip System which mimics the biomechanical microenvironment of the air-blood barrier of the human lung by applying positive and negative pressures on a porous membrane. Lung cells can be cultured under ALI on the apical side of the membrane, and endothelial cells cultured on the basal side, mimicking the alveolar environment with the porous membrane allowing passive diffusion between the chambers (A. O. Stucki *et al.*, 2015; J. D. Stucki *et al.*, 2018). The cyclic strain/stretch has been proven to influence the metabolic activity of primary human pulmonary alveolar epithelial cells, increasing the permeability of the epithelial barrier and an increase in cytokine secretion greater than static conditions (A. O. Stucki *et al.*, 2015).

Other MPS devices combine ALI tissue culture inserts with flow such as CN Bio's PhysioMimix®. Lung cultures are conducted in the Barrier-12 (MPS-12) plate with the media

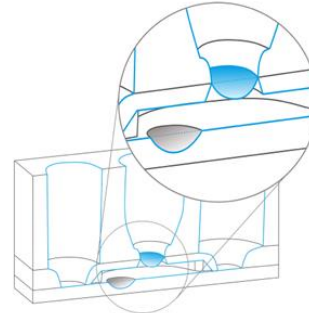
flow in the basal compartment at a flow rate of 0.5 $\mu\text{L/s}$ utilising inserts such as the Transwell® and CellQart® culture inserts (Phan *et al.*, 2023). The cell culture medium is circulated through an inlet valve, the movement of this valve pumps approximately 1 μL per cycle with capacitors regulating flow to ensure consistent fluid movement, simulating physiological condition. The pump's operating range matches *in vivo* observations, maintaining physiological shear stress levels (Domansky *et al.*, 2010). The plates are built with a mix of polystyrene, polycarbonate and polyurethane, avoiding the divisive PDMS (Domansky *et al.*, 2010). The Barrier-12 MPS has been used to optimise healthy and diseased coculture models of the human lung at ALI using primary human lung epithelial and fibroblast cells, highlighting the effective culture of these models resulting in a more physiological relevant lung model than the static equivalent (Phan *et al.*, 2023).

These commercial systems also have their drawbacks. They are limited in terms of flexibility with cell manipulation and customisation as a disease-specific donor is required for primary cells (Zscheppang *et al.*, 2018). Additionally, the portability and reproducibility of the systems needs to be proven to validate the models and make the technology more widely accessible (Low & Tagle, 2017). The PhysioMimix system has further flexibility as the Barrier-12 plates can house commercially available models (e.g. MucilAir) or novel culture models on inserts (e.g. Transwells) (CN Bio, 2019; Phan *et al.*, 2023). However, due to its dependence on cell culture, inserts it lacks the capacity to induce stretch unlike the AlveoliX and Emulate devices. The stretch force on the Emulate chip stretch is unilateral whereas stretch seen in the AlveoliX chips are across three dimensions, which is more akin to the stretch cells experience *in vivo* than the stretch exhibited in the Emulate device (D. Huh, Matthews, Mammoto, Montoya-Zavala, Hsin, *et al.*, 2010; A. O. Stucki *et al.*, 2015). The AlveoliX models boast a passive media exchange however, it is not the most physiologically relevant fluid flow whereas the CN Bio PhysioMimix system and the Emulate chip incorporate active fluid flow, exerting shear stress on the cell similar to that seen *in vivo* (Domansky *et al.*, 2010; D. Huh, Matthews, Mammoto, Montoya-Zavala, Hsin, *et al.*, 2010; A. O. Stucki *et al.*, 2015).

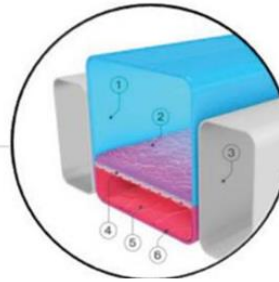
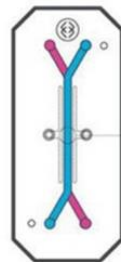
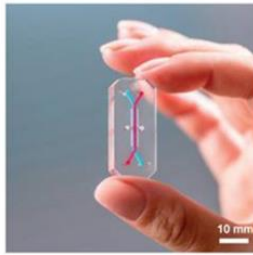
Emulate and AlveoliX both use a PDMS membrane in their MPS which requires coating with fibronectin or collagen to effectively replicate the *in vivo* ECM which increases the complexity of the cell culture protocol when using the chip as well as causing another hurdle for studies involving hydrophobic molecules (D. Huh, Matthews, Mammoto, Montoya-Zavala, Hsin, *et al.*, 2010; A. O. Stucki *et al.*, 2015; J. D. Wang *et al.*, 2012). However, the Barrier-12 MPS from CN Bio uses COC (cyclic olefin copolymer). COC has a low water absorption rate and biological inertness, which is advantageous for the culture of biological models, however the hydrophobicity of COC could pose a challenge to the study of some pharmaceutical compounds whilst advantageous to those not compatible with PDMS (Agha *et al.*, 2022).

The Emulate model has the lowest throughput of the models as each chip is self-encompassing unit, requiring more chips to increase the replicates which reduces the experimental uniformity across the chips due to the aforementioned lack of standardisation in MPS manufacture (D. Huh, Matthews, Mammoto, Montoya-Zavala, Hsin, *et al.*, 2010; Srivastava *et al.*, 2024). Whereas the AlveoliX and PhysioMimix MPS utilise an open-well format similar to the standard cell culture plates with 12 chips in both the AlveoliX and the PhysioMimix MPS, increasing the throughput by having multiple chips per plate and multiple plates that can be maintained at once whilst reducing the complexity of maintain the cultures as the format of the plates is standard across the cell biology industry (Domansky *et al.*, 2010; D. Huh, Matthews, Mammoto, Montoya-Zavala, Hsin, *et al.*, 2010; A. O. Stucki *et al.*, 2015).

The complexity and cost of these systems requires as much information as possible from a single experiment which requires optimisation of as many assays as possible to make the systems cost effective (Dehne *et al.*, 2017). This is made more difficult due to the samples being of such low volume, and therefore it can be expensive to optimise assays and also increases the complexity of translatability and scalability (Sedláková *et al.*, 2019; Wikswo *et al.*, 2013). The low volume of samples is a major issue for models such as the Emulate chip equipped with microchannels as small as 30 μm and the AlveoliX system with wells filled with up to 80 μL of medium (Bhatia & Ingber, 2014b; J. D. Stucki *et al.*, 2018). However, the CN Bio Barrier-12 plate can have up to 1 mL contained in each chip/well (Phan *et al.*, 2023). This challenge in sampling and complexity is why inter-lab reproducibility and transferability has to be tested and validated through wider adoption of the culture systems (Dehne *et al.*, 2017). The MPS culture devices and their schematics are illustrated below (Figure 1.6).

A

©AlveoliX A.G.

B

©Emulate Inc.

C

©CN Bio Innovations Ltd

Figure 1.5: **(A)** AX12 lung chip based on a 96-well plate format, consisting of two chips supported by a plate, each of which comprise six independent units. The ultrathin membrane (blue) is deflected by negative pressure inside the basal chip chamber through an integrated micro-diaphragm (gray). Images from (AlveoliX, 2024) **(B)** The Human Emulation system from Emulate Inc. comprising organ chips which fit into the Pod™ carrier. The Zoë™ culture module controls the rate of flow and stretch for up to 12 chips. The Orb™ provides the precise mixture of gas, power, and vacuum stretch required by the Zoë™ culture module. Images from (Emulate, 2024) **(C)** The Barrier-12 plate allows the culture of cells on commercial inserts such as Transwell® inserts, with circulating flow in the basolateral chamber pumped through microchannels at a customisable flow rate.

1.4.4. CHARACTERISATION APPROACHES FOR TISSUE CULTURE MODELS

1.4.4.1. ANALYSIS OF COMPLEX CELL CULTURE MODELS

Overall, the value of MPS/OOCs has been demonstrated in both academia and commercially with various feasible improvements and discussions illustrating the potential of the technology (Ainslie *et al.*, 2019; Artzy-Schnirman *et al.*, 2020; D. Huh, Matthews, Mammoto, Montoya-Zavala, Hsin, *et al.*, 2010; Klein *et al.*, 2011; Schimek *et al.*, 2020). The main challenges of these *in vitro* systems is scaling and is a result of the micro and nano-scales of volume and area used in cell culture technology, leading to the possibility of less accurate translation of data from the models to the human body (Wikswa *et al.*, 2013). This illustrates the need to ensure the correct tools of analysis are used to produce high quality, translatable and scalable data from small volumes of sample. Characterising these models requires multiple avenues of analysis, incorporating several techniques to create a fully understood picture of the model and its functionalities. An important avenue of characterising the model involves analysing the phenotype of the cells, which is the observable traits of the cells which is a result of the gene expression and environmental factors that influence the expressed characteristics (National Human Genome Research Institute, 2024). There are several assays can be employed to characterise the phenotype of the cell model including, but not limited to:

- Immunofluorescence imaging (IF): Fluorescently labelled antibodies to detect a specific target, primarily proteins, and produce a fluorescent image that can be analysed for expression of the target and represent key features of the lungs such as mucus, tight junctions and cilia (Odell & Cook, 2013)
- Histology: Observe the cell layers in the cross-section view and identify expression of proteins in cells and tissues of the lungs, such as ciliated cells and goblet cells, so that they become visually detectable by light microscopy (Ramos-Vara, 2010).
- Flow cytometry: Rapid analysis of the size, granularity of a single cell and phenotypically characterise and collect the cell using fluorescent reagents similar to those used in IF imaging (Drescher *et al.*, 2021).
- Transepithelial electrical resistance (TEER): Reflecting the ionic conductance of a paracellular pathway in the cell monolayer, TEER is a reliable, continuous and non-destructive method of quantifying the integrity and permeability of the barrier (Srinivasan *et al.*, 2015; Zucco, 2005).
- Quantitative polymerase chain reaction (qPCR): Quantifying the gene expression of key epithelial features such as transporters and mucins, by the qualitative detection of RNA (Wages, 2004).

Once the phenotype has been established, the functionality of the cell model needs to be assessed to understand how the model can be best utilised and if it is fit for purpose. Assessment of functionality includes methods such as:

- Enzyme-linked immunosorbent assays (ELISAs): Measurements of antibodies, antigens, proteins and glycoproteins for the analysis of cellular response to flow- coculture or drug compounds (British Society for Immunology, 2024; Junaid *et al.*, 2017).
- Apparent permeability (P_{app}): The *in vitro* gold standard of the assessment of the formation and function of cellular barriers through the uptake rate of chemicals/drugs, with radiolabelled compounds frequently used (Alsenz & Haenel, 2003; Artursson *et al.*, 2012; K.-J. Lee *et al.*, 2005; Srinivasan *et al.*, 2015; Thiel-Demby *et al.*, 2009).

These methods can be used to study and validate the differentiation of cultures in 3D as well as assess the effects of assays on disease models (Lin *et al.*, 2020).

However, there are disadvantages to these assays. TEER has high inter-experiment and inter-lab variability when conditions are not standardised including temperature, passage number and cell culture medium composition (Srinivasan *et al.*, 2015). Conducting multiple ELISAs is expensive and labour-intensive as they have long incubation stages and multiple washes, with high likelihood of false positive/negative results due to insufficient blocking of the microplate or antibody instability (S. Sakamoto *et al.*, 2018). The use of such tracer compounds to determine P_{app} , can interfere with the transport process under study and can affect the barrier integrity (Srinivasan *et al.*, 2015). An improvement on this approach would be the incorporation of high sensitivity chemical analytical instrumentation such as liquid/gas chromatography with mass spectrometry (LC-MS/GC-MS) for the evaluation of drug flux, metabolomic, and proteomic studies which can enhance the power of MPS assays (Junaid *et al.*, 2017; Lin *et al.*, 2020). Liquid chromatography coupled to mass spectrometry, alongside the assays mentioned above, is a common approach for the study of biological systems including proteomics, metabolomics and for understanding drug disposition (Lynch, 2017). Even though it is a highly generic and known analytical technique, chromatography and MS are still little used in OOC analysis (Junaid *et al.*, 2017; Lin *et al.*, 2020). Currently, LC/GC-MS has only been used as a readout for only a few MPS models even though there is great potential in its use (Filla *et al.*, 2016; H. Lee *et al.*, 2017; Maschmeyer, Hasenberg, *et al.*, 2015; Shah *et al.*, 2016; Zeller *et al.*, 2017). This is further explored in Chapter Two of this thesis.

1.4.4.2. BIOANALYTICAL METHODOLOGIES IN TISSUE CULTURE RESEARCH

1.4.4.2.1. OVERVIEW OF ANALYTICAL INSTRUMENTATION FOR BIOANALYSIS

There are many types of analytical instrumentation that can be used to quantify compounds in a robust and repeatable method. Analysing the multiple types of compounds that are present in cell culture media requires a selective method that can separate these compounds from each other to reduce the interference at the detector. Analysing drug compounds and their metabolites in cell culture media can be complex due to the variability in the percentage of protein bound drug differing between drug classes/types which can lead to a high loss of drug if the sample preparation is not adequate (Rasmussen *et al.*, 2011). In addition, the amount of sample available is often minimal and so requires a highly sensitive instrument to analyse the processed sample. These two main challenges need to be addressed through the sample process method and the instrument type utilised.

Gas chromatography (GC) is used for screening prohibited substances in doping control analysis; however, GC methods are highly labour-intensive and more time consuming than liquid chromatography (LC) alternatives. High performance liquid chromatography (HPLC) is the most commonly used chromatographic technique in industry and academia for determining drug quantities in pharmaceutical preparations or biological samples (Harris, Daniel C., 2010; Rasmussen *et al.*, 2011). The sample and mobile phase is forced through a column packed with a material that retains the analyte, the eluted analytes are then distinguished by a detector system (Rasmussen *et al.*, 2011). LC enables separation of a sample to identify individual compounds as a result of the chemical or physical interaction of compounds with stationary and mobile phases (Hadavi *et al.*, 2023). LC instrumental analysis of biological samples is difficult due to the complexity and high abundance of matrix components (e.g., proteins, plasma etc) that can interfere with the analysis. LC alone is not sufficient for full separation of complex samples, so a purification of the sample is needed through a sample extraction method (Hadavi *et al.*, 2023). Ultra high-performance liquid chromatography is increasingly adopted due to its ability to reduce solvent consumption, reduce elution times and lower detection limits (Rasmussen *et al.*, 2011).

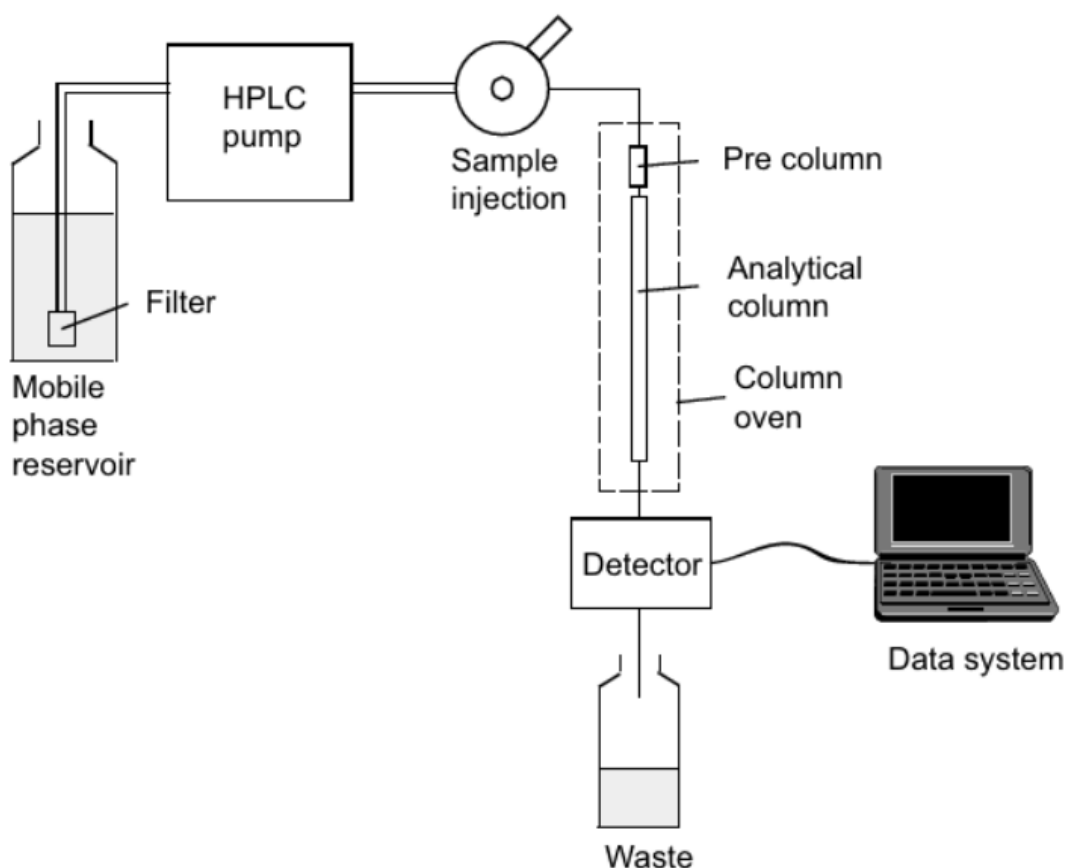


Figure 1.6: Diagram highlighting the main structure of an LC system. Figure obtained from (Rasmussen *et al.*, 2011).

The detectors that can be coupled to LC instrumentation is varied in their selectivity and sensitivity. The most common detectors used are ultraviolet light detectors (UV/Vis) as they can detect compounds that absorb light from a deuterium light source at a fixed wavelength and a photodiode array detector can record the entire spectrum at once in a fraction of a second (Harris, Daniel C., 2010). HPLC-UV is used in industry for the determination of drug compounds in blood and urine and costs are relatively lower than the alternative detection methods. However, the sample must be able to absorb light or be transformed into a sample that can absorb light and that can be challenging with biological samples (Rasmussen *et al.*, 2011). Biological samples are complex, and target analytes are often in extremely small amounts. Also, UV/Vis detection is not the most sensitive detection method, with the limit of detection ranging from low $\mu\text{g/mL}$ to ng/mL . Subsequently, mass spectrometry detection (MS) is more typically required for bioanalysis (Rasmussen *et al.*, 2011; Sharma, 2024).

1.4.4.2.2. MASS SPECTROMETRY

Mass spectrometry (MS) is an analytical technique for studying the masses of atoms/molecules/fragments of molecules ('Introduction to Mass Spectrometry', 2008). MS is typically coupled with gas chromatography (GC-MS) or liquid chromatography (LC-MS) and is the most sensitive and costly detector coupled to LC. It is a key technique in the analysis of drugs in biological samples (Rasmussen *et al.*, 2011).

Once the sample leaves the LC and reaches the MS it is ionised (either positive or negative). This leads to an unstable molecular ion which quickly splits into smaller fragment ions. The ions are then accelerated out of the ion source and separated according to the ratio (m/z) between the mass (m) and the electric charge (z) in a magnetic or electrostatic field. The ions are then transferred to the detector which measures the amount/intensity of the different ions at each m/z value (Harris, Daniel C., 2010; Rasmussen *et al.*, 2011). Ionisation can occur through chemical ionisation, which is most common in GC-MS or atmospheric pressure chemical ionisation (APCI), (Figure 1.7) both of which are particularly relevant for LC analytes that do not contain acidic or basic functional groups (Rasmussen *et al.*, 2011). An extremely important ionisation technique is electrospray ionisation (ESI) (Figure 1.7) and is the most used technique for MS coupled to HPLC (LC-MS). The liquid sample (mobile phase containing the analyte) is sprayed as a fine aerosol and the droplets are charged by an electrode, evaporating the mobile phase/solvent, and leaving behind the charged analyte which is then extracted for further analysis by the mass analyser (Ho *et al.*, 2003; Rasmussen *et al.*, 2011).

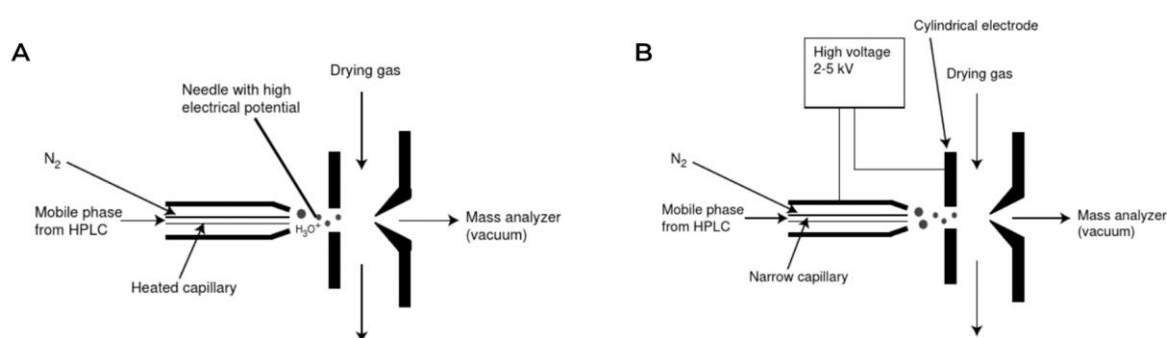


Figure 1.7: Diagrams of the two common ionisation techniques for mass spectrometry. (A) Chemical ionisation and (B) Electrospray ionisation. Figures obtained from (Rasmussen *et al.*, 2011).

The ions travel through a magnetic or electrical field and their movement is affected by their m/z which separates the ions. This is achieved through a quadrupole mass analyser where 4 parallel metal rods are connected electrically allowing stable ions to travel through to the

detector impeded whereas unstable ions hit the metal rods and are neutralised (Ho *et al.*, 2003).

Tandem-MS (MS/MS) is where the quadrupole system is set up in with three quadrupoles in a linear fashion. The first quadrupole (Q1) selects the analyte of interest, this step eliminates complicated and time-consuming sample purification procedures prior to the MS analysis. The analyte reaches the second quadrupole (Q2) where the ions are activated by collisions and further fragment this is known as collision-induced dissociation (CID). The daughter ion mass spectrum from CID can be monitored by the third quadrupole (Q3) providing the structural information of the molecular ions (Ho *et al.*, 2003; Rasmussen *et al.*, 2011). LC-MS/MS is the most sensitive technique to analyse and quantify drug compounds in complex biological samples due to the separation of analytes by the HPLC and then the analysis of the compounds in the MS/MS component, with instrument limits of detection ranging from 20 pg/mL to 100 ng/mL dependent on the compound (Easterling *et al.*, 2020). However, the samples are still considered 'dirty' and require purification and extraction to produce a sample that is compatible with LC-MS/MS.

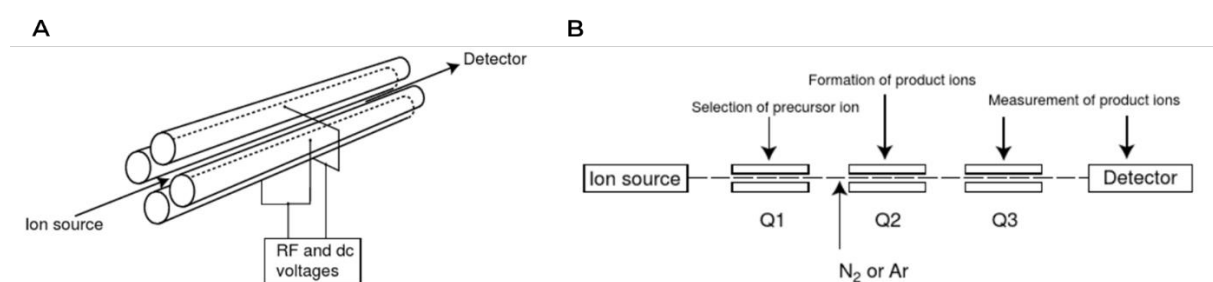


Figure 1.8: Diagram of a (A) quadrupole and a (B) triple quadrupole found in mass spectrometry detectors. Diagrams obtained from (Rasmussen *et al.*, 2011).

1.4.4.2.3. SAMPLE PREPARATION OF BIOLOGICAL SAMPLES

80% of analysis time of biological samples is sample preparation to remove unwanted matrix components such as proteins and exchange the solvent from the aqueous biological fluid to a solvent compatible with HPLC systems (Rasmussen *et al.*, 2011). Protein precipitation, liquid-liquid extraction (LLE), and solid phase extraction (SPE) are the most commonly used techniques for the preparation of biological samples for LC-MS (H. Jiang *et al.*, 2012). Liquid-liquid extraction (LLE) is the traditional extraction technique by the partitioning of the analyte between two immiscible solvents, providing a clean extract (H. Jiang *et al.*, 2012; Rasmussen *et al.*, 2011). A single extraction step can extract the analyte into the organic solvent leaving behind the inorganic salts, proteins, and hydrophilic matrix components in the aqueous phase. LLE is widely used in industry; however, it is labour-intensive and difficult to automate. The

solvents used are harsh and can cause safety concerns for the user as well as causing emulsion issues and present phase separation (H. Jiang *et al.*, 2012; Rasmussen *et al.*, 2011).

Solid-phase extraction (SPE) is based on partitioning the analyte from aqueous biological fluid and a solid phase which is made of sorbent particles contained in a disc/column (Rasmussen *et al.*, 2011). SPE provides a clean extract, however it is a time consuming extract for method development and sample analysis due to selecting the appropriate sorbents and washing and elution conditions being critical to eliminate matrix effect (Lahaie *et al.*, 2010). Although SPE is feasible for automation with greatly reduced time and solvent consumption compared to LLE, it has a much higher cost per sample than LLE (H. Jiang *et al.*, 2012; Rasmussen *et al.*, 2011).

Protein precipitation by organic solvents is a simple sample preparation technique and is used for fast sample clean-up and disrupting protein–drug binding (H. Jiang *et al.*, 2012; Rasmussen *et al.*, 2011). Procedures are based on denaturing proteins to release any drug compounds bound to them. This is performed by an addition of an excess precipitating reagents such as acid or water-soluble organic solvents. The sample is then centrifuged and the supernatant is collected and analysed (Polson *et al.*, 2003; Rasmussen *et al.*, 2011). Solvents such as acetonitrile or methanol are used because of the compatibility with HPLC mobile phases and excellent solubility properties with water. Acetonitrile has been found to be a superior organic plasma protein precipitant and lower volume ratios than other organic solvents (Polson *et al.*, 2003). However, the process can lead to loss as some drug may co-precipitate with the denatured proteins and small molecule components such as serum or plasma are still present and can cause some interference with the signal (Rasmussen *et al.*, 2011). Protein precipitation has been shown to show the most significant matrix effect when compared to SPE and LLE (Bonfiglio *et al.*, 1999; Taylor, 2005). Protein precipitation is the preferred method for sample preparation in drug discovery due to its simplicity and easy automation (Rasmussen *et al.*, 2011).

1.5. AIMS AND OBJECTIVES

There is limited predictability in responses from animal models due to cross species differences resulting in 90% of drugs recently reported failing at human trials after showing promising results in animal models. (B. Jiang *et al.*, 2014; Moeller *et al.*, 2008; Mullard, 2016; van der Worp *et al.*, 2010) The FDA modernisation Act 2.0 in 2023 detailed the adoption of new approach methodologies (NAMs) such as MPS/OCC for the submission of preclinical safety and efficacy data, replacing the need to exclusively use animal models (Stresser *et al.*, 2023).

With the employment of MPS technology, there are a diverse range of tissue-tissue interfaces with 3D multicellular structures that can be cultured to resemble functional human organs (Bhatia & Ingber, 2014a). Utilising MPS devices for the perfusion of media to mimic the *in vivo* blood flow or interstitial fluid flow experienced by cells can enhance the nutrient and oxygen availability as well as exposing cells to physiologically relevant shear stress (Artzy-Schnirman *et al.*, 2020; Sedláková *et al.*, 2019). Incorporating ALI culture and facilitating continuous perfusion of culture medium results in a more physiologically relevant environment (Bhatia & Ingber, 2014a; Trieu *et al.*, 2014; Y. Wang *et al.*, 2018; Zepp *et al.*, 2017). The value of MPS devices have been demonstrated in both academic labs and commercially in various organs and differing technology (Ainslie *et al.*, 2019; Artzy-Schnirman *et al.*, 2020; D. Huh, Matthews, Mammoto, Montoya-Zavala, Hsin, *et al.*, 2010; Klein *et al.*, 2011; Schimek *et al.*, 2020).

Using stem or primary cells, a MPS device could be used to study human lung development, pathophysiology and study the responses to inhaled compounds to study pharmacodynamics (PD) and pharmacokinetics (PK) and toxicity to ultimately discover new diagnostics and therapeutics (Artzy-Schnirman *et al.*, 2020; Nawroth *et al.*, 2019). Although the benefit of MPS devices have been proven, there are few commercially available lung coculture MPS models that have been characterised extensively. The majority of the lung *in vitro* models available are static insert-based primary cell culture (EpiAirway 3D in Vitro Microtissues, 2015; Epithelix, 2024).

Many of the primary cell models are expensive and require specialist media and additives for culture, reducing the access to these models to only a few research groups that can afford the expense and time to optimise the cultures. The advantages of cell line sources were explored earlier in this chapter. As an almost unlimited human cell source, lung epithelium cell lines are a cost effective alternative to by-pass the many costs and ethical concerns associated with primary human cell harvesting (Hickey & da Rocha, 2019; Kaur & Dufour, 2012). There have been well documented academic models utilising human lung epithelial cell lines for drug toxicity and flux as well as used to model disease and immune responses (A. L. Cozens *et al.*,

1994; Ehrhardt, Kneuer, *et al.*, 2002; Forbes, 2000; Furubayashi *et al.*, 2020; Heijink *et al.*, 2010; Inoue *et al.*, 2020; Kerschner *et al.*, 2023; Mukherjee *et al.*, 2012; Reddel *et al.*, 1988; S. Sakamoto *et al.*, 2018; Selo *et al.*, 2021; Stewart *et al.*, 2012a; Yoshisue *et al.*, 2004; Zabner *et al.*, 2003).

A coculture model would be the most representative model of the human lung, combining epithelium and relevant a second pulmonary cell type in a physiologically relevant environment such as a perfused MPS device, would increase the complexity and physiology relevance of the lung model and produce a more representative cell model of the human lung. Interest in understanding the interactions between smooth muscle and epithelium has been increasing, particularly how the interactions contribute to respiratory disease and their response to therapeutic compounds (Deacon & Knox, 2015). However, many of the coculture models that have been published were not directly cultured in the same well or cultured for extended periods, so there is not enough data to indicate an influence or resultant differentiation due to the coculture environment (Haghi *et al.*, 2015; Lan *et al.*, 2018a; Malavia *et al.*, 2009; Muddle *et al.*, 2020). This is an area that is yet to be fully understood and investigated. Considering this, the aim in this project is to use an MPS device to establish and characterise an *in vitro* bronchial coculture model that is representative of the human *in vivo* microenvironment. This model should have the potential for use in investigate the biological responses of the lung microenvironment to inhaled drug compounds and stimulants in a manner that is translatable to the *in vivo* situation. Using various assays to characterise the model to determine gene expression, morphological changes and barrier functionality. The measurement of biological response to drug compounds e.g. smooth muscle relaxation coupled with the use of analytical tools such as LC-MS to determine the delivered drug concentration to determine the elucidation of biological responses in the MPS coculture model.

The specific objectives and aims of this thesis were as follows:

1. Develop and optimise cell culture assays to characterise and assess the model.
 - a. Optimise assays for the assessment of the barrier properties of the epithelial monolayer and characterise the model.
 - b. Develop and optimise assays for the assessment of drug compounds efficacy and flux.
2. Investigate the influence of basolateral perfusion on Calu-3 epithelium cells.
 - a. Assess the influence of basolateral perfusion on Calu-3 epithelium over long-term culture.
 - b. Determine of the ideal window for interrogation of the epithelial model.
3. Develop and optimise a perfused MPS bronchial coculture model.
 - a. Optimise a novel coculture model with *in vivo* representative architecture of the bronchial epithelium-smooth muscle interface.
 - b. Assess of the influence of the coculture on the cell model characteristics.
 - c. Assess the influence of basolateral perfusion on the MPS coculture model.
4. Assess the application of the epithelial barrier and smooth muscle MPS model to ADME and efficacy evaluation of pulmonary beta-2 agonists.
 - a. Evaluate the influence of perfusion on the transport of beta-2 agonist, terbutaline, across the Calu-3 epithelial barrier.
 - b. Assess the influence of perfusion on the transport of terbutaline across the epithelial – smooth muscle MPS model.
 - c. Assess the influence of perfusion on the efficacy of terbutaline on the smooth muscle target.

Chapter Two

Methods and Materials

2. METHODS AND MATERIALS

2.1. INTRODUCTION

Complex cell culture systems such as microphysiological systems (MPS) devices require high-content end-point analysis to characterise the differentiated cells and tissues and provide quality control parameters. This will include but is not limited to the analysis of supernatant for drug content and bio-marker measurements (Dehne *et al.*, 2017). Analysing compounds and biomarkers is a critical step in the utilisation of MPS devices and must be addressed to produce more accurate, precise, and reproducible models for use in drug studies (toxicity, metabolism, pharmacokinetic/pharmacodynamic studies (PK/PD) etc.) (B. ill Lee *et al.*, 2018). The primary obstacles encountered by the *in vitro* systems revolve around scaling of data and is a result of the micro and nanoscales of volume and area used in cell culture technology which can potentially result in less accurate translation of data from the models to the human body (Wikswa *et al.*, 2013).

Another significant issue is that the samples are very limited in amount, usually in microlitre volumes. This requires highly sensitive biochemical methods, which limits the high throughput capability of the systems (Sedláková *et al.*, 2019). Furthermore, scaling the data is different for each function and limit the transability e.g. surface-volume ratio of tissue (Wikswa *et al.*, 2013). However, the low volume is advantageous for reducing the costs for drug development processes as it allows smaller amounts of scarce compound to be employed during testing. The latter reduction of compound requirements has been exploited in various physiological studies including absorption, distribution, metabolism and excretion (ADME), and toxicity (Ahadian *et al.*, 2018; Ishida, 2018; S. H. Lee & Sung, 2018).

The latter challenges highlight the need to develop and optimise high quality, informative biochemical assays that can use small volumes of sample in a suite of analyses to determine changes in the model and characterise any effects from drug/xenobiotic/allergen treatments. Common endpoint assays used include luminescence assays such as Promega® Cell Titre Glo for cell viability analysis or, colorimetric assays such as Promega® CytoTox 96® Non-Radioactive Cytotoxicity Assay for the determination of cell stress through the detection of lactate dehydrogenase (LDH) release.

There are various non-destructive assays that can be utilised in MPS culture to further determine tissue health and functionality. One such assay is transepithelial electrical resistance (TEER). TEER reflects the ionic conductance of the paracellular pathway in the epithelial monolayer (Zucco, 2005). TEER is a non-invasive technique to continuously monitor the barrier integrity of a cellular monolayer. By measuring the electrical resistance across the

monolayer, TEER can be reliable method to verify the integrity and permeability of the barrier (Srinivasan *et al.*, 2015).

During TEER measurement, the epithelium is washed using phosphate-buffered saline (PBS). This PBS wash can be analysed for respiratory mucus glycoproteins using a protocol that was reported by (Hall *et al.*, 1980). This protocol was adapted and optimised for use in the current study using a similar method to Hall *et al.* (1980) but utilising bovine submaxillary gland mucin as an alternative for the generation of the calibration curve as was adapted by (Sontheimer-Phelps *et al.*, 2020). This allows for a non-invasive analysis of the mucus glycoproteins present on the cell surface of air-liquid interface (ALI) cultured lung epithelium cell lines without disrupting the culture or sacrificing wells.

Apparent permeability (P_{app}) assessment is considered the *in vitro* gold standard to assess the uptake rate of chemicals/drugs into the body across an epithelial barrier (Alsenz & Haenel, 2003; Artursson *et al.*, 2012; K.-J. Lee *et al.*, 2005; Thiel-Demby *et al.*, 2009). These tests are time and cost effective (Hubatsch, 2007), and as a result are readily adopted for the assessment of the permeability of lung epithelial monolayers, and have been well documented as a reliable assay by multiple academic groups (Cingolani *et al.*, 2019; Forbes & Ehrhardt, 2005; Frost *et al.*, 2019; George *et al.*, 2015; Grainger *et al.*, 2006; Min *et al.*, 2013; Srinivasan *et al.*, 2015; M. V. Suresh *et al.*, 2012). High sensitivity bioanalytical approaches are required to quantify the low concentrations of molecules undergoing permeation. This has frequently been achieved using radiolabelled compounds (Srinivasan *et al.*, 2015). An apparent permeability assay can be used to characterise the barrier function of an epithelial monolayer in various conditions.

Immunofluorescent (IF) antibody staining is a technique that utilises fluorescently labelled antibodies to detect a specific target and is a widely used technique in academic and clinical research (Odell & Cook, 2013). The detection can be direct through binding of a fluorescently labelled antibody directly to the protein or indirect detected through the binding of a secondary fluorophore-labelled antibody bound to the first antibody that is unlabelled (Odell & Cook, 2013). This allows images to be taken on a fluorescent microscope to create a 3D image of the structures in the cell monolayer.

Histology is used to identify expression of proteins in cells and tissues so that they become visually detectable by light microscopy (Ramos-Vara, 2010). This is performed through embedding cell and/or frozen tissue samples in paraffin wax, sectioning and then staining through various staining techniques that can be applied to examine specific tissue or cell structures (Ramos-Vara, 2010). A routine stain used to study changes in morphology is the haematoxylin and eosin (H&E) stain. Haematoxylin is a basic dye that binds to the nucleic

acids of the cell nucleus and eosin is an acidic dye that binds to the cytoplasmic structures of the cells. This assay results in blue nuclei and red cytoplasm to visualise tissue/cell morphology in a cross-section (Ramos-Vara, 2010).

MPS tissue culture systems have also been analysed with several different methods for nucleic acid analysis such as polymerase chain reaction (PCR) (Li & Tian, 2018). PCR amplifies deoxynucleic acid (DNA) fragments. Being a very sensitive technique, PCR is a qualitative tool for the detection of DNA from a single molecule and can be used to quantify (qPCR) the number of target molecules synthesized in the tissue under specific conditions. Although other nucleic acid amplification technologies are used, PCR remains the most used (Wages, 2004). Utilising qPCR to analyse the cell model would aid the characterisation and phenotyping of the cell development within the MPS culture system by quantifying expression of key characteristics such as transporters and mucin expression.

All the methods mentioned above can be used to study and validate the differentiation of cultures in 3D as well as to assess the utility of cell-based assays as disease models (Lin *et al.*, 2020). An important aspect of comparative bioavailability/bioequivalence studies or toxicokinetic/pharmacokinetic studies are the measurements of chemical and biological drugs in biological matrices. These results can be used in regulatory documents on the safety and efficacy of drug products. This illustrates the need to develop and characterise an appropriately validated bioanalytical method (EMA, 2022). Ensuring the bioanalytical method is fit for purpose is essential for the method to be robust and relevant to industry standards. When developing and validating the bioanalytical method a set of criteria should be adhered to and worked towards as a point of improvement for the method. The International Council for Harmonisation (ICH) has released a guidance document on bioanalytical method validation (ICH M10). This has been adopted by the European Medicines Agency (EMA) and the US American Food and Drug Administration (FDA) (EMA, 2022; FDA, 2022).

The EMA ICH M10 guideline document details key areas and criteria to meet for the chromatography of the analyte including selectivity, matrix effect, calibration curve, range (lower limit of quantification (LLOQ) to the highest concentration or upper limit of quantification (ULOQ)), accuracy and precision (EMA, 2022). Following this document for the development of a LC-MS method and its subsequent validation is paramount to ensuring a robust and reliable bioanalytical method.

2.2. CHAPTER AIMS

The main aims of this chapter are to detail the materials and methods employed to characterise and monitor the development of the Transwell cell models in the PhysioMimix OOC system.

2.3. MATERIALS

2.3.1. GENERAL CHEMICALS

All chemicals used were obtained from Sigma Aldrich (Poole, Dorset, UK). All water was deionised (dH₂O) unless stated otherwise, obtained using a Milli-Q® IQ 7003 Pure & Ultrapure Water Purification System (Sigma Aldrich, UK). All cell culture reagents were purchased sterilised or sterilised prior to use through autoclaving at 121°C at 1 bar for 20 mins using the Touchclave-R 160H from LTE Scientific™ (Oldham, UK).

2.3.2. TRANSWELLS® COLLAGEN COATING REAGENTS

Rat tail type 1 collagen (3780 µg/mL) (Corning Life Sciences, The Netherlands), Glacial Acetic Acid (>99%) (Fisher Scientific, UK), Polyester Transwells® 0.4 µm pore size (Cat# 13216768) (Corning Costar, UK). 50 mL Falcon tubes (Greiner Bio-One, Austria). Sterile water for irrigation (ddH₂O) (Baxter Healthcare, UK).

2.3.3. CELL CULTURE REAGENTS

Calu-3 cell line was obtained from the American Type Culture Collection (ATCC) (ATCC, USA). Calu-3 cells were cultured in Eagle's minimum essential medium (with Earle's salts, L-glutamine, and sodium bicarbonate) with the addition of sodium pyruvate, Non-Essential Amino Acids (NEAA) and penicillin/streptomycin. Additionally, foetal bovine serum (FBS) non-USA origin used throughout the project is the same batch (M4655). All reagents were obtained from Sigma Aldrich (Poole, Dorset, UK). Medium was supplemented with a final concentration of 1% sodium pyruvate, 1% NEAA, 1% Penicillin/Streptomycin and 10% FBS.

Human bronchial smooth muscle cells (BSMC) (Cat No. CC-2576, Lot No.18TL138668) were cultured in SmGM™-2 smooth muscle cell growth medium -2 BulletKit™ (#CC-3182) (Lonza, UK). The following were used for general culture - Gibco TrypLE™ Express Enzyme (1X), Recovery™ cell culture freezing medium, 0.4% w/v Trypan Blue solution (Sigma Aldrich, UK).

2.3.4. PHYSIOMIMIX® ORGAN-ON-A-CHIP (OOC) MICROPHYSIOLOGICAL SYSTEMS (MPS) INSTRUMENTS

All MPS materials and plates were obtained and used on-site in CN Bio Innovations Ltd (CN Bio Innovations Ltd, UK). This includes the PhysioMimix OOC MPS controllers, controller desiccant, docking station and MPS plate drivers. The PhysioMimix Barrier-12 plate was used in conjunction with coated Transwell inserts (Section 2.3.2) in the Barrier plate as detailed in Section 2.4.6.

2.3.5. LUNG MUCUS QUANTIFICATION REAGENTS

Alcian blue powder and glacial acetic acid (>99%) (Fisher Scientific, UK). Bovine submaxillary gland mucin, magnesium chloride (MgCl), sodium dodecyl sulphate (SDS) (Sigma Aldrich, UK). Sterile water for irrigation (ddH₂O) (Baxter Healthcare, UK). 1.5 mL Eppendorf vials (Greiner Bio-One, Austria), 96 well white/clear bottom plate (Thermo Fisher Scientific, UK).

2.3.6. APPARENT PERMEABILITY REAGENTS

Hank's balanced salt solution (HBSS) supplemented with 20 mM 4-(2-hydroxyethyl)-1-piperazine-ethanesulfonic acid (HEPES) (Thermo Fisher Scientific, UK) and supplemented with 200 mM D-glucose (Sigma Aldrich, UK). Fluorescein sodium salt (NaFL) and Lucifer Yellow salt (LY) (Sigma Aldrich, UK). Opaque-bottomed black 96-well plates (Thermo Fisher Scientific, UK).

2.3.7. QUANTITATIVE POLYMERASE CHAIN REACTION (QPCR) REAGENTS

Zymo Quick-RNA Miniprep Kit (Zymo Research, USA) used for RNA extraction and purification from cells. Qiagen RNase-free water (Qiagen, Germany), Applied Biosystems™ TaqMan™ Universal PCR Master Mix, Applied Biosystems TaqMan® Gene Expression Assay (FAM): GAPDH, MUC5AC, FOXJ1, SCGB1A1, ZO1 (TJP1), Claudin-1 (CLDN1), MDR1 (ABCB1), MRP1 (ABCC1), OCT1 (SLC22A1), OCTN2 (SLC22A5), α -Smooth Muscle Actin (ACTA2), and SM22, Applied Biosystems High-Capacity RNA-to-cDNA™ Kit and MicroAmp™ Fast Optical 96-Well Reaction Plate (Thermo Fisher Scientific, UK).

2.3.8. FIXATION AND IMMUNOFLUORESCENCE (IF) REAGENTS

4% v/v paraformaldehyde (PFA) solution in PBS, IgG (H+L) goat anti-rabbit Alexa Fluor 488 super clonal, and IgG (H+L) goat anti-mouse Alexa Fluor 647, and Hoechst 33342 (Thermo Fisher Scientific, UK). ZO1 rabbit anti-human polyclonal antibody, MUC5AC mouse anti-human antibody and bovine serum albumin (BSA), EpreDia™ Immu-Mount™, EpreDia SuperFrost Plus™ Adhesion slides, EpreDia Cover Slips 54x50mm, and Swann-Morton™ sterile disposable stainless-steel scalpels (Fisher Scientific, UK). Goat serum, Tween-20,

phalloidin–tetramethyl rhodamine B isothiocyanate (TRITC), and Triton-X100 (Sigma Aldrich, UK).

2.3.9. HISTOLOGY REAGENTS

Alcian blue powder, Nuclear fast red (Acros), haematoxylin, eosin Y, aluminium sulphate, and glacial acetic acid (>99%) (Fisher Scientific, UK).

2.3.10. LIQUID CHROMATOGRAPHY-MASS SPECTROMETRY (LC-MS) REAGENTS

Terbutaline hemi-sulphate salt and D3-salbutamol (Sigma Aldrich, UK). Optima LC-MS grade water (H₂O), acetonitrile (MeCN), and formic acid, LC-MS grade methanol and high-performance liquid chromatography (HPLC) grade ammonium acetate (Fisher Scientific, UK). 1.5 mL Eppendorf vials (Greiner Bio-One, Austria). Thermo Scientific™ Matrix™ Blank and alphanumeric storage tubes and 96-well plate (Thermo Fisher Scientific, UK). Micronic 1.40 mL round bottom sample storage Ttubes and TPE CAPCLUSTER-96 (VWR, USA).

2.4. EQUIPMENT

Microbiological safety cabinets (MBSC) used were TriMAT Class 2 (CAS, UK). Incubators used were Eppendorf CellXpert® C170i (Eppendorf, UK). The solvent hood used was from Monmouth Scientific – Circulaire CT1100 (Monmouth, UK). Aspirator used was the Vacusafe from Integra (Integra, Switzerland). Centrifuges used were the Heraus Megafuge 40R (Thermo Fisher Scientific, UK) and the Eppendorf 5430 (Eppendorf, UK). Transepithelial electrical resistance (TEER) was measured using the Epithelial Volt/Ohm Meter 3 (EVOM3) with STX2 Chopstick Electrode for EVOM2 and EVOM3 Legacy Adaptor (World Precision Instruments, Hertfordshire, UK). Plate readers used were FLx800 fluorescence plate reader (Biotek, USA) and the Byonoy absorbance 96 plate reader (Enzo Life Sciences, UK). The analytical balance used was the Sartorius MSE125P-100-DU Cubis Semi-Micro balance (Sartorius, Germany). For qPCR analysis, Jenway™ Genova Nano Micro-volume spectrophotometer (Cole-Parmer Ltd, UK), Applied Biosystems QuantStudio™ 6 Flex Real-Time PCR system and Veriti™ 96-Well Fast Thermal Cycler (Applied Biosystems, United States) was used. For imaging the fluorescent labelled cell samples, the Axio Imager M2 with the Apotome 2 module (Carl Zeiss Microscopy GmbH, Germany) was used. For LC-MS/MS analysis, the Waters TQS Xevo Micro was used (Waters Limited, United States).

2.5. METHODS

2.5.1. CELL THAWING METHOD

Cells were removed from liquid nitrogen cryostorage using rapid thawing (< 1 min) in a 37 °C water bath. The cell suspension was transferred dropwise to a 15 mL Falcon tube containing 10 mL of the appropriate pre-warmed cell culture medium. The cell vial was washed with 1 mL medium to retrieve residual cells. The cell suspension was centrifuged at 200 x g for 5 min to remove dimethyl sulfoxide (DMSO). The supernatant was aspirated, and the cells were re-suspended in 10 mL medium. Thawed cells were plated at a high density to optimise recovery. The seeded flasks were incubated at 37 °C, 5 % v/v carbon dioxide (CO₂) for 2 days to allow them to settle before changing medium.

2.5.2. CALU-3 CELL CULTURE METHOD

Calu-3 cells (passage 12-24) were maintained using 6 mL Eagle's Minimum Essential Medium (EMEM) with all supplements added in T75 flasks and subculture was performed at 80-95% confluence. For subculture, cells were aspirated of all media then rinsed with 3 mL of PBS before aspiration again. Afterwards, 3 mL TrypLE (1X) was added and incubated at 37°C for 10 min. The cells were then suspended in 10 mL of the cell culture medium containing FBS to neutralise the trypsin, collected into a 15 mL Falcon tube and the suspension centrifuged at 200 x g for 5 min. The medium was subsequently aspirated, and the cells were resuspended in 1 mL of cell culture medium. The cells were then counted using a volume of cells into a volume of Trypan Blue solution. Thereafter 10 µL of the mixture transferred to a haemocytometer and live cells were counted. The cells were then resuspended into 3 mL of medium and split in a 1:3 flask ratio by adding 1 mL of cells into a new T75 flask with 6 mL of medium. When seeding on Transwells, the cell density used was 3 x10⁵ cells/cm² unless specified.

2.5.3. HUMAN BRONCHIAL SMOOTH MUSCLE CELL (BSMC) CULTURE METHOD

BSMC cells (passage 1 to 4) were maintained using 6 mL SmBM basal medium supplemented with the SmGM-2 SingleQuot Kit in T75 flasks and subculture performed at 80-95% confluence. For subculture, cells were rinsed with 5 mL of PBS and then incubated with 3 mL TrypLE at 37°C for 3 mins. The cells were then resuspended in 10 mL of cell culture medium containing FBS to neutralise the TrypLE, collected into a 15 mL Falcon tube and the suspension was centrifuged at 200 x g for 5 min. The medium was aspirated, and cells resuspended in 1 mL of cell culture medium. The cells were then split in a 1:2 ratio into a new T75 flask. When seeding, the cell density used was 1 x10⁴ cells/cm² unless specified.

2.5.4. CRYOSTORAGE OF CELLS

When freezing cells, a freezing medium was prepared (10% w/w DMSO in the appropriate medium for the cells) or Recovery™ Cell Culture Freezing Medium was used. Cells were detached using TrypLE (1X) as previously described and then resuspended in 1 mL medium before being counted. After counting, cells were centrifuged and then supernatant was removed before being re-suspended in the freezing medium in a minimum concentration of 1×10^6 cells/mL. 1.5 mL aliquots were dispensed into cryovials and placed in an isopropanol chamber and stored at -80°C overnight before being transferred to the gas phase of a liquid nitrogen cryostorage container.

2.5.5. TRANSWELLS® COLLAGEN COATING METHOD

Using sterile ddH₂O, glacial acetic acid (17.4 M) was diluted in a solvent hood to a final concentration of 0.02 M. The solution was then placed on ice for 20 min to cool to the point of being ice-cold before addition of the stock collagen solution. Rat tail type 1 collagen (3780 µg/mL) was diluted using ice-cold acetic acid to form a final concentration of 10 µg/mL collagen solution. The solution was mixed by inversion 10 times before being used to coat the Transwells in the supplied 24 well plate. 100 µL of the collagen solution was added to the apical compartment of the insert and 500 µL to the basolateral chamber of a Transwell plate. The plate of Transwells was subsequently placed in the incubator at 37°C for 60 min. The collagen solution was then aspirated using the Vacusafe aspirator and the Transwells were washed with PBS using 100 µL in the apical compartment and 500 µL in the basolateral chamber. The PBS was aspirated, and the PBS wash was repeated 3 times. The plate was then left in the MBSC with the lid slightly askew to dry the Transwells for at least 30 min. Once dry, the plate was closed and sealed with autoclave tape and to be used immediately or stored in the fridge (4-8°C) for up to 2 weeks.

2.5.6. PHYSIOMIMIX® ORGAN-ON-A-CHIP (OOC) MICROPHYSIOLOGICAL SYSTEMS (MPS) METHOD

The MPS system was set up and used in accordance with the standard operating procedures (SOPs) that are followed internally by CN Bio Innovations and by external customers. The set up is shown in Figure 2.1. Briefly, the system was set up by wiping the docking station with 10% Chemgene, followed by 70% ethanol, before it was placed in a cleaned incubator. The controller was set up outside the incubator with fresh desiccant in the compartment to reduce system humidity. Electrical and pneumatic umbilical cords link the controller to the docking station. Upon switching on the controller, checks were completed to ensure the pressure in the system was within the correct parameters and was stable. The drivers were cleaned with 10% Chemgene and 70% Ethanol before being placed in an MSBC. A sterile Barrier-12 MPS

plate was taken into the MSBC, opened, and placed into the driver and locked into place. Medium was added to the wells before the plate-driver was placed on the docking station in the incubator. The perfusion speed was set to 0.5 $\mu\text{L/s}$ and left for 2 h minimum to ensure good flow and priming in the plate.

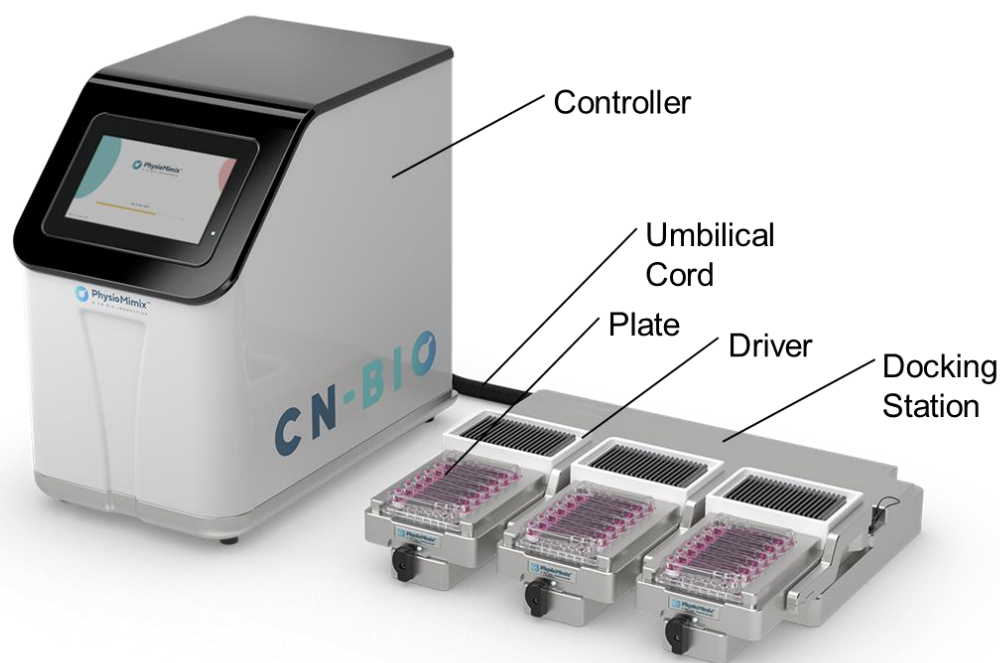


Figure 2.1: Labelled diagram of the PhysioMimix OOC system components and set up.

2.5.7. CULTURE OF CELLS IN THE PHYSIOMIMIX OOC SYSTEM

Perfusion flow was stopped after priming (Section 2.5.6) and the plate-driver were placed in the MSBC. All medium was aspirated and replaced with 600 μL fresh media in each well.

The collagen coated Transwells (Section 2.5.5) were used for seeding the cells. For BSMC seeding, the Transwells were flipped upside down in a sterile empty tip box in an MSBC. The BSMC cells were detached as previously described in Section 2.5.3, resuspended and counted. After counting, the cells were diluted to a density to seed 3,000 cells/ cm^2 . 50 μL of the cell suspension was added to the basolateral face of each Transwell and then the droplet was supplemented with 25 μL of medium. The lid was then closed on the box and the box carefully transferred to an incubator for 2 h minimum to allow the cells to attach to the membrane. After, the Transwell inserts were flipped into a 24-well or MPS plate and either 200 μL medium was added to the apical compartment, or the Transwells were then seeded with Calu-3 cells.

For Calu-3 cell seeding, cells were detached as previously described (Section 2.5.2), counted, and then diluted to a density of 100,000 cells/cm². 200 µL of the cell suspension was added to the apical chamber of the insert and the plate-driver was placed in the incubator with no flow set. After 24 h, perfusion speed was set to 0.5 µL/s. Medium was replenished every 2-3 days.

2.5.8. AIR-LIQUID INTERFACE (ALI) CULTURE METHOD

All medium was removed from the apical and basolateral compartments of the Transwells 48 h after seeding. 600 µL of medium was added to the basolateral compartment and the apical compartment was left empty, exposing the Calu-3 cells to air to establish the air-liquid interface (ALI).

2.5.9. TRANSEPITHELIAL ELECTRICAL RESISTANCE (TEER) METHOD

TEER was measured by adding 200 µL of PBS to the apical chamber of the ALI cultured cells and incubated for a minimum of 20 min before being measured. Using the Epithelial Volt/Ohm Meter 3 (EVOM3) with STX2 Chopstick Electrode, the electrode was placed with the short stick in the apical chamber and the long stick in the basolateral chamber, once the measurement had stabilised the resistance (Ohms, Ω) was measured. This was performed on a Transwell with no cells to be used as a blank that was subtracted from the cell resistance. The measurement was then normalised to surface area (cm²). The PBS was aspirated or collected for analysis from the cell layer as detailed in Section 2.5.10 and media replaced in the basolateral side as described.

2.5.10. LUNG MUCUS QUANTIFICATION METHOD

Buffer solution (0.1 M acetic acid and 25 mM magnesium chloride) was prepared by adding 2 mL glacial acetic acid to 18 mL ddH₂O and 0.048 g of magnesium chloride in a 15 mL Falcon tube. Alcian blue (0.1% w/v) solution was prepared by adding 15 mL of buffer solution to 0.015 g of alcian blue powder. SDS 10 % w/v solution was prepared by dissolving 1.5 g SDS in 15 mL of PBS solution. The solutions were inverted and vortexed until homogenous and were maintained in a water bath at 37°C until use. This was especially necessary for the SDS as it did not all dissolve at room temperature. Standard preparation required a stock solution of 1 mg/mL of bovine submaxillary gland mucin in PBS solution. Using this stock solution, a series of standards were prepared by serial dilution in PBS: 100, 75, 50, 40, 30, 15, and 10 µg/mL to a final volume of 1 mL for each solution.

For sample collection, 200 µL of warmed PBS was added to the apical side of the Transwell and incubated at 37°C and 5% CO₂ for 30 min. TEER measurements were performed at this point as described in Section 2.3.6. Following the 30 min incubation, the PBS samples were

carefully collected into 1.5 mL Eppendorf tubes and frozen at -80°C until analysis. Once thawed, the samples were vortexed to ensure homogeneity, and then 50 μL was taken and diluted in 150 μL PBS (1:4 dilution). This step was optimised for Calu-3 cells and generated 4 replicates per sample. 200 μL of each standard was pipetted in duplicate into separate 1.5 mL Eppendorf tubes. Then, 66 μL of the Alcian blue solution was added to each sample and standard replicate tube. The samples and standards were then incubated in the dark at room temperature for 2 h. After incubation, the Eppendorf tubes were centrifuged at 10,000 rpm for 30 min. The supernatant was then carefully removed, without disturbing the pellet, and discarded in a suitable container. The pellets were then dissociated using 100 μL of the 10% SDS solution, pipetting the suspension up and down to help the pellet dissolve. The samples and standards were transferred to a white walled 96 well plate, taking care to not introduce bubbles. If bubbles were present, misting the plate with 70% EtOH at arm's length was employed to collapse the bubbles. The plate was then read at 620 nm on the Byonoy Absorbance 96 Plate Reader absorbance plate reader.

2.5.11. APPARENT PERMEABILITY (P_{APP}) METHOD

Fluorescein sodium salt (NaFL) was diluted to 22.38 μM in P_{app} buffer (200 mM D-glucose, 20 mM HEPES in HBSS). Standards were made using 11 serial dilutions from the 22.38 μM stock of NaFL to a final concentration of 0.02 μM . These standards were plated in duplicates into a black 96-well plate with blank P_{app} buffer, ensuring to leave an empty well between each sample to avoid signal bleaching through to adjacent wells.

200 μL and 750 μL of the buffer was added to the apical and basolateral chambers of the Transwell, respectively. The Transwell plate was then incubated for 30 min at 37°C and 5% CO_2 . The buffer was aspirated and 750 μL of fresh P_{app} buffer was added to the basolateral chamber and 200 μL of the NaFL at 22.38 μM was added to the apical chamber. The Transwell plates were then incubated at 37°C and 5% CO_2 on a plate shaker at 200 rpm. At timepoints 30, 60, 120 and 180 min, 3 x 50 μL of samples from the basolateral side of each Transwell were taken and placed into an opaque-bottomed black 96 well plate. The basolateral chamber was replenished with 150 μL buffer before being placed on the plate shaker in the incubator again. At 180 min, 3 x 50 μL was also taken from the apical chamber of each Transwell. The plates were read immediately after sampling on a fluorescent plate reader (Excitation 460 nm and Emission 528 nm). Transwells/cells were washed in PBS (100 μL apical and 500 μL basolateral) 3 times before either being returned to culture or taken for endpoint analysis. A logarithmic standard curve was generated using the Log_{10} of the concentration and the fluorescence values. The equation of the resulting line was used to calculate the concentration of the samples at each time point. The samples are then anti-logged (10^{\wedge}) to obtain Molar concentration (μM). This was multiplied by the volume to calculate the amount of NaFL in

micromoles (e.g. $\mu\text{M} \times 750 \mu\text{L} / 1,000,000 = \mu\text{mol}$). The cumulative amount of the probe (μmol) was then calculated by the addition of the amount of NaFL at each timepoint with all previous timepoints. Using these values the SLOPE function in Excel was used to calculate the slope of the line against the timepoints in s ($=\text{SLOPE}(\text{Y values}, \text{X values})$). Using this slope value as dQ/dt ($\mu\text{mol/s}$), Equation 2.1 was used to calculate Apparent Permeability (P_{app}):

$$P_{app} = \frac{dQ}{dt} / (A \times C_0)$$

Equation 2.1

dQ/dt: amount of a compound in the basolateral compartment as function of time ($\mu\text{mol/s}$)

A: surface area of Transwell (cm^2)

C₀: initial concentration in apical compartment ($\mu\text{mol/mL}$)

2.5.12. QUANTITATIVE POLYMERASE CHAIN REACTION (QPCR) METHOD

Cell lysis, RNA extraction and purification was performed using the Zymo Quick-RNA Miniprep Kit and the protocol provided by the manufacturer was followed to generate RNA from the Transwell models. The RNA was quantified using the Jenway™ Genova Nano Micro-volume Spectrophotometer. To synthesise cDNA, 9 μL of the RNA sample was taken through the Applied Biosystems High-Capacity RNA-to-cDNA™ Kit with 11 μL of RNA Buffer (1 μL 20x Enzyme Mix and 10 μL 2x RT Buffer). This 20 μL mixture was then processed on the Veriti™ 96-Well Fast Thermal Cycler with the program set to 37°C for 60 mins then 95°C for 5 mins and holding at 4°C.

Using the calculated RNA concentration, the cDNA was then diluted using Qiagen RNase-Free water to give a final concentration of 10 ng/ μL . A master mix solution for each cDNA target was prepared using 10 μL of the Taqman Universal Master ix II (2x), 1 μL of the Taqman Gene Expression Assay (20x) primer and 7 μL of RNase-Free water. This 18 μL mix was then plated in a MicroAmp™ Fast Optical 96-Well Reaction Plate and 2 μL of the cDNA sample was added to the 18 μL in one well. The QuantStudio™ 6 Flex Real-Time PCR System was used to analyse samples, with each cDNA sample analysed against the house keeping gene GAPDH.

2.5.13. FIXATION AND IMMUNOFLOUORESCENCE (IF) METHOD

In this protocol, all volumes used were 100 μL in the apical chamber and 500 μL in the basolateral chamber unless specified. Transwells were washed in PBS twice before being fixed with 4% PFA for 10-15 min. After, the PFA was removed and the Transwells were washed

in PBS and aspirated 3 times. The cells were then either processed instantly or placed in PBS and then kept in at 4°C for a maximum of 2 weeks.

Cells were permeabilised using 0.3% TritonX-100 in PBS by incubation for 5 min before being washed in PBST (PBS with 0.1% Tween-20) and aspirated 3 times. The cells were then incubated for 1 h in blocking buffer (1% w/v BSA, 0.5% goat serum and 0.5% FBS in PBST). Primary antibodies were made up in blocking buffer (200 µL per Transwell). After they were prepared, the solution was vortexed for 10 s before centrifuging for 2 min at 10,000 rpm. Blocking buffer was aspirated from the Transwells and washed 3 times using PBST. Parafilm was taped on to the bench and 50 µL of primary antibody mix was pipetted on to the parafilm, ensuring adequate space between the droplets. Transwells were aspirated of any PBST and placed on the droplet, then 100 µL of the primary antibody mix was added to the apical side of the Transwell. The inserts were covered using a pipette tip box and incubated for a minimum of 2 h at room temperature in the dark.

The Transwells were returned to the plate and washed three times in PBST. The secondary antibodies were made up in blocking buffer (200 µL per Transwell). Parafilm was taped on to the bench and 50 µL of secondary antibody mix was pipetted on to the parafilm, ensuring adequate space between the droplets. Transwells were aspirated of any PBST and placed on the droplet, then 100 µL of the secondary antibody mix was added to the apical side of the Transwell. The inserts were covered using a pipette tip box and incubated for a minimum of 1 h at room temperature in the dark. The Transwells were returned to the plate and washed three times in PBST.

Glass slides were labelled with conditions and stains before a drop of mounting media was squeezed on to the slide. All PBST was aspirated and the edge of the Transwell was dabbed on a tissue to ensure all liquid has been removed. Using a scalpel the membrane was excised from the Transwell. Once the membrane had been released, tweezers were used to pick up the membrane and placed into the drop of mounting media, cell side up to the coverslip. The membrane was completely submerged in the mounting media and a cover slip was placed on top of the mounting media/membrane. The slides were left to dry at room temperature overnight before taking images and subsequent storage at 4°C.

2.5.14. HISTOLOGY METHOD

After the fixation step in Section 2.5.13, using a scalpel, the membrane was excised from the Transwell. Once the membrane had been released, tweezers were used to pick up the membrane and placed in a 2mL Eppendorf tube containing 70% Ethanol. The samples were then transported to the University of Cambridge: Pathology Department for the histology to be carried out.

Briefly, the membranes were placed on lens paper and the wrapped membranes were placed in an embedding cassette and submerged in 70% ethanol. The cassettes were then placed in 10 min steps of increasing grades of ethanol (70%, 80%, 2 x 95%, 3 x 100%) and two changes of xylene as a clearing solvent. The wrapped membranes were then removed from the cassette and infiltrated with two changes of melted paraffin for 30 min each. After, the membranes were cut in half with a microtome blade and the membrane halves were embedded in paraffin with the cut surface down, slightly diagonal in the mould and the cassette placed on top. The mould/cassette was then quickly placed in ice to cool the wax to form the paraffin block with the membrane embedded. The block was then sectioned at 5 μ m slices and collected on positively charged glass slides and then baked in 60°C for 1 h.

A routine haematoxylin and eosin (H&E) procedure was used after. Briefly, the sections were deparaffinised with three changes of xylene for 5 min each and then sections were rehydrated with two changes of 100% ethanol and 95% ethanol for 2 min each. The slides were then washed in gently running tap water for 3 min before they were placed in haematoxylin solution for 4 min then washed again for 3 min. The slides were then placed in 5% acetic acid for 1 min then washed again for 2 min then placed in 0.1% sodium bicarbonate for 1 min before a final wash with tap water. The slides were then placed in 95% ethanol for 1 min before being placed in eosin Y solution for 15 s. The slides were then placed in three changes of 95% ethanol for 1 min each and then the same performed with 100% ethanol. Finally, the slides were cleared in xylene three times for 3 min each before mounting medium was placed on the slide and a glass coverslip was placed on the slide.

For the alcian blue staining for acidic mucins, the following procedure was carried out. First, the staining solutions were made up as follows: 1g of alcian blue was dissolved in 100 mL 3% acetic acid solution. 20 g aluminium sulphate was dissolved in 400 mL double-distilled water (ddH₂O) followed by the addition of 0.4 g Nuclear fast red. The solution was then slowly heated to a boil before cooling and filtering before use.

The sections were deparaffinised with three changes of xylene for 5 min each and then sections were rehydrated with two changes of 100% ethanol and 95% ethanol for 2 min each before placed in 1% alcian blue solution for 30 min. After, the slides were washed in water for 5 min before being placed in Nuclear Fast Red solution for 10 min. The slides were then washed in water for 5 min before rinsing in 100% ethanol twice, and then cleared in xylene and then mounting medium placed on top before a glass coverslip.

2.5.15. STATISTICAL TESTING METHODS

All experiments had a minimum of three technical replicates with a one exception where only two technical replicates were possible. Results were evaluated by several statistical tests as appropriate for the data and were performed using the software GraphPad Prism 10.3.0.507.

Normality of the data was evaluated by using the Kolmogorov - Smirnov normality test. Unpaired T-tests were used to compare the results of two groups with Mann-Whitney post-hoc test performed. ANOVA analysis was performed on experiments where three or more groups were compared with Tukey post-hoc test performed. Repeated measure two-way ANOVA to understand the effect of, and the differences between, two variables across three or more groups, with Tukey post-hoc test performed. Significance of data was reported if $P = <0.05$.

2.6. LC-MS MATERIALS AND METHODS

2.6.1.1. STANDARDS AND SOLUTIONS PREPARATION

Ammonium acetate 200 mM was prepared by adding 770 mg to a 50 mL volumetric flask and then dissolving and making up to volume using Optima grade water. Internal standard was prepared by dissolving 1 mg of D3-salbutamol in 1 mL of Optima grade water for a concentration of 1,000,000 ng/mL. This was further diluted in 5 litres of Optima grade water to obtain a final concentration of 200 ng/mL. This was aliquoted into 50 mL falcon tubes and frozen at -80°C . When required a tube was thawed out to room temperature and 2.5 mL of D3-Salbutamol (200 ng/mL) was added to 47.5 mL Optima grade acetonitrile to produce 10 ng/mL D3-Salbutamol in 95:5 acetonitrile: water. A salt form calculation was employed to calculate the concentration of the free base in the stock solution. Terbutaline hemi-sulphate salt was weighted out (mg) and multiplied by 0.8212 ((molecular weight of free base/ molecular weight of salt) ($225.8 \text{ g/mol} / 274.32 \text{ g/mol} = 0.8212$)) to calculate the volume of acetonitrile: water (50:50) solvent (mL) required to give a final concentration of 1mg/mL. Three working standards were made up from the stock solution: 100 μL of stock + 900 μL of cell culture medium = 100,000 ng/mL, 100 μL of 100,000 ng/mL + 900 μL of media = 10,000 ng/mL, 100 μL of 10,000 ng/mL + 900 μL of media = 1,000 ng/mL. Using these working standards, 9 standards are made up: 600 (x2), 500, 400, 300, 200, 100, 50 (x2) ng/mL. A second set of working standards were made up to then produce a second set of standards for accuracy and precision at 600, 450, 300, 150 and 50 ng/mL.

2.6.1.2. SAMPLE PROCESSING METHOD

To process the standards and the samples, 50 μL samples were taken and pipetted into a 1.5 mL Eppendorf tube. 250 μL of 10 ng/mL D3-Salbutamol 95:5 (MeCN: H_2O) was added and vortexed for 30 s. Then, the samples were centrifuged for 15 min at 13,200 rpm using the Eppendorf centrifuge 541D. 250 μL of the supernatant was taken and placed in a 1.5 mL tube

and then capped with a pre-slit septum. The samples were then shaken for 5 min on an IKA MS3 Digital plate shaker at 750/min before injection. This process was performed on all standards, samples, and blank samples.

2.6.1.3. MOBILE PHASE PREPARATION AND MASS SPECTROMETRY SETTINGS

Mobile phase preparation required every 100 mL of mobile phase to have 0.1 mL formic acid (0.1%) and 77 mg ammonium acetate (10mM). Mobile phase A was a ratio of 95:5 acetonitrile water e.g., 20 mL 200 mM ammonium acetate in water + 380 mL acetonitrile and 0.4 mL formic acid. Mobile Phase B was a ratio of 50:50 acetonitrile: water e.g., 10 mL 200 mM ammonium acetate in water + 90 mL water + 100 mL acetonitrile and 0.2 mL formic acid. The samples were then run on a Waters Xevo TQ-S Micro using Acquity Premier BEH Amide 1.7 μ m VanGuard fit 2.1 x 50 mm column. Run time was 5 min at a flow rate of 0.4 mL/min with an injection volume of 1 μ L. The gradient used was (A%:B%) 0 min 90:10, 0.8 min 90:10, 2 min 80:20, 2.5 min 1:99, 3.5 min 1:99, 3.6 min 90:10, 5min 90:10. Mass spectrometry was performed in electrospray positive mode with instrument settings set as follows: Capillary voltage 1.0 kV, source temperature 100 °C, desolvation temperature 500 °C, cone voltage at 20 V, cone gas flow 150 L h⁻¹, and desolvation gas flow 1000 L h⁻¹. Multiple reaction monitoring (MRM) settings employed for each compound are as detailed in Table 2.1.

Table 2.1: MRM setting for positive ion MS/MS analysis of terbutaline and D3-salbutamol.

Compound	Parent Ion (M/Z)	Daughter Ion (M/Z)	Dwell (s)	Cone (V)	Collision (V)
Terbutaline	226.1204	107.0095	0.081	40	28
Terbutaline	226.1204	124.9688	0.081	40	22
D3-Salbutamol	243.2235	151.1301	0.081	2	18
D3-Salbutamol	243.2235	169.1513	0.081	2	12

Once analysed, the peak area response of the terbutaline was divided by the area response of the internal standard to give rise to the relative response factor (RRF). The RRF was then plotted against the concentration to give rise to the calibration line. The equation of this line was used to quantify the samples analysed.

2.7. CHAPTER CONCLUSIONS

The methodologies and materials utilised in this thesis to generate experimental data were outlined in this chapter. Methods have been optimised and the LC-MS method that will be employed has been developed and validated using the EMA ICH M10 guidelines (EMA, 2022) to establish a criterion for the development and validation of the bioanalytical LC-MS method. Consequently, the aims set out in Section 2.2 were achieved in this chapter. Subsequent chapters will reference the appropriate section in Chapter 2 for the methods used when addressing specific research objectives in those chapters, and for the generation of the LC-MS data.

Chapter Three

Development of the Perfused Calu-3 Bronchial Epithelium Model

3. DEVELOPMENT OF THE PERFUSED CALU-3 BRONCHIAL EPITHELIUM MODEL

3.1. INTRODUCTION

3.1.1. LUNG EPITHELIUM FEATURES

The primary barrier for absorption for inhaled xenobiotics and drug compounds is the lung epithelium (Labiris & Dolovich, 2003). Bronchial epithelial tissue has been characterised as predominately lined with ciliated cells, mucus-secreting goblet cells and club cells. Ciliated cells are pseudostratified columnar cells in the larger airways and are cuboidal in the bronchioles. Goblet cells produce mucus, which traps inhaled matter. This is subsequently pushed up the airways to the oesophagus by the action of ciliated cells to be disposed of in the digestive tract (Breeze & Turk, 1984; Franks *et al.*, 2008; Levitzky, 2018; Stanfield, 2016). Goblet cells are less abundant in the bronchioles and are replaced by Club cells which secrete lipids, glycoproteins and inflammatory cytokines (Breeze & Turk, 1984; Franks *et al.*, 2008; Levitzky, 2018; Stanfield, 2016).

The polarised epithelial cells function as barriers and mediators of selective transport, preventing the free diffusion of substances through the extracellular space between the cells. Tight junctions function to hold cells together to form a robust tissue and control the flow of solutes from one side to the other, with the tight junction encircling the cell with the appearance of an interlocking network of ridges across the plasma membrane at locations where adjacent cells are in contact within a cell layer (Lodish *et al.*, 2016). Pulmonary epithelium cell culture has been advantageous in its ability to study mechanisms of drug transport including but not limited P-glycoproteins and organic ion transporters (Forbes & Ehrhardt, 2005; Gardiner & Schanker, 1976; Hamilton *et al.*, 2001).

3.1.2. LUNG EPITHELIUM CELL SOURCES

The three main cell sources for *in vitro* models were explored in Section 1.5.1. These sources are relevant for the purchase of human bronchial epithelial cells but as explored earlier, there are significant drawbacks and concerns for the different sources. Primary cultures of human lung epithelial cells serve as representative models of normal lung epithelial cells (Sachs *et al.*, 2003; Sato *et al.*, 2020; Widdicombe *et al.*, 2003; Yamaya *et al.*, 1992). However, primary cells are difficult to obtain sustainably, have significant variation between donors, and are expensive (Ainslie *et al.*, 2019; Sato *et al.*, 2020). Stem cells are another source of cells that have the potential to differentiate into several cell types and are seen as a solution to the lack of available primary cells (Kasendra *et al.*, 2018). However, there are ethical concerns in gene editing human cells and they are costly to purchase and maintain (Sedláková *et al.*, 2019). Cell lines are a widely used source for cell culture models. The main advantages over other cell sources is they are almost an unlimited human cell source, are cost-effective and bypass

many ethical concerns that are typically associated with animal and human tissue (Hickey & da Rocha, 2019; Kaur & Dufour, 2012). Cell lines have been used in many applications (e.g. vaccine production, drug testing for metabolism and toxicity, gene function and therapeutic proteins) and have greatly furthered scientific research as they provide a consistent population of cells.

Despite their utility, it is important to note that many cell lines are cancer-derived cells which have a high proliferation rate and can lead to misleading results compared to healthy *in vivo* organs (Courcot *et al.*, 2012; Hogan *et al.*, 2014). Cell lines can display major differences in gene and protein expression such as lacking tight junctions (A549) or mucus production (16HBE14o-) (Braakhuis *et al.*, 2015; Hickey & da Rocha, 2019). Consequently, this can reduce their representative ability of the healthy organ response (Ekert *et al.*, 2014). It is therefore important to consider the advantages and disadvantages of each cell line prior to their use for specific applications.

3.1.3. LUNG BRONCHIAL EPITHELIUM CELL LINES

Within this project, a substantial aim was to develop a lung model that can be reproduced in any cell culture laboratory by using commercially available cell sources. To achieve this, a sustainable and accessible cell source was required. Cell lines, whilst most are cancerous, have many advantages. They can be accessed and distributed to researchers worldwide whilst maintaining key features of bronchial epithelial cells such as tight junctions and mucus production. More predictive outcomes can be made by reproducing these key physiological and biological features, thus allowing identification and testing of novel and conventional therapeutics (Braakhuis *et al.*, 2015; Gazdar *et al.*, 2010; Hickey & da Rocha, 2019).

Ainslie *et al.* (2019) detailed key functional parameters that should be present and characterized in a lung microphysiological system (MPS) model for the airways (Ainslie *et al.*, 2019):

- Pseudostratified epithelium with metabolically active club cells and goblet cells producing mucus.
- Smooth muscle contractility
- Cell viability and functional capabilities maintained for up to 4 weeks.
- Qualification with compounds including bioanalysis for drug exposure.
- Comparability and superiority over existing, simpler 2D *in vitro* models

There are several cell lines that were considered for this project that have previously been reported to express features representative of human bronchial epithelium:

1. 16HBE14o- (A. L. Cozens *et al.*, 1994)

2. BEAS2-B (Forbes, 2000; Heijink *et al.*, 2010; Stewart *et al.*, 2012b)
3. NuLi-1 (Zabner *et al.*, 2003)
4. NCI-H292 (Yoshisue *et al.*, 2004)
5. Calu-3 (Grainger *et al.*, 2006; Kreft *et al.*, 2015)

The 16HBE14o- cell line was established by Couzens *et al.* (1994), who reported an immortalised bronchial epithelial cell line that was isolated from a 1-year-old male heart-lung patient. The 16HBE14o- cells are non-cancerous and successfully retain tight junctions and directional ion transport after multiple passages (A. L. Couzens *et al.*, 1994). This cell line retains the characteristic epithelial cobblestone appearance and as a result, 16HBE14o- has been widely used as an alternative to primary human bronchial epithelium cells (A. L. Couzens *et al.*, 1994; Kerschner *et al.*, 2023). 16HBE14o- cells can form intercellular tight junctions containing key proteins such as zonular occludens (ZO1) as well as E-cadherin, with mucociliary differentiation observed between 14 and 26 days (Heijink *et al.*, 2010). However, 16HBE14o- do not form cilia and most disadvantageous to the use of the cell line, they do not form a polarised cell layer when grown at an air interface (Ehrhardt, Kneuer, *et al.*, 2002; Selo *et al.*, 2021).

BEAS-2B are another immortalised cell line of normal human bronchial epithelial cells from a non-cancerous source, however, there is no further information about age, sex and ethnic background which are all recognised as important factors in considering drug ADME properties (Reddel *et al.*, 1988; Selo *et al.*, 2021). BEAS-2B cells have been used for studies of pulmonary cell biology, pathological process, drug metabolism and drug transport (Z. Yu *et al.*, 2017). However, the cell line has similar disadvantages to 16HBE14o- with the lack of confluent layers of polarised cells, diffuse expression of tight junction proteins and epithelial differentiation markers regardless of the culture condition (Forbes, 2000; Heijink *et al.*, 2010; Stewart *et al.*, 2012b).

NuLi-1 is an immortalised bronchial epithelial cell line from a healthy 36-year old male and generated as a relevant control in parallel to cystic fibrosis cell lines CuFi-1, -2 and -4 from cystic fibrosis patients (Zabner *et al.*, 2003). The cell line expresses tight junction proteins such as ZO1 and Caludin-1 and -3, which corresponds with high impedance values when grown under air-liquid interface (ALI) culture conditions (Molina *et al.*, 2015). The cell line can be passaged multiple times; however, it has been reported that the goblet cell expression increases with passage number whilst the percentage of ciliated cells decreases from >50% to ~5% after passage 20 (Zabner *et al.*, 2003). Long culture times are needed for the cells to fully differentiate, and a biosafety level 2 (BSL-2) is required according to the American Type Culture Collection (ATCC) (Selo *et al.*, 2021). BSL-2 laboratories require more restrictive

access, enhanced safety protocols and specialised training requirements than biosafety level 1 (BSL-1) labs and are not always feasible to establish (CDC, 2020).

NCI-H292 is a non-small cell lung carcinoma cell line derived from a pulmonary mucoepidermoid carcinoma from a 32-year-old black female in 1983 (Yoshisue *et al.*, 2004). NCI-H292 have been reported to form a tight barrier initially however, the transepithelial electrical resistance (TEER) values decrease over 9 days in culture and high paracellular transport rates of Lucifer Yellow have been observed (van Schilfgaarde *et al.*, 1995; Yoshisue *et al.*, 2004). Correspondingly, diffuse localisation of ZO1 has been described, suggesting a lack of tight junctions (Heijink *et al.*, 2010). The cell line has also been reported to have limited ciliary function. With these factors in mind, this cell line has rarely been used in biopharmaceutical research (Yoshisue *et al.*, 2004).

The Calu-3 cell line was originally derived from sub-epithelial gland adenocarcinoma in the bronchial region of a 25-year-old Caucasian male (Fogh & Trempe, 1975). Calu-3 cells have a columnar phenotype and are recognised to exhibit bronchial epithelial phenotype (Cavet *et al.*, 1997; Forbes, 1998). Calu-3 cells have the ability to form a suitably restrictive barrier which is physiologically relevant to the bronchial epithelium (Selo *et al.*, 2021). When grown at ALI, lower levels of ZO1 tight junction and lower TEER values than LLI have been reported ($>1000 \Omega\text{cm}^2$ under LLI vs. $300\text{-}500 \Omega\text{cm}^2$ under ALI conditions) (Grainger *et al.*, 2006; Kreft *et al.*, 2015). MUC5AC mucin secretion has also been detected at ALI (Grainger *et al.*, 2006; Kreft *et al.*, 2015).

Calu-3 cells have demonstrated good correlation (r values >0.9) in the permeability of 22 model drugs when compared across Calu-3 and Caco-2, RPMI 2650 and MucilAir cells grown at LLI and ALI conditions (Sibinovska *et al.*, 2020). The Calu-3 cells have also been found to have comparable P_{app} values with *ex vivo* drug absorption rates from rat nasal mucosa (Furubayashi *et al.*, 2020; Inoue *et al.*, 2020). The physiologically relevant barrier formation is one of the factors contributing to the adoption of the Calu-3 cell line as one of the most widely used organotypic cell line in inhalation biopharmaceutical research.

The expression of various transporters has been confirmed in the Calu-3 cell line and they have showed similar expression to primary cells (Mukherjee *et al.*, 2012, 2017a; Rotoli, Barilli, *et al.*, 2020; A. Sakamoto *et al.*, 2015). Of particular importance, the expression of the efflux transporters MRP1 and BCRP have been confirmed in Calu-3 cells, and the expression was found to be comparable to primary cells from the bronchial region (A. Sakamoto *et al.*, 2015) (Rotoli, Barilli, *et al.*, 2020). MRP1, BCRP and MDR1 are P-glycoprotein ATP-binding cassette (ABC) proteins that play a crucial role in translocation of a broad range of drugs with literature evidence indicating expression in lung tissue at varying levels, which suggests it could be

responsible for the delivery of respiratory drug such as B2-adrenergic agonists, anticholinergic agents and corticosteroids (Bosquillon, 2010; Nickel *et al.*, 2016; van der Deen *et al.*, 2005).

The presence of multiple organic cation transporters has also been confirmed in Calu-3 cells. Data suggests that Organic Cation Transporters (OCT) may facilitate the pulmonary absorption of bronchodilators such as salbutamol (Bosquillon, 2010; Mukherjee *et al.*, 2017a; Nickel *et al.*, 2016; Salomon *et al.*, 2012). The OCT transporters are solute-link carriers and comprise of electrogenic OCT1 (SLC22A1) and pH-dependent OCTN2 (SLC22A5) transporters (Koepsell *et al.*, 2007). Calu-3 cells have been shown to express the same OCT subtypes as normal bronchial epithelium (OCT1, OCT3, OCTN1 and OCTN2) on their apical side (Mukherjee *et al.*, 2012).

For all the points discussed previously, the Calu-3 bronchial cell line has been chosen for development of a bronchial ALI model in a perfused microphysiological system as it is the most appropriate commercially available cell line with desirable morphology such as the formation of tight junctions, mucus expression and physiologically relevant P_{app} values. In the next section, the methods of culture that have been deployed in the application of Calu-3 models will be discussed.

3.1.4. CALU-3 IN VITRO BRONCHIAL MODELS

3.1.4.1. STATIC CALU-3 MODELS

Traditional 2D culture has traditionally been in liquid-submerged culture, however with the discovery of insert-based culture, ALI culture was established which has been adopted as the standard for culturing Calu-3 epithelial cells (Grainger *et al.*, 2006). A major area of study has been the deposition, diffusion and transport of drugs deposited on the Calu-3 epithelium monolayer of dry powders. Drugs such as fluticasone propionate and salbutamol have been studied for their deposition profile and transport across the ALI-cultured epithelium (Cingolani *et al.*, 2019; Haghi *et al.*, 2012a, 2013; V. Kumar *et al.*, 2022, 2022). Other avenues of research have been the evaluation of inhaled toxicants, such as tobacco flavouring extracts and nanoparticles (zinc oxide and titanium dioxide), as well as the investigation of various pathogens (Ji *et al.*, 2022; D. Kim *et al.*, 2021; Mösbauer *et al.*, 2021; Sims *et al.*, 2008; Stuetz *et al.*, 2023).

The culture of Calu-3 cells at ALI has been popular in research across many different academic disciplines. Although Grainger *et al.* (2006) tried to standardise the culture of Calu-3 cells at ALI (Grainger *et al.*, 2006), there have been significant differences reported in many aspects of culture, including (but not limited to): the length of LLI culture before ALI culture; and ALI culture duration before assays and cell seeding densities (summarised in Table 3.1). Cell seeding densities of the Calu-3 cell line in Transwell inserts have ranged between 1×10^5

cells/cm² (Cingolani *et al.*, 2019; Horstmann *et al.*, 2021; Mukherjee *et al.*, 2013; Pasman *et al.*, 2021), 5x10⁵ cells/cm² (Foster *et al.*, 2000; Grainger *et al.*, 2006; Haghi *et al.*, 2012a, 2013, 2019; Ji *et al.*, 2022; Meindl *et al.*, 2015; Min *et al.*, 2013, 2016; Stuetz *et al.*, 2023) and 3.03x10⁵ cells/cm² (V. Kumar *et al.*, 2022). Although many studies used similar seeding densities, the TEER values reported are highly divergent (Table 3.1). As well as demonstrating intra-laboratory variances of Calu-3 culture, this also highlights the challenge of using TEER alone to characterise the barrier function of the bronchial model. There is a significant amount of variation in the length of ALI culture prior to use, with some researchers preferring to interrogate their models at day 8 (Ji *et al.*, 2022; Min *et al.*, 2013, 2016) and others preferring between 11 and 14 days (Haghi *et al.*, 2012a, 2013, 2019; Horstmann *et al.*, 2021; Meindl *et al.*, 2015; Pasman *et al.*, 2021). A small number also prefer longer time culture times (up to 21 days), but this is mostly for the characterisation of the model such as OCT subtype expression (Cingolani *et al.*, 2019; V. Kumar *et al.*, 2022; Mukherjee *et al.*, 2013). The variation between seeding densities and the resultant variation of TEER and P_{app} values whilst considering the ALI culture period is shown in Table 3.1. This highlights the need to optimise the seeding density and the ALI culture period of the Calu-3 Transwell model before moving towards the characterisation.

Table 3.1: Calu-3 models observed under both static and dynamic conditions, culture details on seeding density, TEER, ALI culture duration, and morphological characteristics. The permeability coefficients (P_{app}) of these models were determined for the molecules Lucifer Yellow (LY), FITC-Dextran (Dex), and Fluorescein Sodium (NaFL)

Static/ Dynamic	Density (cells/cm ²)	TEER (Ω*cm ²)	Apical - Basolateral Papp (cm/s)	ALI Days	Morphology	Reference
Static	3.03 x10 ⁵	1000	-	2	-	(V. Kumar <i>et al.</i> , 2022)
Static	1 x10 ⁵	500	NaFL 1x10 ⁻⁷	20	ZO1, E- cadherin	(Ehrhardt, Fiegel, <i>et al.</i> , 2002)
Static	1 x10 ⁵	500- 1500	LY 3.4 x10 ⁻⁷	11	-	(Cingolani <i>et al.</i> , 2019)
Static	1 x10 ⁵	200	Dex 2.5x10 ⁻⁶	14	ZO1	(Pasman <i>et al.</i> , 2021)
Static	5 x10 ⁵	600- 1000	-	8	ZO1, E- cadherin, MUC5AC	(Ji <i>et al.</i> , 2022)
Static	5 x10 ⁵	425	-	14	-	(Haghi <i>et al.</i> , 2013)

Static	5 x10 ⁵	484	NaFL 2.7 x10 ⁻⁷	14	MUC5AC	(Meindl <i>et al.</i> , 2015)
Static	5 x10 ⁵	N/A	NaFL 6.25 x10 ⁻⁶	12	-	(Haghi <i>et al.</i> , 2019)
Static	5 x10 ⁵	101	-	14	Cell size 79.1 µm	Stuetz <i>et al.</i> , 2023)
Static	5 x10 ⁵	400	LY 0.86 x10 ⁻⁷	8	Consistent cell monolayer	(Min <i>et al.</i> , 2016)
Static	5 x10 ⁵	400	LY 0.73 x10 ⁻⁷	8	-	(Min <i>et al.</i> , 2013)
Static	5 x10 ⁵	303	NaFL 3.36 x10 ⁻⁷	11	Microvilli, ZO1, Mucus, pseudostratified monolayer	(Grainger <i>et al.</i> , 2006)
Dynamic	1 x10 ⁵	484	LY 0.5 x10 ⁻⁶	0	Occludin, ZO1	(Carius <i>et al.</i> , 2021)
Dynamic	5 x10 ⁴	600	Dex 2.5 x10 ⁻⁷	5	ZO1, VE- Cadherin	(Sui & Lee, 2023)

3.1.4.2. Calu-3 MPS Models

Biomechanical signals influence the growth and differentiation of all tissues in the human body and are well documented as modulators of cell signalling for healthy and diseased states (Jaalouk & Lammerding, 2009). Within the human body, the cellular environment has a combination of biochemical and biomechanical stimuli to regulate the cellular response (Thompson *et al.*, 2020b). Biomechanical cues are often extracellular and are passive or active. Passive biomechanical stimuli include extracellular matrix stiffness and geometric confinement. Active stimuli include connective tissue tensile stretch and compression, fluid shear stress, interstitial fluid flow and hydrostatic pressure (Thompson *et al.*, 2020b). Many physiological processes rely on biomechanical stimuli, including the response to pharmaceuticals and other stimuli which creates a need for the incorporation of biomechanical cues into *in vitro* systems (Fu *et al.*, 2019; Thompson *et al.*, 2020b). The biomechanical stimuli the lung receives are: airflow from inspiration and expiration of normal breathing, stretch as a result of lung expansion from breathing and blood flow/interstitial fluid flow (Franks *et al.*, 2008; Levitzky, 2018; Stanfield, 2016)

Huh *et al* (2010) first reported the importance of mimicking the lung epithelial stretch on primary human alveolar epithelium by incorporating cyclic tensile strain, by the physiological inflammatory response that was elucidated (D. Huh, Matthews, Mammoto, Montoya-Zavala,

Yuan Hsin, *et al.*, 2010). Cyclic tensile strain, which is a result of the stretch experienced from inhalation and blood flow, is at a low level in the human lung with normal epithelium experiencing around 12% of strain, whilst under diseased conditions the level of cyclic strain is higher as the tissue loses elasticity (Waters *et al.*, 2012). One such example is in the asthma disease state, bronchoconstriction leads to compressive loading of the epithelium as the result of smooth muscle activation, leading to elevated levels of cyclic strain (Tschumperlin & Drazen, 2001).

The pulmonary vasculature is unique as it has thinner walls with less vascular smooth muscle than the systemic circulation, with high blood flow maintained at relatively low intravascular arterial pressure. The pulmonary veins and arteries are involved in the transport of the whole body's blood volume (K. Suresh & Shimoda, 2016). Pulmonary circulation is unique as the arteries carry deoxygenated blood through the capillaries for gaseous exchange to occur before returning to the heart via the veins (K. Suresh & Shimoda, 2016). Among the most physiological important mechanical stimuli, perfusion is recognized as a key component to be employed in *in vitro* MPS systems to improve the cellular differentiation to a more *in vivo*-like phenotype (Thompson *et al.*, 2020b).

Despite the physiological advantages of an MPS model, perfused cell culture has yet to be widely adopted for *in vitro* models of lung epithelial cell culture (Artzy-Schnirman *et al.*, 2020). It is a relatively new technology, and because of this additional training is required for users to use them appropriately. Furthermore, compared to traditional 2D approaches, they are labour intensive (Ainslie *et al.*, 2019). Analysis of some chips is another significant issue as the small sizes and lower fluid volumes require highly sensitive biochemical methods such as ELISA and qPCR. This limits the high throughput capability of the systems however, the lower volume is advantageous for reducing the costs for drug development processes as it allows smaller amounts of compound (Sedláková *et al.*, 2019). The latter reduction of compound requirements has been exploited in various physiological studies including ADME and toxicity (Ahadian *et al.*, 2018; Ishida, 2018; S. H. Lee & Sung, 2018). However, many chips are designed using PDMS, which is a highly hydrophobic material and therefore prone to drug adsorption, thus reducing its suitability for drug studies.

Within MPS models, cell lines have not been widely used and primary cells are highly favoured in MPS model development. (D. Huh, Matthews, Mammoto, Montoya-Zavala, Yuan Hsin, *et al.*, 2010; Lan *et al.*, 2018b; Malavia *et al.*, 2009; J. D. Stucki *et al.*, 2018). However, there have been MPS devices that utilised the Calu-3 epithelium, demonstrating the applicability of the Calu-3 cell line as a suitable alternative to primary or stem cells for bronchial epithelial modelling. Carius *et al* (2021) reported a perfused model of the Calu-3 epithelium model,

grown in parallel to the static Transwell model, with a cell density of 1×10^5 cells/cm² density for both models (Carius *et al.*, 2021). The perfused model established an effective epithelial barrier with the apparent permeability of sodium fluorescein that was decreased by 26% in perfusion compared to the static Transwell model (Carius *et al.*, 2021). This indicated that the perfused model was able to maintain an effective barrier. However, this model was cultured under LLI not ALI so reduces the physiological relevance that ALI culture creates. The authors discussed the potential of incorporating ALI in their perfusion model however, they did not explore the phenotypical differences between the ALI and LLI cultured Calu-3 cells.

Sui and Lee, (2023) reported a microfluidic device that utilised a 2D benchtop rocker to produce flow along a channel underneath a Calu-3 monolayer, of unknown cell seeding density, but 12,500 total cells seeded per device (Sui & Lee, 2023). Despite using the Calu-3 model (a bronchial cell line) to create an alveolar model by a coculture with pulmonary endothelium, they successfully produced a barrier model of the lung with features such as cobblestone epithelium with the presence of ZO1 tight junctions and quantified the barrier function with a flux study of fluorescein isothiocyanate (FITC)-Dextran (Dex) (Sui & Lee, 2023). However, they cultured the epithelium at ALI for 5 days which might not have provided enough time for the cells to differentiate, as they were cultured in LLI for 5 days prior. Although, the use of a bronchial cell line as an alveolar model may explain the limited differentiation as the characteristics of the cell line would have been aimed towards the characteristics of the alveolar epithelium (i.e. a simple barrier function). The authors were able to demonstrate that the flux of FITC-dextran was similar to that seen in *ex vivo* studies (Sui & Lee, 2023).

Baptista *et al.*, (2022) reported a microfluidic device with a density of 0.5×10^5 cells/cm², grown in LLI for 11 days in coculture with human primary endothelial cells with a flow rate of 25 μ L/hr (Baptista *et al.*, 2022). Similarly to Sui & Lee (2023), this model utilised Calu-3 cells in a microcurved porous membrane as a surrogate alveolar epithelium due to its formation of tight junctions in a monolayer. It was reported that the Calu-3 monolayer behaved in a comparable manner to human primary alveolar epithelium in their concave alveolar-like well (Baptista *et al.*, 2022). Primary alveolar cells were also used in monoculture on the microcurved wells with fluid flow, resulting in a 14-day ALI culture. Baptista *et al.* (2022) concluded that their microfluidic device would set a precedent for micro-anatomically inspired membrane based MPS models of epithelial tissue barriers such as the bronchioles when utilised with primary cells grown at ALI (Baptista *et al.*, 2022). However, the Calu-3 model produced lacked the physiological relevance due to the limited differentiation gained from LLI in comparison to ALI, and this study failed to assess the extent of the differentiation that had occurred. This model has immense potential and is a proof of concept of this MPS device. However, Baptista *et al.*

did not intend to assess the cell model function so lacked the interrogation of the barrier function with assays such as TEER or fluorescent-labelled molecules for flux studies.

Madiedo-Podvrsan *et al* (2023) reported a model with Calu-3 epithelium cells cultured on a Transwell insert for 11 days (density 2×10^5 cells/cm²) (Madiedo-Podvrsan *et al.*, 2023). Although the monolayer was established in a Transwell insert, the cells were continuously cultured in LLI. Importantly, the microfluidic flow was only established on day 11 for 72 h at 25 μ L/min with the medium leaving the tissue model and travelling through a hepatic chip, this was established as an inhalation-like toxicity assessment. The authors reported a reduction in Caludin-1 expression (tight junctions) through immunostaining however, this did not significantly affect the Lucifer Yellow flux and was unclear whether the changes were a result of the flow or the coculture with the hepatic chip after only 72 h of flow and coculture.

The models described above incorporated key MPS aspects that have been developed for complex cell culture models (e.g. perfusion, Transwell inserts, cocultures) whilst other models have increased the complexity by incorporating specifically designed structures for the cells to grow on such as microcurved well (Baptista *et al.*, 2022). MPS models that are niche, and purpose built are useful in their application however, they lack the ease of use most commercial devices require for adoption as a replacement for the traditional 2D submerged cell culture. These MPS Calu-3 models were for niche studies such as recapitulating the alveolar barrier, which is not suitable model for the incorporation of the Calu-3 bronchial cell line (Baptista *et al.*, 2022; Sui & Lee, 2023). Others were not cultured at ALI (Carius *et al.*, 2021; Madiedo-Podvrsan *et al.*, 2023) which, as previously discussed, is the superior method of differentiating Calu-3 cells to a more *in vivo-like* phenotype (Baptista *et al.*, 2022; Carius *et al.*, 2021; Cavet *et al.*, 1997; Forbes, 1998; Madiedo-Podvrsan *et al.*, 2023; A. Sakamoto *et al.*, 2015; Sui & Lee, 2023). A major issue of these MPS models is the lack of cell phenotype characterisation described in these articles. This reduces the confidence in the model's ability to accurately replicate the tissue microstructure and function for specific applications.

3.2. CHAPTER AIMS

Literature has shown perfused Calu-3 MPS bronchial models to be beneficial in the development of an effective epithelial barrier (Carius *et al.*, 2021). However, some of the MPS models that have been developed utilised the Calu-3 bronchial cell line in simplified barrier models (Baptista *et al.*, 2022; Sui & Lee, 2023). In the latter use, as the Calu-3 cell line is established as a simple barrier proof-of-concept model, there is a lack of its use as a bronchial MPS model, for which it has much promise, since the Calu-3 cell line has similar expression to normal human bronchial cells (NHBE) when cultured at ALI (Cavet *et al.*, 1997; Forbes, 1998; Grainger *et al.*, 2006; Selo *et al.*, 2021).

Development of a bronchial MPS model requires thorough characterisation to determine the human relevance of culture with perfusion and the suitability of the models for their applications. Furthermore, an understanding of its ease of use for adoption into more laboratories and use for e.g. drug transport, irritation studies etc., are critical to consider (Ainslie *et al.*, 2019). Within this chapter, a perfused bronchial MPS model will be developed and characterised, utilising the Calu-3 bronchial cell line cultured at an air-liquid interface (ALI) over a long-term culture (up to 28 days). The model will be optimised for seeding density and culture length and assessed using relevant assays such as TEER and flux studies to quantify barrier function, mucus assays to assess bronchial epithelial function and immunofluorescence and histology imaging to assess expression of bronchial epithelium features such as tight junctions and mucins. The phenotype of the model will be described through qPCR analysis of gene expression of transporters such as OCT1, OCTN2 and MRP1 and bronchial features such as ZO1, MUC5AC and Claudin-1.

3.3. METHODS

3.3.1. OPTIMIZING THE SEEDING DENSITY OF CALU-3 BRONCHIAL EPITHELIAL CELLS ON A TRANSWELL INSERT

The Calu-3 cells underwent culture and maintenance procedures outlined in Sections 2.5.1, 2.5.2, and 2.5.4 with Transwells coated with collagen as described in Section 2.5.5. The cells were seeded onto the coated inserts and placed in either a standard 24-well plate or a Barrier-12 MPS plate, following the method in Section 2.5.7. The PhysioMimix system was set up according to Section 2.5.6. In both static and MPS plates, cells were seeded at three densities: 1×10^5 , 3×10^5 , and 5×10^5 cells/cm². After 24 h of seeding, the flow rate was set to 0.5 μ L/s in the MPS plate. All cells were transitioned to air-liquid interface (ALI) conditions 48 h post-seeding and cultured for 7 days at ALI. TEER measurements were conducted at each change of medium, following the protocol in Section 2.5.9. Permeability coefficients (Papp) were determined using Lucifer Yellow (LY), dosed at a concentration of 0.1 mg/mL (221 μ M) by diluting a stock solution of 25 mg/mL in HBSS (Hank's Balanced Salt Solution), as detailed in Section 2.5.11. Brightfield images were captured using a EVOS XL Core microscope (Invitrogen, USA) at each media change.

3.3.2. PERFUSION ACCELERATED THE FORMATION OF A FUNCTIONAL CALU-3 EPITHELIAL BARRIER MODEL BY 7 DAYS

The Calu-3 cells underwent culture and maintenance procedures outlined in Sections 2.5.1, 2.5.2, and 2.5.4 with Transwells prepared according to the method in Section 2.5.5. The cells were seeded onto the Transwells in standard 24-well plates and the Barrier-12 MPS plate, as described in Section 2.5.7, with the PhysioMimix system configured according to Section

2.5.6. Flow was initiated at 0.5 $\mu\text{L/s}$ in the MPS plate after 24 h of seeding. All cells were transitioned to air-liquid interface (ALI) condition 48 h post-seeding and maintained for 14 days. TEER measurements were conducted at each media change following the protocol outlined in Section 2.5.9. Brightfield images were captured using a EVOS XL Core microscope (Invitrogen, USA) during each media change. Cell Titer-Glo[®] luminescence assay (Promega, USA) was used to determine cell number by the amount of adenosine triphosphate (ATP) present in the cells. The manufacturer's protocol was followed. Briefly, 100 μL of the Cell Titer-Glo substrate solution was added to the cell layer and left to incubate in the dark at room temperature for 12 min before 100 μL of cell culture medium was added and then the 200 μL solution was transferred to a black bottomed 96 well plate and the samples were read on the FLx800 Fluorescence plate reader.

Permeability coefficients (P_{app}) were determined using Lucifer Yellow (LY), as above and detailed in Section 2.5.11. qPCR analysis was performed at ALI days 7 and 14, following the procedures outlined in Section 2.5.12, with immunofluorescence (IF) staining carried out as described in Section 2.5.13. IF intensity was measured using Fiji Image J software to measure the intensity of average of Hoechst 33342 and then the intensity of ZO1 and MUC5AC IF images. The intensity of the latter two was then divided by the intensity of Hoechst 33342 of the same area to normalise the intensity of ZO1/MUC5AC to the DNA intensity. This was performed on multiple areas of a single images before averaging for a single replicate and then performed on a total of 3 images per condition per day. Mucus quantification procedures were conducted as specified in Section 2.5.10.

3.3.3. LONG TERM CHARACTERISATION OF THE ALI PERFUSED CALU-3 MPS BRONCHIAL EPITHELIAL MODEL

The Calu-3 cells underwent culture and maintenance procedures outlined in Sections 2.5.1, 2.5.2, and 2.5.4 with Transwells prepared according to the method in Section 2.5.5. The cells were seeded onto the Transwells in standard 24-well plates and the Barrier-12 MPS plate, as described in Section 2.5.7, with the PhysioMimix system configured according to Section 2.5.6. Flow was initiated at 0.5 $\mu\text{L/s}$ in the MPS plate after 24 h of seeding. All cells were transitioned to air-liquid interface (ALI) condition 48 h post-seeding and maintained for 28 days. TEER measurements were conducted at each change of medium following the protocol outlined in Section 2.5.9. Permeability coefficients (P_{app}) were determined by performing the flux study as detailed in Section 2.5.11. Mucus quantification procedures were conducted as specified in Section 2.5.10.

3.4. RESULTS AND DISCUSSION

3.4.1. OPTIMISING THE SEEDING DENSITY OF CALU-3 BRONCHIAL EPITHELIAL CELLS ON A TRANSWELL INSERT

Initially, the model was optimised for seeding density by exploring three densities previously described in the literature: 1×10^5 cells/cm² (Cingolani *et al.*, 2019; Horstmann *et al.*, 2021; Mukherjee *et al.*, 2013; Pasman *et al.*, 2021), 3.03×10^5 cells/cm² (V. Kumar *et al.*, 2022), and 5×10^5 cells/cm² (Foster *et al.*, 2000; Grainger *et al.*, 2006; Haghi *et al.*, 2012a, 2013, 2019; Ji *et al.*, 2022; Meindl *et al.*, 2015; Min *et al.*, 2013, 2016; Stuetz *et al.*, 2023). In a 24 well Transwell with a surface area of 0.33 cm² this equated to 33,000 cells per well (1×10^5 cells/cm²), 100,000 cells per well (3.03×10^5 cells/cm²), or 165,000 cells per well (5×10^5 cells/cm²).

The lowest density, 33,000 cells/well, showed a full monolayer by day 7 ALI in both the static and perfused conditions (Figure 3.1). However, the monolayers had gaps at day 0 and day 4 in both conditions. This indicates that the cells were still in their growth phase and had not achieved the optimum coverage of the Transwell surface to start differentiating. The 100,000 cells/well density showed similar gaps at day 0, but by Day 4 the cells achieved a consistent monolayer that was maintained at Day 7 (Figure 3.2). The highest density at 165,000 cells/well showed a complete monolayer at Day 0, and so theoretically could be at the stages of differentiation by the start of the air-liquid interface culture (Figure 3.3). No obvious differences between the static and perfused morphology of the cells from the brightfield images were observed in the conditions. However, for cells seeded at 100,000 cells/well the static Day 7 image shows the initial culture growing more as patches undergoing integration into a monolayer, whereas the perfused Day 7 images show a consistent, confluent monolayer of cells (Figure 3.2).

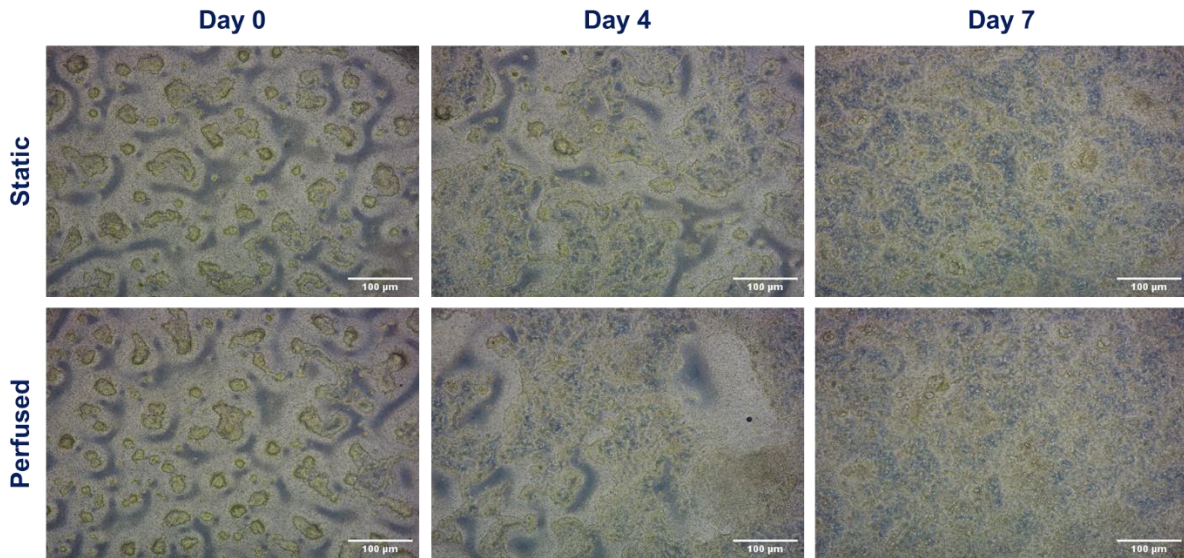


Figure 3.1: Seeding density 1×10^5 cells/cm² (33,000 cells/well) required up to 7 days of ALI culture to reach confluency. Brightfield images of Calu-3 cell growth in static and perfused conditions seeded at a density of 1×10^5 cells/cm² (33,000 cells/well), on days 0, 4 and 7 of ALI culture. Scale bar = 100 µm.

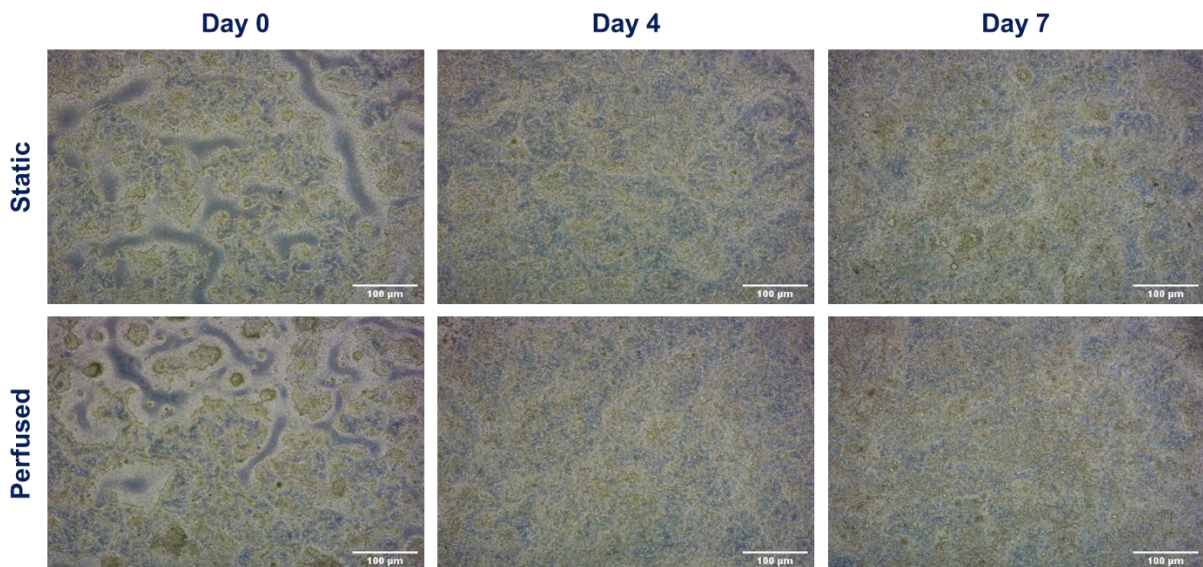


Figure 3.2: Seeding density 3×10^5 cells/cm² (100,000 cells/well) required up to 4 days of ALI culture to reach confluency. Brightfield images of Calu-3 cell growth in static and perfused conditions seeded at a density of 3×10^5 cells/cm² (100,000 cells/well), on days 0, 4 and 7 of ALI culture. Scale bar = 100 µm.

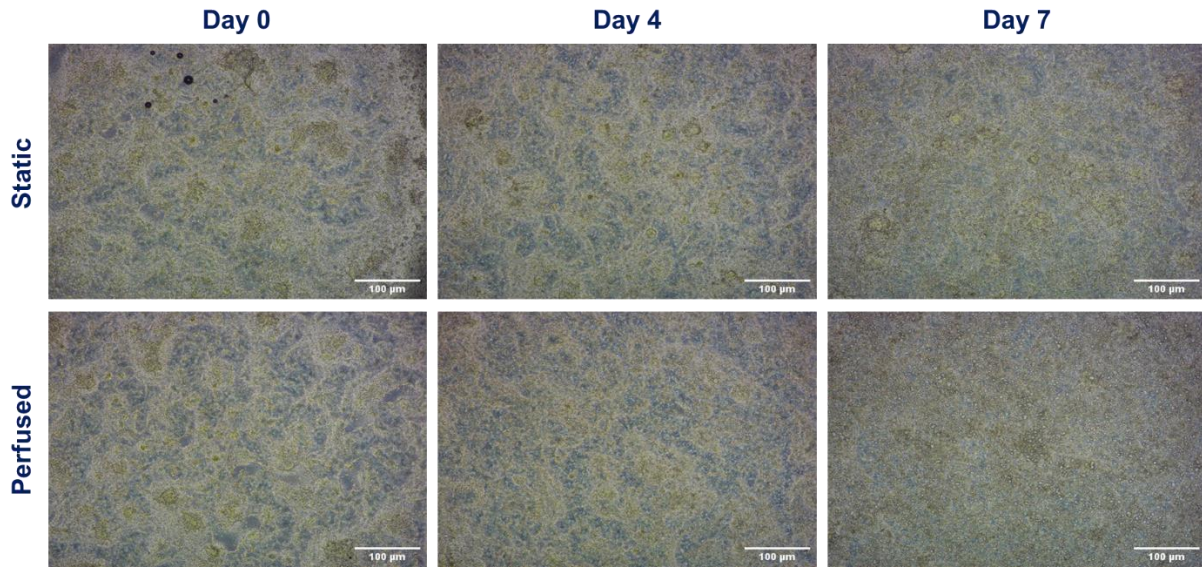


Figure 3.3: Seeding density 5×10^5 cells/cm² (165,000 cells/well) reached confluency at day 0 ALI. Brightfield images of Calu-3 cell growth in static and perfused conditions seeded at a density of 5×10^5 cells/cm² (165,000 cells/well), on days 0, 4 and 7 of ALI culture. Scale bar = 100 μ m.

Barrier formation as assessed by TEER measurements showed similar measurements for the 100,000 and 165,000 cells/well in the static and perfused conditions (Figure 3.4 A and B). However, the perfused condition seeded at 100,000 cells/well showed a steady increase of TEER until Day 7 when the resistance was the same as 165,000 cells/well (Figure 3.4 B). Overall, the TEER measurements in the perfused condition were lower than the static condition but, in both conditions, the 33,000 cells/well showed negligible TEER until Day 7, when in the static system it reached similar values to the other two seeding densities. 33,000 cells/well in the perfused system reached approximately half the resistance of the other two densities. This suggested that the perfused Calu-3 barrier would be more permeable than the barrier achieved in the static condition.

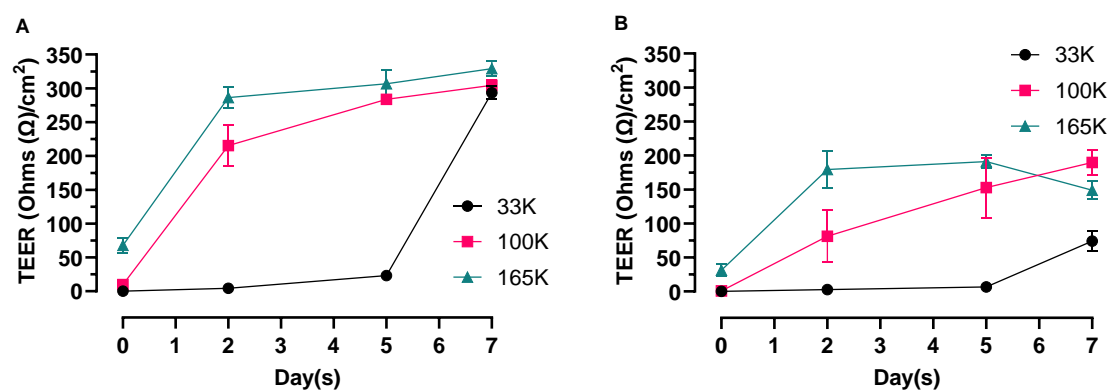


Figure 3.4: Perfused cells had a lower TEER profile than their static equivalent, whilst 100K and 165K cells/well had similar TEER profiles. Transepithelial Electrical Resistance (TEER) measurements reported as Ohms (Ω)/cm² for the static (A) and perfused (B) conditions with all three densities in each graph. 33K = 1×10^5 cells/cm², 100K = 3×10^5 cells/cm², 165K = 5×10^5 cells/cm² (N \geq 3).

The fluorescent dye Lucifer Yellow (LY) was used to interrogate the passive permeability of the monolayers by the movement of a solute through the tight junctions of the paracellular pathway. Lucifer Yellow is a fluorescent molecule that mimics the transport of small drug molecules through the paracellular pathway which is why it is a useful assay to characterise the barrier function of epithelial cells. The apparent permeability (P_{app}) of LY indicates the integrity of the barrier and has been used by many research groups as a measurement alongside TEER (Carius *et al.*, 2021; Cingolani *et al.*, 2019; Min *et al.*, 2013, 2016). Figure 3.5 A shows in the static condition, the 165,000 cells/well density had the highest P_{app} , thus indicating a low barrier integrity, despite this density displaying the highest TEER. There was no significant difference between the 33,000 and 100,000 cells/well densities. Although the 33,000 cells/well had a lower mean P_{app} value than the 100,000 cells/well, the variance of the P_{app} value for 33,000 cells/well seeding density meant that this difference was not significant. The 100,000 cells/well density had a much more consistent P_{app} across replicates than either 33,000 or 165,00 cells/well. In the perfused condition, 100,000 cells/well had the lowest P_{app} (Figure 3.5 B). Although there was no significant difference between 100,000 and 165,000 cells/well seeding density, the large variation between the replicates for 165,000 cells/well could indicate inconsistencies when seeding at this density. This could be a result of variation in the successful seeding of cells on to the membrane or a variation in functional tight junction formation.

Figure 3.6 shows the comparison of the P_{app} values between static and perfused conditions at each respective cell seeding density. The perfused condition had a significantly higher P_{app}

than the static culture when seeded at 33,000 cells/well (Figure 3.6 A). This was concluded to arise from the barrier not being as sufficiently formed by day 7 in the perfused system compared to the static culture. This was also indicated by the TEER not reaching the same value as the other two seeding densities (Figure 3.4 B). A significant decrease in P_{app} was achieved in the perfused Calu-3 model when seeded at 100,000 and 165,000 cells/well compared to the same conditions in static culture (Figure 3.6 B and C).

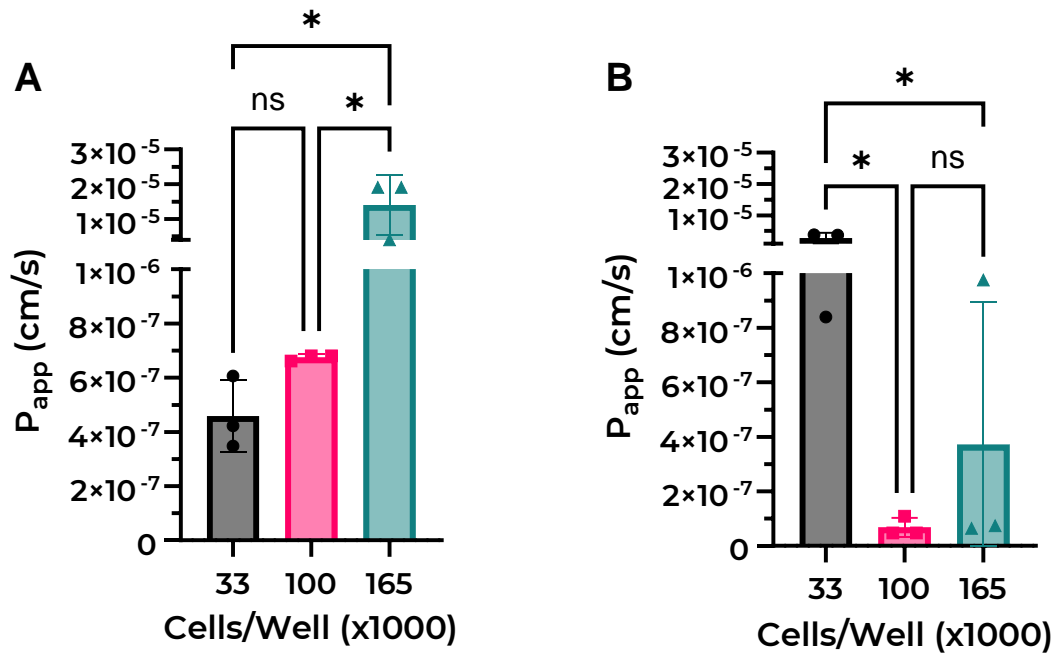


Figure 3.5: The P_{app} of LY is variable across seeding densities and culture conditions.

P_{app} of LY across the Calu-3 monolayer at Day 7 of ALI culture in the (A) static and (B) perfused conditions. Both graphs show the P_{app} of all three densities (ANOVA * = $P < 0.05$) (N=3).

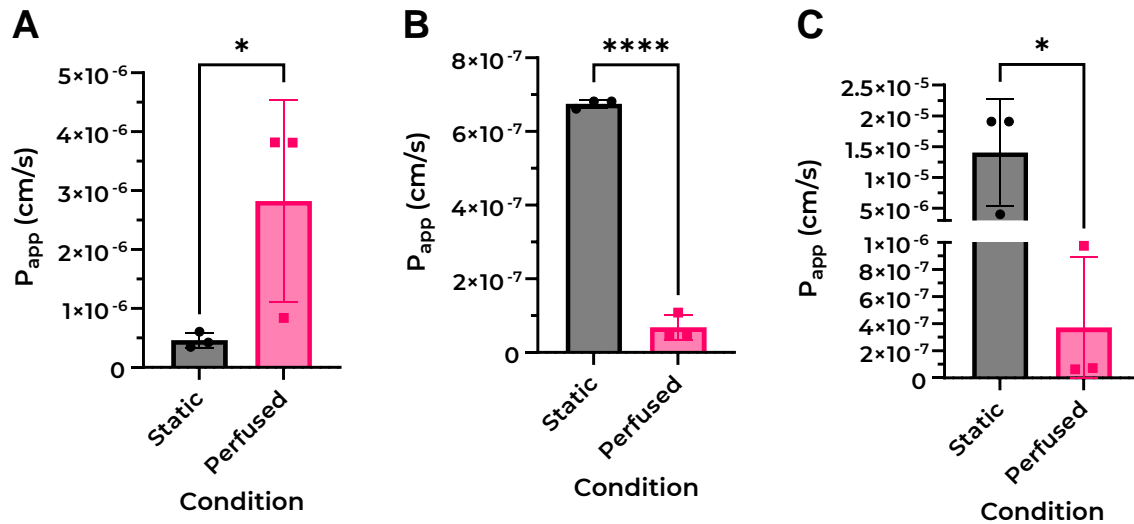


Figure 3.6: P_{app} of LY was lowest in the 3x10⁵ cells/cm² (100,000 cells/well) density in both conditions. Comparison of the P_{app} of LY in the static and perfused conditions across the Calu-3 monolayer at Day 7 in the three densities: **(A)** 1x10⁵ cells/cm² (33,000 cells/well), **(B)** 3x10⁵ cells/cm² (100,000 cells/well) and **(C)** 3x10⁵ cells/cm² (165,000 cells/well) (Unpaired T-test * = P<0.05, **** = P<0.0001) (N=3).

Previously, Calu-3 models have been reported to show P_{app} values of LY as low as 3.4 x10⁻⁷ cm/s with cells seeded at a density of 1 x10⁵ cells/cm² (Cingolani *et al.*, 2019) and at 7.3 and 8.6 x10⁻⁸ cm/s when seeded at 5x10⁵ cells/cm² (Min *et al.*, 2013, 2016) with maximum TEER values recorded at 400-500 Ω/cm², as detailed in Table 3.1. Within this experiment, 1x10⁵ cells/cm² was observed to produce highly variable results in P_{app} and TEER measurements as was also seen in the 5x10⁵ cells/cm² density. The 3x10⁵ cells/cm² was the optimum seeding density in terms of variability between replicates and with the lowest average P_{app} value at 6.77x10⁻⁸ cm/s with a maximum TEER value of 240 Ω/cm² in the perfused condition. Taking into consideration the seeding density and the resultant TEER and P_{app} values, it was apparent that the 100,000 cells/well generated an effective barrier by Day 7. As the most efficient, consistent, and functional seeding density, 100,000 cells/well was chosen as the seeding density for all experiments with Calu-3 epithelium models in this thesis.

3.4.2. PERFUSION ACCELERATES THE FORMATION OF A FUNCTIONAL CALU-3 EPITHELIAL BARRIER MODEL BY 7 DAYS

To determine if the perfused condition resulted in altered cell viability, the Cell Titer-Glo® assay was used to determine the number of cells present through the amount of ATP generated by the cells. To determine the number of cells more accurately in each sample, the assay was first performed on an increasing number of cells to generate a calibration curve of ATP raw

values against cell number. Figure 3.7 A shows the number of cells in the Calu-3 cell models in the perfused and static conditions. The results were not different from each other at each day (7 and 14) regardless of condition. There was a reduction in cell number from Day 7 to Day 14, but this was not statistically significantly different. This may have been due to a reduction of cell activity, as by Day 14 the cells are likely to have reduced cell division and are increasingly in a differentiated state due to both spatial and environmental cues from ALI induction. In this case, it is likely that they are not as metabolically active as they will have been up to Day 7, since ATP increases when utilised for cell growth and DNA replication (Ahn *et al.*, 2017).

Figure 3.7 B illustrates that the TEER values of the static and perfused models of the Calu-3 epithelial barrier exhibited similar patterns. Overall, the static model demonstrated a higher TEER profile than the perfused model. However, by Day 7, the TEER values were nearly identical between the two models. This was a result of the fluctuations in TEER profile observed in the static model over the 14-day culture period. Specifically, a large increase from Day 2 to Day 5 was followed by a sizable drop by Day 7, another increase until Day 12, and another drop by Day 14. Similarly, the perfused model exhibited a sharp rise in TEER values from Day 2 to Day 5, followed by a decline by Day 7, although not as large as in the static model. From Day 7 to Day 12, the perfused model maintained a steady TEER, indicating the formation of a stable barrier, before experiencing a drop by Day 14, similar to the static model.

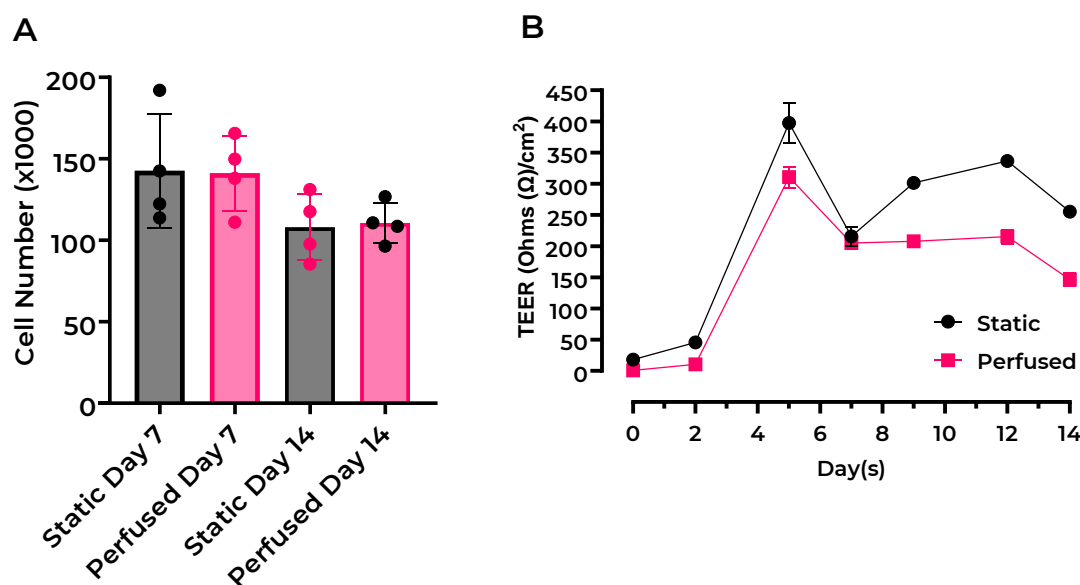


Figure 3.7: Perfusion did not affect cell viability but reduced the TEER profile of Calu-3 epithelium. Cell viability determined by number of viable cells present at Day 7 and Day 14 of ALI culture in the static and perfused condition determined by using the **(A)** Cell Titer-Glo[®] luminescence assay which was not significantly different between the samples (ANOVA ns = $P > 0.05$). **(B)** Transepithelial Electrical Resistance (TEER) measurements of the static and perfused Calu-3 models performed every 2/3 days with from day 0 ALI till day 14 ALI ($N \leq 4$).

The apparent permeability of Lucifer Yellow was used to assess the paracellular permeability of the epithelial barrier models, as previously shown. Figure 3.8 A illustrates the significantly tighter barrier in the perfused model compared to the static at Day 7, with lower variance of the replicates of the perfused model compared to the static. No significant differences were observed between the static and perfused models at Day 14, as a result of the increased variation in both the static and perfused models (Figure 3.8 B). An almost 10-fold decrease in the average P_{app} of LY in the perfused condition (3.59×10^{-8} cm/s) was evident compared to the average value of the static model (2.78×10^{-7} cm/s), which may be a result of a higher expression of tight junctions or lower permeability of the expressed tight junctions in the perfused condition. When directly compared, the difference between the days was evident with both the static and perfused having higher variance on Day 14 (Figure 3.9). This caused the average value to be higher for Day 14 than Day 7 in both the static (1.21×10^{-6} cm/s) and perfused (1.74×10^{-7}) conditions however, the difference was not significant due to the large error bars.

This increase in variance between Days 7 and Day 14 for both the static and perfused condition was interesting and although there was no significant difference between the P_{app}

values on each respective day, it would be beneficial to determine the extent of this variance by increasing replicate numbers, repeating the P_{app} assay on the same well for each timepoint, and the length of culture at ALI for example, Day 21 and Day 28. At 3.59×10^{-8} cm/s, the perfused Calu-3 model at day 7 ALI had a lower P_{app} value than the literature values at a higher density and an extra day in ALI culture (Min *et al.*, 2013, 2016), showing the perfused Calu-3 epithelial barrier to have a tighter barrier than previously reported in static cultures.

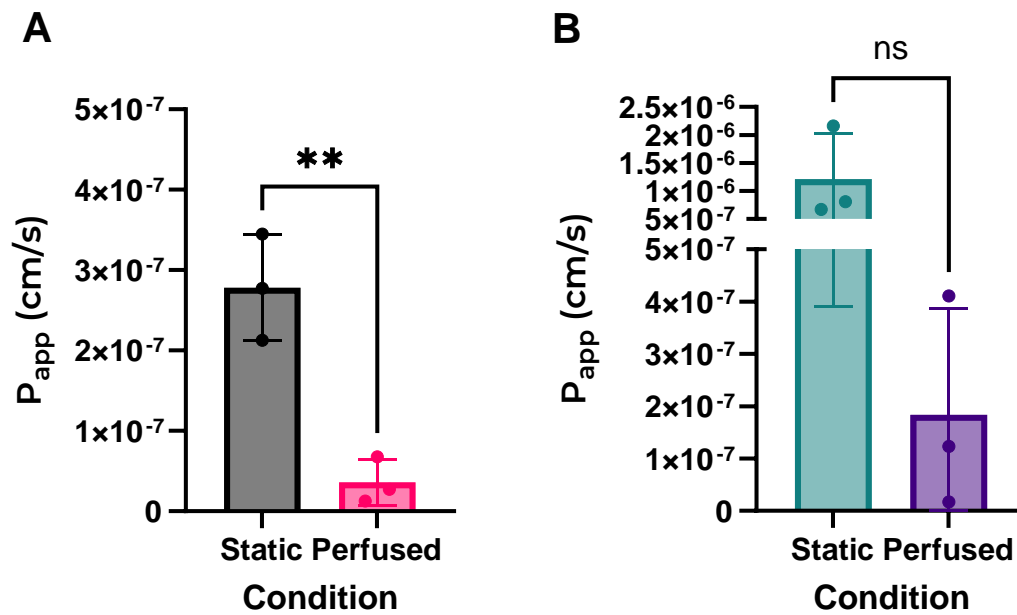


Figure 3.8: Perfusion resulted in a significantly lower P_{app} value than the static model at day 7 ALI. Comparison of the apparent permeability (P_{app}) of Lucifer Yellow (LY) across the Calu-3 epithelial Transwell model in the static and perfused conditions at **(A)** Day 7 ALI and **(B)** day 14 ALI culture (Unpaired T-test ns = $P > 0.05$, ** = $P < 0.005$) (N=3).

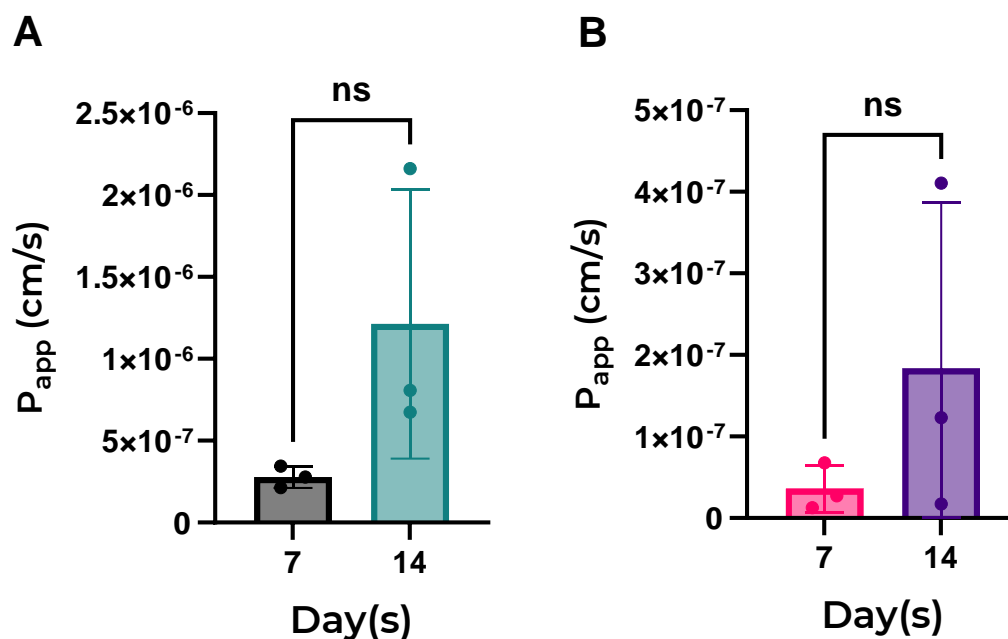


Figure 3.9: There was an increase in variability in P_{app} between Day 7 and Day 14 of the Calu-3 epithelial barrier in both conditions but no significant difference in permeability. Comparison of the apparent permeability (P_{app}) of Lucifer Yellow (LY) across the Calu-3 epithelial Transwell model at day 7 and day 14 of air-liquid interface (ALI) culture in the **(A)** static and **(B)** perfused conditions (Unpaired T-test ns = $P > 0.05$) (N=3).

After assessing the barrier integrity, the cell models were further investigated for changes in phenotype. From analysis of tissues immuno-stained for mucus (MUC5AC) and tight junctions (ZO1), it was evident that the morphology of the static model was different from that of the perfused system at Day 7 (Figure 3.10). Calu-3 cells cultured in perfused conditions exhibited a more uniform layer of epithelial cells whereas the static model displayed patches of cells growing on top of a lower Calu-3 epithelial monolayer. This was even more evident on Day 14, where the static model seemed to have further significant patches of cells on top of the Calu-3 monolayer (Figure 3.11). Interestingly, by Day 14 the perfused model also showed early signs of these second layer patches. This may be the reason for the significant increase in well-to-well variation in the P_{app} of LY at Day 14 (Fig. 3.9) as these patches may be interfering with the barrier integrity and tight junctions.

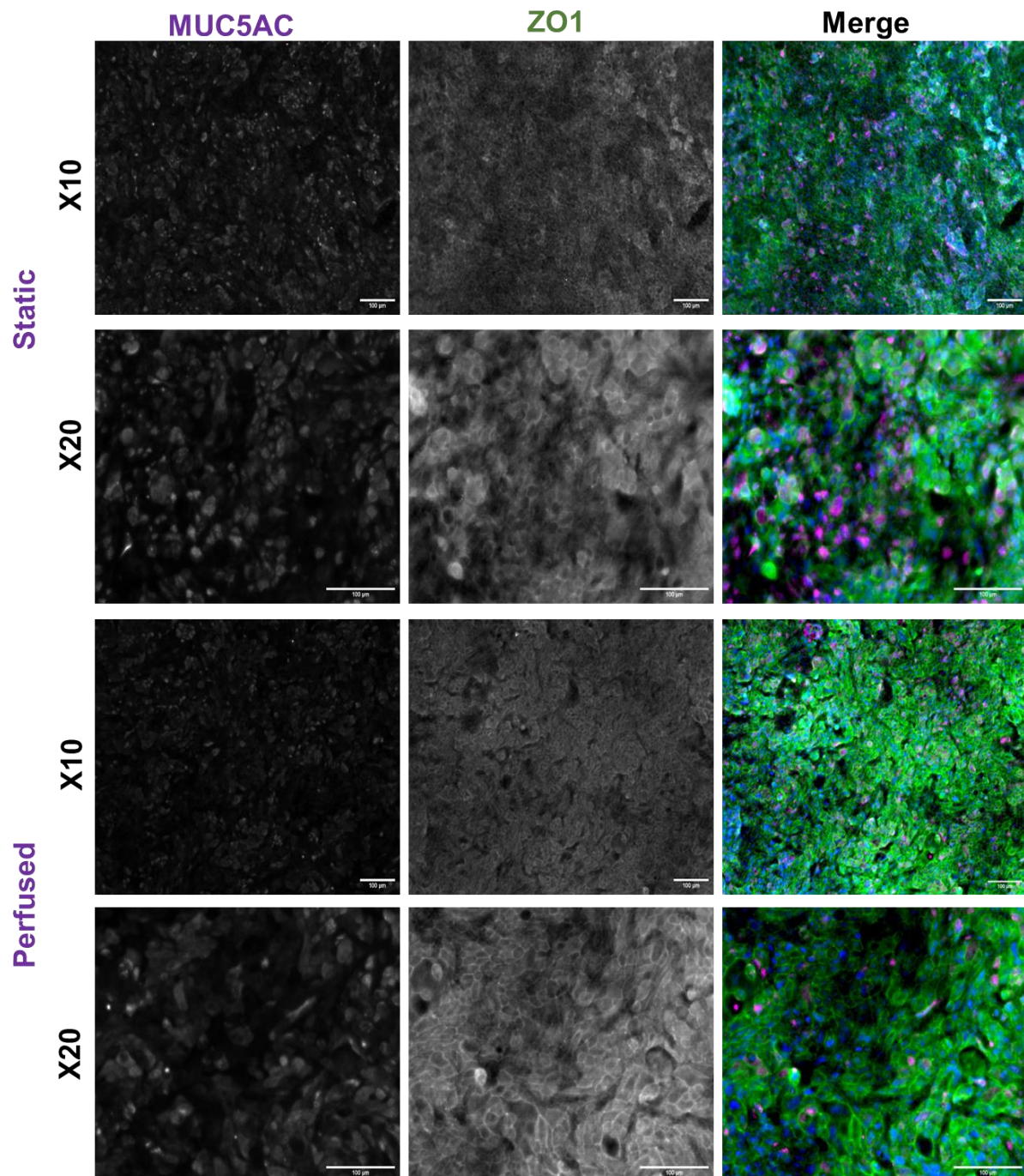


Figure 3.10: Perfused Calu-3 Transwell model established a more uniform monolayer than the static model at Day 7. Calu-3 cells cultured in static or perfused conditions were cultured for 7 days before being fixed and stained with antibodies against ZO1 (green), MUC5AC (magenta) and Hoechst for DNA (blue). Scale bar = 100 µm

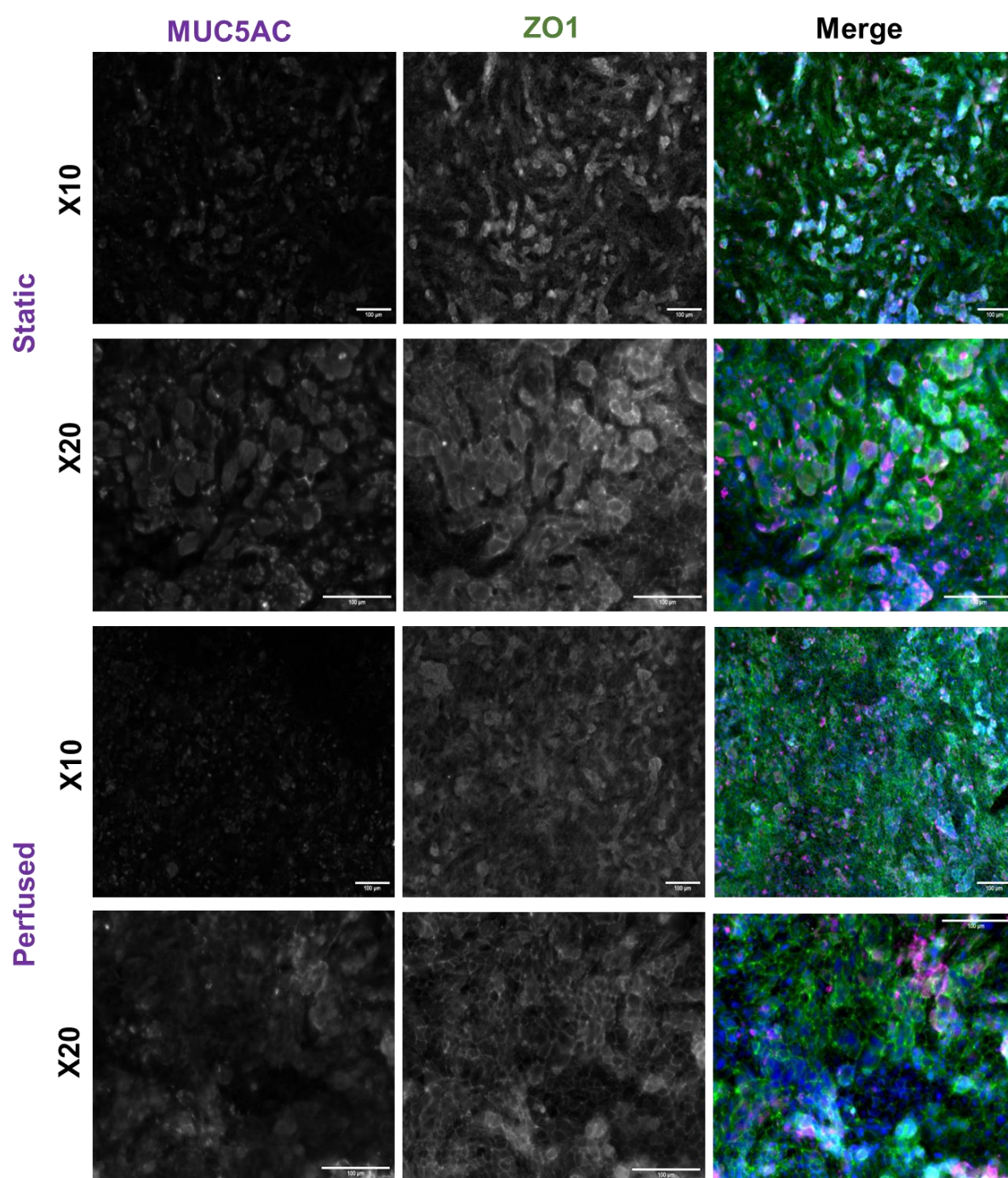


Figure 3.11: At Day 14, the perfused Calu-3 Transwell model exhibited a more uniform monolayer than the static model. Calu-3 cells cultured in static or perfused conditions were cultured for 7 days before being fixed and stained with antibodies against ZO1 (green), MUC5AC (magenta) and Hoechst for DNA (blue). Scale bar = 100 μ m

Using ImageJ/Fiji, the pixel intensity of specific stains was analysed. A significant increase was detected in the intensity of DNA from Day 7 to Day 14 in both static and perfused conditions (Figure 3.12 A). When normalised to the DNA intensity of each condition, significant increase in expression of ZO1 in the perfused condition was detected compared to the static condition in both Day 7 and Day 14 of ALI culture, indicating the barrier was better formed in the perfused model than the static model (Figure 3.12 B). Interestingly, both the static and the perfused model had significantly decreased ZO1 expression at Day 14 compared to Day 7 but this could be a result of the increased DNA intensity suppressing these values, since the 'leakier' barrier indicated by such a result was not seen in the P_{app} assay (Figure 3.8) however, this could explain to reduction in TEER at Day 14 for both the static and perfused conditions (Figure 3.7).

The MUC5AC staining intensity was similar in the static and perfused conditions at both timepoints however, a reduction was observed in the MUC5AC expression of the static model from Day 7 to Day 14 which was not seen in the perfused model, indicating a more consistent MUC5AC expression in the perfused Calu-3 epithelial barrier.

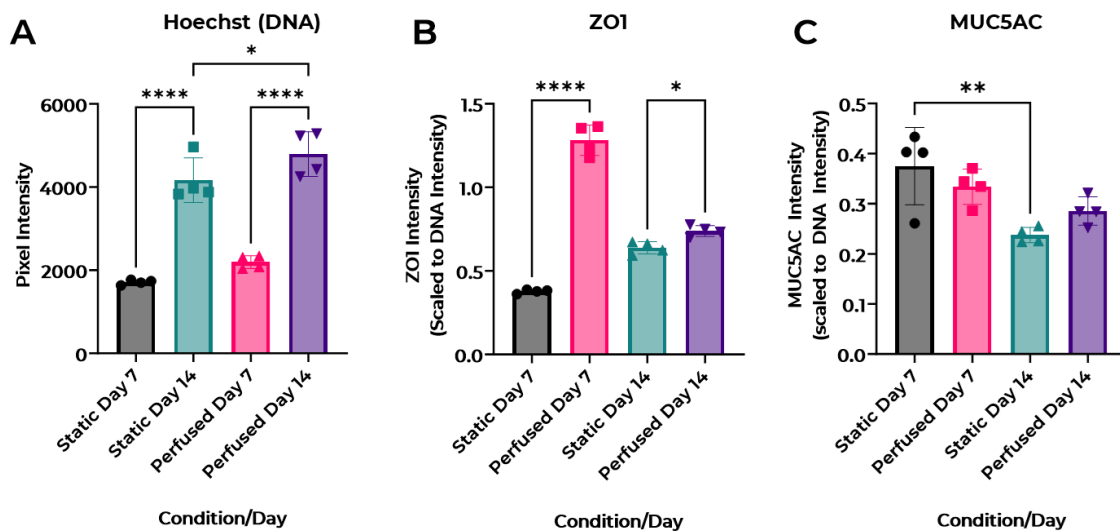


Figure 3.12: Perfusion causes increased ZO1 expression and maintains mucus expression. DNA fluorescence intensity of the greyscale image showing (A) Hoechst 33342. (B) ZO1 intensity of the greyscale image showing only ZO1 scaled to the DNA intensity of the same image shown in (A). (C) MUC5AC intensity of the greyscale image showing only MUC5AC scaled to the DNA intensity of the same image shown in (A) (ANOVA * = <0.05, ** = <0.005, **** = <0.0001) (N=4).

qPCR analysis was used to determine the expression of three transporters indicated in beta-2 (β_2) adrenoreceptor agonist transport to explore whether the culture conditions altered their expression. Calu-3 cells have been found to exhibit expression of OCT1 and OCTN2 cation transporters and proven responsible for the transport of β_2 -adrenoreceptor agonists such as salbutamol (Mamlouk *et al.*, 2013; Mukherjee *et al.*, 2013, 2017b; Salomon *et al.*, 2012). Consequently, these transporter subtypes were analysed by qPCR in this experiment. The OCT1 (SLC22A1) transporter was highly expressed in the perfused model at Day 7 with a 50-fold increase whereas the static model displayed less than a 25-fold increase compared to the GAPDH housekeeping gene, respectively (Figure 3.13 A). By Day 14 the static model had reached similar levels of expression to the perfused model at Day 14. SLCC22A1 expression was previously shown to be higher in Calu-3 than the primary cell bronchial model, EpiAirway, and perfusion enhances this expression however, the RPL15 housekeeping gene was used in this instance (Barilli *et al.*, 2020).

A significant increase in expression of the solute transporter OCTN2 (SLC22A5) was detected at Day 14 when compared to the Day 7 counterparts of each model (Figure 3.13 B). However, no difference was observed between the two conditions at either timepoint. In previous studies, expression of OCTN2 in Calu-3 was determined as comparable in expression at Day 8 ALI to the primary bronchial model, EpiAirway (Rotoli, Visigalli, *et al.*, 2020). There was no difference between the static or perfused conditions at Day 7 for the expression of the MRP1 (ABCC1) transporter (Figure 3.13 C). In both conditions, a significant increase in MRP1 expression was observed from Day 7 to 14, with the static model showing the highest expression at Day 14 overall. ABCC1 has previously been quantified with a 20-fold expression in Calu-3 compared to the housekeeping gene RPL15, whereas in this study only a maximum of a 10-fold increase was observed compared to GAPDH (Rotoli, Barilli, *et al.*, 2020).

Claudin-1 and ZO1 tight junctions were also assessed for their expression via qPCR analysis. There was no noticeable difference between the static and perfused models at either timepoint for ZO1 expression, however there was a significant increase from Day 7 to Day 14 in the static model (Figure 3.14 A). A significant increase in Claudin-1 expression was observed from Day 7 to Day 14 for both models (Figure 3.14 B), highlighting the tight junction expression between the conditions was similar. However, functionally the tight junctions were different as evident from the P_{app} values generated from the paracellular transport assay (Figure 3.9).

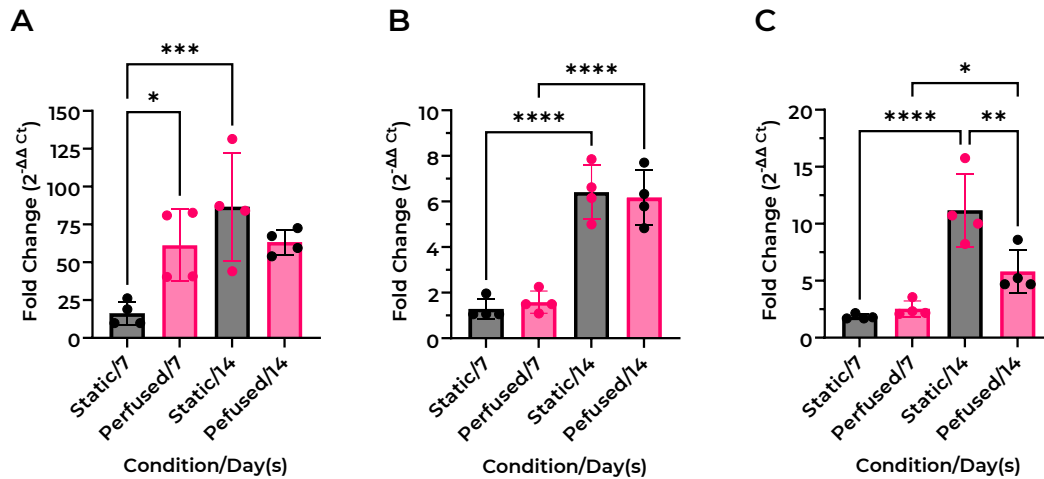


Figure 3.13: Perfusion increased the expression of the cation transporter OCTN2 in Calu-3 epithelium at Day 7. qPCR expression of three different transport proteins that are present in the Calu-3 epithelial cells in the static and perfused model at Days 7 and 14 when cultured at ALI. **(A)** SLC22A1/OCT1, **(B)** SLC22A5/OCTN2 and **(C)** ABCC1/MRP1. (ANOVA * = $P < 0.05$, ** = $P < 0.005$, *** = $P < 0.0005$, **** = $P < 0.0001$) (N=4).

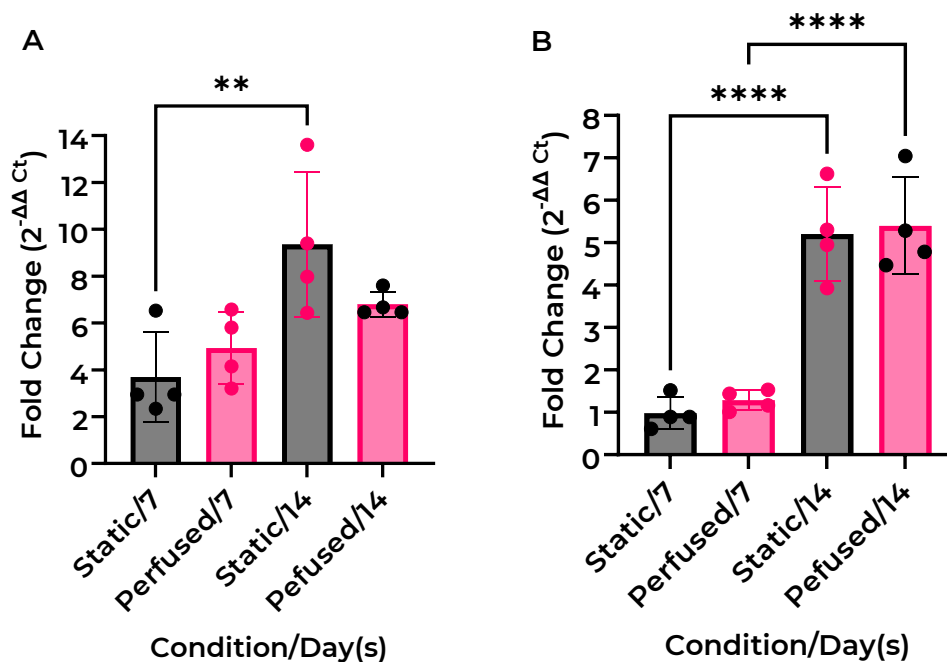


Figure 3.14: Static and perfused conditions resulted in a similar expression of tight junction proteins. qPCR expression of two tight junction proteins that are present in the Calu-3 epithelial cells in the static and perfused models at Days 7 and 14 of ALI culture. **(A)** TJP1/ZO1 and **(B)** CLDN1/Claudin-1. (ANOVA * = $P < 0.05$, ** = $P < 0.005$, *** = $P < 0.0005$, **** = $P < 0.0001$) (N≤4).

Together, these experiments determined that the perfused condition resulted in the Calu-3 Transwell model to express a tighter epithelial barrier than the standard static model as seen from the P_{app} values of the Lucifer Yellow paracellular marker. The P_{app} values generated by the perfused model were lower than the values recorded in literature and although the ZO1 expression was similar for the static and perfused conditions, the perfused model resulted in a tighter barrier indicating the perfusion may have resulted in enhanced functionality of those tight junctions. The IF images and subsequent image intensity analysis showed an increase of ZO1 tight junction expression at Day 7, potentially the cause of the reduction in P_{app} for the Calu-3 barrier in perfused conditions. This highlights the need for extensive characterisation of the model as genetic and protein level expression differences can lead to functional differences such as the passive permeability of compounds. This study highlights the perfused Calu-3 MPS bronchial model is superior in its barrier function compared to the standard static Calu-3 Transwell model.

3.4.3. LONG-TERM MAINTENANCE OF THE ALI PERFUSED CALU-3 BRONCHIAL EPITHELIAL TRANSWELL MODEL FOR 28 DAYS

The next assessment was to determine the potential for long-term culture of the Calu-3 model in the different culture conditions, to understand how perfusion may affect longevity of the culture. The Calu-3 Transwell model was cultured successfully over 28 days, with the barrier integrity assessed using TEER at every media change. Overall, the static model had a higher TEER measurement especially at days 7-12 and days 23-28 (Figure 3.15). However, the TEER values were not significantly different at Days 5, 14, 19 and 21 showing there were fluctuations in the TEER profile of both static and perfused models (Figure 3.15) which could be a result of the morphological changes previously seen with the patches growing on top of the initial Calu-3 monolayer.

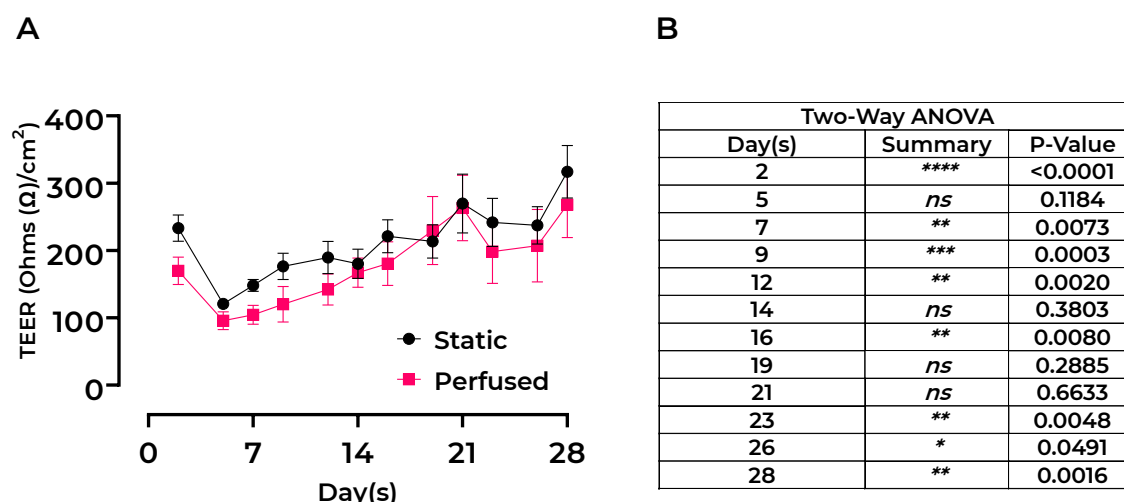


Figure 3.15: Perfusion resulted in a lower TEER profile than the static Calu-3 model.

(A) TEER measurements of the Calu-3 Transwell model across 28-days at ALI in the static and perfused conditions with the **(B)** statistical P-values of the Two-Way ANOVA showing the significant differences between the two conditions (Static vs Perfused) on each timepoint (N≤12)

The ability of the epithelial barriers to resist paracellular permeability was assessed by the permeability of sodium fluorescein (NaFL) and has been used extensively as a paracellular permeability marker for Calu-3 culture models (Ehrhardt, Fiegel, *et al.*, 2002; Grainger *et al.*, 2006; Haghi *et al.*, 2019; Meindl *et al.*, 2015). The P_{app} of NaFL was assessed every 7 days on the same Transwells in both the static and perfused plates. Intriguing results were detected, as seen in the previous experiment, the P_{app} value of the perfused model was lower than the static model (Figure 3.16). By Day 14 the static model had reached similar P_{app} values to the perfused model, as previously seen (Figure 3.16 A and B). However, by Day 21 the perfused model displayed lower P_{app} values than the static model, before rising to similar levels to the static model on Day 28 (Figure 3.16 C and D).

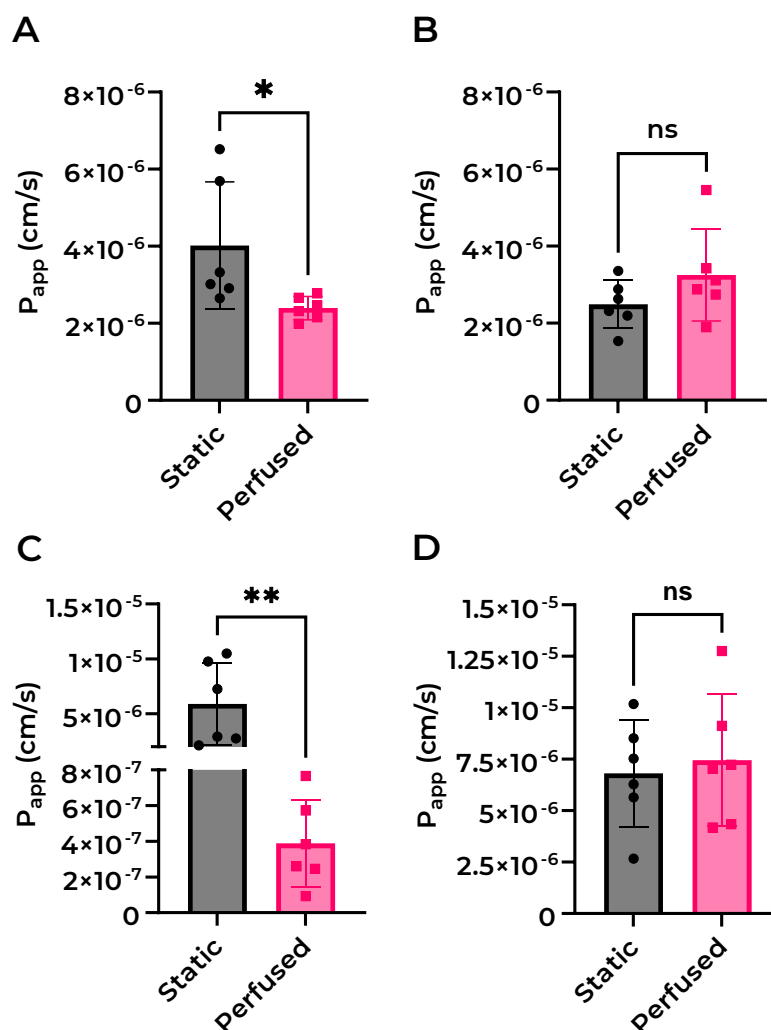


Figure 3.16: P_{app} was significantly lower in the perfused model than the static at Days 7 and 21. P_{app} values of NaFL across the Calu-3 monolayer in the static and perfused conditions on Days (A) 7, (B) 14, (C) 21 and (D) 28. (Unpaired T-test * = $P < 0.05$, ** = $P < 0.002$). (N=6)

The perfused Day 21 P_{app} was significantly lower than Days 7, 14 and 28 (Figure 3.17 B). However, the Day 28 P_{app} was significantly higher than Day 14 and Day 7, indicating that the barrier was more permeable after 28 days in culture but up to Day 21 the barrier permeability was maintained. The static model showed little differences between the days except for Day 14 being significantly lower than Day 28 due to the increased error of Days 21 and 28 raising the mean P_{app} value, 5.89×10^{-6} and 6.81×10^{-6} cm/s respectively. The data on Days 21 and 28 became more variable, although the difference between Day 21 and 14 was not significant, the difference between the mean values showed an increase in permeability from Day 14 (2.49×10^{-6} cm/s) to Day 21 (5.89×10^{-6} cm/s) in the static model. Together, this suggests that the perfused model generated a tighter, functional barrier up to 21 days in culture, with better inter-experimental robustness achievable than the static model.

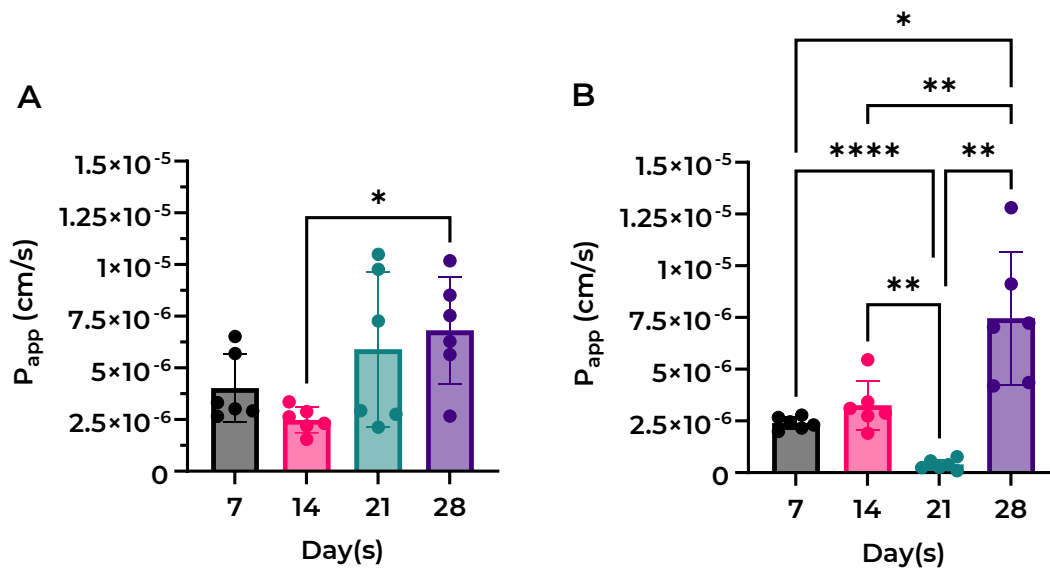


Figure 3.17: Perfusion resulted in a consistent Calu-3 barrier for up to 21 days. P_{app} of NaFL across the 28-day ALI culture for the **(A)** static and **(B)** perfused Calu-3 Transwell and MPS models. (ANOVA * = $P < 0.05$, ** = $P < 0.001$, *** = $P < 0.0002$, **** = $P < 0.0001$) (N=6).

To understand more about the functionality of the models over time, an optimised alcian blue mucus quantification assay was used to quantify acidic mucins produced by goblet cells. PBS washes from Day 2 post-ALI onwards were collected and analysed. From Figure 3.18 A, it can be confirmed that the mucin expression of the static model reached its highest level at Day 21 and was maintained until Day 28, whereas the perfused model reached the highest value at Day 14, and this was maintained until Day 28 (Figure 3.18 B). The data became more variable in both the static and perfused models from Day 14 onwards, compared to Days 2 and 7 which had more consistent values. There was no significant difference between the amount of mucus generated from the static and perfused model for day-to-day comparators.

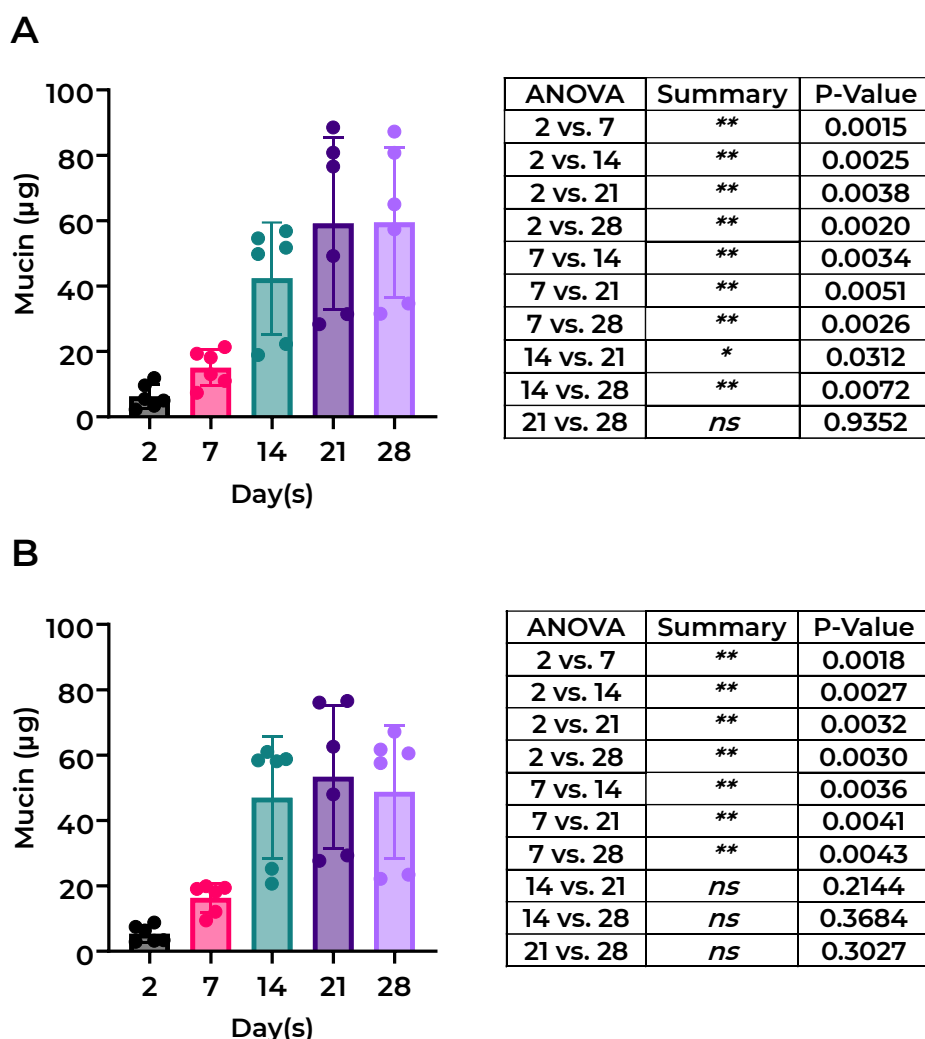


Figure 3.18: Maximum mucus expression was reached at Day 14 for both the perfused model and static model. Mucus quantification of the PBS wash post-TEER measurements on Days 2, 7, 14, 21 and 28 for the **(A)** static and **(B)** perfused Calu-3 Transwell models with the tables showing the statistical differences between the days within the condition as evaluated using an ANOVA statistical test. (ANOVA * = $P < 0.05$, ** = $P < 0.001$) (N=6)

Within this experiment, a Calu-3 epithelial barrier was formed by Day 2 ALI for static and perfused models and was successfully maintained until Day 28, as confirmed by the TEER measurements. The perfusion resulted in the Calu-3 MPS model generating a more consistent barrier for 21 days with reduced variance and a faster rate of differentiation, leading to a tighter barrier than the static model at Day 7 and Day 21. The maximum mucus expression was reached at Day 14 for the perfused model, up to 7 days faster than static model. This confirmed that by Day 7, the perfused model had established a functionally tight barrier that could be used to investigate transport/flux of inhaled drugs, such as β_2 -adrenergic receptor agonists.

3.5. CHAPTER CONCLUSIONS

The aim of this Chapter was to characterize the effects of long-term culture during perfused culture of the Calu-3 Transwell model at an air-liquid interface utilising a microphysiological system. This was successfully achieved, and the data generated has identified the perfused model to differentiate into an effective barrier by Day 7 ALI with key bronchial epithelium characteristics such as mucus expression and tight junction formation. These features were maintained until Day 21 ALI, highlighting the perfused model can be used for assessment between Day 7 and Day 21 of ALI culture. The static model showed similar features, however, it required up to 7 days longer to establish a barrier similar in function to the perfused model at Day 14 ALI. Again, this is maintained until Day 21 ALI however, the static model had much higher functional variability than the perfused model. This led to the conclusion that the perfused Calu-3 epithelial model generated a more consistent, bronchial-like epithelium seven days sooner than the static model, increasing the throughput of the model by reducing the minimum culture period required before use in the various assessments e.g. stimulation, drug studies, disease modelling etc. Moving forward, the perfused Calu-3 model will be assessed from Day 7 ALI and the assays established will be used to assess the model in the coculture format with human bronchial smooth muscle cells in the next chapters.

Chapter Four

Development of the Perfused Bronchial Coculture Model

4. DEVELOPMENT OF THE PERFUSED BRONCHIAL COCULTURE MODEL

4.1. INTRODUCTION

In the lungs, the epithelial layer is attached to a basement membrane which separates the epithelial layer and the layer below, the lamina propria, which consists of fibroblasts and immune cells embedded in extracellular matrix (ECM) expressed by the fibroblasts (Lan *et al.*, 2018b). ECM is made up of proteins such as elastin, laminins, fibronectin, and collagen (Liu *et al.*, 2021). Collagen is the main component of ECM proteins with fibrillar collagen type I, II, III, V and XI making up almost 90% of total collagen content. Collagen type I and III are most abundant in the lung tissue with the former being rigid, while type II is more pliable (Asgari *et al.*, 2017; Ricard-Blum, 2011).

The smooth muscle layer is located below the lamina propria, (Lan *et al.*, 2018b). Smooth muscle lines the airway walls from the upper airways down to the alveoli (Lumb, 2016). There is a positive correlation between the thickness of the bronchial smooth muscle and the diameter of the airway lumen (Ebina *et al.*, 1990). Bronchial smooth muscle cells (BSMCs) have a fusiform shape with a single nucleus, in contrast to skeletal muscle, which is multinucleated (Lumb, 2016) (Figure 4.1). BSMCs maintain minimal tone in the airways and are crucial in regulating the calibre of the airways (Yan *et al.*, 2018). They control the distribution of airflow throughout the lung and mediate functions such as deep breathing, forced expiration and coughing (James & Carroll, 2000). The smooth muscle cells run in various directions, unlike skeletal muscle which is organised in striations (Figure 4.1) (Stanfield, 2016). This organisation allows contraction in various directions. In proximal biopsies obtained through bronchoscopy, airways smooth muscle cells have been shown to be close to the epithelial layer (Pepe *et al.*, 2005) (Figure 4.2). This proximity of the different cell types may have an impact on the phenotype expressed by the cells of the two tissue layers.

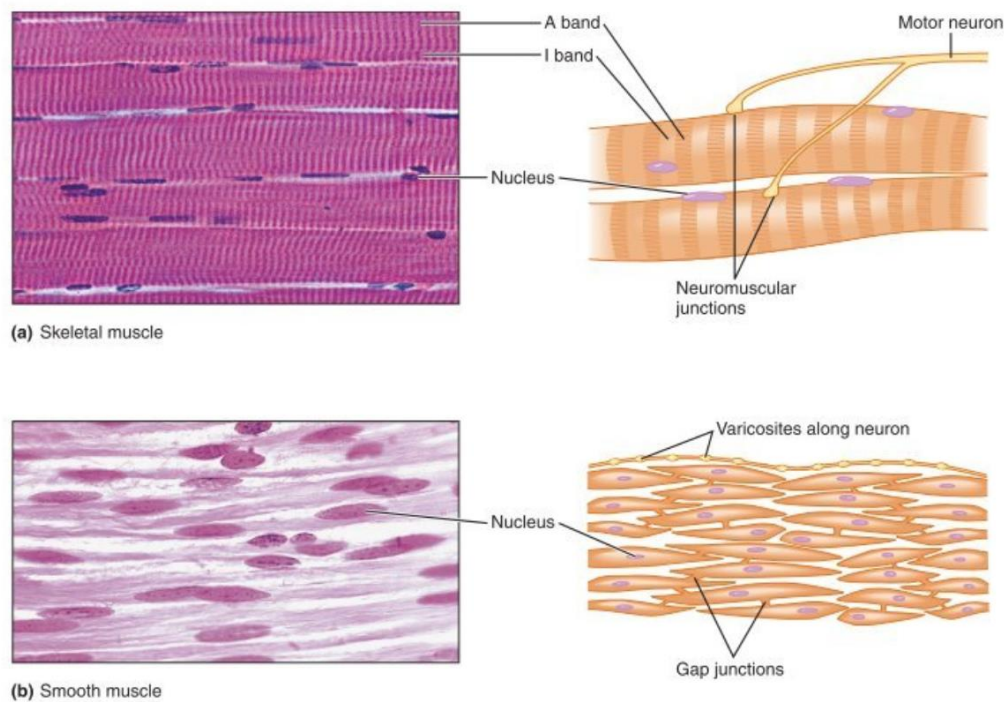


Figure 4.1: Comparison of the histology cross-section images and diagrams of the (A) structure of skeletal muscle cells and the (B) structure of smooth muscle. Figure taken from (Stanfield, 2016).

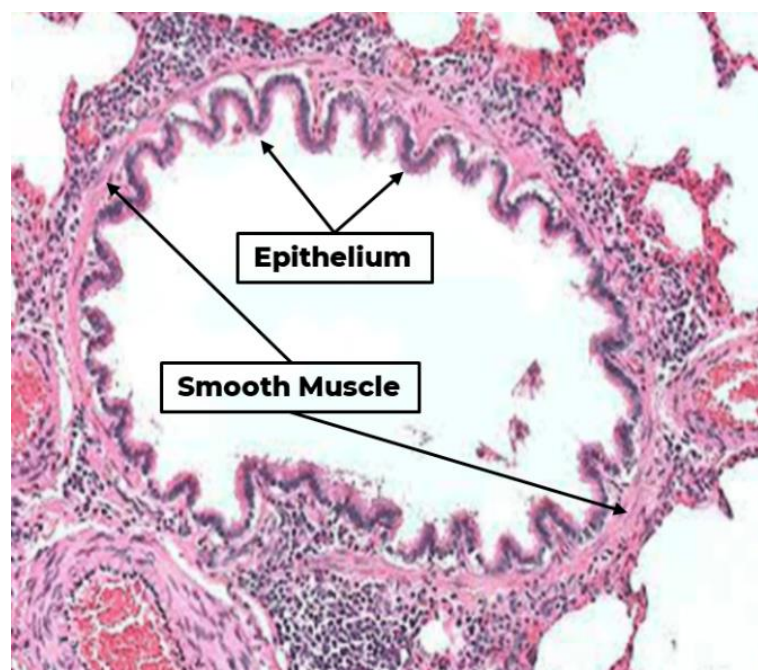


Figure 4.2: Histology cross-section image of the human bronchiole wall highlighting the proximity of the epithelium and smooth muscle tissue layers. Image obtained from (Sheffield, 2017)

4.1.1. CONTRACTION AND RELAXATION IN SMOOTH MUSCLE CELLS

The maturation and differentiation of smooth muscle cells is characterised by the expression of contractile proteins (Mack, 2011). These cells exhibit several markers of differentiation or maturation including alpha-smooth muscle actin (α -SMA), calponin, transgelin (TAGLN or SM22) and SM-MHC isoforms (Latif *et al.*, 2015). Alongside the latter proteins, myosin heavy chain (MYH11) is the major contractile protein in smooth muscle. MYH11 contains a region that can bind to actin thereby facilitating the shortening of the muscle fibre (J. R. Sellers *et al.*, 1985). α -SMA is another major contributor to smooth muscle contraction. It is a protein that forms the filament lattice to which myosin heads attach to shorten the muscle (Webb, 2003). SM22 is a protein that binds to actin filaments and generates a more ordered actin filament network (Shapland *et al.*, 1993). Alterations in the expression or activity of MYH11, α -SMA, and SM22 could contribute to changes in smooth muscle force production, shortening capacity or shortening velocity (Pascoe *et al.*, 2015).

Smooth muscle contraction is regulated through intracellular calcium ions (Ca^{2+}). Ca^{2+} is released from within the cell or from extracellular space through the activation of muscarinic acetylcholine receptors (M_2 and M_3) by acetylcholine. (Cazzola *et al.*, 2012; Matera *et al.*, 2020; Meurs *et al.*, 2013). Once the Ca^{2+} enters the cytoplasm, it then starts a signalling cascade that eventually activates myosin light chain kinase (MLCK). Once this has occurred, the actin filaments are pulled inward by the myosin which leads to the muscle cell shortening and resulting in contraction (Sieck & Gransee, 2012; Stanfield, 2016). Relaxation is thought to occur because of the decrease in intracellular Ca^{2+} concentrations in the smooth muscle cells. This is through the closing of the calcium channels subsequently stopping the flow of Ca^{2+} into the cell or by the sarcoplasmic reticulum absorbing the excess Ca^{2+} (Webb, 2003).

4.1.2. BRONCHIAL SMOOTH MUSCLE IN DISEASE STATES

Bronchial epithelial cells and smooth muscle cells play a significant role within the pathogenesis of chronic lung disease. For example, bronchial epithelial damage results in enlarged smooth muscle mass and increased cytokine production in asthma pathology (Deacon & Knox, 2015; Güney *et al.*, 2021; Humayun *et al.*, 2018). Asthma is a chronic inflammatory disorder of the airways with increased responsive of the bronchi to various stimuli resulting in episodes of coughing, wheezing and chest tightness. Characteristics include remodelling and narrowing of the airways with increased smooth muscle content, non-specific airway hyperresponsiveness and hypersecretion of mucus. Together, these limit the effectiveness of bronchodilators (Ward, J.P.T., Ward, J. and Leach, 2010). It has been reported that the distance between the basal membrane of epithelial cells and smooth muscle layer in the airways of asthmatic patients was shorter compared to healthy subjects (Celle *et al.*, 2022;

Pepe *et al.*, 2005). The thickening of the smooth muscle layer in airway walls is the most significant characteristic of bronchial remodelling, with links between the increased smooth muscle mass to asthma severity shown in adults and children (Beaufils & Berger, 2022).

Increased smooth muscle thickness has also been observed in chronic obstructive pulmonary disease (COPD) patients with airway hyperreactivity, and the area of the smooth muscle is greater than healthy subjects but not as much as asthmatic patients (Kuwano *et al.*, 1993; Riess *et al.*, 1996). COPD is a diagnosis that includes several respiratory pathologies including inflammation, remodelling of the lower airways and lung parenchyma together with activation of inflammatory and immune processes. Due to the increasing habit of cigarette smoking, COPD prevalence is increasing globally (Uwagboe *et al.*, 2022). As previously mentioned, changes in the expression of MYH11, α -SMA and SM22 in smooth muscle cells could contribute to changes in smooth muscle force production, shortening capacity or velocity. These proteins are therefore being considered as targets to treat the exaggerated airway narrowing of airway hyper-responsiveness in asthma and other disease states (Pascoe *et al.*, 2015).

4.1.3. PRIMARY BRONCHIAL EPITHELIUM AND PRIMARY SMOOTH MUSCLE COCULTURE CELL MODELS

Animal *in vivo* models are used for a whole organism response to potential inhaled drugs as well as inducing respiratory diseases to unveil potential targets for drugs (Y. Wang *et al.*, 2018; Williams & Roman, 2016). However, most animal models have a significant lack of disease features that are present in humans and the deposition of inhaled compounds is different to human oral inhalation (Movia *et al.*, 2020; Ogi & Aruga, 2013; Yaddanapudi *et al.*, 2013). Animal models have a limited predictability of human response due to cross species differences, resulting in 90% of drugs failing at human trials after positive animal studies (B. Jiang *et al.*, 2014; Moeller *et al.*, 2008; Mullard, 2016; van der Worp *et al.*, 2010). This highlights the need for *in vitro* models that can address concerns of better reflecting *in vivo* anatomy and (patho-)physiology to study disease and evaluating drug transport and responses (Ge *et al.*, 2010; Kasper *et al.*, 2013).

The communication between epithelial cells and smooth muscle cells in the airways is a crucial aspect in the response of smooth muscle cells to pathogens and air pollutants. These stimulants interact with the epithelium, triggering responses in the smooth muscle leading to airway contraction which can be exacerbated in chronic lung diseases such as asthma or COPD leading to increase smooth muscle proliferation and airway obstruction and narrowing (Chung & Adcock, 2008; Erle & Sheppard, 2014). The bronchial epithelium can release mediators which diffuse through the lamina propria to act on the smooth muscle, resulting in

airway narrowing, which is exacerbated in asthma and COPD patients (Humayun *et al.*, 2018). Studies have shown that the epithelium influences smooth muscle in healthy conditions too (Abohalaka, 2023). Airway epithelium is also the primary source of endogenous neurotransmitters that result in airway smooth muscle relaxation (Gallos *et al.*, 2013).

Cell culture models of the bronchial epithelium have been developed to provide a basis for studying drug transport and uptake, with the 2D monocultures of epithelial cells most suited for low cost, high throughput screening. However, they are reductionist due to their lack of complexity and a result are less suited to monitor changes in the epithelial barrier because of disease or the therapeutic effectiveness of drugs on the target cells (Haghi *et al.*, 2015). Combining two or more cell types into the same cell culture model is defined as a coculture model. Coculture can be direct or indirect: direct coculture is where cells share a culture well and are in direct contact with one another, indirect coculture involves a physical separation of the cells, but they share the same medium (Vis *et al.*, 2020). Transwell inserts are commonly used to compartmentalise different cell types within the same well.

Interest in understanding the interactions between smooth muscle and epithelium has been increasing, particularly how the interactions contribute to respiratory disease (Deacon & Knox, 2015). Co-culturing requires a highly specific environment to meet the potentially disparate requirements of the different cell types and, therefore, requires optimisation. This can achieve the goal of developing more complex, reproducible, *in vitro* tissue models (Vis *et al.*, 2020). There have been several coculture models of bronchial epithelial cells cultured with airway smooth muscle cells for various purposes. In one such study, primary normal bronchial epithelial (NHBE) cells were differentiated in ALI for 14 days before mechanical compression was applied via a silicon plug on the top of each Transwell, creating a seal pressure chamber over the apical surface of the NHBE cells, resulting in a continuous apical-to-basal transcellular pressure similar to that predicted during maximum airway constriction during an asthma exacerbation (Lan *et al.*, 2018b). The basolateral media collected from compressed epithelial cells were transferred to primary airway smooth muscle cells and this indirect coculture was cultured for 1 h prior to administration of a histamine contraction stimulus. This coculture was observed to amplify the contractile response of BSMCs (Lan *et al.*, 2018b).

Malavia *et al* (2009), reported an indirect coculture model of NHBE differentiated at ALI for 14-21 days on Transwells before an 8-day coculture with BSMCs grown on the baseplate. This coculture increased the proliferation of BSMCs with a higher level of inflammatory chemokines in the coculture supernatant such as IL-6, IL-8, and matrix metalloproteinase (MMP-9) than BSMCs only (Malavia *et al.*, 2009). The coculture with the chemokines contributed to the BSMCs proliferation, observed by injuring the epithelium leading to an increase of MMP-9

released from the epithelium which in turn increased BSMCs proliferation, as seen *in vivo* when rabbit trachea was injured leading to increase smooth muscle mass (Malavia *et al.*, 2009).

Another model of an indirect coculture was produced to investigate rhinovirus-induced asthma exacerbation by the culture of NHBE at ALI for 21 days before exposure to the rhinovirus. The culture medium was then used in culture with either asthmatic BSMCs or non-asthmatic BSMCs on a baseplate for 24 h, resulting in asthmatic BSMCs migrating towards the epithelial layer as seen *in vivo* in severe asthmatic patients and was not seen in the non-asthmatic BSMCs. There are no *in vivo* models for non-allergic severe asthma, and so this model filled an area of unmet need (Celle *et al.*, 2022). However, this was again an indirect coculture and so the model lacked the physiological relevance of the proximity of the cell types as is the model reported by Malavia *et al.*, (2009). In a model reported by Haghi *et al.* (2015), NHBE cells were cultured at ALI for 72 h before a coculture with BSMCs grown on the baseplate to assess the transport of bronchodilators, specifically salbutamol (Haghi *et al.*, 2015). This model not only lacked relevant coculture contact time with the BSMCs, but also the time required for differentiation of the epithelium as primary epithelium was differentiated for at least 14 days in the previously discussed models.

4.1.4. CELL LINE AIRWAY EPITHELIUM AND PRIMARY SMOOTH MUSCLE COCULTURE MODELS

Only a single coculture model pairing smooth muscle with an epithelial cell line (rather than primary cell), other than Calu-3, was identified. In this study, the BEAS-2B epithelial cell line or NHBE cells were indirectly cocultured with human BSMCs on a base plate for 24 h, resulting in a proliferative phenotype of the smooth muscle cells with down regulated α -SMA a lower intracellular calcium concentration and higher cAMP level in response to histamine, which is a molecule that elicits contraction in BSMCs (O'Sullivan *et al.*, 2017). Humayun *et al.* (2018) described a OOC model of Calu-3 epithelium grown at ALI for 7 days before a 7-day direct coculture with BSMC on a hydrogel platform that incorporated airflow and pollutant exposures. The coculture showed the Calu-3 retained tight junction expression in a monolayer whilst the BSMC expressed α -SMA as confirmed by immunofluorescence staining (Humayun *et al.*, 2018). Despite the model being developed to include the perfusion of fluid and air, this study did not detail their incorporation, resulting in the lack of physiological relevance of the model.

Muddle *et al.*, (2020) reported a Transwell coculture model with a similar set up to Haghi *et al.* (2015) but used the Calu-3 epithelial cell line instead of primary bronchial epithelium. The Calu-3 epithelium was cultured for 11-14 days at ALI before use during the deposition of salbutamol onto the epithelium, whilst in indirect coculture with BSMCs on the baseplate of

the culture well for 30 min. The model was described as a bioassay interfaced with an aerosol deposition system that could be used as an alternative to *in vivo* pharmacodynamics to compare different formulations of inhaled drugs (Haghi *et al.*, 2015; Muddle *et al.*, 2020). The presence of the Calu-3 layer significantly reduced the transport of salbutamol sulphate from the donor to receiver chamber compared to a Transwell with no epithelial cells, showing 30 min to be the effective incubation time to produce reproducible and sensitive cAMP response from the BSMC cultured on the baseplate (Muddle *et al.*, 2020).

Table 4.1 summarises all the *in vitro* coculture models described with the increased the complexity and human lung relevance; However, the cocultures reported by Haghi and Muddle were not maintained for longer than 72 h (Haghi *et al.*, 2015; Muddle *et al.*, 2020) whilst the previous models reported by Malavia and Lan only used the medium of the epithelial cells after stimulation (Lan *et al.*, 2018b; Malavia *et al.*, 2009). Therefore, the cells were not established in coculture for enough to indicate an influence on the cell-to-cell signalling or resultant differentiation due to the coculture environment, so this is an area that is yet to be fully investigated.

Table 4.1: Summary of all coculture models discussed. Normal Human Bronchial Epithelium (NHBE), Bronchial Smooth Muscle Cells (BSMCs), air-liquid interface (ALI), BEAS-2B (human epithelial cell line).

Epithelial Cells	Smooth Muscle Cells	ALI Period	Coculture period	Application	Indirect or Direct	Reference
NHBE	BSMCs	14 days	1 hour	Disease Model	Indirect	(Lan <i>et al.</i> , 2018b).
NHBE	BSMCs	14-21 days	8 days	Epithelium Injury	Indirect	(Malavia <i>et al.</i> , 2009)
NHBE	BSMCs and Asthmatic BSMCs	21 days	1 day	Disease Model	Indirect	(Celle <i>et al.</i> , 2022)
NHBE	BSMCs	3 days	3 days	Drug Transport	Indirect	(Haghi <i>et al.</i> , 2015)
NHBE or BEAS-2B	BSMCs	N/A	1 day	Contraction Model	Indirect	(O'Sullivan <i>et al.</i> , 2017)

Calu-3	BSMCs	7 days	7 days	OOC Model	Direct	(Humayun <i>et al.</i> , 2018)
Calu-3	BSMCs	11-14 days	30 minutes	Drug Transport	Indirect	(Muddle <i>et al.</i> , 2020)

4.2. CHAPTER AIMS

The aim of this Chapter was to develop and assess a more complex, functional, and physiologically representative coculture model of differentiated Calu-3 epithelium cultured at air-liquid interface and primary bronchial smooth muscle cells cultured either side of a Transwell insert for a prolonged period. This required the investigation into the viability of seeding BSMCs on the basolateral face of a Transwell insert as well as optimising the seeding density of BSMCs in co- and monoculture. The effect of culture medium composition and perfusion was also assessed, utilising assays previously explored including transepithelial electrical resistance (TEER) apparent permeability (P_{app}) of sodium fluorescein (NaFL), mucin quantification, immunofluorescence (IF) staining and qPCR to characterise the coculture model and the resultant effects of the perfusion from the culture in the Barrier-12 plate used in conjunction with the PhysioMimix OOC system.

4.3. METHODS AND MATERIALS

4.3.1. BRONCHIAL SMOOTH MUSCLE SEEDING DENSITY AND PLACEMENT OPTIMISATION

The primary bronchial smooth muscle cells were sourced from Lonza (Lonza, 2024) as a reputable cell provider with sustainable, reliable stock levels that were commercially accessible within the cost limitations of the project budget. The primary BSMCs required a Lonza specific medium, Smooth Muscle Cell Growth Medium (SmGM). This medium was made up with multiple supplements that are listed in Table 4.1 and the medium kit was purchased alongside the cells. The donor of the primary BSMCs was a 65-year-old Caucasian male that was a non-smoker. The optimum seeding density and the placement of the BSMC had to be determined and the two locations chosen were the baseplate of the 24-well Transwell plates similar to the previously-described models (Haghi *et al.*, 2015; Malavia *et al.*, 2009; Muddle *et al.*, 2020) and the basolateral face of the Transwell insert membrane to decrease the distance between the epithelium and smooth muscle cells, replicating (Humayun *et al.*, 2018). Three densities were chosen using the previous models as guidance: 3,000 cells/well (1×10^4 cells/cm²) (Malavia *et al.*, 2009), 15,000 cells/well (8×10^4 cells/cm²), and 30,000 cells/well (1.5×10^4 cells/cm²) (Haghi *et al.*, 2015; Muddle *et al.*, 2020).

BSMC cells were maintained as described in Section 2.5.3. For seeding BSMCs on the basolateral face of the Transwells, the Transwells were flipped upside down in a sterile empty tip box in an MSBC. The BSMCs were detached from culture flasks as previously described in Section 2.3.1.2 and resuspended and counted. After counting, the cells were diluted to the densities described above. 50 μ L of the cell suspension was added to the basolateral face of each Transwell (n = 3 replicates) and then the droplet was supplemented with 25 μ L of medium. The lid was then closed on the box and the box carefully transferred to an incubator for 2 h minimum to allow the cells to attach to the membrane. Thereafter, the Transwell inserts were flipped into a 24-well culture plate and 200 μ L medium was added to the apical compartment and 600 μ L of medium was added to the basolateral chamber. After 48 h, the apical medium was removed.

For the baseplate seeding of the BSMCs, the cells were detached and counted as previously described. Thereafter, the cells were diluted to the three densities and 600 μ L of the cell suspension was added to the 24-well plate and incubated for 48 h before the first change of medium. Medium changes were performed on each well on Days 2 and 5 before the endpoint analysis on Day 7.

Table 4.2: Supplements in the Lonza Smooth Muscle Cell Growth Medium (SmGM). Components in the SmGM medium with the final concentrations and their purposes in *in vitro* cell culture

Name	Concentration	Purpose	References
Human Epidermal Growth Factor (hEGF)	3 ng/ml	Stimulates proliferation in epithelial cells	(Fitzgerald <i>et al.</i> , 2001)
Human Fibroblastic Growth Factor (hFGF)	2 ng/ml	Regulates biological functions such as cellular proliferation, survival, and differentiation.	(Yun <i>et al.</i> , 2010)
Gentamicin sulphate and Amphotericin (GA-1000)	30 µg/ml Gentamicin and 15 ng/ml Amphotericin	Gentamicin: broad spectrum antibiotic preventing bacterial infection Amphotericin: antifungal agent preventing yeast and multicellular fungi	(<i>Amphotericin B</i> , 2024; <i>Gentamicin</i> (50 Mg/mL), 2024)
Insulin	0.1%	Acts as a growth factor with anti-apoptotic and mitogenic effects, synergistic with hFGF.	(Straus, 1981)
Foetal Bovine Serum (FBS)	5%	Nutrients for cell growth	(<i>The Basics of Fetal Bovine Serum Use</i> - UK, 2024)

On Day 7, the several assays to determine cell health and differentiation were performed. The CytoTox 96® Non-Radioactive Cytotoxicity Assay (Promega, USA) for the determination of cell stress/cytotoxicity through the detection of intracellular lactate dehydrogenase (LDH) released by lysed cells. The manufacturer protocol was followed. Briefly, 50 µL of the cell culture medium was taken and placed in a black bottomed 96-well plate and 50 µL of the LDH Substrate Mix was added in the same well. The plate was incubated for 30 min on a plate shaker and then 50 µL of the Stop Solution was added. The plate was then read on the Byonoy Absorbance 96 Plate Reader (Enzo Life Sciences, UK) at 490 nm. Cell Titer-Glo® luminescence assay (Promega, USA) was used to determine cell number by the amount of ATP present in the cells. The manufacturer's protocol was followed. Briefly, 100 µL of the Cell Titer-Glo substrate solution was added to the cell layer and left to incubate in the dark at room temperature for 12 min before 100 µL of cell culture medium was added and then the 200 µL

solution was transferred to a black bottomed 96 well plate and the samples were read on the FLx800 Fluorescence plate reader. The cells were stained in accordance with Section 2.5.13 with volumes adjusted for the baseplate. The primary antibody used was anti-mouse alpha-smooth muscle actin Catalogue Number:14-9760-82 (Sigma Aldrich, UK) and the secondary antibody used was Alpha-Smooth Muscle Actin Monoclonal Antibody (1A4), eBioscience™ # 14-9760-82 and, Goat anti-Mouse IgG (H+L), Superclonal™ Recombinant Secondary Antibody, Alexa Fluor™ 488 #A28175 (Thermo Fisher Scientific, UK).

4.3.2. ESTABLISHING THE COCULTURE MODEL IN STATIC CONDITIONS AND MEDIUM OPTIMISATION

Calu-3 cells and BSMC cells were maintained as described in Section 2.5.2 and Section 2.5.3, respectively. BSMC and Calu-3 cells were seeded as described in Section 2.5.7, but the PhysioMimix system was not employed for these optimisation experiments. The media evaluated for culturing were either 100% of the smooth muscle medium (SmGM) or a 50:50 (v/v) ratio of the SmGM: Calu-3 Medium. Cells were either seeded as Calu-3 monoculture, BSMC monoculture or coculture on either side of a Transwell in either 50:50 SmGM: Calu-3 medium or 100% SmGM medium. The culture was raised to ALI after 48 h and maintained for 14 days with medium changes every 2-3 days. TEER was performed at every change of medium as described in Section 2.5.9. The CytoTox 96® Non-Radioactive Cytotoxicity Assay (Promega, USA) for the determination of cell stress through the detection of lactate dehydrogenase (LDH) release was performed at Day 0, 2 7 and 14 ALI. The manufacturer protocol was as described in Section 4.3.1, above. Mucus quantification assay was performed as described in Section 2.5.10 on Days 7 and 14 ALI. Apparent permeability (P_{app}) was performed as described in Section 2.5.11 on Days 7 and 14 of ALI.

4.3.3. EVALUATING THE EFFECTS OF PERFUSION ON THE COCULTURE MODEL

Calu-3 cells and BSMC cells were maintained as described in Section 2.5.2 and Section 2.5.3, respectively. BSMC and Calu-3 cells were seeded as described in Section 2.5.7 and cultures were maintained for 7 days. The culture was raised to ALI after 48 h and maintained for 14 days with medium change every 2-3 days. TEER was performed at every change of medium as described in Section 2.5.9.

Mucus quantification assay was performed as described in Section 2.5.10 on days 7 and 14. Apparent permeability (P_{app}) was performed as described in Section 2.5.11 on days 7 and 14 of ALI. Fixation and immunofluorescence were conducted as described in Section 2.4.13. The primary antibodies used were ZO1 anti-rabbit # 40-2200 and Alpha-Smooth Muscle Actin Monoclonal Antibody (1A4), eBioscience™ #14-9760-82 and the secondary antibodies were Goat anti-Rabbit IgG (H+L) Highly Cross-Adsorbed Secondary Antibody, Alexa Fluor™ Plus

488 Cat #A32731 and Goat anti-Mouse IgG (H+L) Highly Cross-Adsorbed Secondary Antibody, Alexa Fluor™ Plus 647 Cat # A32728 (Thermo Fisher Scientific, UK). The immunofluorescence stains used were Phalloidin–Tetramethylrhodamine B isothiocyanate Cat #P1951 (Sigma Aldrich, UK) for the staining of F-actin in the cell cytoskeleton and Hoechst 33342 Cat #H3570 (Thermo Fisher Scientific, UK) for staining DNA. Quantitative Polymerase Chain Reaction (qPCR) was performed as described in Section 2.3.12 with Taqman primers α -SMA (ACTA2) and SM22 (TAGLN) Cat # 4351372 (Thermo Fisher Scientific, UK). Histology was performed as described in Section 2.5.14.

4.4. RESULTS AND DISCUSSION

4.4.1. BRONCHIAL SMOOTH MUSCLE SEEDING DENSITY AND PLACEMENT OPTIMISATION

When developing the coculture model described in this chapter, sourcing the bronchial smooth muscle proved a challenge as there was not an established bronchial smooth muscle cell line that was commercially and readily available. Although there are some immortalised smooth muscle cells (T0493 | Immortalized Human Bronchial Smooth Muscle Cells - Academic, 2024), they were not readily available for purchase and would prove difficult to be a sustainable source. Alongside this, there is limited published research to support the use of these cells. Stem cells were considered but as previously discussed in Chapter 1, they are expensive and complex to culture and can easily lose the phenotype induced, alongside the ethical concerns of the origins of the cell source. Again, this was not a sustainable, commercially available cell source.

Primary bronchial smooth muscle cells were more readily available from several reputable cell repositories including ATCC (American Type Culture Collection) (Primary Bronchial/Tracheal Smooth Muscle Cells; Normal, Human - PCS-130-011 | ATCC, 2024) and ABM (Applied Biological Materials Incorporated) (Immortalized Human Bronchial Smooth Muscle Cells | Applied Biological Materials Inc., 2024). However, the cells from ABM were priced outside of the project budget and ATCC did not have the cells available at the time of enquiry. The primary bronchial smooth muscle cells (BSMCs) from Lonza had a reasonable variety of donors with and without disease states and a large repository of cell vials available for purchase. Lonza was identified as the vendor of choice due to the availability of the number of vials and the cost of each vial keeping within the budget of the project, with potential to expand to disease state cells (Lonza, 2024).

The cell density of BSMCs was optimised on the basal face of a Transwell insert to produce a more *in vivo*-like architecture of the Calu-3 epithelium and BSMC cell layers. As this was a novel concept of seeding on a Transwell for this coculture, the seeding on the basal face of the membrane required optimisation. Seeding densities from previous studies of BSMC and lung epithelium cocultures were used as a guide for surface area densities of BSMCs. Three densities were chosen using the previous models as guidance: 3,000 cells/well (1×10^4 cells/cm²) (Malavia *et al.*, 2009), 15,000 cells/well (8×10^4 cells/cm²), and 30,000 cells/well (1.5×10^4 cells/cm²) (Haghi *et al.*, 2015; Muddle *et al.*, 2020). This was then seeded on the basal face of Transwells, and the equivalent densities were seeded on the 24-well plate the Transwells are shipped in (baseplate).

In both the Transwell-seeded and baseplate-seeded cell groups, there was no significant difference in the number of viable BSMCs observed at Day 7 of culture (Figure 4.3 A). This confirms the equivalence of outcome for seeding densities of 30,000 cells/well and 3,000 cells/well, as both result in the same number of cells by Day 7 which was around 40,000 cells/well. The 30,000 cells/well density increased by one third of its original population whereas the 3,000 cells/well increased by 13.3 times. An interesting result was the large variance in the number of cells at Day 7 in the baseplate seeded cells. There is understandably a larger cell number present in the baseplate seeded compared to the Transwell seeded cells, as the cells have a larger surface area upon which to grow (0.332 cm² Transwell compared with 1.9 cm² baseplate well). However, there was significantly higher variance in the cell growth on the baseplate compared to the Transwell insert, with the larger error bars in the 15,000 cells/well seeding density, resulting in no significant difference calculated between the Transwell and baseplate seeding locations. This may be a result of increased error in seeding cells as they are less likely to be homogenous in the larger seeding volumes required for the baseplate compared to the Transwell.

The cell stress exhibited by the location of the seeding was investigated. The objective for this assessment was to understand if the effect of seeding the cells on the basolateral face of the Transwell had a detrimental effect on the cell viability of the BSMCs. The Transwell-seeded cells displayed no more stress than the baseplate-seeded cells at the same density, and this was seen across all three densities (Figure 4.3 B). There was an increase in the amount of LDH release in the higher densities, but this can be explained by the larger number of cells, and therefore more pronounced LDH release is detected from cellular activities such as proliferation.

The formation of the BSMCs at each location and concentration was analysed using immunofluorescence microscopy (Figures 4.4-4.6). The images showed a positive staining of α -SMA in all cell densities after 7 days of culture with the smooth muscle cells growing in multiple directions, however this was more prominent in the Transwell insert seeded cells than the baseplate similar to the *in vivo* morphology of smooth muscle cells (Stanfield, 2016). The cells aligned in muscle-like fibres in both seeding locations, positively expressing the α -SMA contractile proteins confirming the characteristic smooth muscle contractile phenotype was retained.

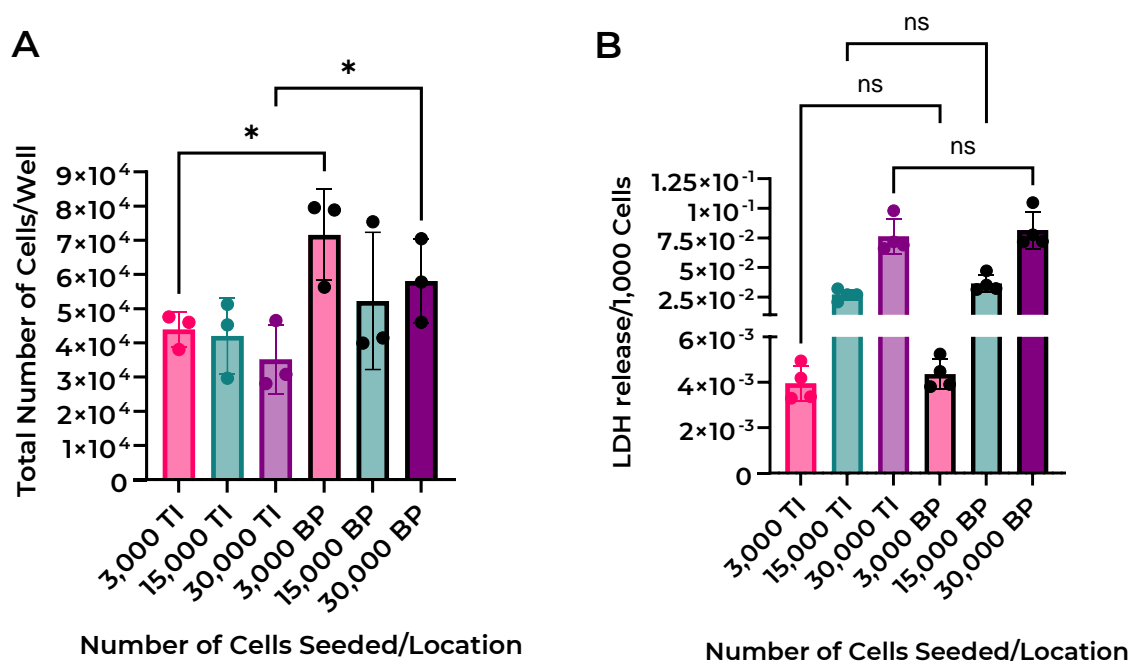


Figure 4.3: Transwell- or baseplate-seeded BSMCs showed little significant difference in cell number or cellular stress after 7 days of culture. BSMCs were seeded at three densities (3,000, 15,000 or 30,000 cells/well) on either the baseplate of the well (BP) or on the underside of the Transwell (TI). **(A)** Total cell number and **(B)** LDH release were assessed after 7 days of culture (ANOVA ns = $P > 0.05$, * = $P < 0.05$) ($N \leq 3$)

The intensity of the α -SMA immunofluorescence was measured as a ratio of the DNA stain (Hoechst 33342) and examined for the impact of the seeding densities and locations (Figure 4.7 A), which revealed the baseplate to have a higher ratio of α -SMA intensity compared to the Transwell. No significant difference was observed in the α -SMA intensity between the seeding densities on the baseplate seeding location. However, this was not the case for the three densities on the Transwell insert. 3,000 cells/well density on the Transwell insert had a significantly higher intensity of α -SMA on the Transwell insert compared to the other two densities (Figure 4.7 B), implying that there was more α -SMA present per cell as the number of cells were similar between the three densities on the Transwell insert (Figure 4.3 A).

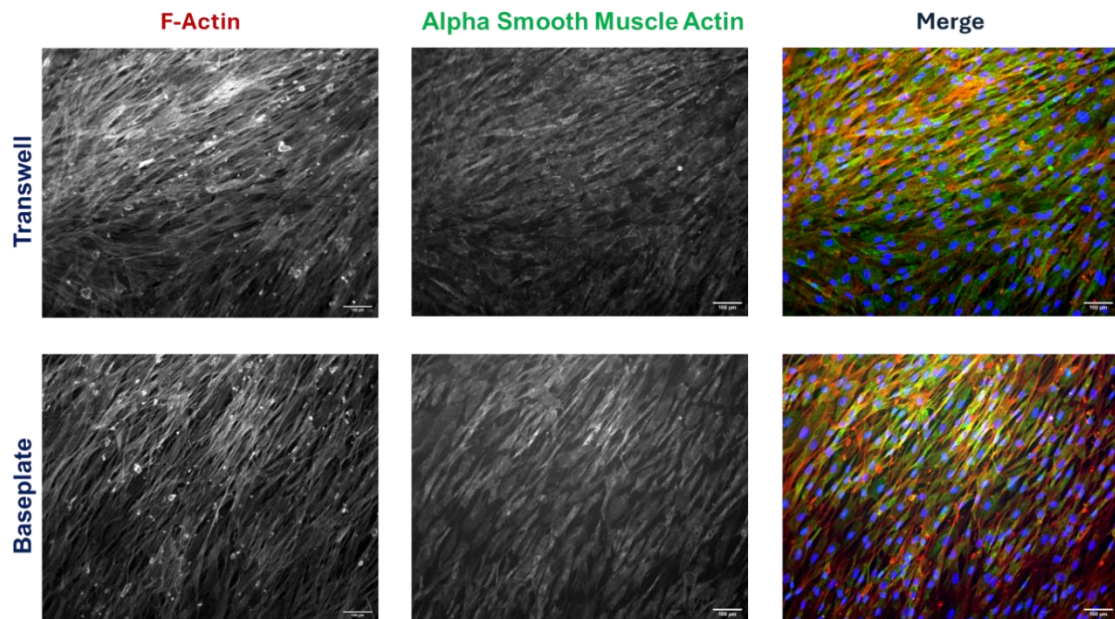


Figure 4.4: Baseplate and Transwell-seeded BSMCs at 3,000 cells/well were morphologically similar. 3,000 BSMCs were seeded on either the baseplate or the underside of a Transwell insert for 7 days, before being fixed and stained using antibodies against anti- α -SMA (green), Phalloidin (actin- red) and Hoescht-3332 (DNA – blue). Scale bar = 100 μ m.

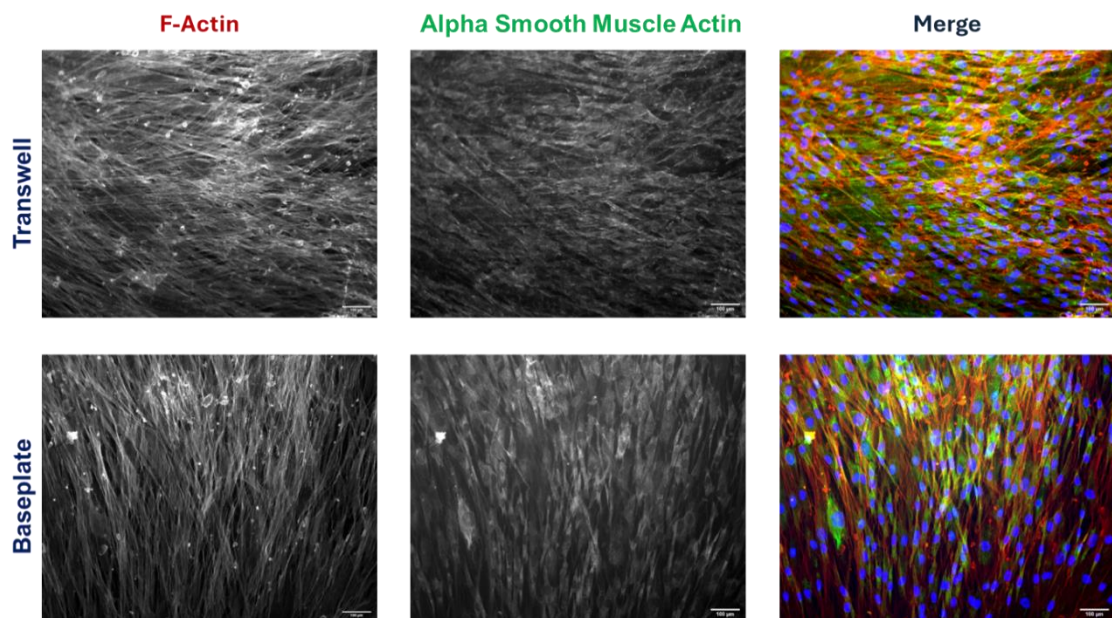


Figure 4.5: Baseplate and Transwell-seeded BSMCs at 15,000 cells/well were morphologically similar. 15,000 BSMCs were seeded on either the baseplate or the underside of a Transwell insert for 7 days, before being fixed and stained using antibodies against anti- α -SMA (green), Phalloidin (actin- red) and Hoescht-3332 (DNA – blue). Scale bar = 100 μ m.

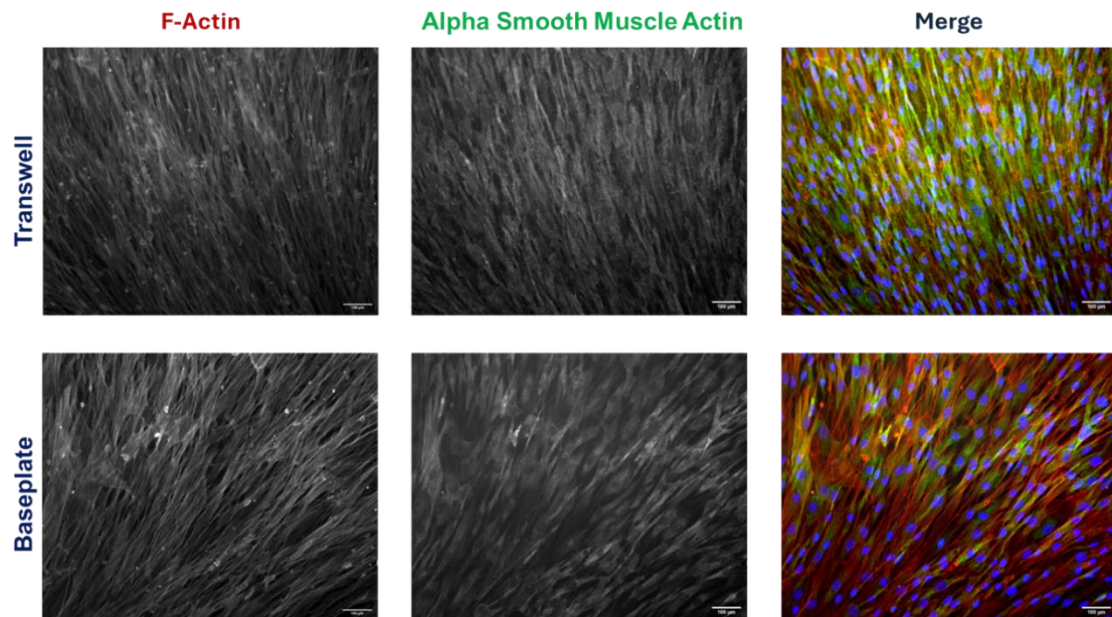


Figure 4.6: Baseplate and Transwell-seeded BSMCs at 15,000 cells/well were morphologically similar. 15,000 BSMCs were seeded on either the baseplate or the underside of a Transwell insert for 7 days, before being fixed and stained using antibodies against anti- α -SMA (green), Phalloidin (actin- red) and Hoescht-3332 (DNA – blue). Scale bar = 100 μ m.

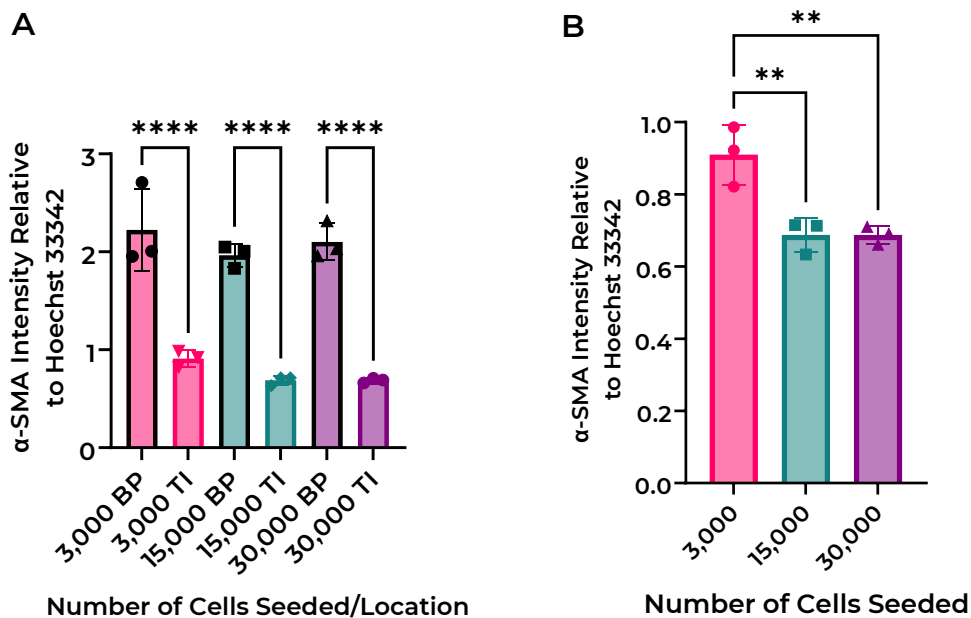


Figure 4.7: 3,000 cells/well had the highest expression of α -SMA when grown on the Transwell inserts. (A) The intensity of α -SMA is reported as a ratio of the Hoechst 33342 intensity in the same image with all densities in both seeding locations, with the **(B)** intensity for the Transwell insert (ANOVA ** = $P < 0.01$, **** = $P < 0.0001$) (N=3)

Together, these results confirmed that seeding on the basolateral face of the Transwell insert was as viable as the traditional culture on the 24-well culture plate with no additional cell stress observed. The 3,000 cells/well density appeared to express a higher amount of α -SMA, and equivalent viability to seeding at a density ten-times higher. The smooth muscle cells grown on the basolateral face of the Transwell insert is more representative of the *in vivo* architecture than the baseplate seeded BSMCs as the smooth muscle cells were closer in proximity to the epithelium as seen in Figure 4.2. Consequently, going forward, the Transwell insert was used to seed the BSMCs on the basolateral face at a density of 3,000 cells/well (1×10^4 cells/cm²) for the coculture and monoculture of the BSMCs.

4.4.2. ESTABLISHING THE COCULTURE MODEL IN STATIC CONDITIONS AND MEDIUM OPTIMISATION

To determine optimal coculture conditions, BSMCs were seeded on the basolateral side of a Transwell insert before Calu-3 cells were seeded on the apical side and then raised to ALI. The wells were maintained in either 100% SmGM media or 50/50 SmGM media/Calu-3 media. LDH release was examined on days 0, 2, 7 and 14 of ALI culture with interesting results. LDH release was detected to be higher in the 100% SmGM media for all cultures than the 50/50 at Day 0 ALI (48 h after seeding) (Figure 4.8 A). However, LDH was not different between the coculture and monoculture Calu-3 wells. LDH release was at a low level at Day 0 and did not indicate increased cell stress.

At Day 2 (Figure 4.8 B), the pattern of significant difference was the same, except for BSMC monoculture having similar LDH release for the two media compositions. This shows that the BSMC and Calu-3 cells were more stressed in the 100% SmGM medium at the early timepoints in the culture compared to the 50/50 medium. This may be a result of the higher concentrations of the supplements such as the hFGF and hEGF. There was also an increase in LDH released from Day 0 to 2 ALI, which may be a result of the cell stress as a portion of cells undergo apoptosis under continued culture in the 100% SmGM medium composition (P. Kumar *et al.*, 2018). However, by Day 7 the LDH levels decreased to Day 0 levels (Figure 4.8 C). This shows the LDH release at Day 2 could have been derived from the epithelial cells still undergoing a growth phase and as they differentiated, leading to the shedding of some cells resulting in a higher level of LDH release. Although the pattern of significant differences shows the LDH release in the coculture to be higher than the Calu-3 monocultures, there was a higher level of LDH release in the coculture model in general. Specifically, the 100% SmGM medium showed higher levels of LDH release for the coculture compared to the 50/50 composition. This was not true for the Calu-3 monoculture however, so it may be a result of the coculture with the BSMCs in the coculture model.

At Day 14, all the cells had a higher LDH release than Day 7, with the coculture having the highest LDH release for both medium compositions. There were no significant differences in LDH release between the two medium types for the coculture, and the Calu-3 monoculture (Figure 4. D). This shows the cell models had reached a point where the medium type was not determining the cell stress. For both the 50/50 and the 100 % medium composition, the highest LDH release was on Day 14 for the coculture model showing the coculture itself was a cause of stress on the cells. Unfortunately, this experiment did not have positive and negative controls for LDH as this would require the sacrifice of wells and there was no capacity to employ such controls with a need to prioritize more informative assays of cell function and health. Positive controls would have been cells seeded in the same density and combination as the sample wells and dosed with a detergent (e.g. 1% Triton X-100) to release the maximum amount of LDH and the negative control would be the blank medium that had no contact with cells.

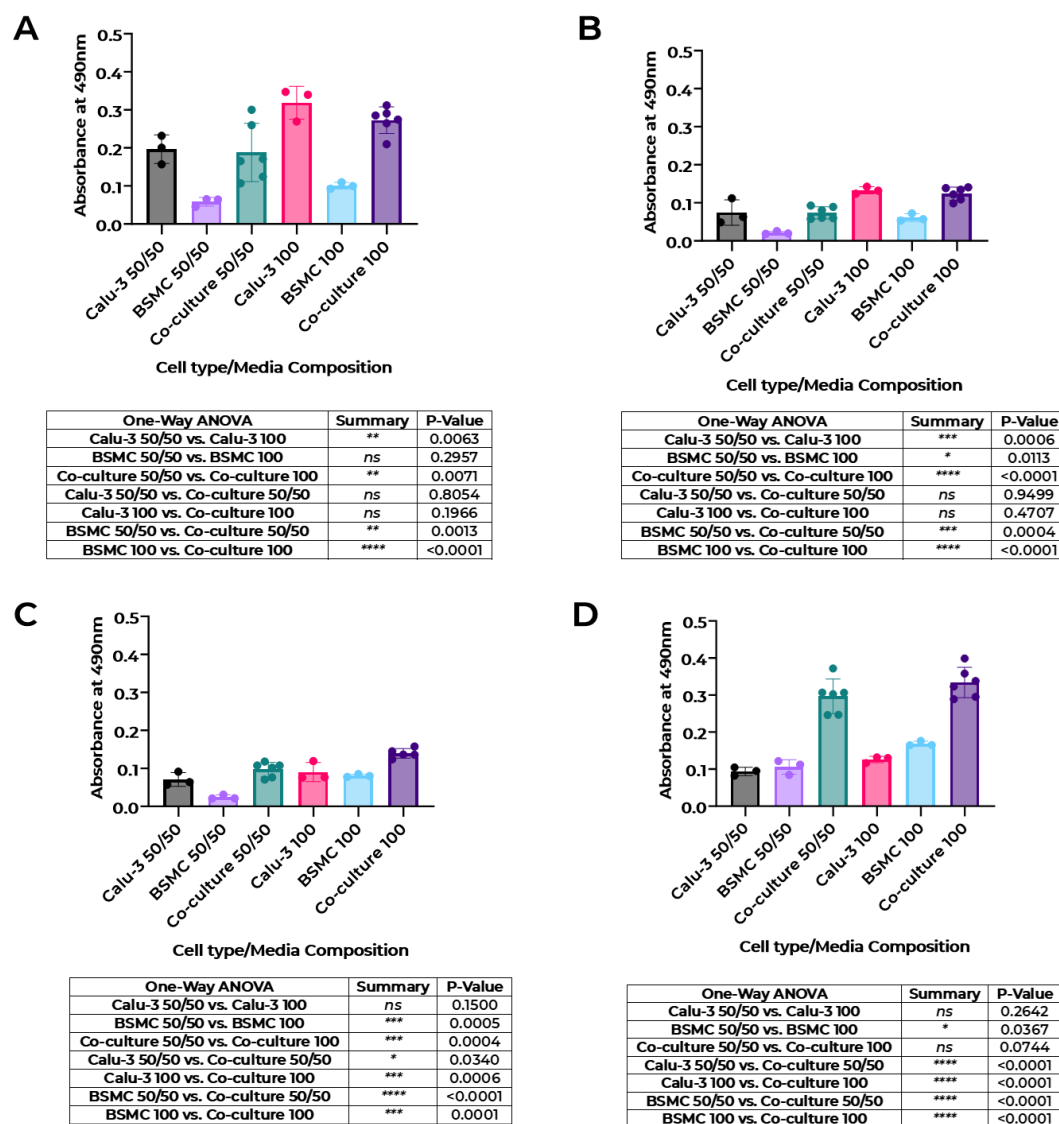


Figure 4.8: No significant increase of LDH release from culture in 50/50 SmGM medium: Calu-3 medium or 100% SmGM medium. LDH was monitored on days (A) 0, (B) 2, (C) 7 and (D) 14 of air-liquid interface (ALI) and are presented with the Two-way ANOVA results alongside the graph. (Two-Way ANOVA * = $P < 0.05$, ** = $P < 0.01$, *** = $P < 0.001$, **** = $P < 0.0001$) ($N \leq 3$).

The barrier integrity was assessed at every change of medium using the non-destructive TEER assay. Overall, it was found that TEER of the epithelium in the 100% SmGM medium was higher than that of the 50/50 composition for both monoculture and coculture comparisons, (Figure 4.9 A and Figure 4.9 B). The coculture had a significantly higher TEER in the 100 % compared to the 50/50 composition from Day 5 onwards. The Calu-3 monoculture epithelium had the same significant increase in TEER for the 100 % compared to the 50/50 medium composition starting from Day 0 ALI. This confirmed that the 100 % SmGM medium

was better at establishing a tight epithelial barrier than the 50/50 composition medium with the highest TEER at Day 14. When comparing the TEER profiles of the Calu-3 epithelium against the coculture epithelium in each medium, the highest TEER for all cultures was measured on Day 12 and 14. However, the coculture had a significantly higher increase in TEER compared to the Calu-3 monoculture for both medium compositions. Overall, the 100 % SmGM medium was associated with a higher TEER profile than the 50/50 composition (Figures 4.9 C and Figure 4.9 D).

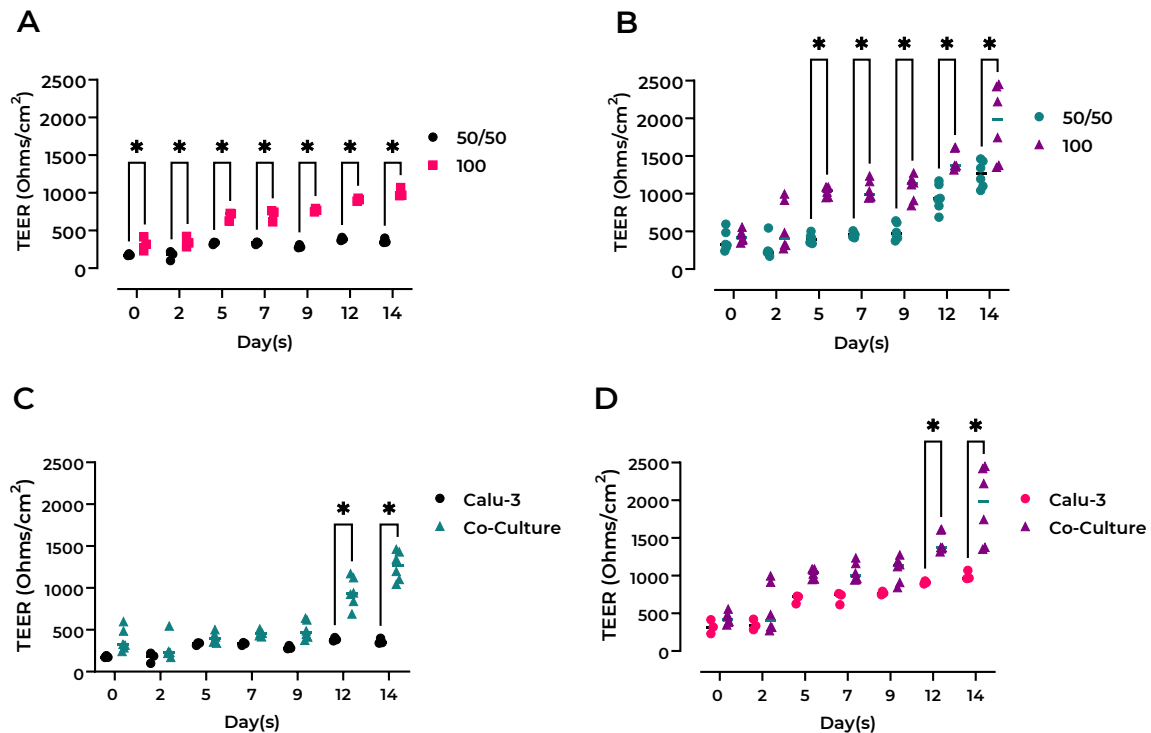


Figure 4.9: Transepithelial Electrical Resistance (TEER) of the 100% SmGM media was higher than the 50:50 composition. (A) Calu-3 epithelial barrier integrity of the Calu-3 monoculture in both medium types and the **(B)** coculture epithelium in both medium types. **(C)** Comparison of the barrier integrity of the Calu-3 monoculture against the coculture epithelium in the 50/50 medium and the **(D)** 100 media (Two-Way ANOVA * = $P < 0.05$) (N=6)

Another assessment of the barrier integrity was the P_{app} of NaFL on Days 7 and 14. Between the two days there was no significant difference in P_{app} , however the Day 7 values had high variance, and the spread of data was marginally larger than at Day 14 (Figure 4.10). The large error bars on Day 7 meant there was no statistical difference in NaFL P_{app} between the mono- or cocultures in either of the medium composition. By Day 14, however, the differences between the culture models were evident. Between both culture types, the 100 % SmGM medium seemed to have established a tighter barrier, with lower P_{app} values produced for

NaFL transport. P_{app} was significantly lower for the coculture epithelium than the Calu-3 epithelium in both media compositions (Figure 4.10 B). This assay, combined with the TEER profiles, confirmed the 100% SmGM medium with a BSMC/Calu-3 coculture to produce a tight, more impermeable epithelium barrier than the monoculture of Calu-3 alone regardless of the medium.

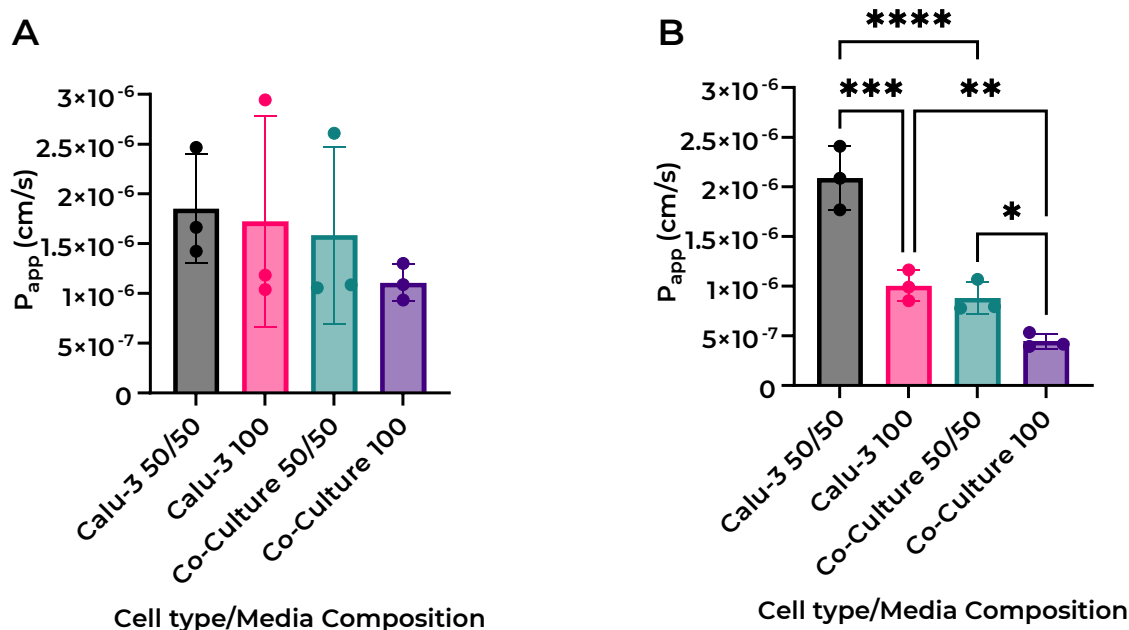


Figure 4.10: Apparent permeability (P_{app}) of sodium fluorescein (NaFL) through the Calu-3 epithelium barrier was lowest in the coculture 100% SmGM media. P_{app} in either monoculture or coculture with BSMCs in the 50/50 or 100 media at **(A)** Day 7 and **(B)** Day 14 (ANOVA * = $P < 0.05$, ** = $P < 0.01$, *** = $P < 0.001$, **** = $P < 0.0001$) (N=3)

To determine the functionality of the bronchial epithelium, the mucus produced by the Calu-3 epithelium in the monoculture and coculture was washed off using PBS and analysed using the lung mucus quantification assay that was developed and detailed in Section 2.4.9. The mucus produced by the Calu-3 cells in the 100 % SmGM medium was higher than those cultured in the 50/50 medium composition (Figure 4.11 A). This was seen again with a much higher mucus amount in all the cultures at Day 14 (Figure 4.11 B). However, by Day 14 the coculture model in the 100 % SmGM medium had a significantly lower amount of mucus (70 μ g) than the Calu-3 monoculture (85 μ g). One consideration to be kept in mind, is that the number of wells available for the Calu-3 monoculture was lower ($n = 3$) whereas the coculture had more replicates ($n = 6$), which could have affected the statistical analysis with the Calu-3 monoculture wells having a lower statistical power, with larger error bars. Figure 4.11 (C) details the increase from the mucus quantified from Day 7 to 14, expressed as a percentage.

Calu-3 100 had a significantly higher increase in mucus expression from Day 7 to 14 than Calu-3 50/50 and Coculture 100, showing the 100% SmGM medium to induce a higher mucus expression in the Calu-3 cells than the 50/50 medium.

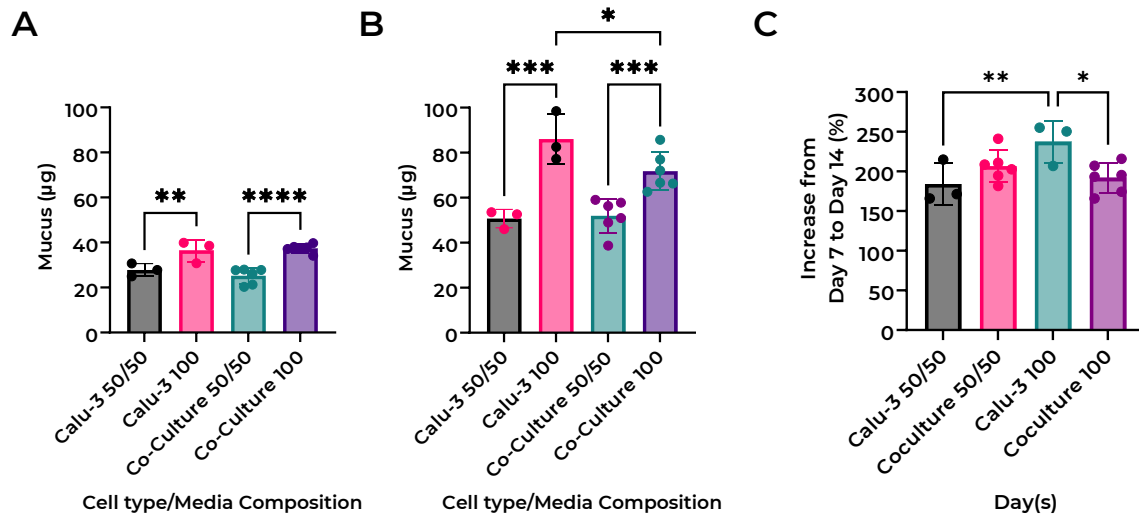


Figure 4.11: Mucus produced by the Calu-3 epithelium in the 100% SmGM was higher than the 50/50 media in the monoculture and coculture. Calu-3 cells were grown at ALI and mucus removed using a PBS wash and then analysed using the alcian blue mucus quantification assay. Mucus (µg) was analysed at **(A)** Day 7 and **(B)** Day 14 and **(C)** percentage increase of mucus from day 7 to 14 (ANOVA * = $P<0.05$, ** = $P<0.01$, *** = $P<0.001$, **** = $P<0.0001$) ($N\leq 3$).

This experiment confirmed that the coculture of Calu-3 cells with BSMCs on opposite side of a Transwell insert membrane was not only possible, but the presence of the BSMC positively altered the characteristics of the Calu-3 epithelium, resulting in a tighter barrier as seen from the TEER profile and the P_{app} values. Despite the higher levels of LDH, the 100% SmGM generated positive effects seen on epithelial function, such as increased mucus and a tighter barrier, and is recommended medium composition for the culture of primary bronchial smooth muscle cells. As a result, the 100% SmGM medium was deemed optimal for continued experimentation.

4.4.3. EVALUATING THE EFFECTS OF PERFUSION ON THE CALU-3/BSMC COCULTURE MODEL

The effect of perfusion on the coculture model optimised in the previous experiment are investigated and evaluated using the same assays as before (Section 4.4.3). The aim was to identify the key areas of differentiation in the smooth muscle and epithelial cells affected by the perfusion. To evaluate the effects of perfusion, the coculture model was cultured in static and perfused conditions along with Calu-3 and BSMC monocultures in both conditions.

The barrier integrity of the epithelium was monitored using TEER. The barrier integrity in the perfused and static conditions of the Calu-3 monoculture (Figure 4.12 A) and in the Calu-3/BSMC coculture (Figure 4.12 B) were similar from Day 0 ALI up to Day 7 ALI, except for Day 3, when the perfused condition in both cultures was significantly lower than the static culture. However, the perfused cultures in both mono- and coculture had a much lower TEER variance and maintained a more consistent TEER profile across the days as was seen in the Calu-3 experiments in Chapter 3. The coculture was more consistent both in replicate values and across the seven-day culture. It was evident that the coculture resulted in a more consistent barrier from Day 0 ALI whereas the Calu-3 monoculture had not established a TEER value of any note at Day 0 (Figure 4.13 A). The spread of TEER values was also significantly larger in the Calu-3 static culture than the static coculture. In the perfused condition this was also evident, although the perfusion resulted in reduced TEER variance for both the coculture and Calu-3 monoculture (Figure 4.13 B). The combination of the perfusion and coculture seemed to generate a more reproducible and robust epithelial barrier.

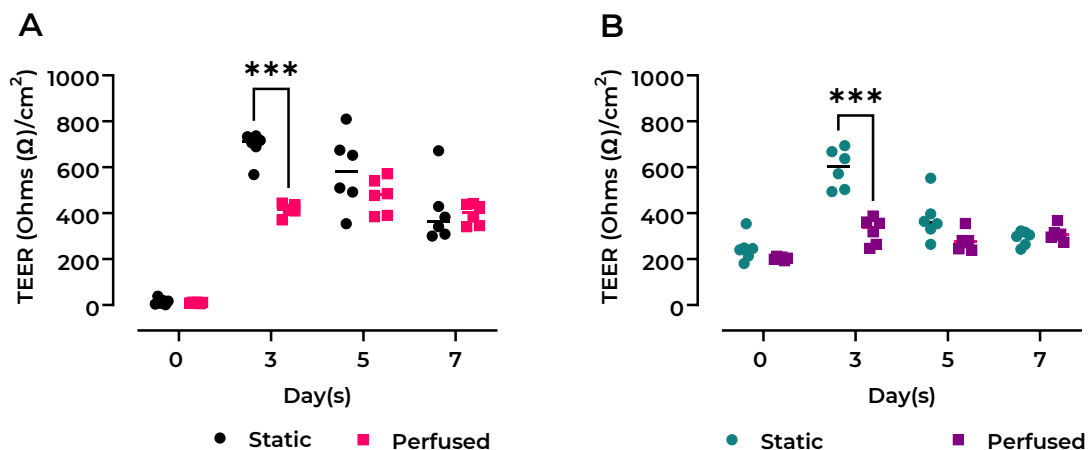


Figure 4.12: Transepithelial electrical resistance (TEER) profiles of the static and perfused conditions of both cultures was similar across seven days. (A) Calu-3 monoculture and the (B) Calu-3/BSMC coculture (Two-Way ANOVA * = $P < 0.001$) (N=6)**

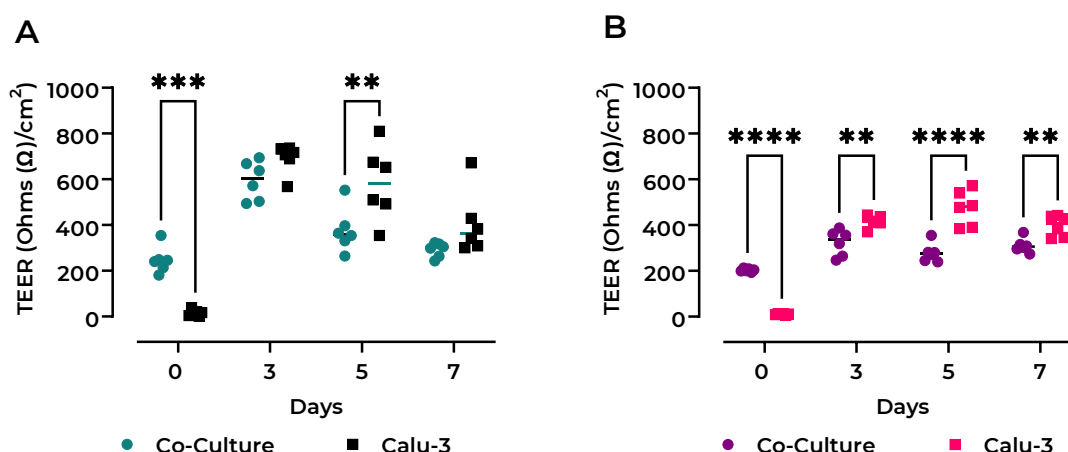


Figure 4.13: Transepithelial electrical resistance (TEER) profiles of the coculture were lower than the Calu-3 monoculture. (A) Static and the (B) perfused conditions of the Calu-3 monoculture and Calu-3/BSMC coculture (Two-Way ANOVA ** = $P < 0.01$, * = $P < 0.001$, **** = $P < 0.0001$) (N=6)**

The Day 7 P_{app} data (Figure 4.13 A and Figure 4.13 B) agreed with the TEER data in terms of the differences in the variance for the models in both conditions. The controls of the blank insert and the BSMC monoculture were also assessed to determine if the presence of BSMCs had an influence on the passive diffusion of NaFL. In both the static and perfused condition, the passive diffusion of NaFL was lower in the BSMC than the blank Transwell so the physical presence of BSMCs did affect the diffusion rate of the paracellular marker, regardless of the culture condition (Figure 4.13 A and Figure 4.13 B), however, permeation was an order of magnitude higher (10^{-4}) than when an epithelial layer was in place (10^{-5}).

As previously seen with the TEER profile, the static condition of the coculture and monoculture had a wide P_{app} variance, resulting in no significant difference between the two model types. However, once the perfusion was introduced, the P_{app} variance became much tighter with less variation between replicates. This resulted in a clearer difference between the two models and a significantly lower P_{app} was established in the coculture model compared to the Calu-3 monoculture. Without the perfusion, the coculture epithelium was closer in functionality to the Calu-3 monoculture, however the perfusion resulted in a consistently (i.e. lower variance) tighter barrier, implying a differentiation that occurred for the combination of the coculture and the perfusion.

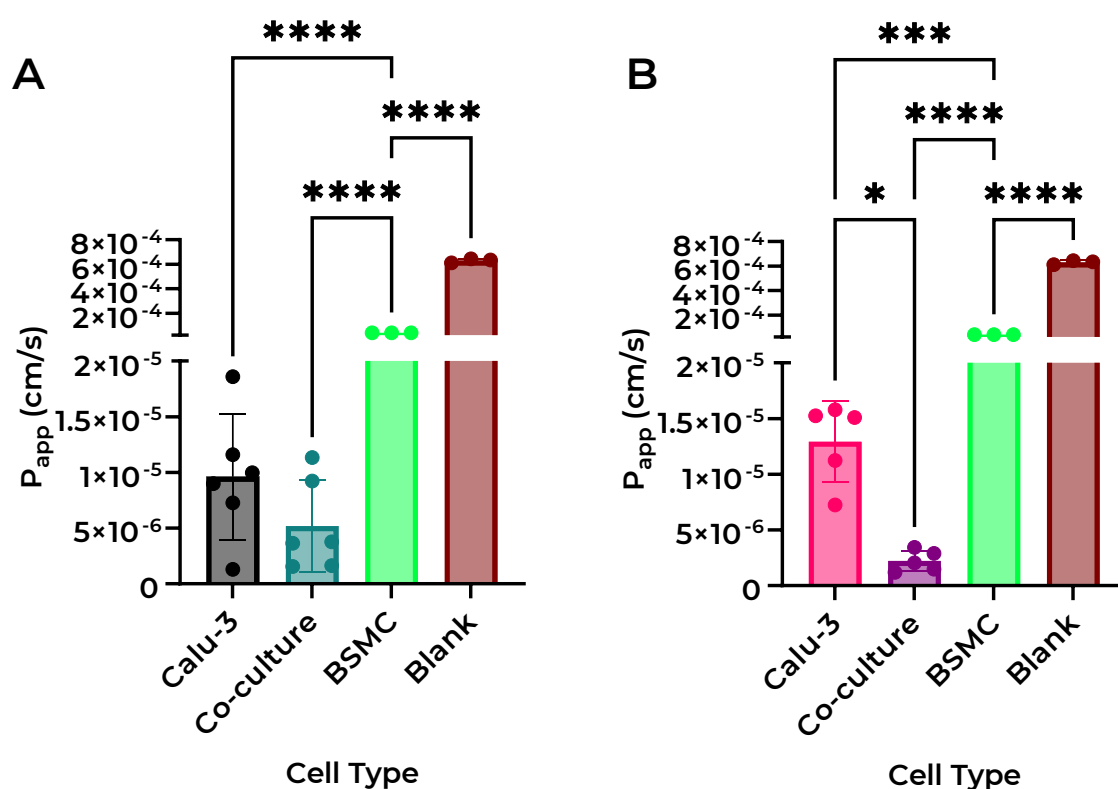


Figure 4.14: Apparent permeability (P_{app}) of sodium fluorescein (NaFL) across the barrier model was lower in coculture perfused than Calu-3 perfused. Transwell insert with no cells (Blank), Bronchial Smooth Muscle Cell Monoculture (BSMC), Calu-3 monoculture, or Calu-3/BSMC coculture grown on the membrane. The P_{app} is expressed in cm/s in the **(A)** static and **(B)** perfused conditions. (ANOVA * = $P < 0.05$, *** = $P < 0.0002$, **** = $P < 0.0001$) ($N \leq 3$).

From Figure 4.15, the apparent permeability of the two conditions in the static and perfused conditions can be seen to possess no significant difference. Although in Chapter 3, the effect of perfusion in reducing the apparent permeability of the Calu-3 barrier was established, it seems the inter-experiment reproducibility is yet to be determined and those cultures established a significant difference at Day 14 whereas this culture was analysed at Day 7 of culture. However, the P_{app} of the barrier is not the only determinant for the transport of all molecules, only this paracellular marker, NaFL.

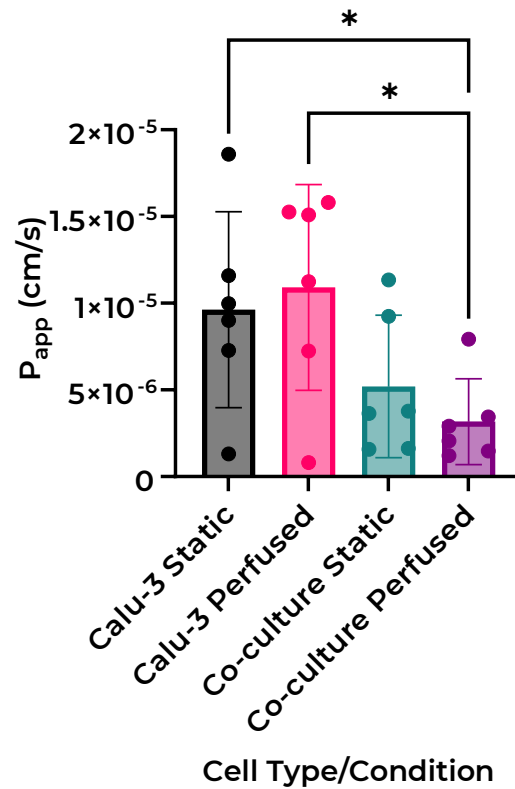


Figure 4.15: Apparent permeability (P_{app}) of the static Calu-3 monoculture was similar to the Calu-3 perfused monoculture which in turn was significantly higher than the perfused coculture model (ANOVA * = $P < 0.05$) (N=6).

The mucus expression at Day 3 ALI was similar in the Calu-3 monoculture and the Calu-3/BSMC coculture regardless of perfusion (Figure 4.16 A). By Day 7, the coculture perfused model generated more mucus than the coculture static and the Calu-3 monoculture static and perfused. This identified the combination of the perfusion with the coculture model to generate a higher mucus-expressing phenotype from the Calu-3 epithelium when grown at ALI.

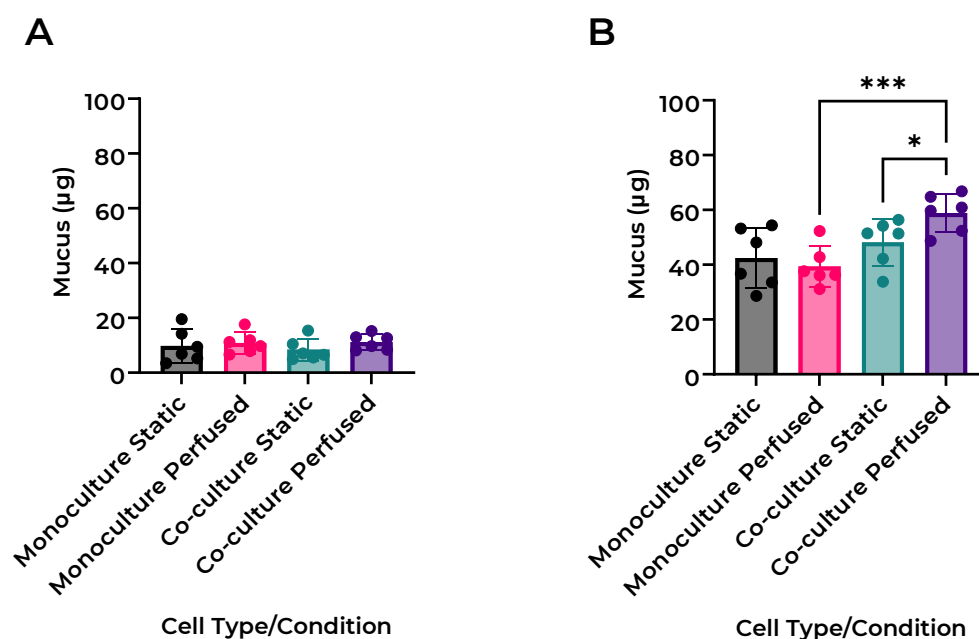


Figure 4.16: Significantly higher mucus expression from the Calu-3 epithelium in the perfused coculture model compared to the static equivalent and perfused monoculture.

Calu-3 cells were grown at ALI and mucus removed using a PBS wash and then analysed using the alcian blue mucus quantification assay. Mucus (µg) was analysed at **(A)** Day 3 and **(B)** day 7 air-liquid interface (ALI) measured using the alcian blue mucus quantification assay (ANOVA * = $P < 0.05$, *** = $P < 0.0002$) (N=6).

The qPCR of the MUC5AC mucin expressing gene (used as a marker for mucus-expressing Goblet cells (Stewart *et al.*, 2012b)) showed the same trend as the mucin data (Figure 4.16 B) where the perfused coculture model had a higher expression of the MUC5AC gene than static coculture or either monoculture Calu-3 model. This shows the differentiation and expression the MUC5AC mucin and resultant mucus expression was enhanced in the perfused coculture condition. The latter trend in expression was also seen in the FOXJ1 gene, a gene indicative of cilia expression (M. S. Walters *et al.*, 2013) and the SLC22A1 gene which encodes for the organic cation transporter OCT1. The OCT1 organic cation transporter is implicated in the transport of drugs such as salbutamol (Mukherjee *et al.*, 2017a). Figure 4.17 C confirms that the coculture alone was not sufficient to generate a differentiation in gene expression of the Calu-3 cells but the combination of the perfusion with the coculture generated a phenotype that had differentiated away from the Calu-3 monoculture in static and perfused culture, indicating a significant differentiation occurred by combining perfusion and coculture with BSMCs.

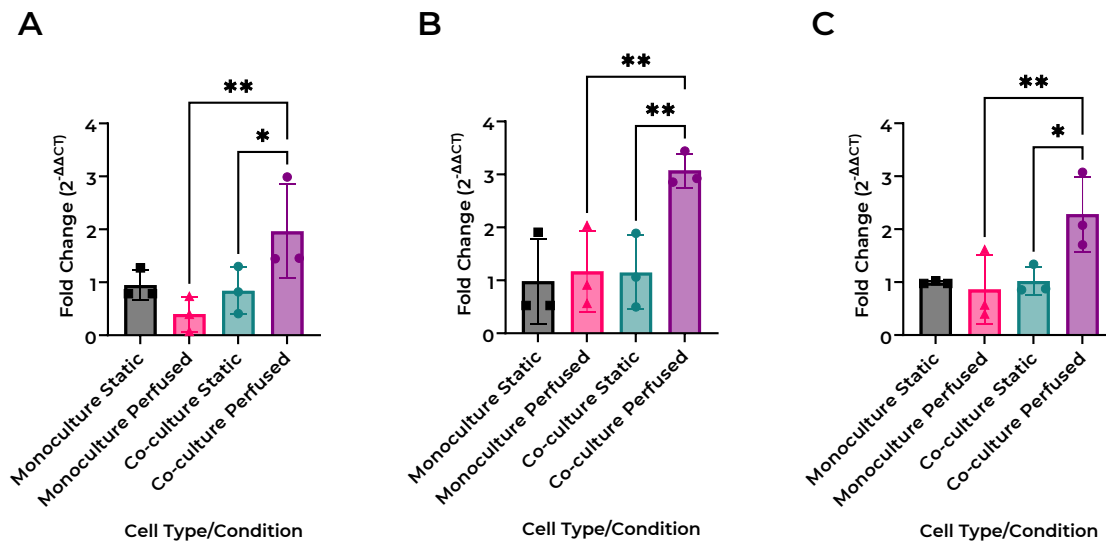


Figure 4.17: Quantitative polymerase chain reaction (qPCR) analysis of the Calu-3 epithelium showed the coculture perfused model to express MUC5AC, FOXJ1 and SLC22A1 genes by one-fold higher than the static equivalent. Cells quantified for the genes **(A) MUC5AC**, **(B) FOXJ1**, and **(C) SLC22A1**. The gene expression is expressed as fold change difference from Calu-3 static cells after difference in expression from undifferentiated cells was calculated to give rise to $2^{-\Delta\Delta Ct}$ (ANOVA * = $P < 0.05$, ** = $P < 0.01$) (N=3).

The bronchial smooth muscle cells were analysed for the alpha smooth muscle actin (α -SMA) gene, ACTA2, which is one of the major contractile proteins in the smooth muscle cells (Webb, 2003). Another key marker is the SM22 gene, which is an early marker for smooth muscle differentiation (GeneCards, 2024). The ACTA2 expression increased significantly in the BSMCs when in coculture with the epithelium compared to the monoculture in both conditions (Figure 4.18 A). There was no significant difference between the static and perfused conditions, however, showing that the presence of the Calu-3 epithelium contributed to the differentiation into a more contractile phenotype in the BSMCs regardless of perfusion. More interestingly, the SM22 marker showed a similar trend of improved differentiation, in that the perfused coculture model had significantly higher expression of SM22 compared to the monoculture Calu-3 perfused and the coculture static (Figure 4.18 B). This further confirmed that the perfused coculture model generated a more contractile phenotype than the static equivalent.

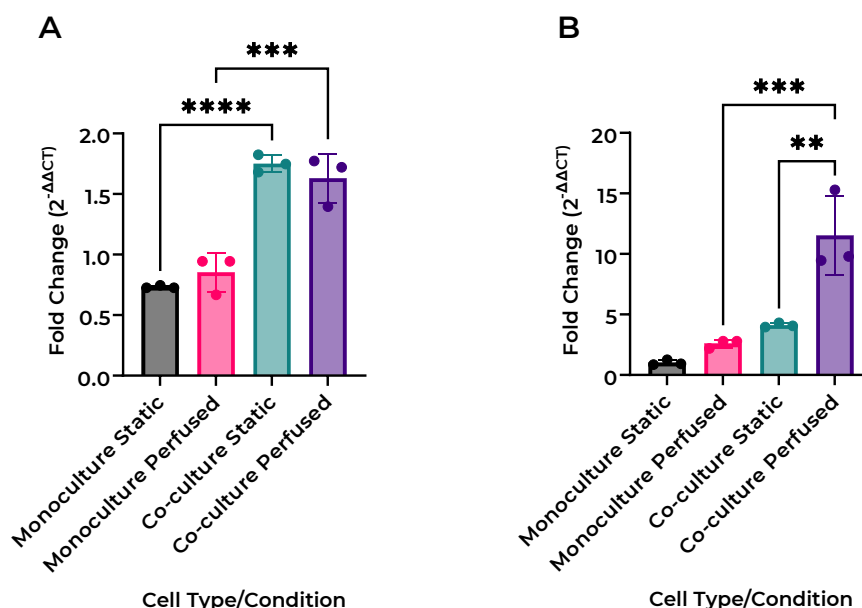


Figure 4.18: Quantitative polymerase chain reaction (qPCR) analysis of the Bronchial Smooth Muscle Cells (BSMCs) showed the coculture perfused model to have the highest contractile phenotype expressed. BSMCs quantified for the genes **(A)** ACTA2 and **(B)** SM22. The gene expression is expressed as fold change difference from monoculture BSMC static cells after difference in expression from undifferentiated cells was calculated to give rise to $2^{-\Delta\Delta Ct}$ (ANOVA ** = $P < 0.01$, *** = $P < 0.001$, **** = $P < 0.0001$) (N=3).

Immunofluorescence microscopy analysis of the cells painted an interesting picture of the morphological changes that occurred in the BSMCs and the Calu-3 epithelium under perfusion and in coculture. The BSMCs stained for α -SMA and F-actin, and under perfusion the BSMCs seem to align in a defined direction, reminiscent of fibres, whereas the static model seemed to grow without a defined polarity, with cells overlapping and crossing (Figure 4.19). This may be a result of the shear stress resulting from the perfusion, with the cells growing in the direction of the flow, but this has not yet been determined. The Calu-3 monoculture epithelium grew in patterns as previously seen (Section 3.4.2) with the static epithelium showing patches of cells growing on top of the original monolayer whereas the perfused epithelium displayed a more uniform sheet of epithelial cells (Figure 4.20). The Calu-3 epithelium in the coculture model (static and perfused conditions) was more akin to the morphology of the perfused Calu-3 monoculture with a uniform monolayer of epithelium cells with defined ZO1 tight junctions (Figure 4.21). The perfused coculture epithelium exaggerated this further, with an approximately single sheet of cells with defined ZO1 tight junction expression. Unfortunately, it was not possible to image the BSMCs in coculture in isolation, due to the density of the Calu-3 cells on the transparent membrane obscuring the BSMC-specific immunofluorescence.

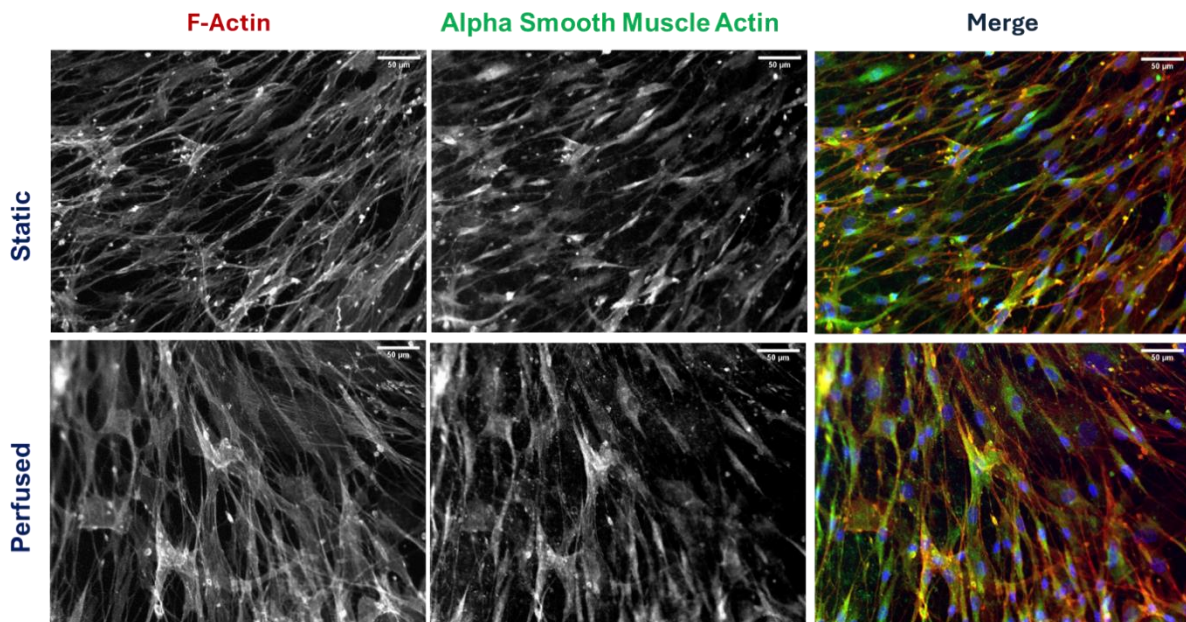


Figure 4.19: Static and perfused BSMCs were morphologically similar. BSMCs were maintained on the underside of a Transwell insert in static and perfused conditions for 7 days, before being fixed and stained using antibodies against anti- α -SMA (green), Phalloidin (actin- red) and Hoescht-3332 (DNA – blue). Scale = 50 μ m.

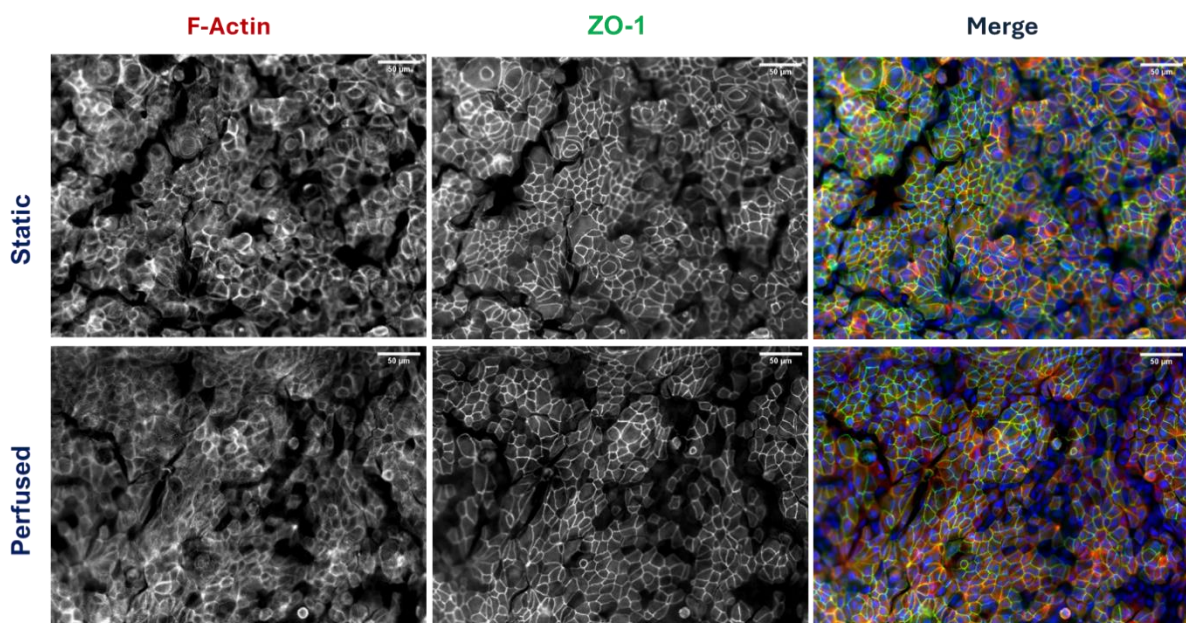


Figure 4.20: Static Calu-3 had more ‘patches’ of cells than the perfused Calu-3 barrier. Calu-3 cells were maintained at ALI on a Transwell insert in static and perfused mono-culture conditions for 7 days, before being fixed and stained using antibodies against anti- ZO1 (green), Phalloidin (actin- red) and Hoescht-3332 (DNA – blue). Scale = 50 μ m.

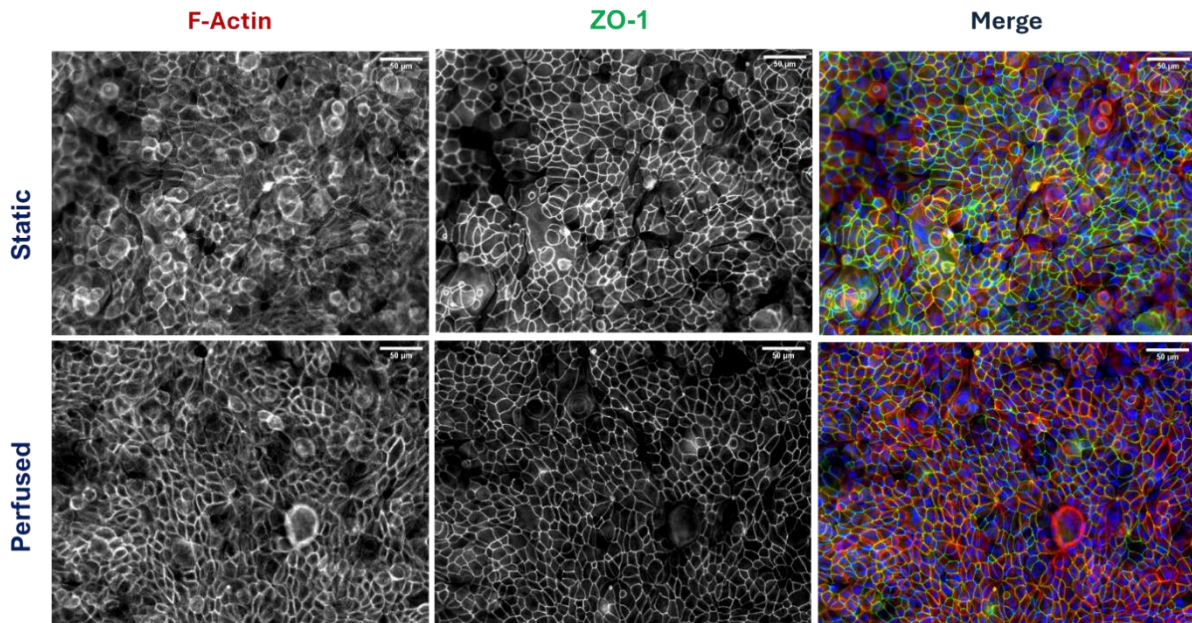


Figure 4.21: Perfused coculture epithelium had a more uniform cell barrier cells than the static coculture barrier. Calu-3 cells were maintained at ALI on a Transwell insert in coculture with BSMC cells in static and perfused conditions for 7 days, before being fixed and stained using antibodies against anti- ZO1 (green), Phalloidin (actin- red) and Hoescht-3332 (DNA – blue). Scale = 50 µm.

The histology images showed a cross-sectional view of the cells to gauge a better idea of the morphology in two dimensions (Figure 4.22). The ‘patches’ of cells observed in the static immunofluorescence microscopy analysis were visualised in the histology analysis (Figure 4.22 A and Figure 4.22 B). The perfused epithelium showed a somewhat similar trend (Figure 4.22 D) however, with the perfused coculture differing significantly in morphology. The epithelium had become more columnar, with a single layer of cells and a consistent mucus layer covering the apical membrane (Figure 4.22 C). This confirmed the morphology of the perfused coculture was significantly different to the static equivalent and the Calu-3 monoculture regardless of perfusion. This differentiation in morphology may be a result of the differentiation that occurred during the coculture combined with perfusion.

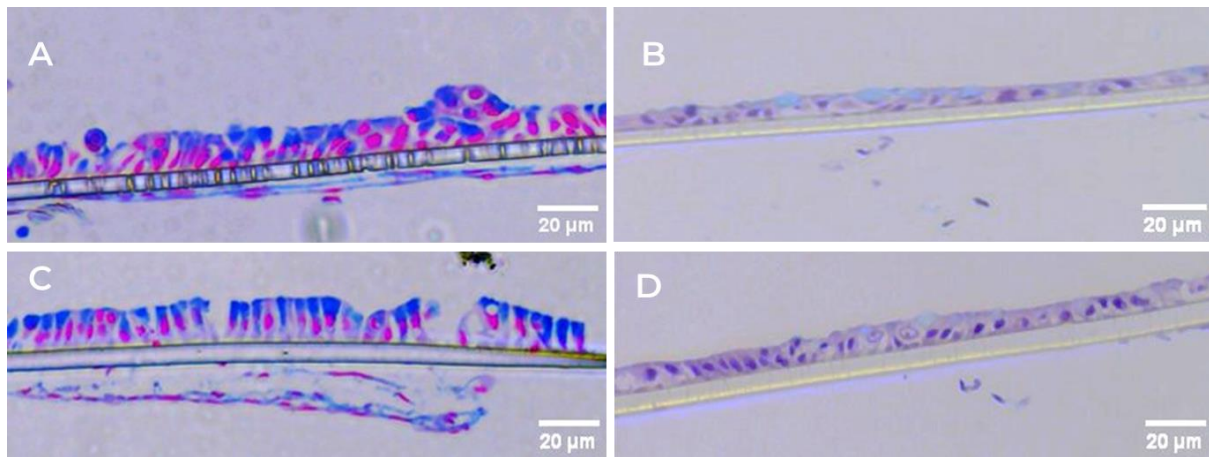


Figure 4.22: Histological samples of the different culture conditions showed differences in morphology between the conditions and cultures. (A) Static coculture, (B) Static monoculture, (C) Perfused coculture, and (D) Perfused monoculture. Cells are stained for cytoplasm (light pink/red), nucleus (dark purple/pink), and acidic mucins (blue), as stained by alcian blue. Scale = 20 μm .

To conclude, seven days coculture of the Calu-3 epithelium differentiated at air-liquid interface in combination with the bronchial smooth muscle cells and perfusion has led to a significant change in cell morphology with a more uniform cell barrier established with defined tight junctions in contrast to the static equivalent which had less defined barrier with patches similar to the static Calu-3 monoculture morphology. The barrier functionality of the perfused coculture was less permeable than the static coculture as seen by the apparent permeability of sodium fluorescein. The perfused coculture had a higher expression of mucus than the static equivalent and the perfused Calu-3 monoculture, which was reflected with a 1-1.5-fold higher expression of the MUC5AC gene, quantified by qPCR. The BSMCs also differentiated more in this model with qPCR analysis confirming a 1-fold increase in the ACTA2 gene expression when in coculture compared to monoculture and the perfused coculture resulting in a 5-fold increase of the differentiation gene marker SM22 compared to the static coculture BSMCs. This experiment confirmed the combination of coculture with perfusion resulted in a highly differentiated cell phenotype for the Calu-3 epithelium and BSMCs that the coculture alone did not elicit.

4.5. CHAPTER CONCLUSIONS

Within this chapter, the coculture of BSMCs on the basolateral side of a Transwell insert with Calu-3 epithelium differentiated at the air-liquid interface was established successfully. The impact of perfusion on this coculture was also examined and found to enhance the differentiation of both the Calu-3 epithelium and the BSMCs within the coculture when cultured in the PhysioMimix Organ-on-Chip system. The next steps will involve evaluating the perfused coculture model's suitability as a drug transport assay for drugs targeting the epithelium and BSMCs, such as bronchodilators, and optimising an assay to evaluate the effectiveness of these drugs on the target cells.

Chapter Five

Evaluation of the Perfused Bronchial Coculture Model

5. EVALUATION OF THE PERFUSED BRONCHIAL COCULTURE MODEL

5.1. INTRODUCTION

Treatment with inhaled therapeutics is critical in managing symptoms of lung disease. There are many lung diseases that affect the global population. Within this chapter, the two major diseases that burden many people, asthma, and chronic obstructive pulmonary disorder (COPD), will be explored to fully understand the requirements of an *in vitro* model for use in screening pharmacological treatments for the diseases. Asthma is a chronic disease of the lower airways with symptoms including inflammation and airway hyper-reactivity leading to wheezing, breathlessness, coughing and chest tightness (Cevhertas *et al.*, 2020; Mims, 2015). The Global initiative for Asthma (GINA) classifies asthma into three categories: mild, moderate and severe asthma (Global Initiative for Asthma, 2022). Asthma affects between 5-16% of people globally (Akinbami *et al.*, 2001) and affects 10-15% of the UK population (Sugawara & Nikaido, 2014). Chronic obstructive pulmonary disease (COPD) is the 3rd leading cause of death in the world, responsible for 6% of global mortalities (WHO, 2020b). COPD is a chronic respiratory disorder that progressively leads to an obstructive ventilatory pattern and chronic respiratory failure (Raheison & Girodet, 2009). COPD is an umbrella term for multiple ailments including:

1. Chronic bronchitis, which is a permanent obstruction of airways (Raheison & Girodet, 2009).
2. Chronic respiratory failure, which is defined by the existence of chronic obstructive bronchitis with hypoxaemia (Raheison & Girodet, 2009).
3. Emphysema, which is destruction of the walls of the alveolar sacs/ducts beyond the terminal bronchiole with an abnormal increase in size of distal airways (MacNee, 2005; Snider, 1985).

COPD is often linked to tobacco smoking, however epidemiological studies have shown that around 20-40% of COPD patients globally are non-smokers, so environmental factors such as vehicle fumes, occupational hazards (dust, lead etc) and pesticides also affect the progression of this disease (Elonheimo *et al.*, 2022; Raheison & Girodet, 2009; Salvi & Barnes, 2009). There are patients with simultaneous asthma and COPD and the co-morbidities are recognised as asthma-COPD overlap (ACAAI, 2024; HU Medical Review Board, 2015). Understanding the symptoms and disease pathogenesis allows a better understanding of why and how inhaled therapeutics can help manage and alleviate symptoms of COPD and asthma.

5.1.1. INHALED TREATMENTS FOR ASTHMA AND COPD

Asthma and COPD have been traditionally treated through bronchodilation and suppression of the inflammatory cell response (Abohalaka *et al.*, 2020). Initially, mild asthma is treated with bronchodilator medication such as short-acting β_2 -agonists (SABA) salbutamol or terbutaline, often termed “reliever” medication. For individuals with moderate asthma who do not gain control with these treatments, inhaled corticosteroids (ICS) such as fluticasone propionate are recommended (BTS/SIGN, 2019; Global Initiative for Asthma, 2022). Regular use of ICS treatments by patients have resulted in improved lung function and reduction in the need for the reliever medications (Adams, Bestall, Lasserson, *et al.*, 2005, p. 2; Adams, Bestall, Malouf, *et al.*, 2005). However, there are patients that cannot control their asthma on the ICS alone and there is insufficient evidence to establish a dose-response relationship of inhaled corticosteroids in children (L. Zhang *et al.*, 2014). If the reliever medication in conjunction with ICS does not achieve sufficient control of the asthma exacerbations, guidelines recommend long-acting β_2 -agonists (LABA) as the preferred additional therapy to inhaled corticosteroids for severe asthma (BTS/SIGN, 2019; Global Initiative for Asthma, 2022). Randomised trials have shown LABA with ICS treatment has a significant benefit for uncontrolled asthma patients including improved lung function, reduction in reliever use and reduction in number of exacerbations (Ducharme *et al.*, 2010).

COPD treatment is similar to asthma treatment and ranges from SABA to alleviate symptoms immediately to LABA and/or long-acting muscarinic antagonists (LAMA) for long-term maintenance for moderate to severely affected patients. Inhaled corticosteroids are central to the treatment for asthma, but they have been used in COPD patients to decrease the risk of exacerbations alongside LABA and/or LAMA treatment for patients with severe airflow obstructions (Maqsood, 2016). Due to their ubiquity in management of both asthma and COPD, the utility of the model developed in Chapter 4 for the investigation of bronchodilation pharmacology will be explored in this chapter. For this reason, it is appropriate to discuss the pharmacology of bronchodilation in brief.

5.1.2. MECHANISM OF CONTRACTION AND RELAXATION IN SMOOTH MUSCLE CELLS

Smooth muscle contraction is regulated through intracellular calcium ions (Ca^{2+}). Ca^{2+} is released from within the cell or from extracellular space through the activation of muscarinic acetylcholine receptors (M_2 and M_3). Acetylcholine is a neurotransmitter of the parasympathetic nervous system and is released from the vagus nerves, activating the muscarinic receptors located on the smooth muscle cells (Cazzola *et al.*, 2012; Matera *et al.*, 2020; Meurs *et al.*, 2013). Smooth muscle contraction is mediated primarily through the activation of G-protein coupled M_3 receptors, subsequently activating phospholipase C,

initiating the release of the secondary messenger inositol 1,4,5-triphosphate (IP_3) (Cazzola *et al.*, 2012, 2021; Matera *et al.*, 2020). IP_3 then activates the sarcoplasmic reticulum within the cell to release Ca^{2+} ions (Webb, 2003). Ca^{2+} ions can also enter the cell from the extracellular space through the voltage-gated calcium channels, which are activated through the depolarisation of the smooth muscle cell after stretch or action potential activation (Sieck & Gransee, 2012; Stanfield, 2016; Ward, J.P.T., Ward, J. and Leach, 2010). Once the Ca^{2+} enters the cytoplasm, it reversibly binds to calmodulin to form a calcium-calmodulin complex. This complex activates myosin light chain kinase (MLCK), which catalyses the phosphorylation of myosin cross bridges. The myosin proteins are then able to bind to actin filaments and the filaments are pulled inward by the myosin which leads to the muscle cell shortening and resulting in contraction (Sieck & Gransee, 2012; Stanfield, 2016). This is illustrated in Figure 5.1.

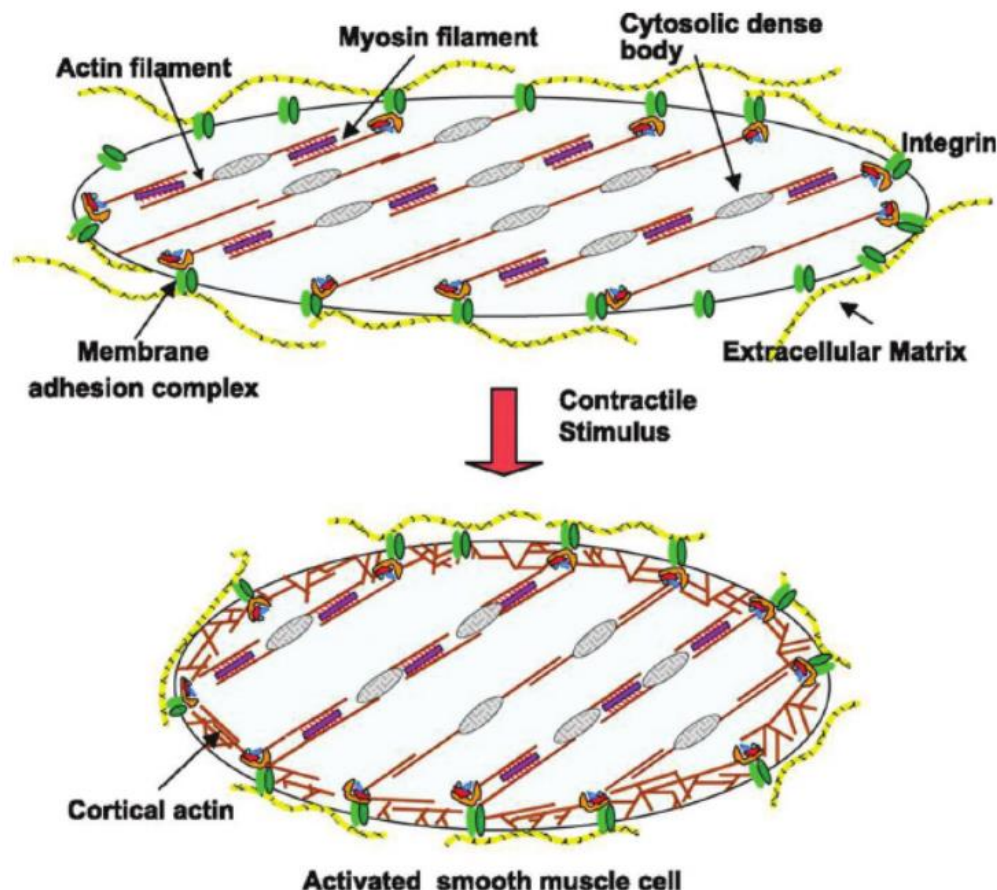


Figure 5.1: Smooth muscle contraction and the resultant muscle fibre shortening from the myosin proteins pulling the actin filaments. Figure from (Gunst & Zhang, 2008).

Relaxation occurs due to the decrease in intracellular Ca^{2+} concentrations in the smooth muscle cells. This is through the closing of the Ca^{2+} channels, which stops the flow of Ca^{2+} into the cell, or by the sarcoplasmic reticulum absorbing the excess Ca^{2+} (Webb, 2003). Smooth muscle cells also express myosin light chain phosphatase (MLCP) which mediates the phosphorylation of myosin even in the presence of a constant intracellular Ca^{2+} concentration (Sieck & Gransee, 2012). A major signalling pathway for the relaxation of the smooth muscle cells are through the beta-2 adrenergic receptors. This receptor, when stimulated by endogenous compounds such as adrenaline, leads to the activation of a G-protein that in turn stimulates adenylyl cyclase (AC). AC then catalyses the conversion of ATP to cyclic adenosine monophosphate (cAMP) which mediates smooth muscle relaxation through plasma membrane hyperpolarisation (leading to decreased Ca^{2+} concentration) and reducing myosin light chain phosphorylation (Nelson *et al.*, 2011; Sieck & Gransee, 2012; Ward, J.P.T., Ward, J. and Leach, 2010). cAMP is recognised as a signalling molecule in bronchial smooth muscle cells (BSMCs) that is heavily involved in the relaxation of airway smooth muscle in response to β_2 -AR agonists such as terbutaline (Matera *et al.*, 2020). Therefore, the changes in cAMP concentrations in BSMCs are used as a proxy measurement of BSMCs relaxation (Haghi *et al.*, 2015; Muddle *et al.*, 2020).

5.1.2.1. INHALED MUSCARINIC ANTAGONISTS

Airway smooth muscle (ASM) contraction is mediated primarily through activation of the G_q -coupled M_3 receptors, which are also the predominant receptors mediating mucus secretion and are involved in the dilation of airway blood vessels (Cazzola *et al.*, 2012; Matera *et al.*, 2020). Another muscarinic receptor, M_2 , is highly expressed on airway smooth muscle and their activation counteracts β_2 -adrenoceptor (β_2 -AR) mediated relaxation due to phosphorylation of G_s protein, with consequent inhibition of adenylyl cyclase (AC) and reduced cyclic adenosine monophosphate (cAMP) generation and accumulation (Gosens & Gross, 2018). M_2 receptors are also located in pre-junctional membranes of neuromuscular junctions of airway smooth muscle where they reduce acetylcholine release in parasympathetic ganglia and nerve terminals (Cazzola *et al.*, 2012).

Long-acting muscarinic antagonists (LAMA) such as tiotropium preferentially block M_3 receptors, whereas short-acting muscarinic antagonists (SAMA) such as ipratropium block both M_2 and M_3 receptors (Lipworth, 2014). SAMA can cause a potential problem of increased pre-junctional acetylcholine release in the extracellular space leading to a delayed contractile response after the effects of the SAMA is worn off (Lipworth, 2014). Muscarinic receptor antagonists are not recommended for long-term management of stable asthma because β_2 -agonists inhibit bronchoconstriction and corticosteroids effectively inhibit inflammation, however they are recommended in conjunction with corticosteroids (National Heart, Lung, and

Blood Institute: National Asthma Education Program.: Expert Panel on the Management of Asthma., 2007).

5.1.2.2. BETA-2 (β_2) ADRENOCEPTOR AGONISTS

β_2 -adrenoceptors in the human lung are widely distributed and are present in airway smooth muscle cells, lung epithelial and endothelial cells, alveolar type II cells and mast cells (Qing *et al.*, 1997). The β_2 -adrenoceptor (β_2 -AR) is a member of the seven G-protein-coupled receptors (GPCRs) family. β_2 -AR are mainly distributed in blood vessels, the heart and lungs (Anakwe *et al.*, 1985; Graziano *et al.*, 1985). β_2 -AR agonists are airway smooth muscle relaxants and are the main course of treatment of bronchodilators used in asthma. Long-acting β_2 -AR agonists (LABA), such as salmeterol and formoterol provide potential pharmacological advantages over short-acting β_2 -ARs (SABAs), namely prolonged bronchodilation and protection against induced bronchospasm (Adkins & McTavish, 1997; Bartow & Brogden, 1998). LABAs have longer onset than SABAs (up to an hour) but effects can last for up to 12 h (E. H. Walters *et al.*, 2002). Salmeterol, a LABA, has a prolonged bronchodilator effect compared to salbutamol in healthy and asthmatic adults with dry powder formulations, thus establishing salmeterol as a more effective treatment in managing asthma symptoms (Lundback *et al.*, 1993; Spring *et al.*, 1992). The prolonged exposure is a result of the compound's lipophilic property which results in the slow clearance of salmeterol from the receptors and tissue (Sichletidis *et al.*, 1993).

Selective SABAs, such as salbutamol and terbutaline (Figure 5.2), are effective at symptomatic management of airway obstruction, and their effectiveness is affected by their transport across the epithelial barrier to reach the β_2 -AR on airway smooth muscle cells (Haghi *et al.*, 2015). The transport of salbutamol and terbutaline is mediated via passive diffusion as well as the transporter proteins (i.e., organic cationic transporters, OCTs) (Haghi *et al.*, 2012b; Horvath *et al.*, 2007). Salbutamol and terbutaline are similar from a clinical point of view, and they are more effective than isoprenaline, a non-selective β -AR agonist, and isoproterenol, a non-selective β_2 -AR agonist (DrugBank Online, 2024). Terbutaline activates the β_2 receptors on bronchial smooth muscle, causing relaxation of the muscle, and can also increase the movement of airway cilia, reduce vascular permeability and reduce the degree of airway submucosal oedema (Beltaief *et al.*, 2019; Q. Zhou *et al.*, 2020). Terbutaline and salbutamol, when administered by a metered-dose inhaler, are equally efficacious in children and adults with mild or moderate acute exacerbations of asthma (Chandra *et al.*, 2004; Lindsay *et al.*, 1994). However, in adults with mild to moderate asthma, terbutaline delivered via Turbuhaler was significantly more effective than salbutamol delivered via Rotahaler in controlling lung function and for 44% of patients it was the preferred treatment (Gioulekas *et al.*, 1996).

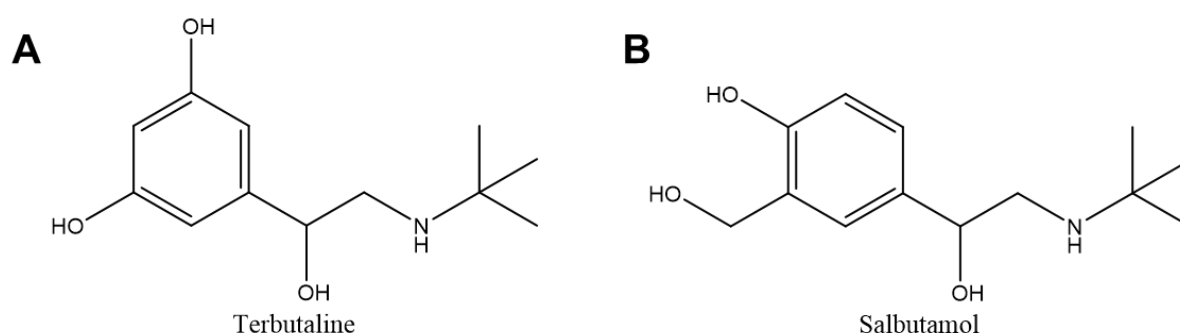


Figure 5.2: Terbutaline and salbutamol have similar molecular structure which could account for their clinical similarities. Molecular structures of the β_2 -adrenoceptor agonists **(A)** terbutaline and **(B)** salbutamol.

5.1.3. *IN VITRO* COCULTURE MODELS FOR ASSESSING BRONCHODILATOR ACTION

In vitro Calu-3 epithelial models currently used for assessing the transport of β_2 -AR agonists are typically cultured in monoculture, static conditions. Often these are characterised for drug transport assessment for drugs such as salbutamol. However, there were no studies assessing terbutaline transport on the Calu-3 epithelial model at the time of this literature review. There are a limited range of studies that evaluated bronchodilators with a coculture of differentiated epithelium with BSMCs, with a further limit on the number of studies using a Calu-3 epithelium. The two models which use similar cocultures are described in detail below. Both models used Transwell inserts to culture epithelial cells at ALI, with BSMCs cultured on the baseplate of the culture well.

Haghi *et al* (2015) described a primary epithelium cultured at ALI for 72 h, before a 72 h coculture with BSMC grown on the baseplate (Haghi *et al.*, 2015). The study evaluated and quantified the cAMP released from BSMCs after stimulation with salbutamol and in the presence of anti-inflammatory cytokine TGF- β . A greater decrease in cAMP release was quantified in the epithelium-BSMC cocultures than in BSMC alone (Haghi *et al.*, 2015). However, this differences from the latter model were variable between donors which highlights a major drawback in utilising primary epithelial cells in cell culture models. It is important to note that the limited differentiation time of the epithelium (72hr), as well as limited coculture time (72hr), may have impacted the results of the study due to lack of phenotypic differentiation. As shown in Chapter 4, coculture of the two cell types over distinct timeframes can critically impact the phenotypes of both cell types. Furthermore, the distance between the two cell types could generate questions of the models' physiological relevance. This three-day coculture may not be sufficient time to generate a significant functional differentiation of the two cell types as seen in Chapter 4 of this thesis alongside the large distance between the epithelium and the BSMC layers with the medium between the two layers generating questions of physiological relevance.

Muddle *et al*, (2020) introduced a Calu-3 epithelial model differentiated at ALI for 11-14 days. This model was developed for use in a coculture assay aimed at assessing the aerosol deposition of salbutamol in various formulations and evaluated the effectiveness of these formulations on primary BSMCs grown when the Calu-3 model was present (Muddle *et al*., 2020). They reported a significant reduction in the transport of salbutamol to the “receiver chamber” (the well below the Transwell insert) when Calu-3 were present, reflecting the *in vivo* scenario of bronchodilators taking up to 30 min to produce reproducible and sensitive cAMP response from the BSMCs. However, like the model seen in Haghi *et al* (2015), the cells were in indirect coculture, with the BSMCs cultured on the baseplate of the well. In this model reported by Muddle *et al*, the coculture was only sustained for 30 min and the cell growth/differentiation stages were performed in monoculture. This means that any cell-cell communication that could influence cellular behaviour, function or differentiation were absent which could further highlight differences in the amount of drug transported and the resultant response from the BSMCs. (Muddle *et al*., 2020).

5.2. CHAPTER AIMS

The aim of this chapter was to investigate and evaluate the coculture model in its functionality of (a) mediating drug flux across an epithelial barrier, and (b) achieving a relaxation response of BSMCs as a result of a β_2 -AR agonist, terbutaline hemisulfate. By utilising the optimised LC-MS method described in Chapter 2 to quantify the amount of drug in each compartment of the MPS model and employing an optimised cAMP assay to quantify the BSMC response to the bronchodilator. This included the development and validation of a novel bioanalytical method to analyse drug concentration in cell culture matrices utilising the highly sensitive liquid chromatography-tandem mass spectrometry (LC-MS/MS) instrument.

5.3. METHODS

5.3.1. OPTIMISING EXTRACTION SOLVENTS FOR BIOANALYSIS METHOD

Standards and 100 ng/mL samples were prepared as previously described in Section 2.6.1.1. The samples were extracted as described in Section 2.6.1.2 with extraction solvents changed for extraction of terbutaline from the 1000 ng/mL media samples, as follows: The extraction solvent compositions were (MeCN: H₂O) 95:5, 90:10, 85:15, 80:20, and 75:25. The extractions were performed in triplicate for each solvent composition, and the instrument parameters were as described in Section 2.6.1.3.

5.3.2. OPTIMISING VOLUME OF EXTRACTION SOLVENT FOR BIOANALYSIS METHOD

Standards and 100 and 1000 ng/mL solutions were prepared as previously described in Section 2.6.1.1. The samples were extracted as described in Section 2.6.1.2 with extraction solvent volumes changed for extraction of terbutaline from the 1000 and 100 ng/mL media samples. The extraction solvent volumes were 150 and 250 µL and the extractions were performed in triplicate for each solvent and the instrument parameters were as described in Section 2.6.1.3.

5.3.3. OPTIMISING THE VOLUME OF EXTRACTED MEDIA SAMPLES FOR BIOANALYSIS METHOD

Standards solutions were prepared as previously described in Section 2.6.1.1 at the following concentrations: 10, 15, 25, 50, 100, 500, 1000 ng/mL and 50 µL or 25 µL samples were taken in triplicate and extracted with 250 µL of extraction solvent MeCN: H₂O (95:5) with 10 ng/mL D3-Salbutamol. The sample and standard extractions were performed in triplicate for each solvent as described in Section 2.6.1.2 and the instrument parameters were as described in Section 2.6.1.3.

5.3.4. ASSESSING EXTRACTION RECOVERY AND MATRIX EFFECT METHOD

All preparation and extraction steps are the same as previously described in Section 2.6.1.1 and 2.6.1.2. Working standards and calibration standards were made up twice: one set in media and one in solvent which was MeCN: H₂O (95:5). These 2 sets of standards were used for matrix effect analysis. Blank medium was extracted in the same fashion but after the supernatant was extracted, the sample was then spiked with the expected amount of terbutaline before injection. Table 2.2 below details the standards used to spike into the blank medium extracts and the volumes of each standard required to make up to the expected amount of terbutaline. The volume was removed from the 250 µL before the volume was then replenished with the drug spike.

Table 5.1: Spiked media samples for determination of recovery.

Concentration (ng/mL)	Expected Amount in 50 μ L Sample (ng)	Volume of Standard (μ L)	Standard Used
50	2.5	25	100 ng/mL
100	5	50	
200	10	10	
300	15	15	1000 ng/mL
400	20	20	
500	25	25	
600	30	30	

5.3.5. VALIDATION OF THE LC-MS METHOD FOR TERBUTALINE HEMI-SULPHATE SALT IN CELL CULTURE MEDIUM METHOD

As previously described in Sections 2.6.1.1, 2.6.1.2, and 2.6.1.3.

5.3.6. ANALYSIS OF SAMPLE INTEGRITY WHEN DILUTED WITHIN THE CALIBRATION RANGE

Calibration curves with A and B samples were generated as in the validated protocol. Samples in culture medium were made up containing 2740 ng/mL (10 mM) of terbutaline hemi-sulphate and 200 μ L samples were taken and diluted 1 in 5 (200 μ L in 1000 μ L) in the same medium. This is the highest concentration of terbutaline hemi-sulphate salt for use in the cell culture experiments, subsequently diluted to be within the calibration range. Then after ensuring homogenisation, 50 μ L was extracted in accordance with Section 2.6.1.2, standards were made up as described in Section 2.6.1.1 and all standards and samples were analysed with the instrument parameters as described in Section 2.6.1.3.

5.3.7. INVESTIGATION OF TOTAL RECOVERY OF TERBUTALINE FROM THE BARRIER-12 PLATES AND TRANSWELL INSERTS WITH NO CELLS PRESENT

Transwell inserts were collagen coated as previously described in Section 2.4.5 and the PhysioMimix OOC System was set up as described in Section 2.4.6.

Terbutaline hemisulfate (3 mg) was weighed in a sterile 7 mL bijou and smooth muscle growth medium (SmGM) was added at a volume that was salt adjusted as described in Section 2.5.1 to generate a concentration of 1000 μ g/mL (3650 μ M) of terbutaline. This was further diluted in SmGM to give rise to a final concentration of 2.74 μ g/mL (10 μ M). The transport of terbutaline hemisulfate was investigated in the apical to basolateral direction as well as the basolateral to apical direction across the Transwell insert. The basolateral compartment

contained 750 μL of medium and the apical contained 200 μL of medium. The compartment which was contained the medium with 10 μM of terbutaline was labelled the “donor chamber”, whilst the opposite compartment which was sampled over time was labelled the “receiver chamber”.

Dosing the inserts consisted of aspirating all medium and adding fresh medium to the receiver chamber. The donor chamber was then dosed with 10 μM terbutaline solution and incubated at 37°C and 5% CO_2 on a plate shaker at 200 rpm. At time points 60, 180, and 360 min all the medium in the receiver chamber was pipetted into an Eppendorf vial and replenished with fresh medium pre-warmed to 37°C. At 1440 min (24 hr post dosing), the receiver and the donor chamber were collected into separate Eppendorf vials. These Eppendorf vials were then stored at -80°C until they were thawed for LC-MS analysis. When analysed for LC-MS, the samples and standards were prepared and analysed as described in Sections 2.5.1 to 2.5.3.

5.3.8. TERBUTALINE TRANSPORT ACROSS A DIFFERENTIATED CALU-3 MPS MODEL

Calu-3 cells were maintained as described in Section 2.5.2 and then seeded and grown in monoculture on the collagen coated Transwells in the Physiomimix OOC system as detailed in Sections 2.5.5 to 2.5.8 and cells were maintained for 7 days post air-liquid interface (ALI) establishment. A solution of terbutaline hemisulfate was prepared in cell culture medium as described in Section 5.3.1, at a concentration of 10 μM terbutaline, and dosed on the appropriate compartment either side of the insert.

The transport of terbutaline hemisulfate was investigated in the apical to basolateral direction as well as the basolateral to apical direction across the Transwell insert. The basolateral compartment contained 750 μL of medium and the apical contained 200 μL of medium. The compartment which was contained the medium with 10 μM of terbutaline was labelled the “donor chamber”, whilst the opposite compartment which was sampled over time was labelled the “receiver chamber”. The dosing and sampling method was the same as described in Section 5.3.1. The Calu-3 epithelial cells were also detached using 100 μL of TrypLE on each well for 15 min in the incubator before the addition of 100 μL of cell culture medium. The full 200 μL with the detached cells were placed into Eppendorf vials. These Eppendorf vials were then stored at -80°C until they were thawed for LC-MS analysis.

When analysed for LC-MS, the samples and standards were prepared and analysed as described in Sections 2.6.1.1 to 2.6.1.3. For the detached cell samples, the samples were thawed and warmed to room temperature before being vortexed for 30 s. After, the 200 μL cell samples were sonicated for 10 min before another 30 s vortex. Then, a 50 μL aliquot was taken and added to 250 μL of 10 ng/mL D3-Salbutamol 95:5 (MeCN: H_2O). The sample then underwent another 10 min sonication before another 30 s vortex. The sample was then

centrifuged and followed the sample preparation steps as in processed as described in Section 2.6.1.2.

5.3.9. OPTIMISATION OF THE cAMP QUANTIFICATION ASSAY

The HitHunter® cAMP Assay for Small Molecules (Eurofins, USA) was used for the quantification of intracellular cAMP of the BSMCs. In Table 5.2 below, the reagents in the kit are listed and the ratio and volumes of the reagents that were used to make up the working cAMP Detection Solution are detailed in Table 5.3.

Table 5.2: Reagents in the HitHunter® cAMP Assay kit

Reagents
cAMP Antibody Reagent
cAMP Lysis Buffer
Substrate Reagent 1
Substrate Reagent 2
cAMP Solution D
cAMP Solution A

Table 5.3: Working cAMP Detection Solution reagent composition with ratio and volumes.

Reagent	Volume Ratio	Volume (mL)
cAMP Lysis Buffer	19	3.8
Substrate Reagent 1	5	1.0
Substrate Reagent 2	1	0.2
cAMP Solution D	25	5.0
Total	50	10

Bronchial Smooth Muscle Cells (BSMCs) were seeded on sterile 96-well white walled optical plates in triplicate for each density in each condition.

The densities seeded were:

1. 3 000 cells/well
2. 6 000 cells/well
3. 12 000 cells/well
4. 20 000 cells/well
5. 30 000 cells/well

6. 40 000 cells/well

The cells were maintained for 24 h to allow the cells to adhere to the plate. 3-isobutyl-1-methylxanthine (IBMX) (Sigma Aldrich, UK), was weighed and dissolved to 0.56 mg/mL (2.5 mM) in cell culture medium. Isoprenaline (Sigma Aldrich, UK) was weighed and dissolved to 1 mg/mL (4048 μ M) in cell culture medium before being serially diluted to 0.00247 mg/mL (10 μ M) in cell culture medium.

The 4 conditions were:

1. Control with IBMX
2. Control without IBMX
3. Dosed with IBMX
4. Dosed without IBMX

The relevant wells were incubated with 100 μ L of IBMX (2.5 mM) in medium for 30 min. The control wells (without IBMX) were incubated with the same volume of blank medium. The cells were then washed with fresh medium before being incubated with 100 μ L isoprenaline (10 μ M) for 30 min. The Control conditions were incubated with the same volume of blank medium. Thereafter, the cAMP assay was performed according to the manufacturers protocol. Briefly, 20 μ L cAMP Antibody Reagent and 80 μ L of working cAMP Detection Solution was added to each well and then the plate was incubated for 1 h at room temperature in the dark. After incubation, 80 μ L of cAMP Solution A was added to each well and incubated in the dark at room temperature overnight. After this incubation step, the plate was transferred to the FLx800 Fluorescence Plate Reader (Biotek, USA) to read the luminescence at 0.1 s/well.

5.3.10. EVALUATION OF THE BRONCHIAL COCULTURE MPS MODEL'S RESPONSE TO A BETA-2 (B_2) ADRENERGIC RECEPTOR AGONIST

Calu-3 and BSMC cells were maintained as described in Section 2.5.2 and 2.5.3 then seeded and grown in coculture on the collagen coated Transwells in the Physiomimix OOC system as detailed in Sections 2.5.5 to 2.5.8 and maintained for 7 days post ALI establishment. 3-isobutyl-1-methylxanthine (IBMX) was weighed and diluted to 0.56 mg/mL (2.5 mM) in cell culture medium. The inserts were aspirated of all medium before being incubated with 600 μ L medium with IBMX (2.5 mM) in the basolateral chamber and incubated for at least 30 min at 37°C and 5% CO₂. After the incubation, the cells were washed with PBS 3 times before dosing with terbutaline. Terbutaline hemisulfate was weighed, dissolved, and diluted to 2.74 μ g/mL (10 μ M) as described in Section 5.3.1.

All medium was removed, and fresh medium added to the basolateral chamber (750 μ L). The apical chamber was dosed with 200 μ L terbutaline solution (10 μ M) and incubated at 37°C

and 5% CO₂. At time points 30, 60, 120 and 180 min all the medium in the basolateral chamber was pipetted into an Eppendorf vial and the chamber replenished with fresh medium (750 µL). At 180 mins, the basolateral and the apical chamber were pipetted into separate Eppendorf vials. These Eppendorf vials were then stored at -80°C until they were thawed for LC-MS analysis.

The HitHunter® cAMP Assay for Small Molecules (Eurofins, USA) was performed at 180 min with the reagents made up as previously described in Table 5.2. The manufacturer protocol was adjusted for use on the Transwell insert. Briefly, the Transwell insert was inverted on to a plate lid with the BSMCs facing up and 80 µL of cAMP detection solution was added as a droplet on the basolateral face of the insert, covering the cells. This was left to lyse the cells for 5 min before the full 80 µL was taken to a 96-white walled optical plate and 20 µL of cAMP Antibody Reagent were added to the wells along with 40 µL PBS and then the plate was incubated at room temperature in the dark for 1 h. After, 80 µL of cAMP Solution A was added and left to incubate over night before reading the luminescence on the FLx800 Fluorescence Plate Reader (Biotek, USA) for 0.1 s/well.

During the first incubation step of the cAMP assay, the Calu-3 epithelial cells were detached using 100 µL of TrypLE on each well for 15 min in the incubator before the addition of 100 µL of cell culture medium. The full 200 µL with the detached cells were placed into Eppendorf vials and transferred to the -80°C. When analysed for LC-MS, the samples and standards were prepared and analysed as described in Sections 2.5.1 to 2.5.3. For the detached cell samples, the samples were processed similarly as described in Section 2.5.2 however, they were first sonicated for 30 min after the addition of 250 µL of 10 ng/mL D3-Salbutamol 95:5 (MeCN: H₂O) to the 50 µL sample. After, the sample processing procedure was the same as described in Section 2.6.1.2.

5.4. RESULTS AND DISCUSSION

5.4.1. OPTIMISING EXTRACTION SOLVENTS FOR BIOANALYSIS

To develop the sample preparation methodology presented in Section 2.6.1.2, it was initially necessary to identify the optimum solvent composition that maximized the extraction of terbutaline hemi-sulphate from the cell culture media. The peak area response for extracts of terbutaline hemi-sulphate in 50 μ L aliquots of cell culture medium at a concentration of 100 ng/mL is presented in Figure 5.3, following extraction in triplicate according to the general methodology of Section 2.6.1.2 with various compositions (v/v) of Optima grade solvent acetonitrile: water mixtures (95:5, 90:10, 85:15, 80:20, and 75:25 v/v). Peak area response was highest at 95:5 (MeCN: H₂O) (ANOVA $P < 0.0001$) which indicates the extraction of terbutaline from the sample of cell culture medium was most effective at this ratio compared to the others with a significantly higher response in peak area. As such, the extraction solvent selected for use in Section 2.6.1.2 was a mixture of 95:5 (v/v) MeCN: H₂O.

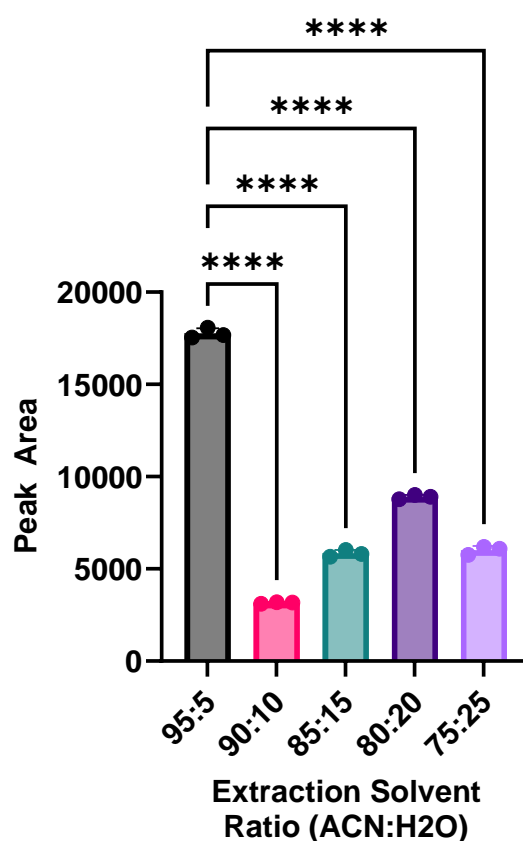


Figure 5.3: Peak area response was highest in 95:5 v/v MeCN: H₂O. Peak area response of terbutaline at 100 ng/mL with the different extraction solvent ratio with statistical significance of 95:5 solvent shown (ANOVA **** = $P < 0.0001$) (N=3).

5.4.2. OPTIMISING THE VOLUME OF EXTRACTION SOLVENT FOR BIOANALYSIS

The best volume of extraction solvent to extract the highest amount of terbutaline from cell culture medium samples was required to optimise the extraction process. This was performed on two concentration levels: 100 and 1000 ng/mL. Figure 5.4 illustrates that at a solvent volume of 250 μ L significantly more drug was extracted than 150 μ L (unpaired t-test 100 ng/mL $P = 0.000518$; 1000 ng/mL $P = 0.000015$), demonstrating the higher volume more effective for extraction of terbutaline from cell culture medium across a range of concentrations. Moving forward, 250 μ L was the extraction volume to be used for extraction of terbutaline from cell culture medium.

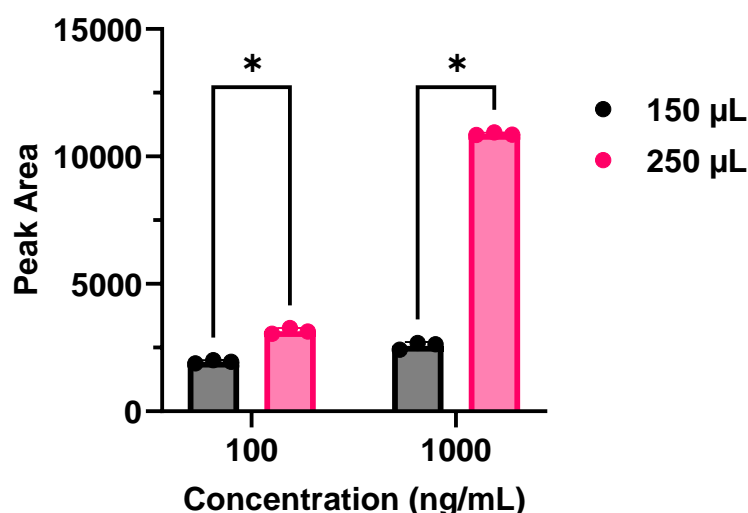


Figure 5.4: 250 μ L extraction volume resulted in the highest peak area response. Peak area response of terbutaline at 100 and 1000 ng/mL at the two extraction solvent volumes 150 and 250 μ L with statistically significant shown (unpaired T-test 100 ng/mL $P = 0.000518$ 1000 ng/mL $P = 0.000015$) (N=3).

5.4.3. OPTIMISING THE VOLUME OF EXTRACTED MEDIUM SAMPLES

The purpose of this experiment was to determine the highest peak area from supernatant extracts of terbutaline hemi-sulphate from two volumes of cell culture media. This was assessed across the calibration range from 10 to 1000 ng/mL to evaluate the difference in linear regression and the use of the equation of the line to determine the concentration of each sample analysed to determine accuracy of the calibration line. Figure 5.5 shows the difference between the slopes of the 25 μ L and 50 μ L samples with the 50 μ L sample extracts resulting in a steeper slope. The higher peak areas for the 50 μ L samples resulted in very different

outcomes when using the linear regression analysis to calculate the concentration of the y-values at each concentration as seen in Table 5.4.

Table 5.4 demonstrates that using a 50 μL sample volume resulted in a more accurate concentration calculation (Equation 5.1) within the acceptance range of 75-125% across the concentration range analysed. The lowest concentration within the acceptable range was at 25 ng/mL for 50 μL volume whereas for the 25 μL volume it was at 50 ng/mL. At 25 μL , the sample volume only achieved 61.39% accuracy at 25 ng/mL, highlighting the greater sensitivity achieved at 50 μL sample volume. Consequently, the 50 μL sample volume successfully quantified as low as 10 ng/mL where the 25 μL failed, however the back-calculation was well below the pass threshold of 75%. This experiment confirms the 50 μL sample volume was the most appropriate for developing a sensitive calibration curve of terbutaline hemi-sulphate extracted from cell culture medium.

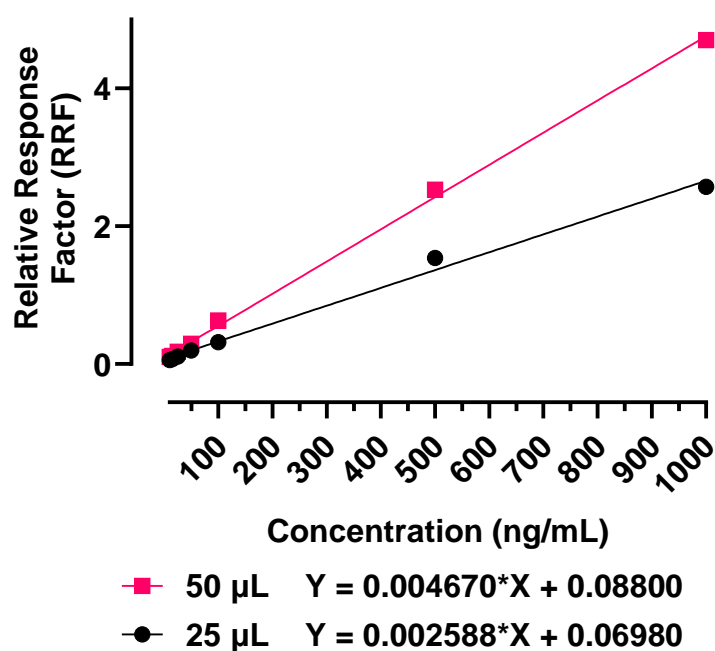


Figure 5.5: 50 μL sample resulted in a higher gradient and y-intercept than the 25 μL sample. Linear regression analysis of terbutaline relative response factor (RRF) extracted from cell culture medium across a range from 10 ng/mL to 1000 ng/mL with the equation of the lines ($N \leq 3$).

Table 5.4: Nominal concentration of each standard level calculated from the calibration curve using Equation 5.1 (N=3)

Sample Volume (μL)	Concentration (ng/mL)						
	10	15	25	50	100	500	1000
25	-49.29	1.69	61.36	96.48	96.24	113.63	96.71
50	31.00	40.37	77.39	88.24	116.89	104.63	98.75

$$\frac{\text{Calculated Concentration } (\frac{\text{ng}}{\text{mL}})}{\text{Actual Concentration } (\frac{\text{ng}}{\text{mL}})} \times 100 = \text{Nominal Concentration } (\%)$$

Equation 5.1

5.4.4. ASSESSING EXTRACTION RECOVERY AND MATRIX EFFECT

Matrix effect is defined as an alteration of the analyte response due to interference from unidentified components in the sample matrix (EMA, 2022). Assessment of recovery from the extraction process is determined by comparing the response of the analyte in the cell culture medium that has been processed against the response of a blank medium sample that has been processed and subsequently spiked with the analyte (EMA, 2022). Figure 5.6 shows the chromatograms of terbutaline at two concentrations in samples from medium and solvent which have been taken through the extraction process. It can be seen the difference between the peak shapes and height are negligible between the two matrices. The baseline noise between the concentrations of each matrix was similar. Figure 5.7 shows the chromatograms of D3-Salbutamol from the same samples as Figure 5.6, illustrating the matrix effect did not alter the chromatography of the internal standard.

Equation 5.2 was used to calculate the percentage recovery values presented in Table 5.4. The recovery of terbutaline from cell culture medium when taken through the extraction process was consistent throughout the concentration range. Table 5.5 shows a range of 81.15 – 89.02% recovery across the calibration range, a difference of 7.87% between the lowest recovery (at 50 ng/mL) and the highest recovery (at 200 ng/mL). This was in agreement with the EMA Bioanalysis Validation requirements which deemed the recovery needs to be consistent but not necessarily 100% (EMA, 2022).

As shown in Table 5.6, the matrix effect was calculated with terbutaline extracted in medium and solvent (95:5 MeCN: H₂O) across the calibration range. The matrix effect was calculated

using Equation 5.3 and indicates the matrix effect ranges from 3.4% to 8.04% which is within the validation criteria of no more than 15% (EMA, 2022). The matrix effect therefore passed the specification, concluding the matrix effect was not detrimental to the analysis of terbutaline from cell culture medium. Concluding, the extraction process resulted in a loss of 11-19% across the calibration range and the matrix effect is between 3.4-8.04% which was within the acceptance criteria and the next steps are to validate the calibration curve.

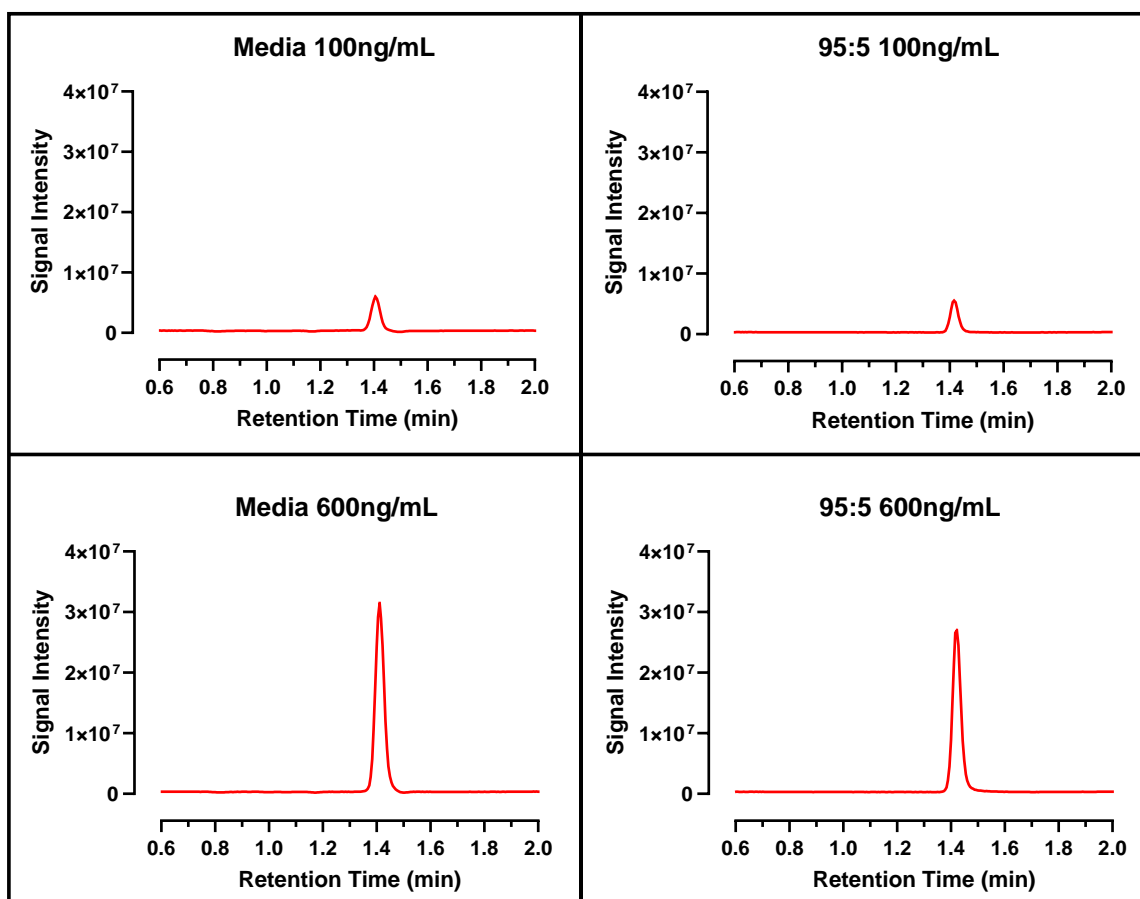


Figure 5.6: The medium sample extracts had a higher signal intensity at each concentration than the solvent equivalent. Chromatograms of terbutaline at 100 ng/mL and 600 ng/mL in extracted medium samples and extracted solvent (95:5 Acetonitrile: Water).

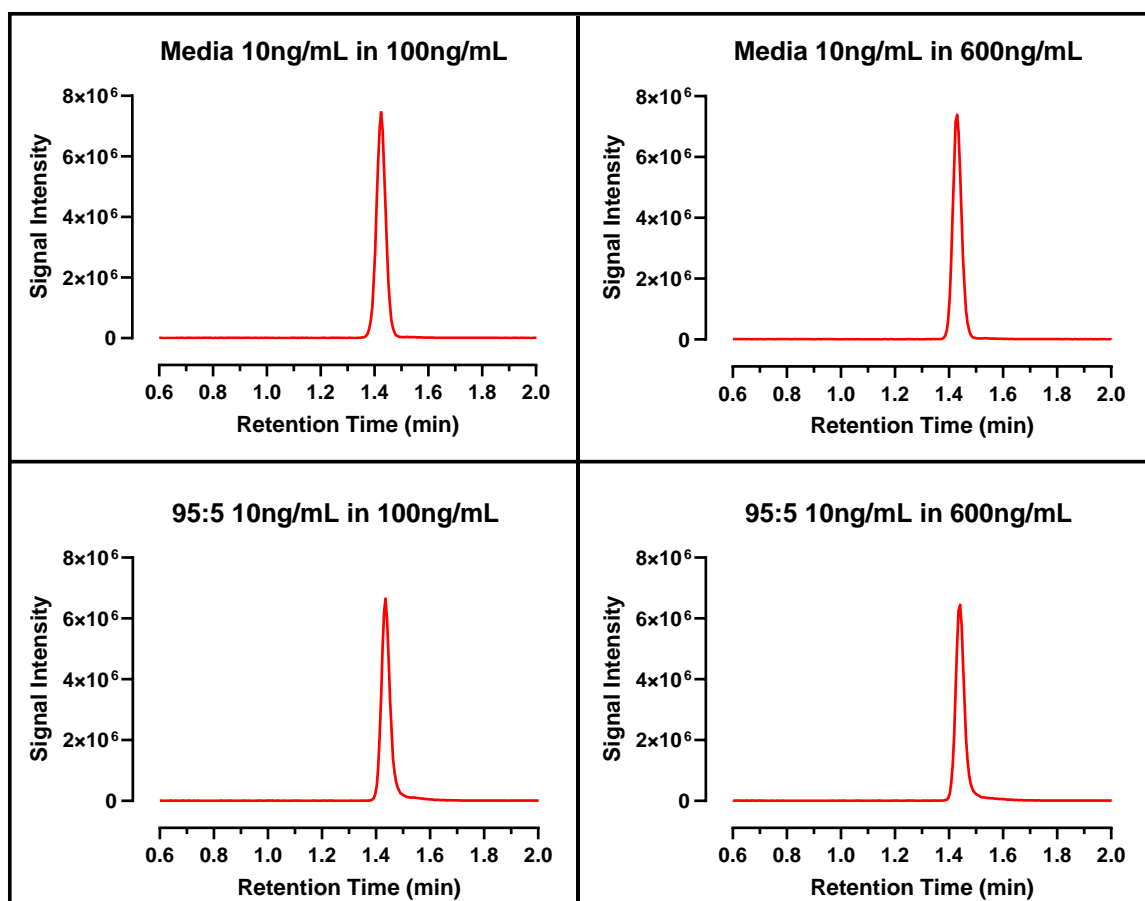


Figure 5.7: The signal intensity of D3-Salbutamol was similar regardless of terbutaline concentration and only a slight increase in signal intensity in medium extracts compared to the solvent extracts. Chromatograms of D3 Salbutamol at 10 ng/mL in medium and solvent (95:5 Acetonitrile: Water) samples of terbutaline at 100 ng/mL and 600 ng/mL after extraction.

Table 5.5: Recovery of terbutaline from cell culture medium. expressed as a percentage of the ratio of the RRF of terbutaline extracted from media samples to the RRF of terbutaline at that concentration spiked into blank media samples extracted in the same method and performed at seven concentration levels (N=3).

	Concentration (ng/mL)						
	50	100	200	300	400	500	600
Medium Extract (RRF (%RSD))	0.273 (10.27)	0.516 (3.12)	1.006 (2.43)	1.474 (19.47)	1.945 (3.10)	2.265 (4.57)	2.650 (4.02)
Medium Spiked (RRF (%RSD))	0.336 (12.56)	0.606 (1.03)	1.131 (3.07)	1.656 (3.00)	2.237 (1.71)	2.630 (1.98)	3.110 (1.64)
Recovery (%)	81.15	85.28	89.02	89.01	86.92	86.13	85.21

$$\frac{\text{RRF of Terbutaline in Media Extract}}{\text{RRF of Terbutaline in Media Spiked}} \times 100$$

Equation 5.2

Table 5.6: Matrix effect of cell culture medium on terbutaline response. Expressed as a percentage of the ratio of the RRF of terbutaline extracted from media samples to the RRF of terbutaline at that concentration extracted from solvent samples extracted in the same method and performed at seven concentration levels (N=3).

	Concentration (ng/mL)						
	50	100	200	300	400	500	600
Medium (RRF (%RSD))	0.273 (10.27)	0.516 (3.12)	1.006 (2.43)	1.474 (10.47)	1.945 (3.10)	2.265 (4.57)	2.650 (4.02)
Solvent (RRF (%RSD))	0.256 (0.39)	0.496 (2.25)	0.973 (0.57)	1.374 (1.80)	1.800 (1.91)	2.148 (1.51)	2.504 (0.80)
Matrix (%)	106.44	104.03	103.40	107.25	108.04	105.43	105.82

$$\frac{RRF \text{ of Terbutaline in Media Extract}}{RRF \text{ of Terbutaline in Solvent Extract}} \times 100$$

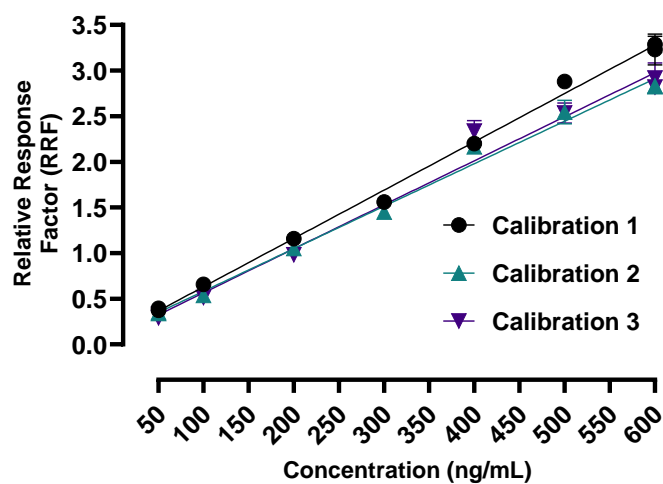
Equation 5.3

5.4.5. VALIDATION OF THE LC-MS METHOD FOR TERBUTALINE HEMI-SULPHATE IN CELL CULTURE MEDIUM

The validation of the LC-MS method for the analysis of terbutaline hemi-sulphate salt was determined by the criteria set by the EMA Bioanalysis Validation document (EMA, 2022). These criteria consisted of the calibration curve having a $\pm 20\%$ nominal concentration at the LLOQ and $\pm 15\%$ at all other concentrations, with a minimum of 6 concentration levels and at least 75% should meet the criteria including the LLOQ. The accuracy of the quality control (QC) standards at $\pm 20\%$ nominal concentration at the lowest level of quantification (LLOQ) and $\pm 15\%$ at all other concentrations, precision of B standards, where the relative standard deviation (%RSD) does not exceed 20% at LLOQ and 15% at all other concentrations. The QC standards must be at 3 levels (low, medium, and high) and consist of at least 5 replicates at each level. Carry over signal should be lower than 20% at the LLOQ. This criterion needs to be met on at least 3 separate runs over 2 days to be accepted. Within this project which required fit-for-purpose, but not clinical bioanalysis, the acceptance criteria were set as $\pm 20\%$ of the nominal concentration for all levels of concentrations in the calibration back-calculated values and the QC standards.

Figure 5.9 shows the calibration lines generated from extracting samples across the calibration range of 50 – 600 ng/mL. The equation of the lines was used to calculate the concentration of the samples and then the percentage of the nominal concentration (calculated using Equation 5.2) as detailed in Table 5.7 for Calibration 1. The equation was also used to calculate the concentration of the QC standards and the percentage of the nominal concentration and is detailed in Table 5.8 for Calibration 1. This data was used to confirm the first run passed the acceptance criteria and the next two validation runs were generated.

The calibration curves generated from validation runs 2 and 3 are shown in Figure 5.8. The validation data for all 3 runs are presented in Table 5.9 with the acceptance criteria, showing all three runs passed the acceptance criteria validating this bioanalytical method for the analysis of terbutaline hemi-sulphate in cell culture medium.



Calibration	Equation	R ²
1	Y = 0.005293 * X + 0.1019	0.99
2	Y = 0.004657 * X + 0.1164	0.99
3	Y = 0.004821 * X + 0.0831	0.99

Figure 5.8: All three calibration curves were similar in gradient and y-intercept. Calibration curves generated from the validation calibration runs across the full concentration range with the linear regression and equation of the lines with the linearity (R^2).

Table 5.7: Summary table of all calculated values of from the calibration curves in Figure 5.9 (N=3).

Calibration Standards (ng/mL)	50	50	100	200	300	400	500	600	600
Average RRF and (RSD%)	0.34 (3.64)	0.35 (7.31)	0.54 (5.29)	1.05 (2.46)	1.45 (3.97)	2.17 (2.19)	2.54 (5.04)	2.82 (2.57)	2.83 (1.41)
Concentration (ng/mL)	47.7	49.8	90.3	200.5	286.4	440.2	521.4	581.1	583.0
Nominal Concentration (%)	95.5	99.5	90.3	100.3	95.5	110.0	104.3	96.9	97.2

Table 5.8: Quality control (QC) standards summary table for all QC samples in the validation runs (N=5).

QC Standards (ng/mL)	50	150	300	450	600
Average RRF and (RSD%)	0.34 (5.65)	0.81 (4.84)	1.37 (4.86)	2.30 (3.24)	2.78 (1.87)
Concentration (ng/mL)	48.7	148.4	268.7	468.8	572.8
Nominal Concentration (%)	97.3	98.9	89.6	104.2	95.5

Table 5.9: Summary table of all LC-MS validation data with the validation criteria from the EMA ICH M10 Bioanalytical Validation (EMA, 2022).

Category	Criteria	Run 1	Run 2	Run 3
Calibration Curve	$\pm 20\%$ Nominal at all concentrations	4.5% at LLOQ 10.04 -0.25% for all others	10.24% at LLOQ 0.19 - 8.31% for all others	86.49% at LLOQ 1.61 – 17.31% for all others
Accuracy and Precision	$\pm 20\%$ Nominal all concentrations	2.71% at LLOQ 10.44 - 1.08% for all others	4.54 % at LLOQ 1.35 – 14.17% for all others	10.20% at LLOQ 6.58 – 18.65% for all others
	%RSD does not exceed 20% at all concentrations	5.65% at LLOQ 1.87 – 4.86% for all others	3.54% at LLOQ 2.96 - 4.23% for all others	10.03% at LLOQ 2.24 – 6.42% for all others
Carry over	Less than 20% of LLOQ	0%	0%	0%

5.4.6. ANALYSING SAMPLE INTEGRITY WHEN DILUTED WITHIN THE CALIBRATION RANGE

Integrity of dilution is the assessment of the sample dilution procedure, when required, confirming that the dilution does not impact the accuracy and precision of the measured concentration of the analyte (EMA, 2022). This experiment validated the integrity of the calibration line when diluting samples that are initially at a higher concentration than the upper limit of quantification (ULOQ) of the calibration curve. The concentration chosen was the highest concentration that was anticipated to be analysed, i.e. the concentration of drug that is dosed on to the cell culture experiments at 2740 ng/mL. The results in Table 5.10 show that the calculated concentrations of the diluted samples were within 85-115% of the nominal

concentration, thus passing the acceptance criteria as detailed in the EMA Bioanalysis Validation document (EMA, 2022).

Table 5.10: Concentration of the diluted samples. Nominal concentration calculated using Equation 5.1 with standard deviation (N=5).

Dilution Sample	Average Concentration (\pm STDEV) (ng/mL)	Nominal Concentration (%)
1	2971.35 (\pm 133.36)	108.44
2	2907.70 (\pm 176.61)	106.12
3	2927.70 (\pm 147.69)	106.85
4	3046.30 (\pm 70.44)	111.18
5	2588.82 (\pm 88.45)	94.48
Total Average	2888.37	105.41

5.4.7. TERBUTALINE CAN BE EFFECTIVELY EXTRACTED FROM CELL CULTURE MEDIUM IN THE TRANSWELL INSERTS AND THE MPS BARRIER-12 PLATES WITH NO CELLS PRESENT

To accurately determine the total amount of terbutaline that can be recovered from the transport studies and quantified by LCMS, the interaction of terbutaline with the perfused Barrier-12 plate and Transwell inserts was first analysed. It was hypothesised that the perfusion microchannels could have an influence on the rate and amount of terbutaline transported in both transport directions (A-B and B-A). Furthermore, the materials of the consumables being used were considered. The Transwell inserts contain polytetrafluoroethylene (PTFE) membranes, whilst a 24-well culture plate is made of polystyrene and the perfused Barrier-12 plate is made of cyclic olefin copolymer (COC). The difference in plastic may have an influence in the amount of non-specific binding of drugs and therefore the extent of this binding by terbutaline needed to be determined for this to be attributed before the introduction of cells. The analysis of the cell culture medium was quantified as previously detailed. Once quantified, the amount of drug present in each chamber was expressed as a percentage of the total amount of terbutaline that was dosed in the donor chamber (Figure 5.9 and Figure 5.10).

The amount of terbutaline recovered in the receiver and donor chambers (expressed as a percentage of the total dose of terbutaline) following transport in the apical to basolateral (A-B) direction of a Transwell insert under static and perfused conditions was calculated (Figure 5.9 A). For the A-B direction, 80.96% and 89.81% on average permeated across the

membrane into the receiver chamber after 24 h in the static and perfused condition, respectively (Table 5.11). In the B-A direction, 30.76% and 30.54% on average permeated across the membrane into the receiver chamber after 24 h in the static and perfused condition, respectively (Table 5.11).

There was no statistical difference between the two conditions (static vs. perfused) in the amount of drug found in the two chambers (Two-Way ANOVA $P < 0.05$). There was a significant difference in the amount of drug in the donor chambers for the B-A direction, with the medium aspirated from perfused condition wells containing significantly lower amounts of terbutaline than the static condition. However, this difference could be accounted for by the difference in the mass balance (Table 5.11) as the perfused condition had more total drug calculated in the two chambers than the static condition. To note, there were two replicates for each condition as the third replicate was lost during an instrument failure on the LC-MS instrument. The amount of drug in the chambers for both conditions for the basolateral to apical (B-A) direction was also calculated (Figure 5.9 B). The average percentage of terbutaline in each compartment for the A-B and B-A directions in each condition can be seen alongside the standard deviation of the replicates (Table 5.11).

There was a large increase in the mass balance in the A-B direction (Table 5.11). This may have been a result of overestimating the magnitude of the volume left in the compartments at the final timepoint as it was assumed to be the same as was added at the beginning. However, after 24 h evaporation of medium in the apical chambers would be expected leaving a lower volume than added initially, resulting in an underestimation of drug present in the chamber. Given the high concentration in the apical chamber, which was subject to evaporation, a small extent of solvent evaporation would have caused a significant increase in the analytically determined amount, since the amount recovered was a function of concentration (which would increase) multiplied by nominal volume (which was over-estimated). In the B-A directions, there was some drug loss observed ($< 100\%$ mass balance). This may have been a result of drug/media not being fully removed from the plate. This was mostly seen in the perfused condition, and it would be expected that a small volume would remain inaccessible in the microfluidic channels of the Barrier-12 plate after aspiration of the volume in the well.

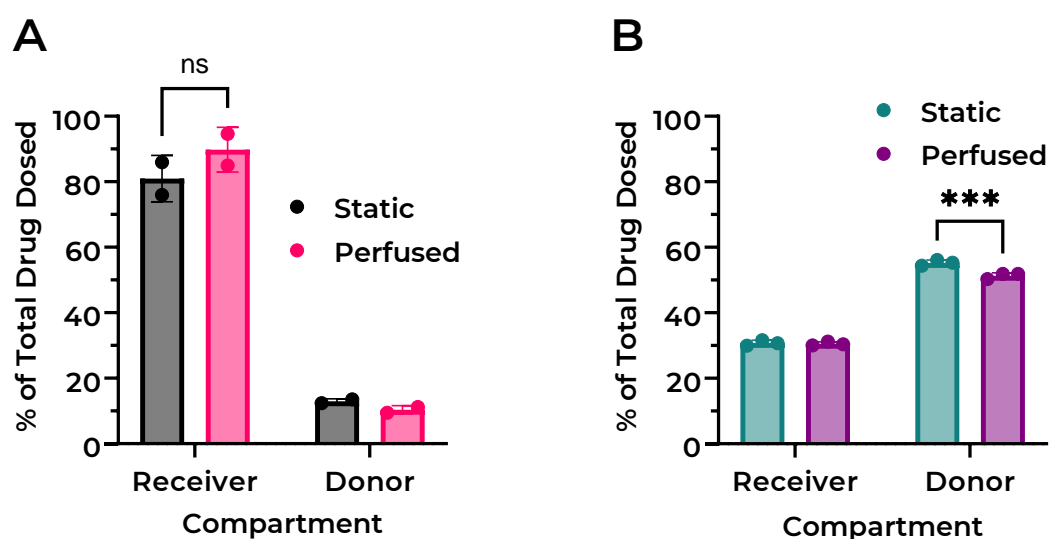


Figure 5.9: Marginal difference in terbutaline permeation and adsorption were observed in perfused and static conditions. Proportion of terbutaline (% total dosed amount) in the compartments in both the static and perfused conditions in the **(A)** apical to basolateral direction and the **(B)** basolateral to apical direction (Two-Way ANOVA ns = $P > 0.05$, *** = $P < 0.001$) ($N \leq 2$).

Table 5.11: Average amount of terbutaline in each chamber relative to the total dosed amount. Percentage of the total amount and standard deviation in each compartment of the Calu-3 epithelial Transwell model in static and perfused in the apical to basolateral direction and the basolateral to apical direction

Direction	Condition	Receiver (%) ±STDEV	Donor (%) ±STDEV	Mass balance (%) ±STDEV
Apical to Basolateral	Static	80.96 ± 7.07	12.94 ± 0.80	93.91 ± 7.87
	Perfused	89.81 ± 6.86	10.36 ± 1.25	100.16 ± 5.60
Basolateral to Apical	Static	30.76 ± 0.84	56.11 ± 0.88	86.00 ± 1.48
	Perfused	30.54 ± 0.60	51.32 ± 1.79	81.86 ± 1.49

Comparing the A-B to B-A transport directions for both perfused and static conditions show an interesting result. The static condition of the A-B transport resulted in a significantly higher amount of terbutaline in the receiver chamber than the B-A direction (Figure 5.10 A). It is to be noted that the receiver chamber in the A-B transport is the basolateral compartment, while in the B-A direction, the receiver chamber is the apical compartment. The donor chamber of the A-B direction had a significantly lower percentage of drug than the B-A direction. This

difference may be attributed to the difference in volumes of the receiver chamber; for the A-B direction, the receiver chamber contained 750 μL while the apical contained only 200 μL , whereas in the B-A direction the receiver chamber only contained 200 μL . As the A-B receiver chamber has a larger 'sink' volume than the donor chamber, this likely resulted in the maintenance of a diffusion gradient into the receiver chamber leading to more drug diffusing into the receiver chamber. Whereas in the B-A direction the donor chamber has a lower volume than the receiver chamber which had been dosed with drug, resulting in an equilibrium of the drug concentration as the diffusion gradient is not as great as the A-B direction.

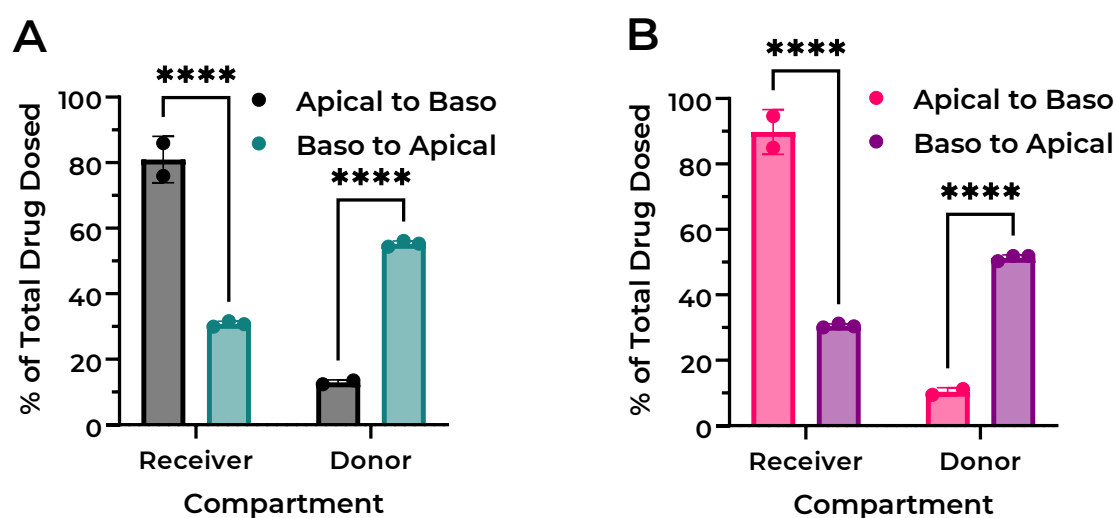


Figure 5.10: There is a significant difference in the amount of drug in each chamber between the two directions in static and perfused conditions. Proportion of terbutaline (% of total dosed amount) in the compartments in the (A) static condition and the (B) perfused condition, comparing the apical to basolateral direction against the basolateral to apical direction. (Two-Way ANOVA **** = $P < 0.0001$) ($N \leq 2$)

The P_{app} of terbutaline across the Transwell insert in the perfused and static condition was calculated for the A-B and the B-A directions (Figure 5.11). The rate of terbutaline diffusion was similar in both directions, regardless of the condition. Although the amounts of terbutaline in each chamber differed depending on the direction of transport, the rate at which the drug reached the receiver chamber was similar in each direction. This can be interpreted as the perfused condition having no effect on the passive permeability of terbutaline through the Transwell membrane and resulting in similar results as the static condition. Although, the A-B static condition had a significantly lower P_{app} (2.35×10^{-5} cm/s) than the B-A static (2.65×10^{-5} cm/s) and the B-A perfused (2.61×10^{-5} cm/s) however, this difference was not indicative of a

significantly faster permeability in the B-A direction and is more indicative of the difference in statistics with 2 replicates in the A-B direction vs 3 replicates in the B-A direction.

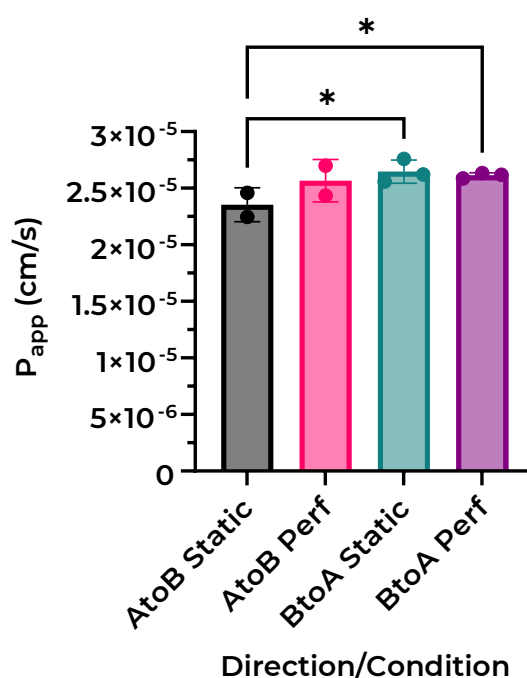


Figure 5.11: The rate of permeability was not different for either transport direction, regardless of condition. Apparent permeability (P_{app}) of terbutaline hemisulphate across the blank Transwell insert in the static and perfused conditions in the two directions (apical to basolateral and basolateral to apical) (ANOVA ns = $P > 0.05$, **** = $P < 0.0001$) ($N \leq 2$).

This experiment has shown the sampling method of the static and perfused Transwell models results in the successful analytical recovery of drug from the two chambers in both A-B and B-A directions across the Transwell support. The mass balance could be attributed to sampling/pipetting error as well as over/under calculated drug concentrations due to volume loss through evaporation during the assay. There was no significant difference between the static plate and the perfused Barrier-12 plate in terms of amount of drug recovered/lost and moving forward, both culture plates can be used in the transport experiments of terbutaline with the cell barrier models. The differences in the amount recovered in the two chambers depending on the diffusion direction can be attributed to the volume differences in the respective donor and receiver chambers affecting the total amount of drug transported. However, the rate of terbutaline diffusing across the membrane was similar in both directions in both conditions. These results suggest that the Barrier-12 plate was not detrimental to the sample collection and subsequent quantification of terbutaline transport study samples. The

next step was to evaluate the transport of terbutaline across the Calu-3 epithelium Transwell barrier model in the static and perfused conditions.

5.4.8. THE TRANSPORT RATE OF TERBUTALINE IS HIGHER IN THE APICAL-TO-BASOLATERAL DIRECTION IN THE CALU-3 MPS MODEL THAN THE BASOLATERAL-TO-APICAL

Assessment of the Calu-3 barrier was carried out using Transepithelial Electrical Resistance (TEER) across the 12 days of culture before dosing (Figure 5.12). The TEER was significantly lower in the perfused cultures compared to the static across all days except Day 7 when there was no significant difference. This was like the TEER profiles seen in the models in the previous chapters. The TEER values themselves were rather low at less than 100 Ω/cm^2 on Day 12 for both conditions, lower than previous Calu-3 monoculture experiments in Chapter 3 which may indicate poor tight junction formation and a more permeable barrier.

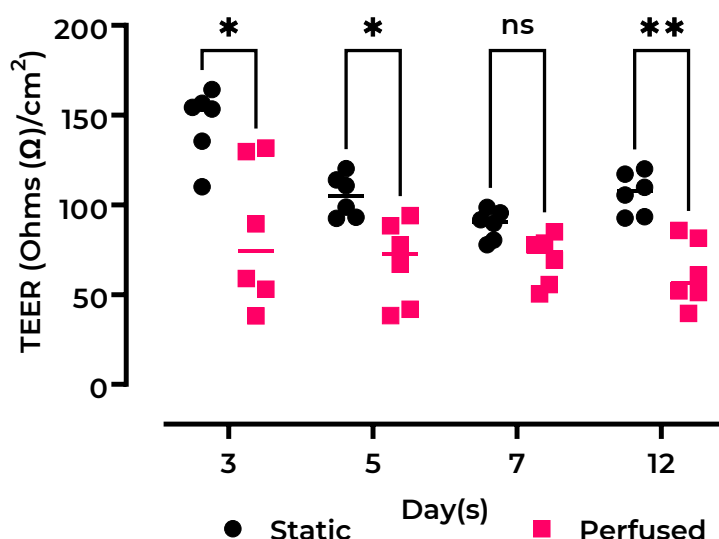


Figure 5.12: The static Calu-3 barrier model had a higher TEER profile than the perfused Calu-3 barrier model. TEER measurements of the Calu-3 Transwell models in the static and perfused conditions from days 3 to 12 post ALI (Two-Way ANOVA ns = $P > 0.05$, * = $P < 0.05$, ** = $P < 0.01$) (N=6).

The amount of terbutaline in the receiver and donor chambers was calculated using LC-MS to quantify the drug concentrations and amounts in each chamber and then expressed as a percentage of the total dose for the A-B direction (Figure 5.7 A) and the B-A direction (Figure 5.13 B). There was no significant difference between in two conditions in either transport direction. An average of 20.23% of the drug reached the receiver chamber in the A-B direction of the static model with the perfused equivalent achieving 29.38% (Table 5.12) after 180 mins

however, these were not statistically difference due to the large error in the perfusion replicates ($\pm 14.38\%$) with the static at lower error ($\pm 1.57\%$) in the respective receiver chambers. The lower TEER in the perfused model compared to the static could indicate a weaker barrier, resulting in the higher average amount of terbutaline permeating through the A-B direction for the perfused model. However, the amount of terbutaline that reached the receiver chamber was not significantly different for either direction so there was no conclusive evidence to make this assumption.

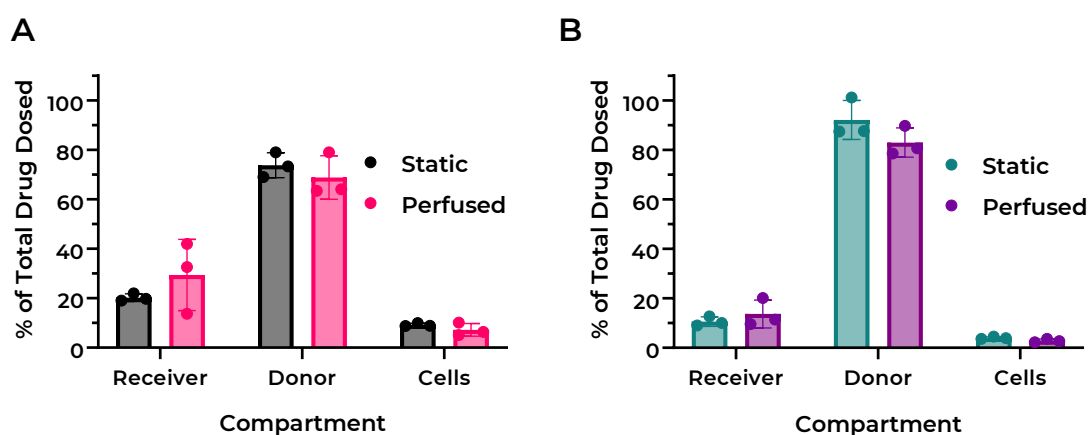


Figure 5.13: There was no significant difference in the amount of drug in each chamber of the cell models, regardless of condition after 180 mins. Proportion of terbutaline (% of total dosed amount) in the compartments in both the static and perfused conditions in the (A) apical to basolateral direction and the (B) basolateral to apical direction (Two-Way ANOVA ns = $P > 0.05$) (N=3).

More terbutaline was transported in the A-B direction than the B-A direction, with a higher percentage of drug present in the receiver chamber in the A-B direction than the B-A direction for both perfusion conditions (Figure 5.14 A and B). This showed that there was a greater transport of terbutaline in the A-B direction across the Calu-3 epithelial barrier than the B-A direction. However, this increase in amount transported was only significant in the static model as the perfused condition had a high variability in the A-B direction ($\pm 14.38\%$) compared to the B-A direction ($\pm 5.64\%$). The volume differences of the chambers may play a role in the amount of drug in each chamber however, the presence of transporters on the Calu-3 epithelial cell layer is more likely to produce this difference. The organic cation transporters (OCT) have a localised expression on the luminal surface of airway epithelial cells like Calu-3 cells, although the relative expression of each subtype of the OCT family is unclear (Bosquillon, 2010).

The higher amount of drug in the receiver chamber was also associated with a higher amount of drug extracted from cells in the static A-B direction compared to the B-A direction (Figure 5.14 A). This may be a result of the transporter uptake of the drug however, the higher cellular uptake for the A-B compared to B-A transport was not seen in the perfused conditions (Figure 5.14 B). This was not a significant difference however the increase was observable (Table 5.12). There was not a cell extraction validation carried out for the extraction of terbutaline from cells within this thesis so these values cannot be depended upon for drawing conclusions, however the observable difference did highlight an interesting finding for future experimentation.

Overall drug mass balance recovery was close to 100%, with a difference of less than $\pm 10\%$ of the total dose of terbutaline applied to the barrier model for both directions in the transport study (Table 5.12). This shows the method described in Chapter 2 for the extraction and quantification of the terbutaline from cell culture media was effective and robust with the Calu-3 cell model present.

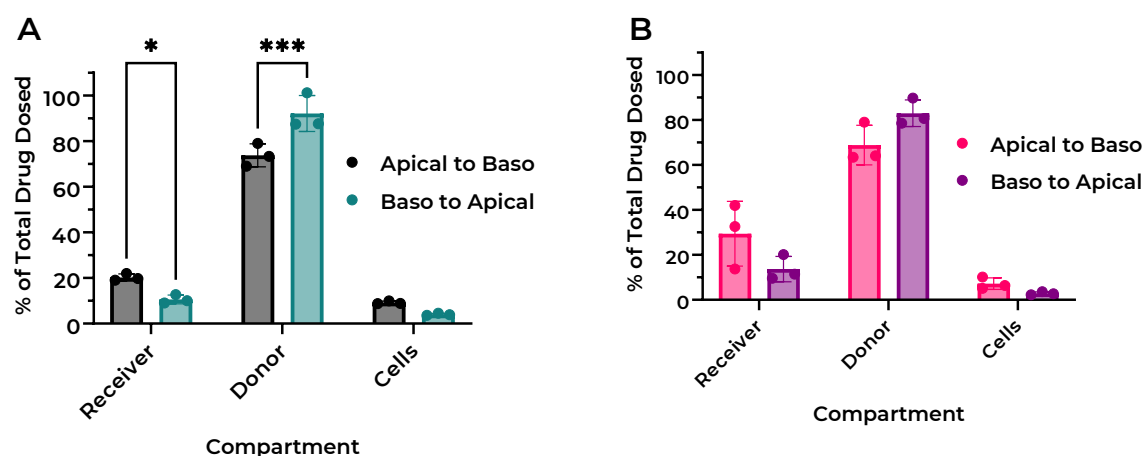


Figure 5.14: More drug was transported in the A-B direction than the B-A direction after 180 mins. Proportion of terbutaline (% of total dosed amount) in the compartments in the **(A)** static condition and the **(B)** perfused condition, comparing the two transport directions (Two-Way ANOVA ns = $P > 0.05$, * = $P < 0.05$, ** = $P < 0.01$, *** = $p < 0.001$, **** = $P < 0.0001$) (N=3).

Table 5.12: Average amount of terbutaline in each chamber relative to the total amount dosed after 180 mins. Percentage (%) of the total amount of terbutaline and standard deviation (STDEV) in each compartment of the Calu-3 epithelial Transwell model in static and perfused in the apical to basolateral direction and the basolateral to apical direction. The associated TEER values for each condition is indicated (N=3).

Direction	Condition	Receiver (%) ±STDEV	Donor (%) ±STDEV	Cells (%) ±STDEV	Mass balance (%) ±STDEV	TEER (Ω/cm^2) ±STDEV
Apical to Basolateral	Static	20.23 ± 1.57	73.73 ± 5.03	9.18 ± 0.67	103.13 ± 3.56	106.45 ± 37.23
	Perfused	29.38 ± 14.38	68.79 ± 8.81	7.21 ± 2.59	105.38 ± 4.12	61.84 ± 40.66
Basolateral to Apical	Static	10.59 ± 1.93	92.04 ± 7.89	4.02 ± 0.44	106.65 ± 6.35	106.45 ± 37.23
	Perfused	13.68 ± 5.64	82.95 ± 5.90	2.85 ± 0.68	99.48 ± 4.20	61.84 ± 40.66

The apparent permeability (P_{app}) of terbutaline across the Calu-3 epithelial barrier model was significantly higher in the A-B direction than the B-A direction (Figure 5.15). The conditions did not affect the rate of the permeability in both directions however, although the average P_{app} values were different (4.94×10^{-6} and $5.83 \times 10^{-6} \text{cm/s}$ respectively), the difference was not statistically significant due to the large variation of the perfused condition (corresponding with the associated TEER values). The amount and rate of terbutaline transport was higher in the A-B direction than the B-A direction, again in agreement with the evidence of increased OCT expression in the apical side of the Calu-3 cells contributing to the transport of drugs like terbutaline.

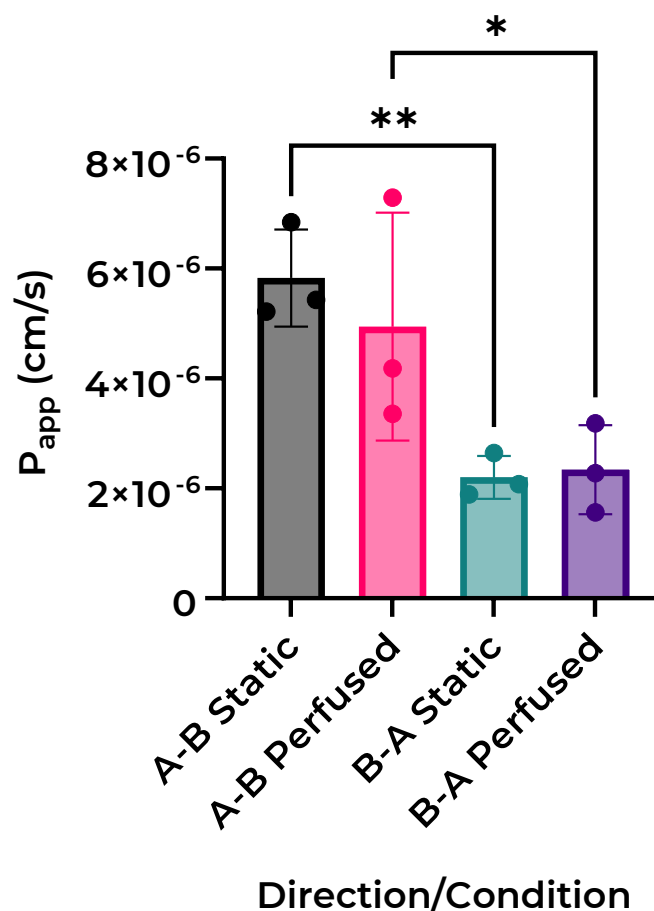


Figure 5.15: Rate of permeability was higher in the A-B direction in both conditions.

Apparent permeability (P_{app}) of terbutaline hemisulfate across the Calu-3 epithelial barrier in the static and perfused conditions in the two directions (apical to basolateral and basolateral to apical) (ANOVA ns = $P > 0.05$, ** = $P < 0.01$) (N=3).

In conclusion, the apical to basolateral direction had a higher rate of permeability of terbutaline than the basolateral to apical direction with more drug moving across to the receiver chamber in A-B direction than the B-A direction. This may be due to the OCT having a localised expression on the apical surface of the Calu-3 cells to transport cation drug such as terbutaline (Bosquillon, 2010). The Calu-3 barrier effectively reduced the amount of drug in the receiver chamber as well as the rate the drug was transported to from the donor to the receiver chamber (29.38 and 13.68 ng/mL B-A) compared to the blank inserts (89.81 and 30.76 ng/mL) in the A-B and B-A direction (Figure 5.3). The P_{app} was reduced by up to in the perfused condition 11-fold compared to the experiment where no cells were present (Figure 5.15).

5.4.9. THE PRESENCE OF 3-ISOBUTYL-1-METHYLYXANTHINE (IBMX) OPTIMISES HITHUNTER® CAMP ASSAY FOR SMALL MOLECULES FOR THE QUANTIFICATION OF INTRACELLULAR CAMP

To assess the muscle relaxation response upon exposure of BSMC to terbutaline, cAMP was assayed as a surrogate marker. This required the optimization of commercially available kit for the cell-type and seeding densities employed in the current study. Optimising the HitHunter® cAMP Assay for Small Molecules (Eurofins, USA) luminescence assay required the addition of 3-isobutyl-1-methylxanthine (IBMX) to evaluate the extent of cAMP degradation throughout the assay. IBMX is a nonspecific inhibitor of phosphodiesterase which breaks down intracellular cAMP, and therefore the presence of IBMX may enhance the levels of cAMP that have been produced intracellularly (Essayan, 2001; Muddle *et al.*, 2020; Schroeder *et al.*, 2012). The influence of the presence of IBMX on the cAMP response that is detected by the HitHunter® cAMP Assay was explored in the presence of isoprenaline, a known non-selective β_2 adrenergic receptor agonist. The addition of isoprenaline should elicit an increase in intracellular cAMP due to the activation of the relaxation pathway as a response to isoprenaline binding to the β_2 adrenergic receptors.

The cAMP response measured in the control cells was significantly higher in the presence of IBMX compared to without IBMX present at all cell densities except 3,000 cells/well, showing the presence of IBMX reduces the breakdown of cAMP in non-stimulated BSMCs, resulting in a higher response of intracellular cAMP when measured by the assay (Figure 5.106A). When comparing the cells dosed with 10 μ M isoprenaline with and without IBMX present, this was even more evident. The IBMX resulted in a much higher cAMP response from the BSMCs at all densities compared to the BSMCs dosed with isoprenaline without IBMX (Figure 5.16 B). When comparing the control and dosed BSMCs without IBMX, there was no significant difference in the amount of cAMP present in the dosed cells compared to the control cells (Figure 5.16 C). This demonstrated that the absence of IBMX resulted in a quick breakdown of cAMP by phosphodiesterase, resulting in the effect of isoprenaline on cAMP generation being negated. In comparison, with the presence of IBMX, the dosed cells show a significantly higher response than the control cells at all densities (Figure 5.16 D).

Across the BSMC densities in dosed and control conditions (with IBMX), a positive relationship between cell number and cAMP was observed, whereby the cAMP quantity increased with increasing cell number. This highlighted the drastic difference IBMX has on the ability to detect increases in intracellular cAMP levels, rendering the HitHunter® cAMP Assay more sensitive to subtle differences in cell response and activity.

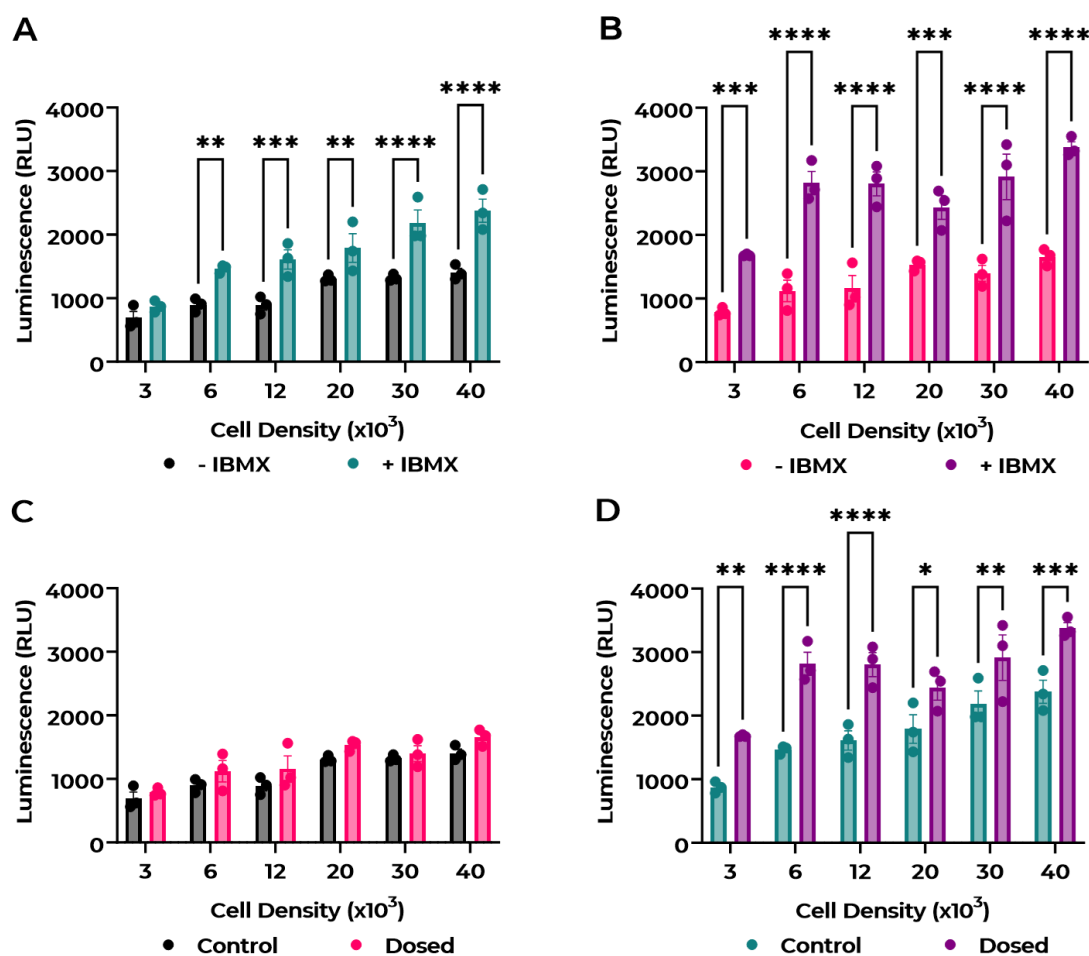


Figure 5.16: 3-isobutyl-1-methylxanthine (IBMX) resulted in more sensitive measurements of cyclic adenosine monophosphate (cAMP). The cAMP response of Bronchial Smooth Muscle Cells (BSMCs) across a range of densities was measured using the HitHunter® cAMP Assay for Small Molecules on **(A)** control cells in the presence and absence of IBMX, **(B)** cells dosed with isoprenaline (10 μ M) in the presence and absence of IBMX, **(C)** control and dosed cells without IBMX and **(D)** control and dosed cells with IBMX present. (Two-Way ANOVA * = $P < 0.05$, ** = $P < 0.01$, *** = $P < 0.001$ and **** = $P < 0.0001$) (N=3).

This experiment confirmed that the presence of IBMX was needed in the cell culture medium to gain a more sensitive response from the HitHunter® cAMP Assay for Small Molecules to measure the intracellular cAMP and subsequent increase from β_2 agonists such as isoprenaline, salbutamol and terbutaline on BSMCs. Going forward, the cAMP assay will be performed with the cells incubated with IBMX prior to exposure to compounds that result in the relaxation of BSMCs such as bronchodilators (e.g. terbutaline).

5.4.10. THE PERFUSED CALU-3/BSMC COCULTURE MPS MODEL ELICITS A MORE SENSITIVE RESPONSE TO B₂-AR AGONISTS THAN THE STATIC MODEL

Utilising the coculture MPS model established in Section 4.4.3 and evaluating the transport of terbutaline across the epithelial/smooth muscle Transwell model as described in Section 5.4.8, combined with the optimized cAMP assay from Section 5.4.9, would provide a robust assessment of the influence of a perfused coculture model and the response to β_2 -AR agonists such as terbutaline.

The barrier integrity of the Calu-3 monoculture was like that as seen in the previous chapters (Figure 5.17 A). The same can be said for the coculture model (Figure 5.17 B) with the perfused models having a lower overall TEER profile than the static equivalent in both the monoculture and the coculture models. Interestingly, at Day 7 the perfused coculture model exhibited a significantly higher TEER value than the static coculture model, which was not previously seen in the coculture model when cultured in the Barrier-12 plate in Section 4.4.3.

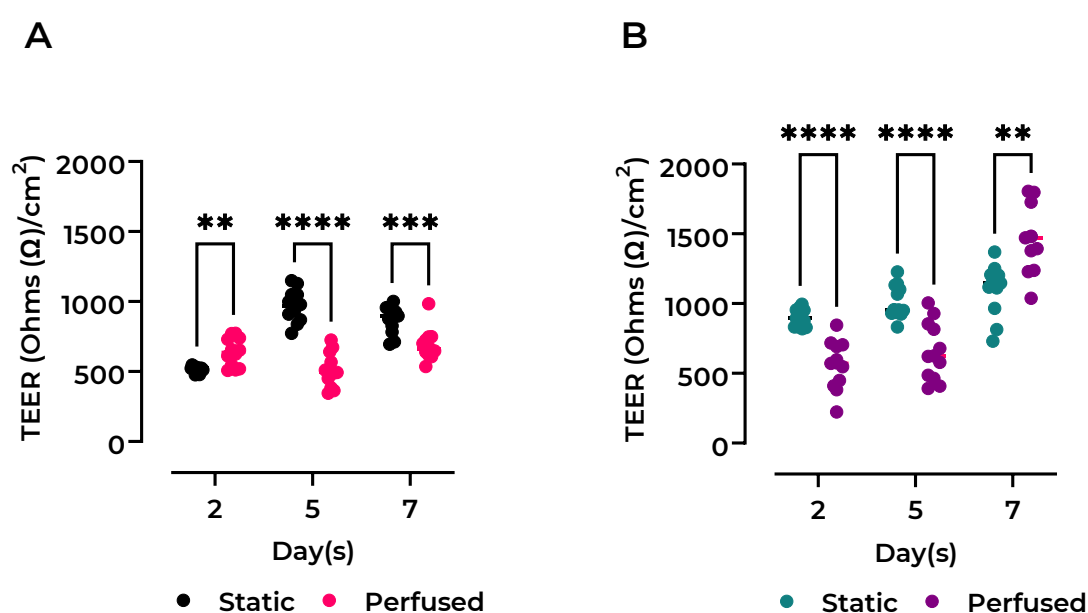


Figure 5.17: Transepithelial Electrical Resistance (TEER) profile of the perfused coculture model was lower than the static equivalent. TEER measurements of the **(A)** Calu-3 monoculture and the **(B)** Calu-3/BSMC coculture Transwell models in the static and perfused conditions (Two-Way ANOVA ** = $P < 0.01$, *** = $P < 0.001$, **** = $P < 0.0001$) ($N \leq 6$).

Comparing the TEER profile of the monoculture Calu-3 model against the coculture model, the static coculture model exhibited significantly higher TEER values at Day 2 and 7 compared to the monoculture model (Figure 5.18 A). The variation of data on Day 7 was greater in the static coculture model compared to the static monoculture model. Although there was a

significant increase in the coculture model TEER, there was some overlap between the replicates. The perfused models of the monoculture and coculture had a very similar TEER profile until Day 7 where the coculture model TEER values were significantly higher than those of the monoculture model (Figure 5.18 B). This was consistent with the data shown in Chapter 4, whereby from Day 7 the barrier properties of the Calu-3 epithelium in the coculture model differentiated to exhibit a phenotype that was significantly different to the monoculture (see Chapter 4).

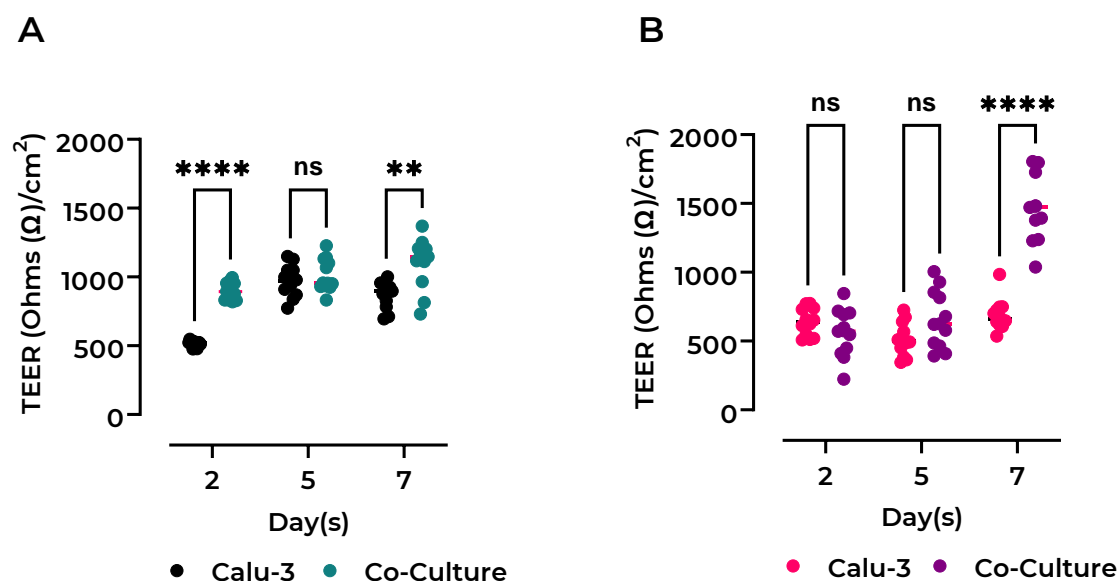


Figure 5.18: Transepithelial Electrical Resistance (TEER) profile of the coculture models was higher than the monoculture models at day 7. Comparison of the TEER measurements of the Calu-3 monoculture and the Calu-3/BSMC coculture Transwell models in the **(A)** static and **(B)** perfused conditions (Two-Way ANOVA ns = $P > 0.05$, ** = $P < 0.01$, **** = $P < 0.0001$) ($N \leq 6$).

Mucin production from the Calu-3 epithelium was quantified to understand the functionality of the epithelium and the resulting drug-epithelial interaction potential. On Day 2 of ALI culture, the mucus was quantifiable and, interestingly, the static monoculture Calu-3 model had a significantly higher mucin expression compared to the other models (Figure 5.19 A). At Day 7, large increases of mucin expression were seen across all models, however, the greatest change was seen in the coculture models (Figure 5.19 B). This again illustrates the importance of the differentiation of the models over time at ALI, as well as the additional and altered differentiation experienced in coculture models. There were minor, non-significant differences between static and perfused monoculture at Day 7, however the coculture perfused model had a significantly lower mucin expression compared to the static coculture model (Figure

5.19 B). Interestingly, previously in Section 4.4.3, it was shown the perfused coculture model expressed a higher level of mucus compared to the static coculture model. In this experiment, the static coculture model reached a greater amount of mucus (79 μ g) compared to the static coculture model in Section 4.4.3 (51 μ g) whereas the perfused coculture model achieved a similar amount of mucus. This increase in mucus expression of the static coculture model was interesting and is unclear what simulated the Calu-3 cells to increase expression of mucus in this experiment as all experimental parameters were kept the same as the study in Section 4.4.3.

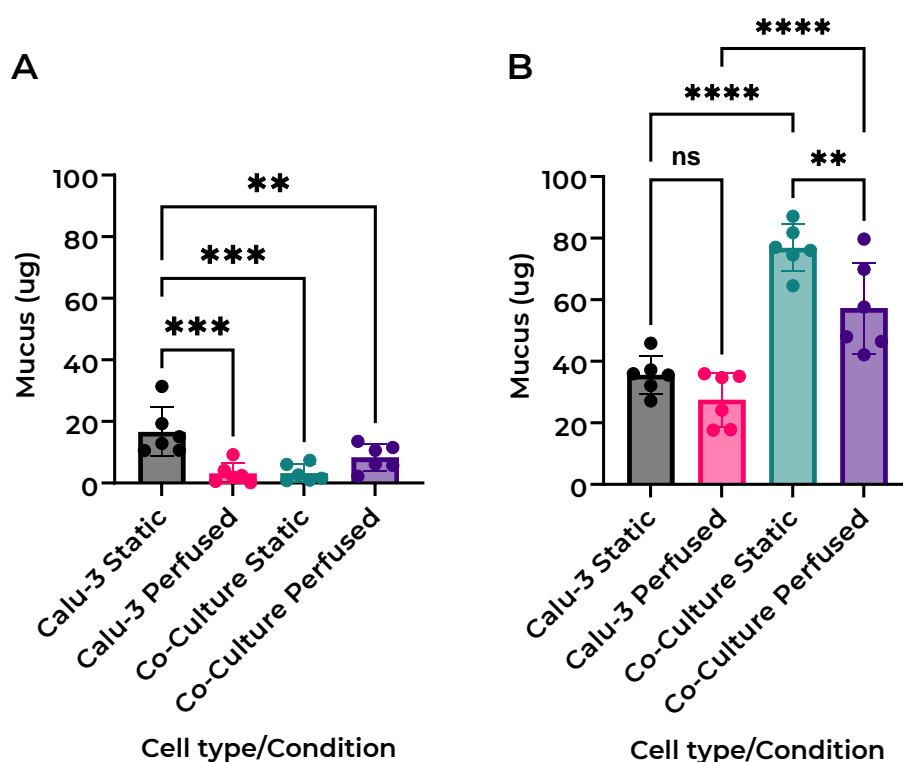


Figure 5.19: More mucus is produced by the coculture epithelium than the monoculture epithelium. Mucus (μ g) produced by the Calu-3 epithelium in the monoculture and coculture models in the static and perfused conditions, quantified on **(A)** day 2 of air-liquid interface (ALI) culture and **(B)** day 7 ALI culture (ANOVA ns = $P > 0.05$, ** = $P < 0.01$, *** = $P < 0.001$, **** = $P < 0.0001$) (N=6).

Next, to determine the differences in permeability between the models, terbutaline was applied to the model and assessed for transport in the apical to basolateral transport direction (A-B). The percentage of the total terbutaline dosed is shown in the receiver chamber, cell fraction and the donor chamber (Figure 5.20 A, B and C). There was no significant difference in the amount of terbutaline reaching the receiver chamber (Figure 5.20 A) or the donor chamber

(Figure 5.20 C) between the Calu-3 monoculture and the coculture models regardless of the condition. However, there was significantly more terbutaline present in the receiver chamber of the BSMC monoculture model than the coculture in both the static and perfused condition, showing the Calu-3 epithelium was acting as the effective barrier to the passive diffusion of terbutaline across the epithelial model. BSMCs do not exhibit tight junction formation and do not form a permeation barrier.

The amount of terbutaline extracted from the Calu-3 epithelial cells after 180 min exposure was quantified. It indicated that there was no significant difference between the coculture and the Calu-3 monoculture model regardless of condition (Figure 5.20 B) however, no drug was extracted from the BSMCs in any condition/cell model due to the cAMP assay requiring the lysis of the cells to extract the intracellular cAMP, resulting in the cell sample being consumed and the cAMP assay matrix cannot be used in the LC-MS analysis. In the static condition, the mass balance of the BSMCs ($102.51 \pm 11.86\%$) and the Calu-3 ($111.02 \pm 28.22\%$) was significantly higher than that of the coculture ($96.72 \pm 1.42\%$). This indicated that there may have been volume loss through evaporation and/or over-estimation of the calculated drug in the chambers for the BSMCs and the Calu-3 samples as this increase in mass balance was similarly observed in the perfused condition (Table 5.13).

Table 5.13: Average amount of terbutaline in each compartment of each model after 180 minutes. Percentage of the total dosed amount with the standard deviation of the replicates (N=3).

Condition	Cell Model	Receiver (%) ±STDEV	Donor (%) ±STDEV	Cells (%) ±STDEV	Unaccounted (%) ±STDEV
Static	BSMC	35.35±3.75	67.16±11.30	N/A	102.51±11.86
	Calu-3	21.55±28.02	88.70±17.79	0.77±0.30	111.02±28.22
	Coculture	6.75±5.75	88.30±4.45	1.67±0.21	96.72±1.42
Perfused	BSMC	40.72±4.41	75.89±14.81	N/A	116.61±19.06
	Calu-3	7.81±3.42	94.06±13.20	0.97±0.44	102.84±15.96
	Coculture	5.74±4.00	92.48±2.60	1.29±1.50	99.51±3.65

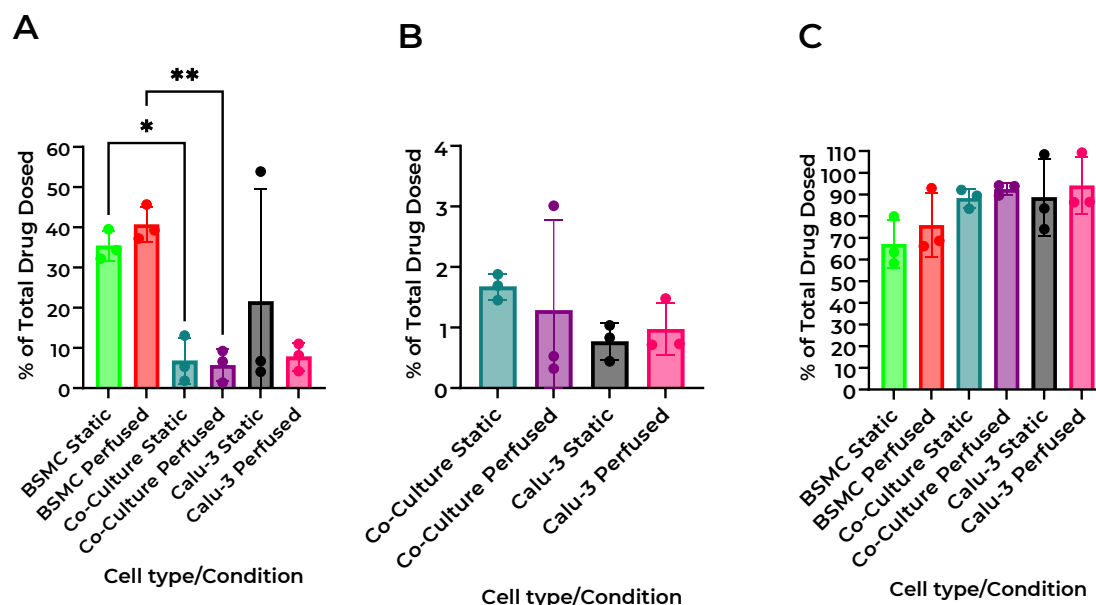


Figure 5.20: The amount of drug in each compartment was similar between the coculture and the Calu-3 monoculture models. Amount of terbutaline (%) in the apical to basolateral direction in both the static and perfused conditions of the different models: BSMC monoculture, Calu-3 monoculture, and the Calu-3/BSMC coculture. **(A)** Percentage of the terbutaline (%) dose in the basolateral chamber after 180 min, **(B)** Percentage of the terbutaline (%) dose in the Calu-3 epithelial cells after 180 min, **(C)** Percentage of the terbutaline (%) dose in the apical chamber after 180 min (ANOVA *** = $P < 0.001$, **** = $P < 0.0001$) (N=3).

After 180 min, the rate of terbutaline transport was calculated as apparent permeability (P_{app}) (Figure 5.21). The P_{app} values demonstrated that the BSMC monoculture had a higher rate of permeability to terbutaline than the coculture models, again showing the Calu-3 epithelium to be a rate-determining barrier for terbutaline transport to the receiver chamber regardless of the perfusion condition. It was also shown that the coculture and Calu-3 monoculture model had no significant differences in permeability. The static Calu-3 model had a higher average P_{app} value than the perfused Calu-3 and the static coculture model. However, this may have been a result of the increased variance in the replicates of the Calu-3 static model compared to the other models which could be corrected by the removal of the outlier which would result a similar average value to the other models.

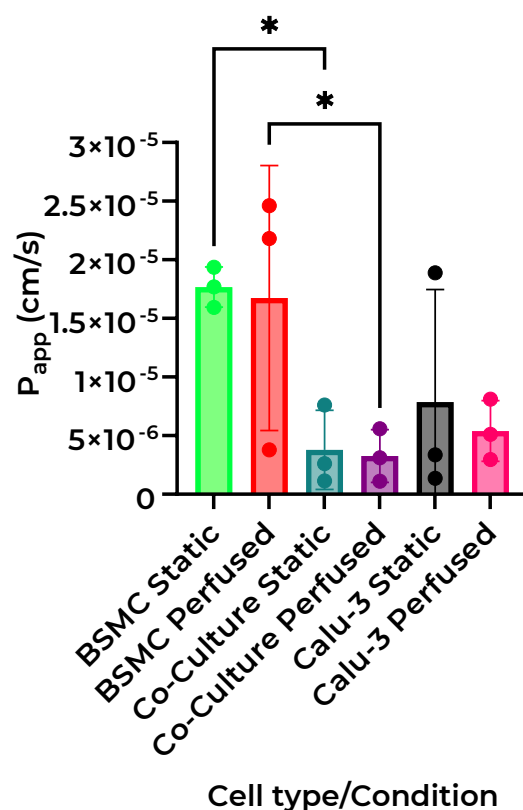


Figure 5.21: The presence of Calu-3 cells significantly reduced the transport of terbutaline. Apparent permeability (P_{app}) of terbutaline across the cell model after 180 minutes (ANOVA ns = $P > 0.05$, * = $P < 0.05$, **** = $P < 0.0001$) (N=3).

The percentage of drug that was calculated in the receiver chamber (Figure 5.22 A) was determined as the total amount of terbutaline that had permeated through the Calu-3 epithelial layer to act upon the BSMCs, which are the drug target. To determine the efficacy of the permeated drug on their target, the response of the BSMCs was determined using the cAMP assay discussed and optimised previously. The total amount of terbutaline (ng) that was available to act upon the β_2 -adrenergic receptors on the BSMCs was calculated and it was observed that a significantly higher amount of drug was available for the BSMC monoculture than the coculture in both the static and perfused conditions (Figure 5.22 A). However, there was no significant difference between the static and perfused conditions for either cell model.

In the coculture model, due to the presence of the Calu-3 epithelial layer which inhibited the passive permeability, less terbutaline reached the coculture BSMCs, thus limiting the available drug to act on the β_2 -adrenergic receptors in the assay window. The resultant relaxation of the BSMCs by the action of terbutaline was assessed after 180 mins by the optimised cAMP assay. IBMX was present in the media before the terbutaline transport, as determined by the optimisation of the assay in Section 5.4.9. The raw cAMP levels detected were similar across

the BSMC monoculture and the coculture models, regardless of the condition (Figure 5.22 B). Although the coculture models had significantly less drug available in the receiver chamber (Figure 5.22 A), the lower cell-available drug dose elicited a similar magnitude of cAMP response to the BSMC monoculture models which had a much higher amount of drug available.

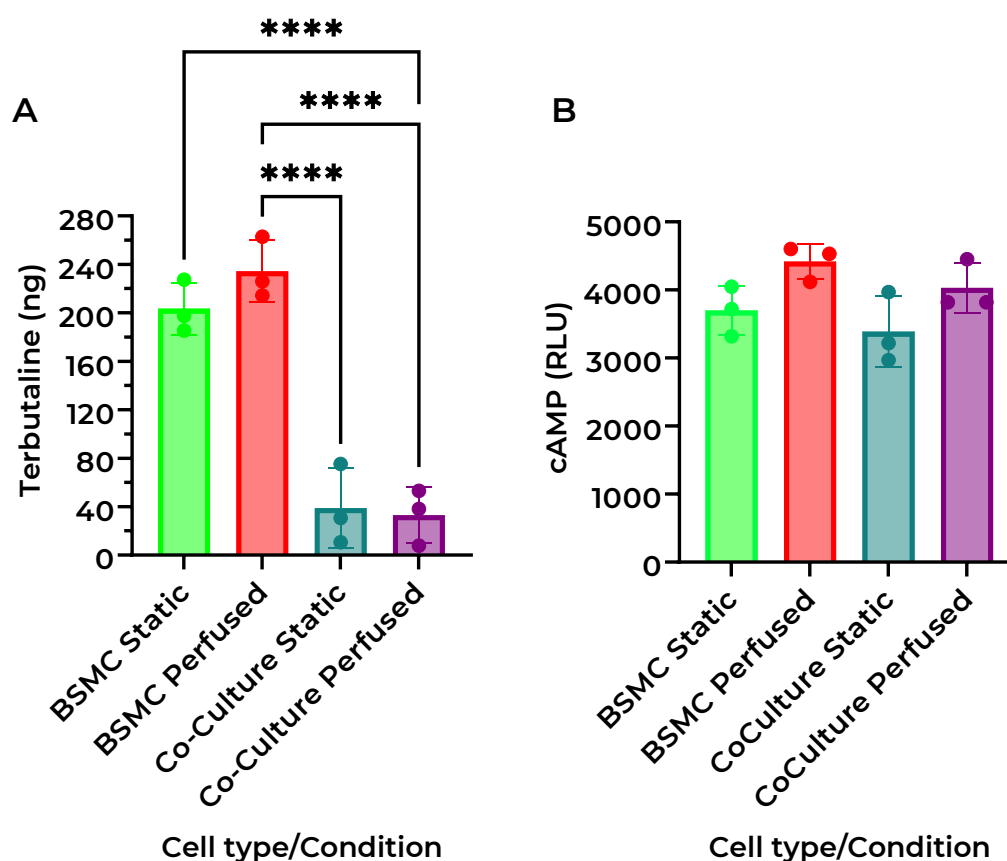


Figure 5.22: The coculture models exhibited a similar cAMP response to terbutaline with less terbutaline reaching the BSMCs in the coculture than the monoculture. (A) Amount of terbutaline (ng) that reaches the BSMCs in the monoculture and coculture model and the resultant **(B)** cAMP response as determined by the HitHunter® cAMP Assay (RLU) (N=3).

To determine the difference in response, the cAMP response was normalised against the total drug available in the receiver chamber for cell model in each condition. The cAMP response per ng of available terbutaline was calculated using the values in Figure 5.22 A and the cAMP data generated from the samples in Figure 5.22 B. The resultant values indicated the BSMC's response to terbutaline on a dose-normalised basis. This indicated that the response was significantly higher in the coculture model than the BSMC monoculture model for both static

and perfused conditions (Figure 5.23). The perfused coculture model displayed a more sensitive cAMP response to terbutaline than the static coculture and BSMC monocultures (Figure 5.23).

Despite the lower amount of drug available for the cocultures than the monocultures, resulting from the barrier properties of the Calu-3 epithelium, the cAMP levels in the coculture models were equivalent the BSMC monoculture models. Through analysing the dose-normalised response, it was clear that the coculture model resulted in a more sensitive response to bronchodilator drugs than the monoculture, and this enhanced sensitivity was magnified for the coculture when maintained under perfusion. Taken together, this data suggests that the perfused coculture model of Calu-3 and BSMC provides a suitable and sensitive model for accessing the ADME and efficacy of inhaled drugs.

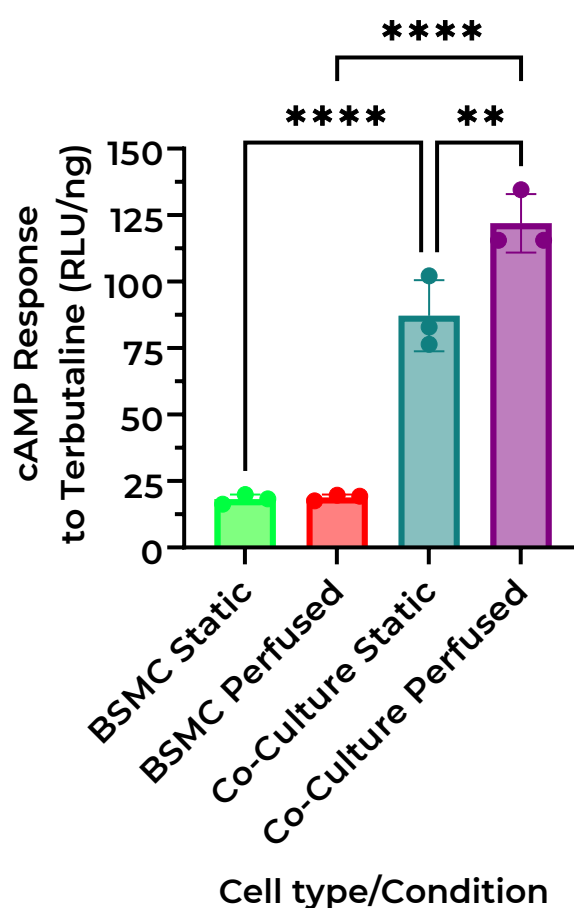


Figure 5.23: The coculture models resulted in a more sensitive cAMP response to terbutaline after 180 mins. cAMP response per ng (RLU/ng) of available terbutaline in the receiver chamber (N=3).

5.5. CHAPTER CONCLUSIONS

The perfused coculture model showed great promise as a highly sensitive cell model for the assessment of bronchodilators such as terbutaline and salbutamol. The coculture model itself resulted in a more sensitive BSMCs phenotype which was enhanced by the perfusion using the Barrier-12 plate. Within this chapter, the optimisation of the commercially available HitHunter® cAMP Assay for Small Molecules assay kit was completed for the analysis of intracellular cAMP levels in BSMCs through the use of IBMX. IBMX generated a higher measurable difference between control and beta-2 agonist dosed cells. Also, in this chapter the transport rate and amount of terbutaline was successfully investigated to calculate the transport across the differentiated Calu-3 epithelium in the static and perfused conditions in both coculture and monoculture. The effect of the coculture combined with perfused conditions was evaluated on drug transported across to the BSMCs and the resultant cAMP response of the smooth muscle, determining the BSMCs exhibit a more sensitive response to terbutaline when in coculture with Calu-3 cells and combined with perfusion than the static equivalent and the monocultured BSMCs.

Chapter Six

General Discussion

6. GENERAL DISCUSSION

6.1. OVERVIEW OF THE SCOPE OF THIS THESIS

Respiratory drug development suffers an overall failure rate of around 70%, with a calculated cumulative probability to reach the clinical market equal to 3%, compared to the 6-14% probability for drugs used to treat other diseases (Barnes *et al.*, 2015). A major cause of failure is the lack of efficacy and safety concerns at human trials after promising animal studies (Jiang *et al.*, 2014; Moeller *et al.*, 2008; Mullard, 2016; van der Worp *et al.*, 2010). There is an overwhelming need to engineer robust *in vitro* models to reduce the attrition rate of drugs as the current models are not representative of the human *in vivo* anatomy, physiology and pathophysiology, which leads to poor predictive power of any adverse effects of a drug candidate (Forbes *et al.*, 2014; Hacker & Rafat, 2020; Hoeng, 2019). There has been increasing interest in the potential of microphysiological system (MPS) models to enhance the understanding of disease states and improve drug candidate selection efficiency, thereby decreasing the reliance on animal models and decreasing drug attrition, all of which will ultimately provide patients with new and alternative therapeutic options (Ainslie *et al.*, 2019). It is within this wider context, that the aim of investigating MPS models of the pulmonary airways for enhanced reliability and prediction values was developed.

6.2. OVERCOMING CURRENT LIMITATIONS OF *IN VITRO* CELL MODELS

2D cell culture has been established as low cost and high throughput alternative for drug toxicity and metabolism screening (Kapałczyńska *et al.*, 2016; Sanyal & Kosovsky, 2017). Cell culture models of the bronchial epithelium have been developed to provide a basis for studying drug transport and uptake, with 2D monocultures of epithelial cells well-suited for low cost, high-throughput screening. However, they are reductionist due to their lack of complexity as most models contain one cell type, resulting in an inability to reproduce an accurate representation of complex interactions between human cell types and tissue seen *in vivo* (de Souza Carvalho *et al.*, 2014; Kapałczyńska *et al.*, 2016). As result, these models are less suited to monitor changes in the epithelial barrier because of disease or the therapeutic effectiveness of drugs on the target cells due to limited representation of cell-to-cell and cell-to-extracellular environment interactions (Haghi *et al.*, 2015). Coculturing bronchial epithelial cells with bronchial smooth muscle cells may achieve the goal of developing more complex, reproducible *in vitro* tissue models, particularly when considering the pharmacodynamics and efficacy of anti-inflammatory respiratory medications (Vis *et al.*, 2020). In combination with MPS to simulate *in vivo* environments, there is great potential to characterise the relationship between biomarkers and clinical outcomes due to the enhanced physiological relevance of tissues cultured in the devices (Bhatia & Ingber, 2014a; Ewart *et al.*, 2018). The key issues to

be addressed are the selection of the cell systems and establishing the culturing factors and MPS conditions that contribute to the validity of the *in vitro* models.

6.3. MICROPHYSIOLOGICAL SYSTEMS AND RECAPITULATING RESPIRATORY BIOMECHANICAL STIMULI

The biomechanical stimuli the lung receives are: airflow from inspiration and expiration of normal breathing, stretch as a result of lung expansion from breathing, and blood flow/interstitial fluid flow (Franks *et al.*, 2008; Levitzky, 2018; Stanfield, 2016). MPS models utilising microfluidics and mechanical stresses such as cyclic pressure for airflow and vacuum chambers to incorporate stretch can recapitulate these movements experienced by the lung tissue *in vivo*. Within this thesis, the advantages of CN Bio's PhysioMimix OOC system were highlighted. The Barrier-12 plate incorporates basolateral perfusion to recapitulate the interstitial fluid flow experienced by lung tissues. A variable flow rate can be applied to the basolateral face of the Transwell inserts based on the requirement of the model, making it flexible for model development. The plate is made of cyclic olefin copolymer (COC) which is biologically inert and advantageous to the study of pharmaceutical compounds that are not compatible with polydimethylsiloxane (PDMS) (Agha *et al.*, 2022). The open-well format of the Barrier-12 plate allowed the use of culture inserts such as Transwells and other scaffolds, allowing for an almost seamless transition from culturing in the traditional 24-well plate the inserts are shipped in, to the Barrier-12 plate. As detailed by Ainslie *et al.* 2019, the PhysioMimix OOC has reasonable throughput with 12 wells that allow sampling from the fluid compartments in a user friendly open-well format in a plate, with little to no drug binding, applicable to small molecules and biologics, allows extended *in vitro* culture times, and is amenable to coculture (Ainslie *et al.*, 2019).

The PhysioMimix system was user friendly with the controller and software easy to use and modify flow rates and troubleshoot any pressure issues within the lines. However, the use of the plate driver and dock within the incubator did increase the risk of contamination if not adequately cleaned along with the umbilical from the controller to the dock which required an open access through the back of an incubator, allowing potential contamination access to a sterile environment.

6.4. ENHANCEMENT OF THE CALU-3 BRONCHIAL EPITHELIUM MODEL

It was previously demonstrated by Grainger *et al.* (2006) that Calu-3 cell layers cultured at ALI provided the closest *in vitro* representation of *in vivo* bronchial epithelial morphology, comprising a pseudostratified columnar epithelium of ciliated and secretory phenotypes (Grainger *et al.*, 2006). For this reason, Calu-3 cells were chosen as the model pulmonary epithelium for development and characterisation in this thesis. The principal findings will be

summarized initially for overview, before progressing to a detailed discussion of the development and characterisation approaches that were employed in reaching these findings.

Within this thesis, barrier functionality and characterisation was conducted utilising transepithelial electrical resistance (TEER) measurements combined with apparent permeability (P_{app}) studies of relevant markers as TEER reflects the ionic conductance of the paracellular pathway in the epithelial monolayer, whereas the flux of non-electrolyte tracers indicates the paracellular water flow, as well as the pore size of the tight junctions (Zucco, 2005).

In Chapter 3 of this thesis, it was clear the perfusion enhanced the barrier function of a Calu-3 epithelial model with the lower transcellular molecular permeability (P_{app}) values achieved by Day 7 which took the static model up to 14 days to achieve. Enhancing the barrier properties and producing a more uniform monolayer from a cancer cell line than the static model highlights the benefits of the MPS system as demonstrated within this thesis. However, there were challenges in maintaining intra-experimental robustness of the model as the P_{app} values varied between experiments across Chapters 3 and 4. However, the latter variation was exhibited by both the static and perfused models, and so may therefore derive from the variation experienced in cell culture in general. Reproducing similar permeability values seems to be an issue that is experienced by many researchers as seen in the variation of the reported literature values of the same markers, luciferase yellow and sodium fluorescein (LY and NaFL) which can be attributed to seeding density and ALI culture periods (as highlighted in Table 3.1 in Section 3.1.4.1). The passage number of the Calu-3 cells is an important consideration as the expression of proteins and transporters can increase by up to 4 times in later passages of Calu-3 cells (Carius *et al.*, 2021; Cingolani *et al.*, 2019; Ehrhardt, Fiegel, *et al.*, 2002; Grainger *et al.*, 2006; Haghi *et al.*, 2015, 2019; Madlova *et al.*, 2010; Min *et al.*, 2013, 2016).

The effect of perfusion on the Calu-3 epithelium was not unprecedented, as Carius *et al.* (2021) previously reported that a perfused model of the Calu-3 epithelium resulted in the P_{app} of NaFL decreasing by 26% compared to the static Transwell model (Carius *et al.*, 2021). However, this model was cultured in liquid-liquid interface (LLI) and so cannot be directly compared to that described in Chapter 3 of this thesis.

Although perfusion was explored by this MPS model, the biomechanical stimuli of cyclic stretch and airflow were not represented in this thesis due to the limitations of the PhysioMimix MPS plates. The recapitulation of stretch must be carefully considered when developing representative models of the healthy human lung. Higher levels of cyclic strain are experienced in the airway epithelium when tissue loses its elasticity in the asthma disease state (Tschumperlin & Drazen, 2001; Waters *et al.*, 2012). Therefore, although theoretically

stretch is experienced by some parts of the lung, particularly the alveoli, *in vitro* model developers must be cautious to model specific parts of the lung with specific physiology in mind. As well as *in vivo* stretch occurring across all dimensions, most MPS models only apply stretch unilaterally (*Emulate*, 2024; D. (Dan) Huh, 2015). Incorporating airflow has been established by some commercial models (Alveolix), however this model mimics the air-blood barrier in the alveolus which was not the aim of the models discussed in this thesis.

A major limitation of these experiments and all subsequent experiments was only technical replicates were explored due to limitations in consumable resource and budget. To further enhance the statistical power of the analysis, experimental replicates could have been performed if consumable resource would have allowed.

6.5. OPTIMISATION OF THE CALU-3 BRONCHIAL EPITHELIUM MODEL

In Chapter 3 of this thesis, the seeding density of Calu-3 was established for the model as there was no consensus in the literature on an optimal seeding density to establish an epithelial barrier. From literature, there were densities as high as 5×10^5 cells/cm² and as low as 1×10^5 cells/cm² used by multiple researchers with insufficient justification for the seeding densities, which were not explored by the authors in depth (Cingolani *et al.*, 2019; Foster *et al.*, 2000; Grainger *et al.*, 2006; Haghi *et al.*, 2012a, 2013, 2019; Horstmann *et al.*, 2021; Ji *et al.*, 2022; V. Kumar *et al.*, 2022; Meindl *et al.*, 2015; Min *et al.*, 2013, 2016; Mukherjee *et al.*, 2013; Pasman *et al.*, 2021; Stuetz *et al.*, 2023).

Within this thesis, in the non-perfused (i.e. non-MPS) conditions, the higher density (5×10^5 cells/cm²) had a TEER at $300 \Omega \cdot \text{cm}^2$ and P_{app} of LY at 1.3×10^{-5} cm/s. The values by Min *et al.*, 2016 after 8 days in ALI culture at the same seeding density were reported as higher in TEER ($400 \Omega \cdot \text{cm}^2$) and significantly lower P_{app} of LY (8.6×10^{-7} cm/s) than in the current study (Min *et al.*, 2016). The TEER measurements for lower density seeding (1×10^5 cells/cm²) indicated potential failure to form a barrier at ALI, only reaching $250 \Omega \cdot \text{cm}^2$ at Day 7 with practically no TEER values established prior to Day 7, compared with literature values of $1500 \Omega \cdot \text{cm}^2$, albeit at Day 11 ALI (Cingolani *et al.*, 2019). However, the P_{app} established in Chapter 3 at this density was 4.3×10^{-7} cm/s, which compared favourably with the value of 3.4×10^{-7} cm/s from Cingolani *et al.* (2019) and significantly lower than the higher density interrogated (5×10^5 cells/cm²). This indicated that, regardless of the lower TEER values, the barrier was as functional in terms of its paracellular permeability as studies reporting higher TEER values.

The seeding density of 3×10^5 cells/cm² was established as the optimal seeding density because the measurement of TEER values and P_{app} of LY indicated a functional barrier was established by Day 7 (6.5×10^{-7} cm/s). The only article that reported this density (V. Kumar *et al.*, 2022) reported a significantly higher TEER ($1000 \Omega \cdot \text{cm}^2$) than the current study (280

$\Omega \cdot \text{cm}^2$). However, Kumar *et al.* measured the TEER when the culture was in LLI, and no paracellular marker used. ALI was only established for 2 days for the purpose of evaluating the deposition of dry powder inhaler formulations in their study. The latter article is one example of several listed above that employed the Calu-3 Transwell model as an established epithelial model without detailed optimization that is likely to perpetuate suboptimal culture approaches for ALI epithelial modelling.

After the optimisation in Chapter 3, Section 3.4.2 described the Calu-3 barrier assessed in the static and perfused conditions using TEER and LY. The static, non-perfused model established an average of $300 \Omega/\text{cm}^2$ TEER across the 14-day ALI culture, with LY P_{app} averaging $2.78 \times 10^{-7} \text{ cm/s}$ at Day 7 ALI and $1.21 \times 10^{-6} \text{ cm/s}$ at Day 14 ALI. Compared to static models of Calu-3 in literature, TEER was lower than Cingolani *et al.* (2019) ($500\text{-}1500 \Omega/\text{cm}^2$) and Min *et al.* (2016) ($400 \Omega/\text{cm}^2$) with their P_{app} at $3.4 \times 10^{-7} \text{ cm/s}$ (Day 11 ALI) and $8.6 \times 10^{-7} \text{ cm/s}$ (Day 8 ALI), respectively (Cingolani *et al.*, 2019; Min *et al.*, 2016). Although the TEER values were lower in the Calu-3 barrier established in Chapter 3 than literature reports, the apparent permeability was lower on average than the two models from literature. This highlights the variability and inconsistencies with the culture of cells for establishing representative cell models across laboratories and users. In particular, the seeding density of cells was lower in the model reported by Cingolani *et al.* (2019) ($1 \times 10^5 \text{ cells/cm}^2$) and higher in the model reported by Min *et al.* (2016) ($5 \times 10^5 \text{ cells/cm}^2$), whilst the seeding density for the model established in Chapter 3 was $3 \times 10^5 \text{ cells/cm}^2$. Optimising the cell seeding density in Section 3.4.2 helped establish a more functional drug diffusion barrier than the two models from literature despite the lower TEER value (Cingolani *et al.*, 2019; Min *et al.*, 2016). This also highlights how the TEER values alone are an insufficient metric to evaluate barrier function, as the TEER values in the model established in Chapter 3, which were lower than previous literature reports, did not translate to a more permeable barrier than those same studies.

6.5.1. ASSESSMENT OF BARRIER FUNCTIONS AND THEIR LIMITATIONS

The perfused model established a TEER of $200 \Omega/\text{cm}^2$ with P_{app} values at an average of $3.59 \times 10^{-8} \text{ cm/s}$ at Day 7 ALI and $1.74 \times 10^{-7} \text{ cm/s}$ at Day 14. This again highlighted that the TEER values are not always indicative of paracellular permeability for the Calu-3 epithelial barrier. The perfusion led to a lower TEER *and* lower P_{app} value than the literature for LY paracellular markers across the perfused Calu-3 Transwell model. Typically, TEER is used as an indication for barrier permeability as the lower TEER values would indicate a higher P_{app} of a paracellular marker however, in the perfused models the relationship between TEER and P_{app} seemed not have as strong a correlation. However, this may be a result of differences in morphology between the two conditions, with the perfused model exhibiting a more uniform monoculture allowing for an more accurate reading than in the non-perfused model which contained several

patches on top of the monolayer that could have given rise to varied measurements on the same well, this may also account for the increased variability of the TEER measurements in the static model compared to the measurements in the perfused model.

Establishing perfusion as an MPS model has led to a tighter, more restrictive epithelium barrier than the comparative static model and the from the models in the literature. Despite the challenges of using TEER as a comparative and quantitative marker of barrier function, TEER measurements do provide a non-destructive method of monitoring barrier formation and cell health across the culture period which was beneficial in determining the barrier establishment before investigating the paracellular permeability. Again, we highlight that it is important to use TEER in conjunction with other quantitative methods to better compare between models and intra-laboratory studies.

From Chapter 3 Section 3.4.3 and across Chapter 4, the Calu-3 barrier model was assessed using the NaFL paracellular marker. The additional use of NaFL after using LY as a permeability marker was to characterise the model with two paracellular markers, because nonradioactive fluorophore compounds lack the sensitivity to reflect the subtle changes in monolayer permeability due to poor specific activity or fluorophore instability (Duffy & Murphy, 2001). Radiolabelled mannitol would have been more suitable however, the instability of radiolabelled markers results in a short-shelf life and increases the cost of a simple permeability assay that NaFL adequately appropriate for (Madara, 1998; Tsukita & Furuse, 1999).

The static Calu-3 model was established to exhibit an average P_{app} ranging from 5×10^{-5} cm/s at Day 7 to 5×10^{-6} cm/s at day 21 ALI, with a TEER averaging from 300 to 400 Ω/cm^2 . The perfused model ranged from an average P_{app} of 1.25×10^{-6} cm/s at Day 7 to 4×10^{-7} cm/s at Day 21 ALI with a TEER of 200 and 400 Ω/cm^2 respectively. There was a significant difference in the range of P_{app} values between the two conditions, exhibiting some general challenges in cell culture, where inter-experiment variability may be a result of passage number increases, supplement/media composition and age, and variations in the equipment that could lead to the health/functionality of cells to vary between experiments. Comparing to literature values of NaFL flux, values as low as 1×10^{-7} cm/s at Day 20 ALI to 6.25×10^{-6} cm/s at day 11 ALI have been reported (Ehrhardt, Fiegel, *et al.*, 2002; Haghi *et al.*, 2019). The P_{app} of the static and perfused model both fall within the reported ranges from literature with the perfused model exhibiting P_{app} of NaFL that has been seen previously in static Calu-3 models.

LY and NaFL were used as they are reliable paracellular markers to assess the permeability of the epithelial barrier and have been used extensively by other researchers for assessing the barrier properties of lung epithelial cells, including the Calu-3 cell line (Cingolani *et al.*,

2019; Min *et al.*, 2016)(Ehrhardt, Fiegel, *et al.*, 2002; Haghi *et al.*, 2019). LY (457 Daltons) and NaFL (376 Daltons) are representative of the small drug molecules that may be inhaled by patients of lung disease such as bronchodilators which have a similar molecular weight/size of under 500 Da. However, larger molecule permeability was not assessed and may have provided more representative view of the barrier function in general for the assessment of tight junction pore size and barrier resistance to foreign bodies. FITC-dextran (4,000 Da) has been used to assess the Calu-3 monolayer in literature and the use of such a large marker in addition to the NaFL and LY used may have produced more exhaustive characterisation of the barrier, tight junction pore size and paracellular permeability (Pasman *et al.*, 2021; Sui & Lee, 2023). However, for the purposes of the study for the inhaled bronchodilators like terbutaline, smaller molecular weight markers like LY and NaFL were more appropriate and representative than the heavier FITC-dextran.

6.5.2. TIGHT JUNCTION EXPRESSION AND LIMITATIONS OF THE ASSAYS

In parallel to the assessment of barrier properties (i.e. TEER and permeability) which are key to epithelial function, the underlying cell biology responsible for the barrier phenotype were characterised. Techniques employed extended to immunofluorescent (IF) imaging of protein expression and histology to determine the morphology of the cell layers, complemented by the gene expression exhibited by the cells in each condition through the analysis of RNA by quantitative polymerase chain reaction (qPCR). Within this thesis, the ZO1 tight junction was characterised in gene and protein expression studies utilising qPCR and immunofluorescence as it one of the major proteins in the airway epithelium that restricts the paracellular movement of water and solutes. The ZO1 tight junction presence in Calu-3 cells grown at ALI has been confirmed by IF and qPCR in literature, therefore the inclusion of the IF and qPCR analysis of the ZO1 protein has precedence in the characterisation of the Calu-3 model (Carius *et al.*, 2021; Ehrhardt, Fiegel, *et al.*, 2002; Grainger *et al.*, 2006; Ji *et al.*, 2022; Pasman *et al.*, 2021; Sui & Lee, 2023).

In Chapter 3, Section 3.4.2, the morphology and expression of the ZO1 tight junction in the Calu-3 model was established in the static and perfused conditions. At Day 7, there were clear differences in the morphology of the cell models between the conditions, whereby the perfused condition exhibited a more uniform, pseudostratified sheet of cells covering the Transwell membrane. Conversely, the static condition exhibited a cell layer that contained patches of cells growing on top of basal layers of cells, disrupting the uniformity of the cell monolayer. This resulted in difficulties in generating a representative image of the static model due to the cell patches residing across multiple planes in the Z direction. This was mitigated by Z-stacking images of the cell layer however this was not successful in removing all the out-of-focus sections of the image. The image clarity may have been increased through the use of a more

powerful, confocal microscope which could differentiate between the multiple Z-planes better than the widefield microscope that was used. The ZO1 expression shown in the static Calu-3 model was similar in morphology to the ZO1 expression exhibited from the literature that has previously investigated the tight junctions of the cell line (Carius *et al.*, 2021; Ehrhardt, Fiegel, *et al.*, 2002; Grainger *et al.*, 2006; Ji *et al.*, 2022; Pasman *et al.*, 2021; Sui & Lee, 2023). Whereas the perfused model showed a morphology consistent with a more uniform monolayer of cells than exhibited in the literature hitherto.

ZO1 expression intensity was higher in the perfused model than in the static model when analysed using Fiji Image J image intensity analysis. The increase in ZO1 expression could have contributed to the reduction in P_{app} values of the NaFL fluorescent marker in the perfused Calu-3 model compared to the static system. Day 14 showed this morphology more prominently, with the static model exhibiting an increased number of peduncular patches of cells growing on top of a basal monolayer, increasing the heterogeneity of the epithelial barrier which increases the artefacts and blurriness seen on the images. The perfused model exhibited fewer of the latter patches than the static model and a more uniformly constructed monolayer. It is currently unclear, but hypothesized, that the observations of higher TEER for static compared to perfused cell models discussed previously, may be associated with the disordered morphology of the non-perfused Calu-3 system, yet similar P_{app} values compared to the monolayer of the perfused system.

Although IF images are a suitable approach for identifying proteins present and visualising morphological differences, the protein expression differences are not adequately represented through fluorescence intensity measurements. As an alternative and complementary approach, gene expression studies for tight junction markers were also performed in Section 3.4.2. The qPCR quantification suggested there to be no significant increase of ZO1 tight junction expression from Day 7 to Day 14 in the perfused condition, however in the static condition a significant 5-fold increase was observed over the same duration. This was not in agreement with the IF intensity measurements, and therefore illustrates the disparity between gene expression measurements and protein expression. Of course, the translation of expressed transcripts to proteins by the time of RNA extraction cannot be ruled out, as intimated by the IF observations. Another analysis technique could have been employed to quantify the increase in fold expression of proteins, such as western blot analysis, that would allow a second physical analysis of tight junction protein expression between the conditions and culture timepoints and reduce the reliance on the qualitative IF images.

Further tight junction proteins, such as occludin and claudin are also present in the Calu-3 epithelium and have a similar function to ZO1 in the restriction of paracellular transport. The

claudin (CLDN1) tight junction expression was not confirmed using IF imaging like ZO1 tight junctions, however its transcription was confirmed and quantified using qPCR analysis. Although there was no significant difference between the static and perfused conditions in CLDN1 gene expression, there was a significant increase in claudin expression between Day 7 and Day 14 in both conditions. The increased expression of tight junction markers could account for the lower P_{app} in the static conditions by Day 14. Occludin presence in the Calu-3 cell line has been confirmed in the literature, so this could have been an additional protein to characterise for the perfused model to provide a fuller understanding of the proteins providing the main barrier function in the epithelial monolayer (Carius *et al.*, 2021). E-cadherin is a cell-cell adhesion protein that has been reported in Calu-3 cells by a number of research groups and contributes to the alignment of the epithelial cells in a monolayer (Carius *et al.*, 2021; Ehrhardt, Fiegel, *et al.*, 2002; Ji *et al.*, 2022; Sui & Lee, 2023). This protein could have added another potential layer of understanding the formation and the morphology of the Calu-3 monolayer in perfused conditions compared to static conditions.

6.5.3. TRANSPORTER EXPRESSION ANALYSIS

Another key cell biology contributor to the permeability barrier of the pulmonary epithelium is the presence of drug transporter proteins. As the organic cation transporters (OCT) have been thought to facilitate the pulmonary absorption of bronchodilators such as salbutamol, the OCT1 and OCTN2 transporter gene expression was quantified using qPCR analysis (Bosquillon, 2010; Mukherjee *et al.*, 2017a; Nickel *et al.*, 2016; Salomon *et al.*, 2012). Calu-3 cells have been shown to express these OCT subtypes, similar to that of NHBE cells (Mukherjee *et al.*, 2012).

In this study, the perfused condition expressed a significantly higher number of transcripts of the OCT1 transporter compared to the static condition and consistently stayed at that expression until Day 14 when the static model reached an equivalent level of gene expression. This indicated that the enhanced level of drug transporter expression under conditions of perfusion may enhance the relevance of the Calu-3 model for studying the transport of bronchodilators like salbutamol and terbutaline. The OCTN2 transporter expression was significantly higher at Day 14 compared to Day 7 in both the static and perfused condition, showing once again the culture past Day 7 ALI was associated with differentiation of the Calu-3 model to a more mature and differentiated phenotype. Further confirmation of protein expression with the use of an assay such as western blotting would be beneficial in future studies to confirm the expression differences between the conditions and timepoints.

6.5.4. DETECTION OF MUCINS PRESENT AND METHOD LIMITATIONS

Airway mucus has been characterised as a key functional parameter that should be present and characterised in a lung MPS model of the airways as bronchial epithelial tissue contains mucus-secreting goblet cells (Ainslie *et al.*, 2019; Stanfield, 2016). Measuring the amount of mucus that has been secreted is a key parameter to be characterised as it is a key feature of healthy and functional tissue, whilst excess or decreased mucus expression can be a disease symptom. Airway mucus consists of a viscoelastic gel which contains a complex mixture of water (ca. 95%), glycoproteins (mucins, ca. 2-5%), and a small minority of non-mucin proteins, salts, lipids, and cellular debris (Bandi *et al.*, 2021; Bansil and Turner, 2006). Mucins are the major component of the mucus, and MUC5AC and MUC5B are the two main mucins of the human airway mucus. MUC5AC is secreted by goblet cells and MUC5B by submucosal glands (Hovenberg *et al.*, 1996; Reid *et al.*, 1997; Thornton *et al.*, 2008). The presence of the mucin MUC5AC was confirmed to be expressed by the Calu-3 cell line when cultured at ALI (Grainger *et al.*, 2006; Ji *et al.*, 2022; Meindl *et al.*, 2015).

In Chapter 3, the expression of the MUC5AC mucin was confirmed through IF imaging (Ji *et al.*, 2022; Meindl *et al.*, 2015). The mucus expressed was also quantified using an optimised alcian blue mucus quantification assay, originally described by Hall *et al.* (Hall *et al.*, 1980). The assay was optimised for analysing mucus that was washed off with PBS during the TEER measurement method. This wash was passive in order to avoid disrupting the cell layer. Consequently, it is likely that not all the mucus may have been washed off. However, there was not a large discrepancy between the replicates between samples and conditions across the experiments in Chapter 3 and Chapter 4, indicating the utility of the method, in particular due to its non-destructive nature suitable for monitoring *in vitro* models over extended time periods. The alcian blue staining of mucus glycoproteins has previously been used on Calu-3 cells but for a qualitative imaging measurement of mucus secretion, utilising the intensity of the blue colour from images taken of the alcian blue stained mucus in ratio to the total intensity of the red, green and blue (Grau-Bartual *et al.*, 2020). The alcian blue mucus quantification assay described by Hall *et al.* was also optimised for the quantification of mucus secreted from a human colon-on-chip model however, after reviewing the literature, this Thesis describes the first instance of utilising this method for the quantification of lung mucus from the Calu-3 cell line, and is therefore a highly beneficial tool that can be used in the analysis of these models in future studies (Sontheimer-Phelps *et al.*, 2020).

6.5.5. MUCUS QUANTIFICATION AND METHOD LIMITATIONS

Mucus quantification was based on linear regression of the assay standard which was bovine submaxillary gland mucin. Whilst it is not the best representation of the mix of glycoproteins

that are expressed by a human cell line such as Calu-3, across the experiments the amount of mucus was consistent proving the assay to be robust. Interestingly, the composition of the medium changed the expression levels of the mucus. In the Calu-3 monoculture in Chapter 4 Section 4.3.2, an average of 59 μg was quantified in the static condition at Day 14 when grown in the EMEM medium, however when mixed in a 50:50 ratio with the SmGM medium the amount of mucus decreased to 30 μg , whereas in 100% SmGM medium the mucus increased to 52 μg (Figure 4.11). Upon investigation of the media compositions, the SmGM medium contained hEGF and hFGF which could have increased the expression of the mucus glycoproteins due to the two growth factors enhancing the growth and differentiation of the goblet cells in the Calu-3 monolayer. The two growth factors may accelerate and amplify the formation of tight junction from Day 7 onwards, further justifying that a 7-day culture is required to establish the epithelial barrier model. It may also translate to the decrease in P_{app} of NaFL in the 100% SmGM cultured Calu-3 cells compared to the 50/50 equivalent at Day 14.

Lansley *et al* (2019) described an enzyme-linked lectin assay that quantified the mucus expression in the Calu-3 cell line and two others. Calu-3 grown at ALI for 18-21 days at a seeding density of 4.46×10^5 cells/cm² expressed 2.18 ng/well of mucus (Lansley *et al.*, 2019). This is extremely low in comparison to mucus quantified in this thesis which reached 60 μg /well by day 21 however, this may be a result of the enzyme-linked lectin assay being more sensitive to mucin glycoproteins than the alcian blue stain which potentially could have bound to cellular debris, resulting in inaccurate mucus quantities. However, the assay could be improved by using mucin extracted from human samples/cells instead of the bovine submaxillary gland to generate a more relevant assay to the human cell line under investigation.

6.6. LIMITATIONS OF THE CURRENT BRONCHIAL COCULTURE MODELS

Having established a functional epithelial barrier model, it was of interest to explore the potential applications of MPS models that replicating the histological architecture of the pulmonary airways. The communication between the epithelial cells and smooth muscle cells in the airways is a vital characteristic in the airways, specifically the response from airway smooth muscle from stimulants in the environment and inhaled therapeutics, in both healthy and disease state tissues (Abohalaka, 2023; Gallos *et al.*, 2013). There has been a rising interest in understanding the interactions between smooth muscle and epithelium and how the interactions can contribute to respiratory disease and reaction to stimuli (Deacon & Knox, 2015). However, models currently used to evaluate drugs, and environmental stimuli lack the physiological features present *in vivo*. In proximal biopsies obtained through bronchoscopy, airways smooth muscle cells have been shown to be close to the epithelial layer (Pepe *et al.*,

2005). This proximity of the different cell types may have an impact on the phenotype expressed by the cells of the two tissue layers.

The models developed in literature do not accurately represent the close proximity of the bronchial smooth muscle to the bronchial epithelium, as most cocultures described are indirect cocultures with a physical separation of the cells which share the same medium (Vis *et al.*, 2020). Other models describe smooth muscle cells exposed to epithelial cell conditioned medium for as short as one hour with the cells not occupying the same well during the culture period (Lan *et al.*, 2018b). Other models only described an indirect coculture for 24 h, which is an insufficient time to determine morphological and phenotypic changes in the cells (Celle *et al.*, 2022; O'Sullivan *et al.*, 2017). Some models described differentiated epithelial cells that were then indirectly cocultured with BSMCs for 8 days before assessment (Malavia *et al.*, 2009). Only one direct coculture model was described with cells on either side of a hydrogel scaffold however, the model was not explored for perfusion or functionality of the cells despite the culture being contained within an OOC model (Humayun *et al.*, 2018).

6.7. ADDRESSING THE NEED FOR A PHYSIOLOGICALLY RELEVANT BRONCHIAL COCULTURE MODEL

All the latter models in the literature describe an indirect coculture with physical distance between the epithelial cells and the smooth muscle cells, which is not representative of the *in vivo* anatomy of the bronchial tissue. Within Chapter 4 of this thesis, a more direct coculture was described where the Calu-3 cells and the BSMCs occupied the same well and were in direct contact with each other on either side of a PTFE Transwell membrane. Although there is a physical separation between the cells due to the membrane, a very thin (10 μm) membrane layer with pores (0.4 μm) allows direct cell-to-cell communication that would be more akin to the basement membranes of the *in vivo* architecture of respiratory tissue.

A key requirement was for the model that was developed to be commercially viable, using cell and consumable sources that were sustainable and accessible from the commercial marketplace. Cell lines were explored for this reason, however, there were few accessible smooth muscle cell lines that were commercially available. Stem cells were identified to be unsustainable and a more expensive option than primary cells due to the need for harvesting and expensive differentiation required. As a result, primary bronchial smooth muscle cells were explored as described in many of the literature models previously mentioned. The vendor was chosen due to the availability of the number of vials allowing the model to be sustainably sourced, reducing donor variability risks and the cost of each vial keeping within the budget of typical research projects, with potential to expand to disease state cells (Lonza, 2024).

The successful creation of the smooth muscle cell phenotype in culture was demonstrated by IF imaging of the α -SMA protein, which is one of the major contractile proteins in the smooth muscle cells and has previously been used to identify the contractile proteins in literature models (Humayun *et al.*, 2018; Webb, 2003). The presence of this protein identified in Figure 4.19 illustrated the contractile potential of the BSMCs. Furthermore, upon gene analysis, the increased expression of the ACTA2 gene that encodes for the α -SMA was significantly increased in the BSMCs when cocultured with the Calu-3. The latter finding suggested the increased expression of the ACTA2 gene may result in a more sensitive contractile response from the BSMCs when in coculture with the differentiated Calu-3 epithelial cells. Another key marker is the contractile SM22 gene, which is an early marker for smooth muscle differentiation (GeneCards, 2024). This gene was highly expressed in the perfused coculture, significantly higher than the static coculture. This identified an increased differentiation of the smooth muscle cells when in coculture combined with the physiologically relevant perfusion in the MPS. The coculture combined with the perfusion has resulted in an increased contractile expression of the BSMCs potentially exhibiting a more *in vivo*-like phenotype.

In the current work, the expression of receptors such as the M_2 and M_3 muscarinic acetylcholine receptors which mediate contractile response of BSMCs (Cazzola *et al.*, 2012; Matera *et al.*, 2020; Meurs *et al.*, 2013) was not performed. The characterisation of the receptor expression responsible for contractile responses of the BSMCs through analysis such as Western blots would have provided an indication of the accuracy of the cell phenotype compared to *in vivo* tissue, and its and potential for contraction-mediated disease processes. Another receptor that could have been identified and quantified was the B_2 -Ars coupled to AC which, when activated, leads to a decreased Ca^{2+} concentration which reduces the contraction of BSMCs (Nelson *et al.*, 2011; Sieck & Gransee, 2012; Ward, J.P.T., Ward, J. and Leach, 2010). As this receptor is the target for bronchodilators such as terbutaline, the pharmacological action of which was explored in Chapter 5 of this thesis, it would be prudent for future work to identify and quantify the expression of this receptor as it would have enhanced the data coupled to the cAMP response of the BSMCs when exposed to terbutaline. A key criticism of the data presented in section 5.4.4 is the limited number of replicates ($n=3$) in the drug dosing experiment. There were large error bars seen in the drug transport data which could have influenced the significance or non-significance between the conditions and cell models. This could be remedied through an increase in replicates which could give a wider understanding of the data ranges and give rise to the 'true values' in each condition. This is a common occurrence in academic studies, and to achieve full validation of the findings from this study for wider industrial application, sufficient statistical powering of the exposure-pharmacological studies remains to be explored. In this instance, the data generated from the

larger number of wells investigated would give rise to a fuller dataset that can be explored in more depth and give rise to more subtle predictions of pharmacokinetics and pharmacodynamics of drug molecules such as short acting bronchodilators.

6.8. RECAPITULATING BRONCHIAL SMOOTH MUSCLE CELLULAR RESPONSE TO BRONCHODILATORS

Terbutaline concentrations in the blood plasma 4 h following an inhaled dose of 10 mg equated to a total dose of 1.3 µg/mL (4.74 µM) (Dyreborg *et al.*, 2016). Multiple literature sources stated a 10 µM concentration of terbutaline was sufficient to elicit a response in cell culture (Hasegawa *et al.*, 2006; Markowska *et al.*, 2001; Niisato *et al.*, 2007). From this rationale, the dose of 10 µM was considered as a sufficient concentration for dosing on the Calu-3 epithelium to be transported across and elicit a relaxation response from the BSMCs. This concentration was sufficient to result in transport across the Calu-3 epithelium and generate a cAMP response from the BSMCs, although a higher concentration may have been more suitable to exaggerate the cAMP response to elicit more subtle differences between the conditions and culture models. The evaluation of terbutaline on *in vitro* respiratory models is limited compared to salbutamol, for which more *in vivo* data is readily available for *in vitro-in vivo* correlations in comparison to terbutaline. In hindsight, it may be advantageous to have studied salbutamol instead of terbutaline, however, the pharmacological similarity to salbutamol allows a wider understanding of the utility of the model for the prediction of bronchodilator response and drug delivery.

The cAMP response was measured by the HitHunter® cAMP Assay for Small Molecules (Eurofins, USA) that was utilised in the study conducted by Muddle *et al* (2020) however in their paper, the cAMP responses of BSMCs to salbutamol were normalized relative to the cAMP response to isoprenaline (10^{-5} M) (Muddle *et al.*, 2020). The cAMP assessment is a terminal assay, requiring cell disruption, which is a limitation of the approach reported in this thesis. An alternative assay that could be utilised is a live cell image assay measuring the changes in intracellular Ca^{2+} during the contractile response of BSMCs using the Fluo-4 indicator, as described in literature (Halaidych *et al.*, 2019). Such assays are suitable to determine the contractile response of the BSMCs and offer the opportunity to employ the coculture model as a longitudinal disease model, studying the impact of exposure to contractile stimuli of disease origins (e.g. vasoconstrictor endothelin-1 or histamine). This would be a logical body of future work based on the utility of the coculture model which will now be discussed.

The coculture model showed significant reduction in the amount of terbutaline that reached the basolateral chamber compared to the blank Transwell, this was also seen in the study of

salbutamol transport by Muddle *et al* (Muddle *et al.*, 2020). Unfortunately, there was no comparison of the transport of salbutamol with and without the coculture of BSMCs in the mentioned article. The model in Chapter 5 of this thesis explored Calu-3 cells and BSMCs differentiated for 7 days in a direct coculture and the resultant response to the bronchodilator, terbutaline. The co-culture model exhibited a more sensitive response to terbutaline when the coculture differentiation was undertaken with MPS perfusion, developing a heightened cAMP response to a lower amount of terbutaline. The Calu-3 epithelium restricted the amount of terbutaline that reached the basolateral chamber of the coculture model, such that the dose of terbutaline reaching the basolateral chamber was lower in the coculture compared to the monoculture of Calu-3 cells alone. Additionally, perfusion of the coculture led to a further decrease in the permeated dose of terbutaline compared to the non-perfused coculture. This reduction in drug permeation was not shown to be due to the BSMC cell layer forming a diffusion barrier to drug permeation.

This evaluation of the perfused coculture model showed a heightened cAMP response of the BSMCs per nanogram of terbutaline present in the basolateral chamber of the culture well, when compared to the monoculture and non-perfused coculture model. In the model developed by Haghi *et al* (2015), there was no significant difference in the cAMP concentration of the monoculture smooth muscle compared to the coculture with NHBE when exposed to salbutamol, which is similar in action to terbutaline (Haghi *et al.*, 2015). However this model was developed with NHBE not Calu-3 cells so may not have developed the crosstalk that was established in the direct coculture in the model described in Chapter 4 and 5. Additionally, this coculture was differentiated for 72 h compared to the 7 days in the model described in this thesis, allowing for a more extensive differentiation to occur in the model presented in this thesis compared to those described in the literature. The model described in Chapters 4 and 5 induced a more sensitive BSMC relaxation response to bronchodilators than the Haghi model as the model was cultured in coculture for 7 days, allowing for complete differentiation to occur ultimately producing a model that is more physiologically relevant resulting in a more sensitive prediction pharmacodynamics and efficacies of bronchodilators.

6.9. FUTURE WORK

Further exploration of the bronchial coculture model would consist of evaluating the contractile response of the model to stimuli such as histamine. Developing an assay to measure the resultant contraction in the coculture model in the perfused and non-perfused conditions to determine the differences between the cells in each condition alongside the influence of the coculture model on the BSMCs contractile potential. Further evaluating the model's response to bronchodilators and if they reach a near-baseline level or if the contractile response is more

akin to the asthmatic patients for whom it does not return to baseline. The model can then be adapted to provide insights into diseases tissue responses from using primary BSMCs from donors with asthma, COPD etc, and the evaluation of these disease models can be conducted to determine translatability/scalability to *in vivo* PK/PD data.

Another key area of research would be the delivery of different drug formulations delivered from dry powder inhalers as this is a key area of inhaled pharmaceuticals, evaluating the dose delivered and the responses from the coculture model as seen in the literature (Muddle et al., 2020). The model could be used in more niche investigational areas such as the effects of chronic agonist exposure on tissue desensitisation which is becoming an increasing area of concern for asthma and COPD treatments (Liao et al., 2010). The need for establishing sufficiently statistically powered exposure studies is key to the further exploitation of the models developed in this study, and such studies should be a priority for future work.

Additional studies could be carried out on the model's response to muscarinic antagonists, corticosteroids and combinatorial therapies (e.g., corticosteroids with long-acting beta-agonists) to determine the perfused coculture model's ability to respond to therapeutic doses of different drug classes and the translatability/scalability of the biological response to *in vivo* data. A full panel of known compounds with varying properties should be tested on this model (e.g. corticosteroids, muscarinic antagonists, long-acting β_2 -adrenergic receptor agonists) and responses correlated to human *in vivo* responses to evaluate the predictive power of this model and determine the extent of predictivity from the sensitivity and specificity of the results. This data generated would be a powerful tool for the novel investigational compounds when combined with *in silico* techniques such as Quantitative Structure-Activity Relationship models, which could then predict the biological responses of the compound and ultimately determine efficacy before any laboratory assays.

6.10. CONCLUSIONS

The aim of this project was to establish and characterise an *in vitro* bronchial coculture MPS model that was representative of the *in vivo* microenvironment. This was achieved using various assays such as IF and qPCR to determine phenotypic changes to key proteins such as ZO1 tight junction expression and ACTA2 expression of the Calu-3 epithelium and BSMCs, respectively. Barrier functionality was successfully characterised with the use of LY and NaFL paracellular permeability compounds that characterised the permeability of the epithelium monolayer. The perfused epithelium barrier was successfully established, monitored and characterised as less permeable than the static Calu-3 model using TEER measurements. A key application of this bronchial coculture MPS model was its potential to investigate biological responses of the bronchial microenvironment to inhaled compounds such as bronchodilators. Measurement of the smooth muscle relaxation response to terbutaline was established by measurement of intracellular cAMP and quantifying the terbutaline that was transported to the basolateral chamber via developed and validated LC-MS method. concluding perfused coculture model was a sensitive model to investigate responses to inhaled compounds. Overall, the aims of the project were achieved with the data demonstrating that the perfused bronchial coculture MPS model to be sustainable and more physiologically relevant to the human *in vivo* microenvironment than the static monoculture and indirect coculture models in literature. Future work would include a validation of the model with other inhaled compounds.

References

1. Abohalaka, R. (2023). Bronchial epithelial and airway smooth muscle cell interactions in health and disease. *Heliyon*, 9(9), e19976. <https://doi.org/10.1016/j.heliyon.2023.e19976>
2. Abohalaka, R., Bozkurt, T. E., Nemutlu, E., Onder, S. C., & Sahin-Erdemli, I. (2020). The effects of fatty acid amide hydrolase and monoacylglycerol lipase inhibitor treatments on lipopolysaccharide-induced airway inflammation in mice. *Pulmonary Pharmacology & Therapeutics*, 62, 101920. <https://doi.org/10.1016/j.pupt.2020.101920>
3. ACAAI. (2024). *Types of Asthma—Causes, Symptoms & Treatment | ACAAI Patient*. ACAAI Public Website. <https://acaai.org/asthma/types-of-asthma/>
4. Adams, N. P., Bestall, J. B., Malouf, R., Lasserson, T. J., & Jones, P. W. (2005). Inhaled beclomethasone versus placebo for chronic asthma. *The Cochrane Database of Systematic Reviews*, 2005(1), CD002738. <https://doi.org/10.1002/14651858.CD002738.pub2>
5. Adams, N. P., Bestall, J. C., Lasserson, T. J., Jones, P. W., & Cates, C. (2005). Fluticasone versus placebo for chronic asthma in adults and children. *The Cochrane Database of Systematic Reviews*, 4, CD003135. <https://doi.org/10.1002/14651858.CD003135.pub3>
6. Adkins, J. C., & McTavish, D. (1997). Salmeterol. A review of its pharmacological properties and clinical efficacy in the management of children with asthma. *Drugs*, 54(2), 331–354. <https://doi.org/10.2165/00003495-199754020-00011>
7. Adler, K. B., Holden-Stauffer, W. J., & Repine, J. E. (1990). Oxygen metabolites stimulate release of high-molecular-weight glycoconjugates by cell and organ cultures of rodent respiratory epithelium via an arachidonic acid-dependent mechanism. *Journal of Clinical Investigation*, 85(1), 75–85. <https://doi.org/10.1172/JCI114436>
8. Agha, A., Waheed, W., Alamoodi, N., Mathew, B., Alnaimat, F., Abu-Nada, E., Abderrahmane, A., & Alazzam, A. (2022). A Review of Cyclic Olefin Copolymer Applications in Microfluidics and Microdevices. *Macromolecular Materials and Engineering*, 307(8), 2200053. <https://doi.org/10.1002/mame.202200053>

9. Ahadian, S., Civitarese, R., Bannerman, D., Mohammadi, M. H., Lu, R., Wang, E., Davenport-Huyer, L., Lai, B., Zhang, B., Zhao, Y., Mandla, S., Korolj, A., & Radisic, M. (2018). Organ-On-A-Chip Platforms: A Convergence of Advanced Materials, Cells, and Microscale Technologies. *Advanced Healthcare Materials*, 7(2), 1700506. <https://doi.org/10.1002/adhm.201700506>
10. Ahn, E., Kumar, P., Mukha, D., Tzur, A., & Shlomi, T. (2017). Temporal fluxomics reveals oscillations in TCA cycle flux throughout the mammalian cell cycle. *Molecular Systems Biology*, 13(11), 953. <https://doi.org/10.15252/msb.20177763>
11. Ainslie, G. R., Davis, M., Ewart, L., Lieberman, L. A., Rowlands, D. J., Thorley, A. J., Yoder, G., & Ryan, A. M. (2019). Microphysiological lung models to evaluate the safety of new pharmaceutical modalities: A biopharmaceutical perspective. *Lab on a Chip*, 19(19), 3152–3161. <https://doi.org/10.1039/C9LC00492K>
12. Akinbami, L. J., Moorman, J. E., Bailey, C., Zahran, H. S., King, M., Johnson, C. A., & Liu, X. (2001). *NCHS Data Brief, Number 94, May 2012: Trends in Asthma Prevalence*,.
13. Alsafadi, H. N., Staab-Weijnitz, C. A., Lehmann, M., Lindner, M., Peschel, B., Königshoff, M., & Wagner, D. E. (2017). An ex vivo model to induce early fibrosis-like changes in human precision-cut lung slices. *American Journal of Physiology-Lung Cellular and Molecular Physiology*, 312(6), L896–L902. <https://doi.org/10.1152/ajplung.00084.2017>
14. Alsenz, J., & Haenel, E. (2003). Development of a 7-Day, 96-Well Caco-2 Permeability Assay with High-Throughput Direct UV Compound Analysis. *Pharmaceutical Research*, 20(12), 1961–1969. <https://doi.org/10.1023/B:PHAM.0000008043.71001.43>
15. AlveoliX. (2024). *AlveoliX - in vitro models inspired by nature*. AlveoliX. <https://www.alveolix.com/>
16. Amann, A., Zwierzina, M., Gamerith, G., Bitsche, M., Huber, J. M., Vogel, G. F., Blumer, M., Koeck, S., Pechriggl, E. J., Kelm, J. M., Hilbe, W., & Zwierzina, H. (2014). Development of an innovative 3D cell culture system to study tumour—Stroma interactions in non-small cell lung cancer cells. *PLoS ONE*, 9(3). <https://doi.org/10.1371/journal.pone.0092511>
17. *Amphotericin B*. (2024). <https://www.thermofisher.com/order/catalog/product/15290018>

18. Anakwe, O. O., Murphy, P. R., & Moger, W. H. (1985). Characterization of β -adrenergic binding sites on rodent Leydig cells. *Biology of Reproduction*, 33(4), 815–826. Scopus. <https://doi.org/10.1095/biolreprod33.4.815>
19. Antman-Passig, M., & Shefi, O. (2016). Remote Magnetic Orientation of 3D Collagen Hydrogels for Directed Neuronal Regeneration. *Nano Letters*, 16(4), 2567–2573. <https://doi.org/10.1021/acs.nanolett.6b00131>
20. Artursson, P., Palm, K., & Luthman, K. (2012). Caco-2 monolayers in experimental and theoretical predictions of drug transport. *Advanced Drug Delivery Reviews*, 64, 280–289. <https://doi.org/10.1016/j.addr.2012.09.005>
21. Artzy-Schnirman, A., Hobi, N., Schneider-Daum, N., Guenat, O. T., Lehr, C.-M., & Sznitman, J. (2019). Advanced in vitro lung-on-chip platforms for inhalation assays: From prospect to pipeline. *European Journal of Pharmaceutics and Biopharmaceutics*, 144, 11–17. <https://doi.org/10.1016/j.ejpb.2019.09.006>
22. Artzy-Schnirman, A., Lehr, C. M., & Sznitman, J. (2020). Advancing human in vitro pulmonary disease models in preclinical research: Opportunities for lung-on-chips. *Expert Opinion on Drug Delivery*, 17(5), 621–625. <https://doi.org/10.1080/17425247.2020.1738380>
23. Asgari, M., Latifi, N., Heris, H. K., Vali, H., & Mongeau, L. (2017). In vitro fibrillogenesis of tropocollagen type III in collagen type I affects its relative fibrillar topology and mechanics. *Scientific Reports*, 7(1), 1392. <https://doi.org/10.1038/s41598-017-01476-y>
24. Atencia, J., & Beebe, D. J. (2005). Controlled microfluidic interfaces. *Nature*, 437(7059), 648–655. <https://doi.org/10.1038/nature04163>
25. Ayliffe, H. E., Frazier, A. B., & Rabbitt, R. D. (1999). Electric impedance spectroscopy using microchannels with integrated metal electrodes. *Journal of Microelectromechanical Systems*, 8(1), 50–57. <https://doi.org/10.1109/84.749402>
26. Bai, Y., Krishnamoorthy, N., Patel, K. R., Rosas, I., Sanderson, M. J., & Ai, X. (2016). Cryopreserved human precision-cut lung slices as a bioassay for live tissue banking a viability study of bronchodilation with bitter-taste receptor agonists. *American Journal of*

- Respiratory Cell and Molecular Biology*, 54(5), 656–663.
<https://doi.org/10.1165/rcmb.2015-0290MA>
27. Bailey, J., Thew, M., & Balls, M. (2015). Predicting human drug toxicity and safety via animal tests: Can any one species predict drug toxicity in any other, and do monkeys help? *Alternatives to Laboratory Animals: ATLA*, 43(6), 393–403.
<https://doi.org/10.1177/026119291504300607>
28. Baker, B. M., & Chen, C. S. (2012). Deconstructing the third dimension-how 3D culture microenvironments alter cellular cues. *Journal of Cell Science*, 125(13), 3015–3024.
<https://doi.org/10.1242/jcs.079509>
29. Baptista, D., Moreira Teixeira, L., Barata, D., Tahmasebi Birgani, Z., King, J., van Riet, S., Pasma, T., Poot, A. A., Stamatialis, D., Rottier, R. J., Hiemstra, P. S., Carlier, A., van Blitterswijk, C., Habibović, P., Giselbrecht, S., & Truckenmüller, R. (2022). 3D Lung-on-Chip Model Based on Biomimetically Microcurved Culture Membranes. *ACS Biomaterials Science & Engineering*, 8(6), 2684–2699.
<https://doi.org/10.1021/acsbiomaterials.1c01463>
30. Barilli, A., Visigalli, R., Ferrari, F., Di Lascia, M., Riccardi, B., Puccini, P., Dall'Asta, V., & Rotoli, B. M. (2020). Organic Cation Transporters (OCTs) in EpiAirway™, a Cellular Model of Normal Human Bronchial Epithelium. *Biomedicines*, 8(5), 127.
<https://doi.org/10.3390/biomedicines8050127>
31. Barkauskas, C. E., Crouse, M. J., Rackley, C. R., Bowie, E. J., Keene, D. R., Stripp, B. R., Randell, S. H., Noble, P. W., & Hogan, B. L. M. (2013). Type 2 alveolar cells are stem cells in adult lung. *Journal of Clinical Investigation*, 123(7), 3025–3036.
<https://doi.org/10.1172/JCI68782>
32. Barnes, P. J., Bonini, S., Seeger, W., Belvisi, M. G., Ward, B., & Holmes, A. (2015). Barriers to new drug development in respiratory disease. *European Respiratory Journal*, 45(5), 1197–1207. <https://doi.org/10.1183/09031936.00007915>
33. Barrila, J., Crabbé, A., Yang, J., Franco, K., Nydam, S. D., Forsyth, R. J., Davis, R. R., Gangaraju, S., Ott, C. M., Coyne, C. B., Bissell, M. J., & Nickerson, C. A. (2018). Modeling

- Host-Pathogen Interactions in the Context of the Microenvironment: Three-Dimensional Cell Culture Comes of Age. *Infection and Immunity*, 86(11), 10.1128/iai.00282-18. <https://doi.org/10.1128/iai.00282-18>
34. Bartow, R. A., & Brogden, R. N. (1998). Formoterol. An update of its pharmacological properties and therapeutic efficacy in the management of asthma. *Drugs*, 55(2), 303–322. <https://doi.org/10.2165/00003495-199855020-00016>
35. Beaufils, F., & Berger, P. (2022). Increased airway smooth muscle cells in asthma: Mechanisms and therapeutic prospects. *Annals of Translational Medicine*, 10(17), 920. <https://doi.org/10.21037/atm-22-3973>
36. Beltaief, K., Msolli, M. A., Zorgati, A., Sekma, A., Fakhfakh, M., Marzouk, M. B., Boubaker, H., Grissa, M. H., Methamem, M., Boukef, R., Belguith, A., Boudia, W., & Noura, S. (2019). Nebulized Terbutaline and Ipratropium Bromide Versus Terbutaline Alone in Acute Exacerbation of Chronic Obstructive Pulmonary Disease Requiring Noninvasive Ventilation: A Randomized Double-blind Controlled Trial. *Academic Emergency Medicine: Official Journal of the Society for Academic Emergency Medicine*, 26(4), 434–442. <https://doi.org/10.1111/acem.13560>
37. Benders, K. E. M., Weeren, P. R. van, Badylak, S. F., Saris, D. B. F., Dhert, W. J. A., & Malda, J. (2013). Extracellular matrix scaffolds for cartilage and bone regeneration. *Trends in Biotechnology*, 31(3), 169–176. <https://doi.org/10.1016/j.tibtech.2012.12.004>
38. Bérubé, K., Aufderheide, M., Breheny, D., Clothier, R., Combes, R., Duffin, R., Forbes, B., Gaça, M., Gray, A., Hall, I., Kelly, M., Lethem, M., Liebsch, M., Merolla, L., Morin, J. P., Seagrave, J., Swartz, M. A., Tetley, T. D., & Umachandran, M. (2009). In Vitro models of inhalation toxicity and disease: The report of a FRAME workshop. *ATLA Alternatives to Laboratory Animals*, 37(1), 89–141.
39. Bérubé, K., Prytherch, Z., Job, C., & Hughes, T. (2010). Human primary bronchial lung cell constructs: The new respiratory models. *Toxicology*, 278(3), 311–318. <https://doi.org/10.1016/j.tox.2010.04.004>

40. Bhatia, S. N., & Ingber, D. E. (2014a). Microfluidic organs-on-chips. *Nature Biotechnology*, 32(8), 760–772. <https://doi.org/10.1038/nbt.2989>
41. Bhatia, S. N., & Ingber, D. E. (2014b). Microfluidic organs-on-chips. *Nature Biotechnology*, 32(8), 760–772. <https://doi.org/10.1038/nbt.2989>
42. Birgersdotter, A., Sandberg, R., & Ernberg, I. (2005). Gene expression perturbation in vitro—A growing case for three-dimensional (3D) culture systems. *Seminars in Cancer Biology*, 15(5 SPEC. ISS.), 405–412. <https://doi.org/10.1016/j.semcancer.2005.06.009>
43. Bissell, M. J., Radisky, D. C., Rizki, A., Weaver, V. M., & Petersen, O. W. (2002). The organizing principle: Microenvironmental influences in the normal and malignant breast. *Differentiation*, 70(9–10), 537–546. <https://doi.org/10.1046/j.1432-0436.2002.700907.x>
44. Bissell, M. J., Rizki, A., & Mian, I. S. (2003). Tissue architecture: The ultimate regulator of breast epithelial function. *Current Opinion in Cell Biology*, 15(6), 753–762. <https://doi.org/10.1016/j.ceb.2003.10.016>
45. Bonfiglio, R., King, R. C., Olah, T. V., & Merkle, K. (1999). The effects of sample preparation methods on the variability of the electrospray ionization response for model drug compounds. *Rapid Communications in Mass Spectrometry*, 13(12), 1175–1185. [https://doi.org/10.1002/\(sici\)1097-0231\(19990630\)13:12<1175::aid-rcm639>3.0.co;2-0](https://doi.org/10.1002/(sici)1097-0231(19990630)13:12<1175::aid-rcm639>3.0.co;2-0)
46. Booth, A. J., Hadley, R., Cornett, A. M., Dreffs, A. A., Matthes, S. A., Tsui, J. L., Weiss, K., Horowitz, J. C., Fiore, V. F., Barker, T. H., Moore, B. B., Martinez, F. J., Niklason, L. E., & White, E. S. (2012). Acellular normal and fibrotic human lung matrices as a culture system for in vitro investigation. *American Journal of Respiratory and Critical Care Medicine*, 186(9), 866–876. <https://doi.org/10.1164/rccm.201204-0754OC>
47. Booth, R., & Kim, H. (2012). Characterization of a microfluidic in vitro model of the blood-brain barrier (μ BBB). *Lab on a Chip*, 12(10), 1784–1792. <https://doi.org/10.1039/C2LC40094D>
48. Borghardt, J. M., Kloft, C., & Sharma, A. (2018). Inhaled Therapy in Respiratory Disease: The Complex Interplay of Pulmonary Kinetic Processes. *Canadian Respiratory Journal*, 2018. <https://doi.org/10.1155/2018/2732017>

49. Bosquillon, C. (2010). Drug transporters in the lung—Do they play a role in the biopharmaceutics of inhaled drugs? *Journal of Pharmaceutical Sciences*, 99(5), 2240–2255. <https://doi.org/10.1002/jps.21995>
50. Braakhuis, H. M., Kloet, S. K., Kezic, S., Kuper, F., Park, M. V. D. Z., Bellmann, S., van der Zande, M., Le Gac, S., Krystek, P., Peters, R. J. B., Rietjens, I. M. C. M., & Bouwmeester, H. (2015). Progress and future of in vitro models to study translocation of nanoparticles. *Archives of Toxicology*, 89(9), 1469–1495. <https://doi.org/10.1007/s00204-015-1518-5>
51. Brandenberger, C., Rothen-Rutishauser, B., Mühlfeld, C., Schmid, O., Ferron, G. A., Maier, K. L., Gehr, P., & Lenz, A. G. (2010). Effects and uptake of gold nanoparticles deposited at the air-liquid interface of a human epithelial airway model. *Toxicology and Applied Pharmacology*, 242(1), 56–65. <https://doi.org/10.1016/j.taap.2009.09.014>
52. Breeze, R., & Turk, M. (1984). Cellular Structure, Function and Organization in the Lower Respiratory Tract. In *Environmental Health Perspectives* (Vol. 55, pp. 3–24).
53. Breslin, S., & O'driscoll, L. (2012). Three-dimensional cell culture: The missing link in drug discovery. *Drug Discovery Today*, 00. <https://doi.org/10.1016/j.drudis.2012.10.003>
54. British Society for Immunology. (2024). *Enzyme-linked immunosorbent assay (ELISA) | British Society for Immunology*. <https://www.immunology.org/public-information/bitesized-immunology/experimental-techniques/enzyme-linked-immunosorbent-assay>
55. Brown, A. C., Fiore, V. F., Sulchek, T. A., & Barker, T. H. (2013). Physical and chemical microenvironmental cues orthogonally control the degree and duration of fibrosis-associated epithelial-to-mesenchymal transitions. *The Journal of Pathology*, 229(1), 25–35. <https://doi.org/10.1002/path.4114>
56. BTS/SIGN. (2019). *Asthma | British Thoracic Society | Better lung health for all*. <https://www.brit-thoracic.org.uk/quality-improvement/guidelines/asthma/>
57. Bukowy-Bieryłło, Z. (2021). Long-term differentiating primary human airway epithelial cell cultures: How far are we? *Cell Communication and Signaling: CCS*, 19, 63. <https://doi.org/10.1186/s12964-021-00740-z>

58. Burgess, J. K., Mauad, T., Tjin, G., Karlsson, J. C., & Westergren-Thorsson, G. (2016). The extracellular matrix – the under-recognized element in lung disease? *The Journal of Pathology*, 240(4), 397–409. <https://doi.org/10.1002/path.4808>
59. Campbell, J. D., McDonough, J. E., Zeskind, J. E., Hackett, T. L., Pechkovsky, D. V., Brandsma, C.-A., Suzuki, M., Gosselink, J. V., Liu, G., Alekseyev, Y. O., Xiao, J., Zhang, X., Hayashi, S., Cooper, J. D., Timens, W., Postma, D. S., Knight, D. A., Lenburg, M. E., Hogg, J. C., & Spira, A. (2012). A gene expression signature of emphysema-related lung destruction and its reversal by the tripeptide GHK. *Genome Medicine*, 4(8), 67. <https://doi.org/10.1186/gm367>
60. Carius, P., Dubois, A., Ajdarirad, M., Artzy-Schnirman, A., Sznitman, J., Schneider-Daum, N., & Lehr, C.-M. (2021). PerfuPul—A Versatile Perfusable Platform to Assess Permeability and Barrier Function of Air Exposed Pulmonary Epithelia. *Frontiers in Bioengineering and Biotechnology*, 0, 904. <https://doi.org/10.3389/FBIOE.2021.743236>
61. Cavet, M. E., West, M., & Simmons, N. L. (1997). Transepithelial transport of the fluoroquinolone ciprofloxacin by human airway epithelial Calu-3 cells. *Antimicrobial Agents and Chemotherapy*, 41(12), 2693–2698. Scopus. <https://doi.org/10.1128/aac.41.12.2693>
62. Cawkill, D., & Eaglestone, S. S. (2007). Evolution of cell-based reagent provision. *Drug Discovery Today*, 12(19–20), 820–825. <https://doi.org/10.1016/j.drudis.2007.08.014>
63. Cazzola, M., Calzetta, L., & Matera, M. G. (2021). Long-acting muscarinic antagonists and small airways in asthma: Which link? *Allergy*, 76(7), 1990–2001. <https://doi.org/10.1111/all.14766>
64. Cazzola, M., & Matera, M. G. (2021). Is it time to look beyond bronchodilators and corticosteroids in treating COPD? *Future Drug Discovery*, 3(2), FDD61. <https://doi.org/10.4155/fdd-2021-0001>
65. Cazzola, M., Page, C. P., Calzetta, L., & Matera, M. G. (2012). Pharmacology and therapeutics of bronchodilators. *Pharmacological Reviews*, 64(3), 450–504. <https://doi.org/10.1124/pr.111.004580>

66. CDC. (2020). *Biosafety in Microbiological and Biomedical Laboratories (BMBL) 6th Edition*. <https://www.cdc.gov/labs/BMBL.html>
67. Celle, A., Esteves, P., Cardouat, G., Beaufile, F., Eyraud, E., Dupin, I., Maurat, E., Lacomme, S., Ousova, O., Begueret, H., Thumerel, M., Marthan, R., Girodet, P.-O., Berger, P., & Trian, T. (2022). Rhinovirus infection of bronchial epithelium induces specific bronchial smooth muscle cell migration of severe asthmatic patients. *The Journal of Allergy and Clinical Immunology*, 150(1), 104–113. <https://doi.org/10.1016/j.jaci.2022.01.022>
68. Cevhertas, L., Ogulur, I., Maurer, D. J., Burla, D., Ding, M., Jansen, K., Koch, J., Liu, C., Ma, S., Mitamura, Y., Peng, Y., Radzikowska, U., Rinaldi, A. O., Satitsuksanoa, P., Globinska, A., van de Veen, W., Sokolowska, M., Baerenfaller, K., Gao, Y.-D., ... Akdis, C. A. (2020). Advances and recent developments in asthma in 2020. *Allergy*, 75(12), 3124–3146. <https://doi.org/10.1111/all.14607>
69. Chandra, P., Paliwal, L., Lodha, R., & Kabra, S. K. (2004). Comparison of terbutaline and salbutamol inhalation in children with mild or moderate acute exacerbation of asthma. *The Indian Journal of Pediatrics*, 71(11), 961–963. <https://doi.org/10.1007/BF02828104>
70. Chen, W. L. K., Edington, C., Suter, E., Yu, J., Velazquez, J. J., Velazquez, J. G., Shockley, M., Large, E. M., Venkataramanan, R., Hughes, D. J., Stokes, C. L., Trumper, D. L., Carrier, R. L., Cirit, M., Griffith, L. G., & Lauffenburger, D. A. (2017). Integrated gut/liver microphysiological systems elucidates inflammatory inter-tissue crosstalk. *Biotechnology and Bioengineering*, 114(11), 2648–2659. <https://doi.org/10.1002/bit.26370>
71. Chen, Y. W., Huang, S. X., De Carvalho, A. L. R. T., Ho, S. H., Islam, M. N., Volpi, S., Notarangelo, L. D., Ciancanelli, M., Casanova, J. L., Bhattacharya, J., Liang, A. F., Palermo, L. M., Porotto, M., Moscona, A., & Snoeck, H. W. (2017). A three-dimensional model of human lung development and disease from pluripotent stem cells. *Nature Cell Biology*, 19(5), 542–549. <https://doi.org/10.1038/ncb3510>

72. Choe, M. M., Tomei, A. A., & Swartz, M. A. (2006). Physiological 3D tissue model of the airway wall and mucosa. *Nature Protocols*, 1(1), 357–362. <https://doi.org/10.1038/nprot.2006.54>
73. Chowdhury, F., Howat, W. J., Phillips, G. J., & Lackie, P. M. (2010). Interactions between endothelial cells and epithelial cells in a combined cell model of airway mucosa: Effects on tight junction permeability. *Experimental Lung Research*, 36(1), 1–11. <https://doi.org/10.3109/01902140903026582>
74. Chung, K. F., & Adcock, I. M. (2008). Multifaceted mechanisms in COPD: Inflammation, immunity, and tissue repair and destruction. *The European Respiratory Journal*, 31(6), 1334–1356. <https://doi.org/10.1183/09031936.00018908>
75. Cingolani, E., Alqahtani, S., Sadler, R. C., Prime, D., Stolnik, S., & Bosquillon, C. (2019). In vitro investigation on the impact of airway mucus on drug dissolution and absorption at the air-epithelium interface in the lungs. *European Journal of Pharmaceutics and Biopharmaceutics*, 141, 210–220. <https://doi.org/10.1016/j.ejpb.2019.05.022>
76. Clevers, H. (2016). Modeling Development and Disease with Organoids. *Cell*, 165(7), 1586–1597. <https://doi.org/10.1016/j.cell.2016.05.082>
77. CN Bio. (2019, December 12). *CN Bio | Organ-on-a-chip company | Human Drug Discovery*. <https://cn-bio.com/>
78. Courcot, E., Leclerc, J., Lafitte, J. J., Mensier, E., Jaillard, S., Gosset, P., Shirali, P., Pottier, N., Broly, F., & Lo-Guidice, J. M. (2012). Xenobiotic metabolism and disposition in human lung cell models: Comparison with in vivo expression profiles. *Drug Metabolism and Disposition*, 40(10), 1953–1965. <https://doi.org/10.1124/dmd.112.046896>
79. Cozens, A. L., Yezzi, M. J., Kunzelmann, K., Ohrui, T., Chin, L., Eng, K., Finkbeiner, W. E., Widdicombe, J. H., & Gruenert, D. C. (1994). CFTR expression and chloride secretion in polarized immortal human bronchial epithelial cells. *American Journal of Respiratory Cell and Molecular Biology*, 10(1), 38–47. <https://doi.org/10.1165/ajrcmb.10.1.7507342>

80. Cozens, D., Sutherland, E., Marchesi, F., Taylor, G., Berry, C. C., & Davies, R. L. (2018). Temporal differentiation of bovine airway epithelial cells grown at an air-liquid interface. *Scientific Reports*, 8(1). <https://doi.org/10.1038/s41598-018-33180-w>
81. Danku, A. E., Dulf, E.-H., Braicu, C., Jurj, A., & Berindan-Neagoe, I. (2022). Organ-On-A-Chip: A Survey of Technical Results and Problems. *Frontiers in Bioengineering and Biotechnology*, 10, 840674. <https://doi.org/10.3389/fbioe.2022.840674>
82. Davies, N. M., & Feddah, M. R. (2003). A novel method for assessing dissolution of aerosol inhaler products. *International Journal of Pharmaceutics*, 255(1–2), 175–187. [https://doi.org/10.1016/S0378-5173\(03\)00091-7](https://doi.org/10.1016/S0378-5173(03)00091-7)
83. de Jong, P. M., van Sterkenburg, M. A., Hesselink, S. C., Kempenaar, J. A., Mulder, A. A., Mommaas, A. M., Dijkman, J. H., & Ponec, M. (1994). Ciliogenesis in human bronchial epithelial cells cultured at the air-liquid interface. *American Journal of Respiratory Cell and Molecular Biology*, 10(3), 271–277. <https://doi.org/10.1165/ajrcmb.10.3.8117445>
84. de Souza Carvalho, C., Daum, N., & Lehr, C. M. (2014). Carrier interactions with the biological barriers of the lung: Advanced in vitro models and challenges for pulmonary drug delivery. *Advanced Drug Delivery Reviews*, 75, 129–140. <https://doi.org/10.1016/j.addr.2014.05.014>
85. Deacon, K., & Knox, A. J. (2015). Human airway smooth muscle cells secrete amphiregulin via bradykinin/COX-2/PGE2, inducing COX-2, CXCL8, and VEGF expression in airway epithelial cells. *American Journal of Physiology. Lung Cellular and Molecular Physiology*, 309(3), L237–249. <https://doi.org/10.1152/ajplung.00390.2014>
86. Dehne, E. M., Hasenberg, T., & Marx, U. (2017). The ascendance of microphysiological systems to solve the drug testing dilemma. *Future Science OA*, 3(2). <https://doi.org/10.4155/fsoa-2017-0002>
87. DiMasi, J. A., Grabowski, H. G., & Hansen, R. W. (2016). Innovation in the pharmaceutical industry: New estimates of R&D costs. *Journal of Health Economics*, 47, 20–33. <https://doi.org/10.1016/j.jhealeco.2016.01.012>

88. Dolovich, M. B., Jordana, M., & Newhouse, M. T. (1987). Methodologic considerations in mucociliary clearance and lung epithelial absorption measurements. *European Journal of Nuclear Medicine*, 13(1 Supplement), S45–S52. <https://doi.org/10.1007/BF00253291>
89. Domansky, K., Inman, W., Serdy, J., Dash, A., Lim, M. H. M., & Griffith, L. G. (2010). Perfused Multiwell Plate for 3D Liver Tissue Engineering. *Lab on a Chip*, 10(1), 51–58. <https://doi.org/10.1039/b913221j>
90. Dowden, H., & Munro, J. (2019). Trends in clinical success rates and therapeutic focus. *Nature Reviews. Drug Discovery*, 18(7), 495–496. <https://doi.org/10.1038/d41573-019-00074-z>
91. Drescher, H., Weiskirchen, S., & Weiskirchen, R. (2021). Flow Cytometry: A Blessing and a Curse. *Biomedicines*, 9(11), 1613. <https://doi.org/10.3390/biomedicines9111613>
92. DrugBank Online. (2024). *Salbutamol: Uses, Interactions, Mechanism of Action*. <https://go.drugbank.com/drugs/DB01001>
93. Duan, Y., Gotoh, N., Yan, Q., Du, Z., Weinstein, A. M., Wang, T., & Weinbaum, S. (2008). Shear-induced reorganization of renal proximal tubule cell actin cytoskeleton and apical junctional complexes. *Proceedings of the National Academy of Sciences of the United States of America*, 105(32), 11418–11423. <https://doi.org/10.1073/pnas.0804954105>
94. Ducharme, F. M., Ni Chroinin, M., Greenstone, I., & Lasserson, T. J. (2010). Addition of long-acting beta2-agonists to inhaled steroids versus higher dose inhaled steroids in adults and children with persistent asthma. *The Cochrane Database of Systematic Reviews*, 4, CD005533. <https://doi.org/10.1002/14651858.CD005533.pub2>
95. Duffy, S. L., & Murphy, J. T. (2001). Colorimetric assay to quantify macromolecule diffusion across endothelial monolayers. *BioTechniques*, 31(3), 495–496, 498, 500–501. <https://doi.org/10.2144/01313st02>
96. Dyreborg, A., Krogh, N., Backer, V., Rzeppa, S., Hemmersbach, P., & Hostrup, M. (2016). Pharmacokinetics of Oral and Inhaled Terbutaline after Exercise in Trained Men. *Frontiers in Pharmacology*, 7. <https://doi.org/10.3389/fphar.2016.00150>

97. E. Cooper, A., Ferguson, D., & Grime, K. (2012). Optimisation of DMPK by the Inhaled Route: Challenges and Approaches. *Current Drug Metabolism*, 13(4), 457–473. <https://doi.org/10.2174/138920012800166571>
98. Easterling, L. F., Yerabolu, R., Kumar, R., Alzarini, K. Z., & Kenttämä, H. I. (2020). Factors Affecting the Limit of Detection for HPLC/Tandem Mass Spectrometry Experiments Based on Gas-Phase Ion–Molecule Reactions. *Analytical Chemistry*, 92(11), 7471–7477. <https://doi.org/10.1021/acs.analchem.9b05369>
99. Ebina, M., Yaegashi, H., Takahashi, T., Motomiya, M., & Tanemura, M. (1990). Distribution of smooth muscles along the bronchial tree. A morphometric study of ordinary autopsy lungs. *American Review of Respiratory Disease*, 141(5 I), 1322–1326. Scopus. https://doi.org/10.1164/ajrccm/141.5_pt_1.1322
100. Ehrhardt, C., Bäckman, P., Couet, W., Edwards, C., Forbes, B., Fridén, M., Gumbleton, M., Hosoya, K. I., Kato, Y., Nakanishi, T., Takano, M., Terasaki, T., & Yumoto, R. (2017). Current Progress Toward a Better Understanding of Drug Disposition Within the Lungs: Summary Proceedings of the First Workshop on Drug Transporters in the Lungs. *Journal of Pharmaceutical Sciences*, 106(9), 2234–2244. <https://doi.org/10.1016/j.xphs.2017.04.011>
101. Ehrhardt, C., Fiegel, J., Fuchs, S., Abu-Dahab, R., Schaefer, U. F., Hanes, J., & Lehr, C.-M. (2002). Drug absorption by the respiratory mucosa: Cell culture models and particulate drug carriers. *Journal of Aerosol Medicine: The Official Journal of the International Society for Aerosols in Medicine*, 15(2), 131–139. <https://doi.org/10.1089/089426802320282257>
102. Ehrhardt, C., Kneuer, C., Fiegel, J., Hanes, J., Schaefer, U., Kim, K.-J., & Lehr, C.-M. (2002). Influence of apical fluid volume on the development of functional intercellular junctions in the human epithelial cell line 16HBE14o-: Implications for the use of this cell line as an in vitro model for bronchial drug absorption studies. *Cell and Tissue Research*, 308(3), 391–400. <https://doi.org/10.1007/s00441-002-0548-5>

103. Ekert, J. E., Johnson, K., Strake, B., Pardinas, J., Jarantow, S., Perkinson, R., & Colter, D. C. (2014). Three-dimensional lung tumor microenvironment modulates therapeutic compound responsiveness in vitro—Implication for drug development. *PLoS ONE*, 9(3), 92248. <https://doi.org/10.1371/journal.pone.0092248>
104. Elonheimo, H. M., Mattila, T., Andersen, H. R., Bocca, B., Ruggieri, F., Haverinen, E., & Tolonen, H. (2022). Environmental Substances Associated with Chronic Obstructive Pulmonary Disease—A Scoping Review. *International Journal of Environmental Research and Public Health*, 19(7), 3945. <https://doi.org/10.3390/ijerph19073945>
105. EMA. (2022). *ICH M10 on bioanalytical method validation—Scientific guideline* | European Medicines Agency. EMA. <https://www.ema.europa.eu/en/ich-m10-bioanalytical-method-validation-scientific-guideline>
106. Emulate. (2024). Emulate. <https://emulatebio.com/>
107. *EpiAirway 3D in vitro Microtissues*. (2015, November 28). MatTek Life Sciences. <https://www.mattek.com/mattekproduct/epiairway/>
108. Epithelix. (2024). *Epithelix—MucilAir, SmallAir, AveolAir*. Epithelix. <https://www.epithelix.com/products/all-tissues>
109. Erle, D. J., & Sheppard, D. (2014). The cell biology of asthma. *The Journal of Cell Biology*, 205(5), 621–631. <https://doi.org/10.1083/jcb.201401050>
110. Essayan, D. M. (2001). Cyclic nucleotide phosphodiesterases. *Journal of Allergy and Clinical Immunology*, 108(5), 671–680. <https://doi.org/10.1067/mai.2001.119555>
111. Evans, M. J., & Kaufman, M. H. (1981). Establishment in culture of pluripotential cells from mouse embryos. *Nature*, 292(5819), 154–156. <https://doi.org/10.1038/292154a0>
112. Ewart, L., Dehne, E.-M., Fabre, K., Gibbs, S., Hickman, J., Hornberg, E., Ingelman-Sundberg, M., Jang, K.-J., Jones, D. R., Lauschke, V. M., Marx, U., Mettetal, J. T., Pointon, A., Williams, D., Zimmermann, W.-H., & Newham, P. (2018). Application of Microphysiological Systems to Enhance Safety Assessment in Drug Discovery. *Annual Review of Pharmacology and Toxicology*, 58(1), 65–82. <https://doi.org/10.1146/annurev-pharmtox-010617-052722>

113. Faure, M., Guibert, E., Alves, S., Pain, B., Ramé, C., Dupont, J., Brillard, J. P., & Froment, P. (2016). The insulin sensitiser metformin regulates chicken Sertoli and germ cell populations. *Reproduction*, 151(5), 527–538. <https://doi.org/10.1530/REP-15-0565>
114. Fiegel, J., Ehrhardt, C., Schaefer, U. F., Lehr, C. M., & Hanes, J. (2003). Large porous particle impingement on lung epithelial cell monolayers—Toward improved particle characterization in the lung. *Pharmaceutical Research*, 20(5), 788–796. <https://doi.org/10.1023/A:1023441804464>
115. Filla, L. A., Sanders, K. L., Filla, R. T., & Edwards, J. L. (2016). Automated sample preparation in a microfluidic culture device for cellular metabolomics. *The Analyst*, 141(12), 3858–3865. <https://doi.org/10.1039/C6AN00237D>
116. Fitzgerald, K. A., O'Neill, L. A. J., Gearing, A. J. H., & Callard, R. E. (Eds.). (2001). *The Cytokine FactsBook and Webfacts*. Academic Press. <https://doi.org/10.1016/B978-0-12-155142-1.60002-8>
117. Florea, B. I., Cassara, M. L., Junginger, H. E., & Borchard, G. (2003). Drug transport and metabolism characteristics of the human airway epithelial cell line Calu-3. *Journal of Controlled Release*, 87(1–3), 131–138. [https://doi.org/10.1016/S0168-3659\(02\)00356-5](https://doi.org/10.1016/S0168-3659(02)00356-5)
118. Fogh, J., & Trempe, G. (1975). New Human Tumor Cell Lines. In J. Fogh (Ed.), *Human Tumor Cells in Vitro* (pp. 115–159). Springer US. https://doi.org/10.1007/978-1-4757-1647-4_5
119. Forbes, B. (1998). Transport characteristics of formoterol and salbutamol across a bronchial epithelial drug absorption model. *European Journal of Pharmaceutical Sciences*. https://scholar.google.com/scholar_lookup?title=Transport%20characteristics%20of%20formoterol%20and%20salbutamol%20across%20a%20bronchial%20epithelial%20drug%20absorption%20model&publication_year=1998&author=B.%20Forbes&author=A.B.%20Lansley
120. Forbes, B. (2000). Human airway epithelial cell lines for in vitro drug transport and metabolism studies. *Pharmaceutical Science & Technology Today*, 3(1), 18–27. [https://doi.org/10.1016/S1461-5347\(99\)00231-X](https://doi.org/10.1016/S1461-5347(99)00231-X)

121. Forbes, B., & Ehrhardt, C. (2005). Human respiratory epithelial cell culture for drug delivery applications. *European Journal of Pharmaceutics and Biopharmaceutics*, 60(2), 193–205. <https://doi.org/10.1016/j.ejpb.2005.02.010>
122. Forbes, B., O'Lone, R., Allen, P. P., Cahn, A., Clarke, C., Collinge, M., Dailey, L. A., Donnelly, L. E., Dybowski, J., Hassall, D., Hildebrand, D., Jones, R., Kilgour, J., Klapwijk, J., Maier, C. C., McGovern, T., Nikula, K., Parry, J. D., Reed, M. D., ... Wolfreys, A. (2014). Challenges for inhaled drug discovery and development: Induced alveolar macrophage responses. *Advanced Drug Delivery Reviews*, 71, 15–33. <https://doi.org/10.1016/j.addr.2014.02.001>
123. *Forum of International Respiratory Societies The Global Impact of Respiratory Disease*. (2012). <https://www.fi>
124. Foster, K. A., Avery, M. L., Yazdanian, M., & Audus, K. L. (2000). Characterization of the Calu-3 cell line as a tool to screen pulmonary drug delivery. *International Journal of Pharmaceutics*, 208(1–2), 1–11. [https://doi.org/10.1016/S0378-5173\(00\)00452-X](https://doi.org/10.1016/S0378-5173(00)00452-X)
125. Foster, K. A., Oster, C. G., Mayer, M. M., Avery, M. L., & Audus, K. L. (1998). Characterization of the A549 Cell Line as a Type II Pulmonary Epithelial Cell Model for Drug Metabolism. *Experimental Cell Research*, 243(2), 359–366. <https://doi.org/10.1006/EXCR.1998.4172>
126. Franks, T. J., Colby, T. V., Travis, W. D., Tuder, R. M., Reynolds, H. Y., Brody, A. R., Cardoso, W. V., Crystal, R. G., Drake, C. J., Engelhardt, J., Frid, M., Herzog, E., Mason, R., Phan, S. H., Randell, S. H., Rose, M. C., Stevens, T., Serge, J., Sunday, M. E., ... Williams, M. C. (2008). NHLBI Workshop Summaries Resident Cellular Components of the Human Lung Current Knowledge and Goals for Research on Cell Phenotyping and Function. *National Institutes of Health*, 19(20). <https://doi.org/10.1513/pats.200803-025HR>
127. Franzen, N., van Harten, W. H., Retèl, V. P., Loskill, P., van den Eijnden-van Raaij, J., & IJzerman, M. (2019). Impact of organ-on-a-chip technology on pharmaceutical R&D costs. *Drug Discovery Today*, 24(9), 1720–1724. <https://doi.org/10.1016/j.drudis.2019.06.003>

128. Frost, T. S., Jiang, L., Lynch, R. M., & Zohar, Y. (2019). Permeability of Epithelial/Endothelial Barriers in Transwells and Microfluidic Bilayer Devices. *Micromachines*, 10(8), 533. <https://doi.org/10.3390/mi10080533>
129. Fu, S., Thompson, C. L., Ali, A., Wang, W., Chapple, J. P., Mitchison, H. M., Beales, P. L., Wann, A. K. T., & Knight, M. M. (2019). Mechanical loading inhibits cartilage inflammatory signalling via an HDAC6 and IFT-dependent mechanism regulating primary cilia elongation. *Osteoarthritis and Cartilage*, 27(7), 1064–1074. <https://doi.org/10.1016/j.joca.2019.03.003>
130. Furubayashi, T., Inoue, D., Nishiyama, N., Tanaka, A., Yutani, R., Kimura, S., Katsumi, H., Yamamoto, A., & Sakane, T. (2020). Comparison of Various Cell Lines and Three-Dimensional Mucociliary Tissue Model Systems to Estimate Drug Permeability Using an In Vitro Transport Study to Predict Nasal Drug Absorption in Rats. *Pharmaceutics*, 12(1), Article 1. <https://doi.org/10.3390/pharmaceutics12010079>
131. Gallos, G., Townsend, E., Yim, P., Virag, L., Zhang, Y., Xu, D., Bacchetta, M., & Emala, C. W. (2013). Airway epithelium is a predominant source of endogenous airway GABA and contributes to relaxation of airway smooth muscle tone. *American Journal of Physiology. Lung Cellular and Molecular Physiology*, 304(3), L191-197. <https://doi.org/10.1152/ajplung.00274.2012>
132. Gao, D., Liu, H., Lin, J.-M., Wang, Y., & Jiang, Y. (2013). Characterization of drug permeability in Caco-2 monolayers by mass spectrometry on a membrane-based microfluidic device. *Lab on a Chip*, 13(5), 978–985. <https://doi.org/10.1039/C2LC41215B>
133. Gardiner, T. H., & Schanker, L. S. (1976). Active transport of phenol red by rat lung slices. *Journal of Pharmacology and Experimental Therapeutics*, 196(2), 455–462. Scopus.
134. Garg, U., & Zhang, Y. V. (2016). Mass spectrometry in clinical laboratory: Applications in therapeutic drug monitoring and toxicology. In *Methods in Molecular Biology* (Vol. 1383, pp. 1–10). Humana Press Inc. https://doi.org/10.1007/978-1-4939-3252-8_1

135. Gazdar, A. F., Gao, B., & Minna, J. D. (2010). Lung cancer cell lines: Useless artifacts or invaluable tools for medical science? *Lung Cancer*, 68(3), 309–318. <https://doi.org/10.1016/j.lungcan.2009.12.005>
136. Ge, Q., Moir, L. M., Black, J. L., Oliver, B. G., & Burgess, J. K. (2010). TGF β 1 induces IL-6 and inhibits IL-8 release in human bronchial epithelial cells: The role of Smad2/3. *Journal of Cellular Physiology*, 225(3), 846–854. <https://doi.org/10.1002/jcp.22295>
137. GeneCards. (2024). *TAGLN Gene—Transgelin*. <https://www.genecards.org/cgi-bin/carddisp.pl?gene=TAGLN>
138. *Gentamicin* (50 mg/mL). (2024). <https://www.thermofisher.com/order/catalog/product/15750060>
139. George, I., Vranic, S., Boland, S., Courtois, A., & Baeza-Squiban, A. (2015). Development of an in vitro model of human bronchial epithelial barrier to study nanoparticle translocation. *Toxicology in Vitro*, 29(1), 51–58. <https://doi.org/10.1016/j.tiv.2014.08.003>
140. Gilpin, S. E., Guyette, J. P., Gonzalez, G., Ren, X., Asara, J. M., Mathisen, D. J., Vacanti, J. P., & Ott, H. C. (2014). Perfusion decellularization of human and porcine lungs: Bringing the matrix to clinical scale. *Journal of Heart and Lung Transplantation*, 33(3), 298–308. <https://doi.org/10.1016/j.healun.2013.10.030>
141. Gioulekas, D., Papakosta, D., Vordoyianni, P., Baloti, H., & Vamvalis, C. (1996). A comparison of the clinical efficacy and patient acceptability of terbutaline Turbuhaler and salbutamol Rotahaler, in adult patients with asthma. *Respiratory Medicine*, 90(4), 205–209. [https://doi.org/10.1016/s0954-6111\(96\)90288-7](https://doi.org/10.1016/s0954-6111(96)90288-7)
142. Global Initiative for Asthma. (2022). *Global Strategy for Asthma Management and Prevention, 2022*. Global Initiative for Asthma - GINA. <https://ginasthma.org/gina-reports/>
143. Gnadt, M., Trammer, B., Freiwald, M., Kardziej, B., Bayliss, M. K., Edwards, C. D., Schmidt, M., Friedel, G., & Högger, P. (2012). Methacholine delays pulmonary absorption of inhaled β 2-agonists due to competition for organic cation/carnitine transporters.

- Pulmonary Pharmacology and Therapeutics*, 25(1), 124–134.
<https://doi.org/10.1016/j.pupt.2011.12.009>
144. Gosens, R., & Gross, N. (2018). The mode of action of anticholinergics in asthma. *The European Respiratory Journal*, 52(4), 1701247. <https://doi.org/10.1183/13993003.01247-2017>
145. Grainger, C. I., Greenwell, L. L., Lockley, D. J., Martin, G. P., & Forbes, B. (2006). Culture of Calu-3 cells at the air interface provides a representative model of the airway epithelial barrier. *Pharmaceutical Research*, 23(7), 1482–1490.
<https://doi.org/10.1007/s11095-006-0255-0>
146. Grau-Bartual, S., Al-Jumaily, A. M., Young, P. M., Traini, D., & Ghadiri, M. (2020). Effect of continuous positive airway pressure treatment on permeability, inflammation and mucus production of human epithelial cells. *ERJ Open Research*, 6(2), 00327–02019.
<https://doi.org/10.1183/23120541.00327-2019>
147. Graziano, M. P., Moxham, C. P., & Malbon, C. C. (1985). Purified rat hepatic β 2-adrenergic receptor. Structural similarities to the rat fat cell β 1-adrenergic receptor. *Journal of Biological Chemistry*, 260(12), 7665–7674. Scopus.
148. Green, J. A., & Yamada, K. M. (2007). Three-dimensional microenvironments modulate fibroblast signaling responses. *Advanced Drug Delivery Reviews*, 59(13), 1293–1298. <https://doi.org/10.1016/j.addr.2007.08.005>
149. Griffith, L. G., & Swartz, M. A. (2006). Capturing complex 3D tissue physiology in vitro. *Nature Reviews Molecular Cell Biology*, 7(3), 211–224. <https://doi.org/10.1038/nrm1858>
150. Güney, T. G., Herranz, A. M., Mumby, S., Dunlop, I. E., & Adcock, I. M. (2021). Epithelial-stromal cell interactions and extracellular matrix mechanics drive the formation of airway-mimetic tubular morphology in lung organoids. *iScience*, 24(9), 103061.
<https://doi.org/10.1016/j.isci.2021.103061>
151. Gunst, S. J., & Zhang, W. (2008). Actin cytoskeletal dynamics in smooth muscle: A new paradigm for the regulation of smooth muscle contraction. *American Journal of*

- Physiology-Cell Physiology*, 295(3), C576–C587.
<https://doi.org/10.1152/ajpcell.00253.2008>
152. Haarst, A., McGarvey, L., & Paglialunga, S. (2019). Review of Drug Development Guidance to Treat Chronic Obstructive Pulmonary Disease: <scp>US</scp> and <scp>EU</scp> Perspectives. *Clinical Pharmacology & Therapeutics*, 106(6), 1222–1235.
<https://doi.org/10.1002/cpt.1540>
153. Hacker, B. C., & Rafat, M. (2020). Organoids as Complex In Vitro Models for Studying Radiation-Induced Cell Recruitment. *Cellular and Molecular Bioengineering*, 13(4), 341–357. <https://doi.org/10.1007/s12195-020-00625-0>
154. Hadavi, D., Tosheva, I., Siegel, T. P., Cuypers, E., & Honing, M. (2023). Technological advances for analyzing the content of organ-on-a-chip by mass spectrometry. *Frontiers in Bioengineering and Biotechnology*, 11, 1197760.
<https://doi.org/10.3389/fbioe.2023.1197760>
155. Haghi, M., Hittinger, M., Zeng, Q., Oliver, B., Traini, D., Young, P. M., Huwer, H., Schneider-Daum, N., & Lehr, C.-M. (2015). Mono- and Cocultures of Bronchial and Alveolar Epithelial Cells Respond Differently to Proinflammatory Stimuli and Their Modulation by Salbutamol and Budesonide. *Molecular Pharmaceutics*, 12(8), 2625–2632.
<https://doi.org/10.1021/acs.molpharmaceut.5b00124>
156. Haghi, M., Traini, D., Bebawy, M., & Young, P. M. (2012a). Deposition, diffusion and transport mechanism of dry powder microparticulate salbutamol, at the respiratory epithelia. *Molecular Pharmaceutics*, 9(6), 1717–1726.
<https://doi.org/10.1021/mp200620m>
157. Haghi, M., Traini, D., Bebawy, M., & Young, P. M. (2012b). Deposition, diffusion and transport mechanism of dry powder microparticulate salbutamol, at the respiratory epithelia. *Molecular Pharmaceutics*, 9(6), 1717–1726.
https://doi.org/10.1021/MP200620M/ASSET/IMAGES/LARGE/MP-2011-00620M_0013.JPEG

158. Haghi, M., Traini, D., Postma, D. S., Bebawy, M., & Young, P. M. (2013). Fluticasone uptake across Calu-3 cells is mediated by salmeterol when deposited as a combination powder inhaler. *Respirology*, 18(8), 1197–1201. <https://doi.org/10.1111/resp.12146>
159. Haghi, M., Windhab, N., Hartwig, B., Young, P. M., & Traini, D. (2019). Human Stimulus Factor Is a Promising Peptide for Delivery of Therapeutics. *Journal of Pharmaceutical Sciences*, 108(4), 1401–1403. <https://doi.org/10.1016/j.xphs.2018.11.017>
160. Halaidych, O. V., Cochrane, A., van den Hil, F. E., Mummery, C. L., & Orlova, V. V. (2019). Quantitative Analysis of Intracellular Ca²⁺ Release and Contraction in hiPSC-Derived Vascular Smooth Muscle Cells. *Stem Cell Reports*, 12(4), 647–656. <https://doi.org/10.1016/j.stemcr.2019.02.003>
161. Hall, R. L., MILLER, R. J., PEATFIELD, A. C., RICHARDSON, P. S., WILLIAMS, I., & LAMPERT, I. (1980). A colorimetric assay for mucous glycoproteins using Alcian Blue. *Biochemical Society Transactions*, 8(1), 72. <https://doi.org/10.1042/bst0080072>
162. Hamilton, K. O., Topp, E., Makagiansar, I., Siahaan, T., Yazdanian, M., & Audus, K. L. (2001). Multidrug resistance-associated protein-1 functional activity in Calu-3 cells. *Journal of Pharmacology and Experimental Therapeutics*, 298(3), 1199–1205. Scopus.
163. Han, C., Labuz, J. M., Takayama, S., & Park, J. (2014). Organs-on-a-Chip. In *Tissue Engineering: Second Edition* (pp. 717–746). Elsevier Inc. <https://doi.org/10.1016/B978-0-12-420145-3.00020-1>
164. Harris, Daniel C. (2010). *Quantitative Chemical Analysis* (8th ed.). W. H. Freeman and Company.
165. Harrison, R. K. (2016). Phase II and phase III failures: 2013–2015. *Nature Reviews Drug Discovery*, 15(12), 817–818. <https://doi.org/10.1038/nrd.2016.184>
166. Hasegawa, I., Niisato, N., Iwasaki, Y., & Marunaka, Y. (2006). Ambroxol-induced modification of ion transport in human airway Calu-3 epithelia. *Biochemical and Biophysical Research Communications*, 343(2), 475–482. <https://doi.org/10.1016/J.BBRC.2006.03.009>

167. Heijink, I. H., Brandenburg, S. M., Noordhoek, J. A., Postma, D. S., Slebos, D.-J., & Van Oosterhout, A. J. M. (2010). *Characterisation of cell adhesion in airway epithelial cell types using electric cell-substrate impedance sensing*. <https://doi.org/10.1183/09031936.00065809>
168. Herrera, J., Henke, C. A., & Bitterman, P. B. (2018). Extracellular matrix as a driver of progressive fibrosis. *The Journal of Clinical Investigation*, 128(1), 45–53. <https://doi.org/10.1172/JCI93557>
169. Hickey, A. J., & da Rocha, S. R. (2019). Pharmaceutical Inhalation Aerosol Technology. In *Pharmaceutical Inhalation Aerosol Technology*. CRC Press. <https://doi.org/10.1201/9780429055201>
170. Hickman, J. A., Graeser, R., de Hoogt, R., Vidic, S., Brito, C., Gutekunst, M., van der Kuip, H., & Imi Prelect consortium. (2014). Three-dimensional models of cancer for pharmacology and cancer cell biology: Capturing tumor complexity in vitro/ex vivo. *Biotechnology Journal*, 9(9), 1115–1128. <https://doi.org/10.1002/biot.201300492>
171. Ho, C., Lam, C., Chan, M., Cheung, R., Law, L., Lit, L., Ng, K., Suen, M., & Tai, H. (2003). Electrospray Ionisation Mass Spectrometry: Principles and Clinical Applications. *The Clinical Biochemist Reviews*, 24(1), 3–12.
172. Hoeng, J. (Ed.). (2019). Organ-on-a-chip. In *Organ-on-a-chip*. Elsevier. <https://www.sciencedirect.com/book/9780128172025/organ-on-a-chip?via=ihub=>
173. Hogan, B. L. M., Barkauskas, C. E., Chapman, H. A., Epstein, J. A., Jain, R., Hsia, C. C. W., Niklason, L., Calle, E., Le, A., Randell, S. H., Rock, J., Snitow, M., Krummel, M., Stripp, B. R., Vu, T., White, E. S., Whitsett, J. A., & Morrissey, E. E. (2014). Repair and regeneration of the respiratory system: Complexity, plasticity, and mechanisms of lung stem cell function. *Cell Stem Cell*, 15(2), 123–138. <https://doi.org/10.1016/j.stem.2014.07.012>
174. Horstmann, J. C., Thorn, C. R., Carius, P., Graef, F., Murgia, X., de Souza Carvalho-Wodarz, C., & Lehr, C.-M. (2021). A Custom-Made Device for Reproducibly Depositing

- Pre-metered Doses of Nebulized Drugs on Pulmonary Cells in vitro. *Frontiers in Bioengineering and Biotechnology*, 9, 643491. <https://doi.org/10.3389/fbioe.2021.643491>
175. Horvath, G., Schmid, N., Fragoso, M. A., Schmid, A., Conner, G. E., Salathe, M., & Wanner, A. (2007). Epithelial Organic Cation Transporters Ensure pH-Dependent Drug Absorption in the Airway. *American Journal of Respiratory Cell and Molecular Biology*, 36(1), 53. <https://doi.org/10.1165/rcmb.2006-0230OC>
176. HU Medical Review Board. (2015). *What Are Different Types of Asthma and Are They Common?* Asthma.Net. <https://asthma.net/types>
177. Huang, G., Li, F., Zhao, X., Ma, Y., Li, Y., Lin, M., Jin, G., Lu, T. J., Genin, G. M., & Xu, F. (2017). Functional and Biomimetic Materials for Engineering of the Three-Dimensional Cell Microenvironment. *Chemical Reviews*, 117(20), 12764–12850. <https://doi.org/10.1021/acs.chemrev.7b00094>
178. Huang, J., Deng, Y., Tin, M. S., Lok, V., Ngai, C. H., Zhang, L., Lucero-Prisno, D. E., Xu, W., Zheng, Z.-J., Elcarte, E., Withers, M., & Wong, M. C. S. (2022). Distribution, Risk Factors, and Temporal Trends for Lung Cancer Incidence and Mortality: A Global Analysis. *Chest*, 161(4), 1101–1111. <https://doi.org/10.1016/j.chest.2021.12.655>
179. Huang, S., Wiszniewski, L., Derouette, J.-P., & Constant, S. (2009). *In vitro* organ culture models of asthma. *Drug Discovery Today: Disease Models*, 6(4), 137–144. <https://doi.org/10.1016/j.ddmod.2009.08.002>
180. Hubatsch, I. (2007). *Determination of drug permeability and prediction of drug absorption in Caco-2 monolayers* | *Nature Protocols*. <https://doi.org/10.1038/nprot.2007.303>
181. Huh, D. (Dan). (2015). A Human Breathing Lung-on-a-Chip. *Annals of the American Thoracic Society*, 12(Supplement 1), S42–S44. <https://doi.org/10.1513/AnnalsATS.201410-442MG>
182. Huh, D., Matthews, B. D., Mammoto, A., Montoya-Zavala, M., Hsin, H. Y., & Ingber, D. E. (2010). Reconstituting Organ-Level Lung Functions on a Chip. *Science*, 328(5986), 1662–1668. <https://doi.org/10.1126/science.1188302>

183. Huh, D., Matthews, B. D., Mammoto, A., Montoya-Zavala, M., Yuan Hsin, H., & Ingber, D. E. (2010). Reconstituting organ-level lung functions on a chip. *Science*, 328(5986), 1662–1668. <https://doi.org/10.1126/science.1188302>
184. Humayun, M., Chow, C. W., & Young, E. W. K. (2018). Microfluidic lung airway-on-a-chip with arrayable suspended gels for studying epithelial and smooth muscle cell interactions. *Lab on a Chip*, 18(9), 1298–1309. <https://doi.org/10.1039/c7lc01357d>
185. Hwang, T. J., Carpenter, D., Lauffenburger, J. C., Wang, B., Franklin, J. M., & Kesselheim, A. S. (2016). Failure of investigational drugs in late-stage clinical development and publication of trial results. *JAMA Internal Medicine*, 176(12), 1826–1833. <https://doi.org/10.1001/jamainternmed.2016.6008>
186. *Immortalized Human Bronchial Smooth Muscle Cells | Applied Biological Materials Inc.* (2024). ABM. <https://www.abmgood.com/immortalized-human-bronchial-smooth-muscle-cells.html>
187. Inoue, D., Furubayashi, T., Tanaka, A., Sakane, T., & Sugano, K. (2020). Quantitative estimation of drug permeation through nasal mucosa using in vitro membrane permeability across Calu-3 cell layers for predicting in vivo bioavailability after intranasal administration to rats. *European Journal of Pharmaceutics and Biopharmaceutics*, 149, 145–153. Scopus. <https://doi.org/10.1016/j.ejpb.2020.02.004>
188. Introduction to mass spectrometry: Instrumentation, applications and strategies for data interpretation. (2008). *Choice Reviews Online*, 45(08), 45-4396-45–4396. <https://doi.org/10.5860/CHOICE.45-4396>
189. Ishida, S. (2018). Organs-on-a-chip: Current applications and consideration points for in vitro ADME-Tox studies. *Drug Metabolism and Pharmacokinetics*, 33(1), 49–54. <https://doi.org/10.1016/j.dmpk.2018.01.003>
190. Jaalouk, D. E., & Lammerding, J. (2009). Mechanotransduction gone awry. *Nature Reviews. Molecular Cell Biology*, 10(1), 63–73. <https://doi.org/10.1038/nrm2597>
191. Jain, A., Barrile, R., van der Meer, A., Mammoto, A., Mammoto, T., Ceunynck, K., Aisiku, O., Otieno, M., Loudon, C., Hamilton, G., Flaumenhaft, R., & Ingber, D. (2018).

- Primary Human Lung Alveolus-on-a-chip Model of Intravascular Thrombosis for Assessment of Therapeutics. *Clinical Pharmacology & Therapeutics*, 103(2), 332–340. <https://doi.org/10.1002/cpt.742>
192. James, A., & Carroll, N. (2000). Airway smooth muscle in health and disease; methods of measurement and relation to function. *European Respiratory Journal*, 15(4), 782–789. Scopus. <https://doi.org/10.1034/j.1399-3003.2000.15d25.x>
193. Ji, X., Sheng, Y., Guan, Y., Li, Y., Xu, Y., & Tang, L. (2022). Evaluation of Calu-3 cell lines as an in vitro model to study the inhalation toxicity of flavoring extracts. *Toxicology Mechanisms and Methods*, 32(3), 171–179. <https://doi.org/10.1080/15376516.2021.1977880>
194. Jiang, B., Zheng, W., Zhang, W., & Jiang, X. (2014). Organs on microfluidic chips: A mini review. *Science China Chemistry*, 57(3), 356–364. <https://doi.org/10.1007/s11426-013-4971-0>
195. Jiang, H., Cao, H., Zhang, Y., & Fast, D. M. (2012). Systematic evaluation of supported liquid extraction in reducing matrix effect and improving extraction efficiency in LC–MS/MS based bioanalysis for 10 model pharmaceutical compounds. *Journal of Chromatography B*, 891–892, 71–80. <https://doi.org/10.1016/j.jchromb.2012.02.031>
196. Jo, J., Xiao, Y., Sun, A. X., Cukuroglu, E., Tran, H.-D., Göke, J., Tan, Z. Y., Saw, T. Y., Tan, C.-P., Lokman, H., Lee, Y., Kim, D., Ko, H. S., Kim, S.-O., Park, J. H., Cho, N.-J., Hyde, T. M., Kleinman, J. E., Shin, J. H., ... Ng, H. H. (2016). Midbrain-like organoids from human pluripotent stem cells contain functional dopaminergic and neuromelanin producing neurons. *Cell Stem Cell*, 19(2), 248–257. <https://doi.org/10.1016/j.stem.2016.07.005>
197. Joint Formulary Committee. (2024, February 8). *British National Formulary (online)*. British National Formulary (Online). <https://www.medicinescomplete.com>
198. Junaid, A., Mashaghi, A., Hankemeier, T., & Vulto, P. (2017). An end-user perspective on Organ-on-a-Chip: Assays and usability aspects. *Current Opinion in Biomedical Engineering*, 1, 15–22. <https://doi.org/10.1016/j.cobme.2017.02.002>

199. Kapałczyńska, M., Kolenda, T., Przybyła, W., Zajączkowska, M., Teresiak, A., Filas, V., Ibbs, M., Bliźniak, R., Łuczewski, Ł., & Lamperska, K. (2016). 2D and 3D cell cultures – a comparison of different types of cancer cell cultures. *Archives of Medical Science*, 14(4), 910–919. <https://doi.org/10.5114/aoms.2016.63743>
200. Kasendra, M., Tovaglieri, A., Sontheimer-Phelps, A., Jalili-Firoozinezhad, S., Bein, A., Chalkiadaki, A., Scholl, W., Zhang, C., Rickner, H., Richmond, C. A., Li, H., Breault, D. T., & Ingber, D. E. (2018). Development of a primary human Small Intestine-on-a-Chip using biopsy-derived organoids. *Scientific Reports*, 8(1). <https://doi.org/10.1038/s41598-018-21201-7>
201. Kasper, J., Hermanns, M. I., Bantz, C., Koshkina, O., Lang, T., Maskos, M., Pohl, C., Unger, R. E., & Kirkpatrick, C. J. (2013). Interactions of silica nanoparticles with lung epithelial cells and the association to flotillins. *Archives of Toxicology*, 87(6), 1053–1065. <https://doi.org/10.1007/s00204-012-0876-5>
202. Kaur, G., & Dufour, J. M. (2012). Cell lines. *Spermatogenesis*, 2(1), 1–5. <https://doi.org/10.4161/spmg.19885>
203. Kerschner, J. L., Paranjapye, A., & Harris, A. (2023). Cellular heterogeneity in the 16HBE14o – airway epithelial line impacts biological readouts. *Physiological Reports*, 11(11), e15700. <https://doi.org/10.14814/phy2.15700>
204. Kim, D., Maharjan, S., Kim, J., Park, S., Park, J.-A., Park, B. K., Lee, Y., & Kwon, H.-J. (2021). MUC1-C influences cell survival in lung adenocarcinoma Calu-3 cells after SARS-CoV-2 infection. *BMB Reports*, 54(8), 425–430. <https://doi.org/10.5483/BMBRep.2021.54.8.018>
205. Kim, S.-H., Lee, S.-H., Lee, J.-E., Park, S. J., Kim, K., Kim, I. S., Lee, Y.-S., Hwang, N. S., & Kim, B.-G. (2018). Tissue adhesive, rapid forming, and sprayable ECM hydrogel via recombinant tyrosinase crosslinking. *Biomaterials*, 178, 401–412. <https://doi.org/10.1016/j.biomaterials.2018.04.057>
206. Kirkstall. (2024). *Quasi Vivo® for organ on a chip | The researchers choice for organ on a chip cell culture*. Kirkstall Ltd. <https://kirkstall.com/>

207. Klein, S. G., Hennen, J., Serchi, T., Blömeke, B., & Gutleb, A. C. (2011). Potential of coculture in vitro models to study inflammatory and sensitizing effects of particles on the lung. *Toxicology in Vitro*, 25(8), 1516–1534. <https://doi.org/10.1016/j.tiv.2011.09.006>
208. Kleinman, H. K., & Martin, G. R. (2005). Matrigel: Basement membrane matrix with biological activity. *Seminars in Cancer Biology*, 15(5), 378–386. <https://doi.org/10.1016/j.semcancer.2005.05.004>
209. Koepsell, H., Lips, K., & Volk, C. (2007). Polyspecific organic cation transporters: Structure, function, physiological roles, and biopharmaceutical implications. *Pharmaceutical Research*, 24(7), 1227–1251. Scopus. <https://doi.org/10.1007/s11095-007-9254-z>
210. Kola, I., & Landis, J. (2004). Can the pharmaceutical industry reduce attrition rates? *Nature Reviews Drug Discovery*, 3(8), 711–715. <https://doi.org/10.1038/nrd1470>
211. Kratochvil, M. J., Seymour, A. J., Li, T. L., Paşca, S. P., Kuo, C. J., & Heilshorn, S. C. (2019). Engineered materials for organoid systems. *Nature Reviews. Materials*, 4(9), 606–622. <https://doi.org/10.1038/s41578-019-0129-9>
212. Kreft, M. E., Jerman, U. D., Lasič, E., Hevir-Kene, N., Rižner, T. L., Peternel, L., & Kristan, K. (2015). The characterization of the human cell line Calu-3 under different culture conditions and its use as an optimized in vitro model to investigate bronchial epithelial function. *European Journal of Pharmaceutical Sciences*, 69, 1–9.
213. Kumar, P., Nagarajan, A., & Uchil, P. D. (2018). Analysis of Cell Viability by the Lactate Dehydrogenase Assay. *Cold Spring Harbor Protocols*, 2018(6). <https://doi.org/10.1101/pdb.prot095497>
214. Kumar, V., Sethi, B., Yanez, E., Leung, D. H., Ghanwatkar, Y. Y., Cheong, J., Tso, J., Narang, A. S., Nagapudi, K., & Mahato, R. I. (2022). Effect of magnesium stearate surface coating method on the aerosol performance and permeability of micronized fluticasone propionate. *International Journal of Pharmaceutics*, 615, 121470. <https://doi.org/10.1016/j.ijpharm.2022.121470>

215. Kuwano, K., Bosken, C. H., Pare, P. D., Bai, T. R., Wiggs, B. R., & Hogg, J. C. (1993). Small airways dimensions in asthma and in chronic obstructive pulmonary disease. *American Review of Respiratory Disease*, 148(5), 1220–1225. Scopus. <https://doi.org/10.1164/ajrccm/148.5.1220>
216. Labiris, N. R., & Dolovich, M. B. (2003). Pulmonary drug delivery. Part I: Physiological factors affecting therapeutic effectiveness of aerosolized medications. *British Journal of Clinical Pharmacology*, 56(6), 588–599. <https://doi.org/10.1046/j.1365-2125.2003.01892.x>
217. Lacroix, G., Koch, W., Ritter, D., Gutleb, A. C., Larsen, S. T., Loret, T., Zanetti, F., Constant, S., Chortarea, S., Rothen-Rutishauser, B., Hiemstra, P. S., Frejafon, E., Hubert, P., Gribaldo, L., Kearns, P., Aublant, J. M., Diabaté, S., Weiss, C., De Groot, A., & Kooter, I. (2018). Air-Liquid Interface in Vitro Models for Respiratory Toxicology Research: Consensus Workshop and Recommendations. *Applied In Vitro Toxicology*, 4(2), 91–106. <https://doi.org/10.1089/aivt.2017.0034>
218. Lahaie, M., Mess, J.-N., Furtado, M., & Garofolo, F. (2010). Elimination of LC–MS/MS matrix effect due to phospholipids using specific solid-phase extraction elution conditions. *Bioanalysis*, 2(6), 1011–1021. <https://doi.org/10.4155/bio.10.65>
219. Lan, B., Mitchel, J. A., O'Sullivan, M. J., Park, C. Y., Kim, J. H., Cole, W. C., Butler, J. P., & Park, J.-A. (2018a). Airway epithelial compression promotes airway smooth muscle proliferation and contraction. *American Journal of Physiology - Lung Cellular and Molecular Physiology*, 315(5), L645–L652. <https://doi.org/10.1152/ajplung.00261.2018>
220. Lan, B., Mitchel, J. A., O'Sullivan, M. J., Park, C. Y., Kim, J. H., Cole, W. C., Butler, J. P., & Park, J.-A. (2018b). Airway epithelial compression promotes airway smooth muscle proliferation and contraction. *American Journal of Physiology. Lung Cellular and Molecular Physiology*, 315(5), L645–L652. <https://doi.org/10.1152/ajplung.00261.2018>
221. Lancaster, M. A., & Knoblich, J. A. (2014). Organogenesis in a dish: Modeling development and disease using organoid technologies. *Science*, 345(6194), 1247125. <https://doi.org/10.1126/science.1247125>

222. Lansley, A. B., Lee, D. F., & Lethem, M. I. (2019). *A comparison of UCN3T and Calu-3 cells as mucus-secreting drug absorption models of the airways*. 15(1), 43–49.
223. Latif, N., Sarathchandra, P., Chester, A. H., & Yacoub, M. H. (2015). Expression of smooth muscle cell markers and co-activators in calcified aortic valves. *European Heart Journal*, 36(21), 1335–1345. <https://doi.org/10.1093/eurheartj/ehv547>
224. Lee, H., Kim, D. S., Ha, S. K., Choi, I., Lee, J. M., & Sung, J. H. (2017). A pumpless multi-organ-on-a-chip (MOC) combined with a pharmacokinetic-pharmacodynamic (PK-PD) model. *Biotechnology and Bioengineering*, 114(2), 432–443. <https://doi.org/10.1002/bit.26087>
225. Lee, B. ill, Park, M. H., Heo, S. C., Park, Y., Shin, S. H., Byeon, J. J., Kim, J. H., & Shin, Y. G. (2018). Quantification and application of a liquid chromatography–tandem mass spectrometric method for the determination of WKYVM peptide in rat using solid-phase extraction. *Biomedical Chromatography*, 32(3). <https://doi.org/10.1002/bmc.4107>
226. Lee, J., Boescke, R., Tang, P.-C., Hartman, B. H., Heller, S., & Koehler, K. R. (2018). Hair follicle development in mouse pluripotent stem cell-derived skin organoids. *Cell Reports*, 22(1), 242–254. <https://doi.org/10.1016/j.celrep.2017.12.007>
227. Lee, J. W., Krasnodembskaya, A., McKenna, D. H., Song, Y., Abbott, J., & Matthay, M. A. (2013). Therapeutic effects of human mesenchymal stem cells in ex vivo human lungs injured with live bacteria. *American Journal of Respiratory and Critical Care Medicine*, 187(7), 751–760. <https://doi.org/10.1164/rccm.201206-0990OC>
228. Lee, K.-J., Johnson, N., Castelo, J., Sinko, P. J., Grass, G., Holme, K., & Lee, Y.-H. (2005). Effect of experimental pH on the in vitro permeability in intact rabbit intestines and Caco-2 monolayer. *European Journal of Pharmaceutical Sciences*, 25(2), 193–200. <https://doi.org/10.1016/j.ejps.2005.02.012>
229. Lee, S. H., & Sung, J. H. (2018). Organ-on-a-Chip Technology for Reproducing Multiorgan Physiology. *Advanced Healthcare Materials*, 7(2), 1700419. <https://doi.org/10.1002/adhm.201700419>

230. Lenz, A. G., Karg, E., Brendel, E., Hinze-Heyn, H., Maier, K. L., Eickelberg, O., Stoeger, T., & Schmid, O. (2013). Inflammatory and oxidative stress responses of an alveolar epithelial cell line to airborne zinc oxide nanoparticles at the air-liquid interface: A comparison with conventional, submerged cell-culture conditions. *BioMed Research International*, 2013. <https://doi.org/10.1155/2013/652632>
231. Leong, D. T., & Ng, K. W. (2014). Probing the relevance of 3D cancer models in nanomedicine research. *Advanced Drug Delivery Reviews*, 79–80, 95–106. <https://doi.org/10.1016/j.addr.2014.06.007>
232. Levitzky, M. G. (2018). *Pulmonary Physiology* (9th ed.). McGraw-Hill Education.
233. Liao, M. M., Ginde, A. A., Clark, S., & Camargo, C. A. (2010). Salmeterol Use and Risk of Admission among Emergency Department Patients with Acute Asthma. *Annals of Allergy, Asthma & Immunology: Official Publication of the American College of Allergy, Asthma, & Immunology*, 104(6), 478–484. <https://doi.org/10.1016/j.anai.2010.04.014>
234. Lin, A., Sved Skottvoll, F., Rayner, S., Pedersen-Bjergaard, S., Sullivan, G., Krauss, S., Ray Wilson, S., & Harrison, S. (2020). 3D cell culture models and organ-on-a-chip: Meet separation science and mass spectrometry. *ELECTROPHORESIS*, 41(1–2), 56–64. <https://doi.org/10.1002/elps.201900170>
235. Lindsay, D. A., Russell, N. L., Thompson, J. E., Warnock, T. H., Shellshear, I. D., & Buchanan, P. R. (1994). A multicentre comparison of the efficacy of terbutaline Turbuhaler and salbutamol pressurized metered dose inhaler in hot, humid regions. *The European Respiratory Journal*, 7(2), 342–345. <https://doi.org/10.1183/09031936.94.07020342>
236. Lipworth, B. J. (1996). Pharmacokinetics of inhaled drugs. *British Journal of Clinical Pharmacology*, 42(6), 697–705. <https://doi.org/10.1046/j.1365-2125.1996.00493.x>
237. Lipworth, B. J. (2014). Emerging role of long acting muscarinic antagonists for asthma. *British Journal of Clinical Pharmacology*, 77(1), 55–62. <https://doi.org/10.1111/bcp.12123>
238. Liu, G., Philp, A. M., Corte, T., Travis, M. A., Schilter, H., Hansbro, N. G., Burns, C. J., Eapen, M. S., Sohal, S. S., Burgess, J. K., & Hansbro, P. M. (2021). Therapeutic targets

- in lung tissue remodelling and fibrosis. *Pharmacology & Therapeutics*, 225, 107839.
<https://doi.org/10.1016/j.pharmthera.2021.107839>
239. Lodish, H., Berk, A., Matsudaira, P., Kaiser, C. A., & Krieger, M. (2016). *Molecular Cell Biology*. W. H. Freeman and Company.
240. Lonza. (2024). *BSMC*. Lonza. https://bioscience.lonza.com/lonza_bs/GB/en/Primary-and-Stem-Cells/p/000000000000185131/BSMC-%E2%80%93Human-Bronchial-Smooth-Muscle-Cells
241. Low, L. A., & Tagle, D. A. (2017). Microphysiological Systems (“Organs-on-Chips”) for Drug Efficacy and Toxicity Testing. *Clinical and Translational Science*, 10(4), 237–239.
<https://doi.org/10.1111/cts.12444>
242. Lumb, A. B. (2016). *Nunn’s Applied Respiratory Physiology EBook: Nunn’s Applied Respiratory Physiology EBook*. Elsevier.
<http://ebookcentral.proquest.com/lib/herts/detail.action?docID=5507971>
243. Lundback, B., Rawlinson, D. W., & Palmer, J. B. (1993). Twelve month comparison of salmeterol and salbutamol as dry powder formulations in asthmatic patients. European Study Group. *Thorax*, 48(2), 148–153. <https://doi.org/10.1136/thx.48.2.148>
244. Lynch, K. L. (2017). Toxicology: Liquid chromatography mass spectrometry. In *Mass Spectrometry for the Clinical Laboratory* (pp. 109–130). Elsevier.
<https://doi.org/10.1016/B978-0-12-800871-3.00006-7>
245. Mack, C. P. (2011). Signaling Mechanisms That Regulate Smooth Muscle Cell Differentiation. *Arteriosclerosis, Thrombosis, and Vascular Biology*, 31(7), 1495–1505.
<https://doi.org/10.1161/ATVBAHA.110.221135>
246. MacNee, W. (2005). Pathogenesis of chronic obstructive pulmonary disease. *Proceedings of the American Thoracic Society*, 2(4), 258–266; discussion 290-291.
<https://doi.org/10.1513/pats.200504-045SR>
247. Madara, J. L. (1998). Regulation of the movement of solutes across tight junctions. *Annual Review of Physiology*, 60, 143–159.
<https://doi.org/10.1146/annurev.physiol.60.1.143>

248. Madiedo-Podvrsan, S., Sebillet, L., Martinez, T., Bacari, S., Zhu, F., Cattelin, M., Leclerc, E., Merlier, F., Jellali, R., Lacroix, G., & Vayssade, M. (2023). Development of a lung-liver *in vitro* coculture model for inhalation-like toxicity assessment. *Toxicology in Vitro*, 92, 105641. <https://doi.org/10.1016/j.tiv.2023.105641>
249. Madlova, M., Bosquillon, C., Asker, D., Dolezal, P., & Forbes, B. (2010). In-vitro respiratory drug absorption models possess nominal functional P-glycoprotein activity. *Journal of Pharmacy and Pharmacology*, 61(3), 293–301. <https://doi.org/10.1211/jpp.61.03.0003>
250. Malavia, N. K., Raub, C. B., Mahon, S. B., Brenner, M., Panettieri, R. A., & George, S. C. (2009). Airway Epithelium Stimulates Smooth Muscle Proliferation. *American Journal of Respiratory Cell and Molecular Biology*, 41(3), 297. <https://doi.org/10.1165/RCMB.2008-0358OC>
251. Mamlouk, M., Young, P. M., Bebawy, M., Haghi, M., Mamlouk, S., Mulay, V., & Traini, D. (2013). Salbutamol sulfate absorption across calu-3 bronchial epithelia cell monolayer is inhibited in the presence of common anionic NSAIDs. *Journal of Asthma*, 50(4), 334–341. Scopus. <https://doi.org/10.3109/02770903.2013.773518>
252. Maqusood, M. (2016). A Study of Prescription Pattern in the Management of COPD in a Tertiary Care Hospital. *Annals of International Medical and Dental Research*. <https://doi.org/10.21276/aimdr.2016.2.3.39>
253. Marinković, A., Mih, J. D., Park, J.-A., Liu, F., & Tschumperlin, D. J. (2012). Improved throughput traction microscopy reveals pivotal role for matrix stiffness in fibroblast contractility and TGF- β responsiveness. *American Journal of Physiology - Lung Cellular and Molecular Physiology*, 303(3), L169–L180. <https://doi.org/10.1152/ajplung.00108.2012>
254. Markowska, M., Oberle, R., Juzwin, S., Hsu, C.-P., Gryszkiewicz, M., & Streeter, A. J. (2001). Optimizing Caco-2 cell monolayers to increase throughput in drug intestinal absorption analysis. *Journal of Pharmacological and Toxicological Methods*, 46(1), 51–55. [https://doi.org/10.1016/S1056-8719\(01\)00161-7](https://doi.org/10.1016/S1056-8719(01)00161-7)

255. Marrazzo, P., Maccari, S., Taddei, A., Bevan, L., Telford, J., Soriani, M., & Pezzicoli, A. (2016). 3D Reconstruction of the Human Airway Mucosa In Vitro as an Experimental Model to Study NTHi Infections. *PLOS ONE*, 11(4), e0153985. <https://doi.org/10.1371/journal.pone.0153985>
256. Maschmeyer, I., Hasenberg, T., Jaenicke, A., Lindner, M., Lorenz, A. K., Zech, J., Garbe, L. A., Sonntag, F., Hayden, P., Ayehunie, S., Lauster, R., Marx, U., & Materne, E. M. (2015). Chip-based human liver-intestine and liver-skin co-cultures—A first step toward systemic repeated dose substance testing in vitro. *European Journal of Pharmaceutics and Biopharmaceutics*, 95(Pt A), 77–87. <https://doi.org/10.1016/j.ejpb.2015.03.002>
257. Maschmeyer, I., Lorenz, A. K., Schimek, K., Hasenberg, T., Ramme, A. P., Hübner, J., Lindner, M., Drewell, C., Bauer, S., Thomas, A., Sambo, N. S., Sonntag, F., Lauster, R., & Marx, U. (2015). A four-organ-chip for interconnected long-term co-culture of human intestine, liver, skin and kidney equivalents. *Lab on a Chip*, 15(12), 2688–2699. <https://doi.org/10.1039/C5LC00392J>
258. Matera, M. G., Page, C. P., Calzetta, L., Rogliani, P., & Cazzola, M. (2020). Pharmacology and Therapeutics of Bronchodilators Revisited. *Pharmacological Reviews*, 72(1), 218–252. <https://doi.org/10.1124/pr.119.018150>
259. Mazzoleni, G., Di Lorenzo, D., & Steimberg, N. (2009). Modelling tissues in 3D: The next future of pharmaco-toxicology and food research? *Genes and Nutrition*, 4(1), 13–22. <https://doi.org/10.1007/s12263-008-0107-0>
260. McAuley, D. F., Curley, G. F., Hamid, U. I., Laffey, J. G., Abbott, J., McKenna, D. H., Fang, X., Matthay, M. A., & Lee, J. W. (2014). Clinical grade allogeneic human mesenchymal stem cells restore alveolar fluid clearance in human lungs rejected for transplantation. *American Journal of Physiology - Lung Cellular and Molecular Physiology*, 306(9), L809. <https://doi.org/10.1152/ajplung.00358.2013>
261. McCauley, K. B., Hawkins, F., Serra, M., Thomas, D. C., Jacob, A., & Kotton, D. N. (2017). Efficient Derivation of Functional Human Airway Epithelium from Pluripotent Stem

- Cells via Temporal Regulation of Wnt Signaling. *Cell Stem Cell*, 20(6), 844-857.e6. <https://doi.org/10.1016/j.stem.2017.03.001>
262. Medeiros, I. L., Pêgo-Fernandes, P. M., Mariani, A. W., Fernandes, F. G., Unterpertinger, F. V., Canzian, M., & Jatene, F. B. (2012). Comparison of lung preservation solutions in human lungs using an ex vivo lung perfusion experimental model. *Clinics*, 67(9), 1101–1106. [https://doi.org/10.6061/clinics/2012\(09\)19](https://doi.org/10.6061/clinics/2012(09)19)
263. Meindl, C., Stranzinger, S., Dzidic, N., Salar-Behzadi, S., Mohr, S., Zimmer, A., & Fröhlich, E. (2015). Permeation of Therapeutic Drugs in Different Formulations across the Airway Epithelium In Vitro. *PLOS ONE*, 10(8), e0135690. <https://doi.org/10.1371/journal.pone.0135690>
264. Meng, M., Wei, R., Wu, Y., Zeng, R., Luo, D., Ma, Y., Zhang, L., Huang, W., Zeng, H., Leung, F. W., Qiu, X., Sha, W., & Chen, H. (2024). Long-term risks of respiratory diseases in patients infected with SARS-CoV-2: A longitudinal, population-based cohort study. *eClinicalMedicine*, 69, 102500. <https://doi.org/10.1016/j.eclinm.2024.102500>
265. Mestre-Ferrandiz, J., Sussex, J., & Towse, A. (2012). *The R&D Cost of a New Medicine*.
266. Meurs, H., Dekkers, B. G. J., Maarsingh, H., Halayko, A. J., Zaagsma, J., & Gosens, R. (2013). Muscarinic receptors on airway mesenchymal cells: Novel findings for an ancient target. *Pulmonary Pharmacology & Therapeutics*, 26(1), 145–155. <https://doi.org/10.1016/j.pupt.2012.07.003>
267. Mims, J. W. (2015). Asthma: Definitions and pathophysiology. *International Forum of Allergy & Rhinology*, 5 Suppl 1, S2-6. <https://doi.org/10.1002/alr.21609>
268. Min, K. A., Rosania, G. R., Kim, C.-K., & Shin, M. C. (2016). Functional and cytometric examination of different human lung epithelial cell types as drug transport barriers. *Archives of Pharmacal Research*, 39(3), 359–369. <https://doi.org/10.1007/s12272-015-0704-6>
269. Min, K. A., Talattof, A., Tsume, Y., Stringer, K. A., Yu, J., Lim, D. H., & Rosania, G. R. (2013). The Extracellular Microenvironment Explains Variations in Passive Drug Transport

- across Different Airway Epithelial Cell Types. *Pharmaceutical Research*, 30(8), 2118–2132. <https://doi.org/10.1007/s11095-013-1069-5>
270. Moeller, A., Ask, K., Warburton, D., Gauldie, J., & Kolb, M. (2008). The bleomycin animal model: A useful tool to investigate treatment options for idiopathic pulmonary fibrosis? *International Journal of Biochemistry and Cell Biology*, 40(3), 362–382. <https://doi.org/10.1016/j.biocel.2007.08.011>
271. Mohammed, J. S., & Murphy, W. L. (2009). Bioinspired Design of Dynamic Materials. *Advanced Materials*, 21(23), 2361–2374. <https://doi.org/10.1002/adma.200803785>
272. Molina, S. A., Stauffer, B., Moriarty, H. K., Kim, A. H., McCarty, N. A., & Koval, M. (2015). Junctional abnormalities in human airway epithelial cells expressing F508del CFTR. *Https://Doi.Org/10.1152/Ajplung.00060.2015*, 309(5), L475–L487. <https://doi.org/10.1152/AJPLUNG.00060.2015>
273. Mösbauer, K., Fritsch, V. N., Adrian, L., Bernhardt, J., Gruhlke, M. C. H., Slusarenko, A. J., Niemeyer, D., & Antelmann, H. (2021). The Effect of Allicin on the Proteome of SARS-CoV-2 Infected Calu-3 Cells. *Frontiers in Microbiology*, 12, 746795. <https://doi.org/10.3389/fmicb.2021.746795>
274. Movia, D., Bruni-Favier, S., & Prina-Mello, A. (2020). In vitro Alternatives to Acute Inhalation Toxicity Studies in Animal Models—A Perspective. *Frontiers in Bioengineering and Biotechnology*, 8, 549. <https://doi.org/10.3389/fbioe.2020.00549>
275. Movia, D., & Prina-Mello, A. (2020). Preclinical development of orally inhaled drugs (Oids)—Are animal models predictive or shall we move towards in vitro non-animal models? *Animals*, 10(8), 1–16. <https://doi.org/10.3390/ani10081259>
276. Muddle, J., Kanabar, V., Brown, M., Page, C., & Forbes, B. (2020). An in vitro bioassay for evaluating the effect of inhaled bronchodilators on airway smooth muscle. *Pulmonary Pharmacology & Therapeutics*, 63, 101943. <https://doi.org/10.1016/J.PUPT.2020.101943>
277. Mukherjee, M., Cingolani, E., Pritchard, D. I., & Bosquillon, C. (2017a). Enhanced expression of Organic Cation Transporters in bronchial epithelial cell layers following

- insults associated with asthma – Impact on salbutamol transport. *European Journal of Pharmaceutical Sciences*, 106, 62–70. <https://doi.org/10.1016/j.ejps.2017.05.052>
278. Mukherjee, M., Cingolani, E., Pritchard, D. I., & Bosquillon, C. (2017b). Enhanced expression of Organic Cation Transporters in bronchial epithelial cell layers following insults associated with asthma – Impact on salbutamol transport. *European Journal of Pharmaceutical Sciences*, 106, 62–70. <https://doi.org/10.1016/j.ejps.2017.05.052>
279. Mukherjee, M., Latif, M. L., Pritchard, D. I., & Bosquillon, C. (2013). In-cell Western™ detection of organic cation transporters in bronchial epithelial cell layers cultured at an air–liquid interface on Transwell® inserts. *Journal of Pharmacological and Toxicological Methods*, 68(2), 184–189. <https://doi.org/10.1016/j.vascn.2013.05.007>
280. Mukherjee, M., Pritchard, D. I., & Bosquillon, C. (2012). Evaluation of air-interfaced Calu-3 cell layers for investigation of inhaled drug interactions with organic cation transporters in vitro. *International Journal of Pharmaceutics*, 426(1–2), 7–14. <https://doi.org/10.1016/j.ijpharm.2011.12.036>
281. Mullard, A. (2016). Parsing clinical success rates. *Nature Reviews. Drug Discovery*, 15(7), 447. <https://doi.org/10.1038/nrd.2016.136>
282. National Heart, Lung, and Blood Institute: National Asthma Education Program.: Expert Panel on the Management of Asthma. (2007). *Expert Panel Report 3: Guidelines for the Diagnosis and Management of Asthma, Guidelines for the Diagnosis and Management of Asthma*. Health and Human Services Department. <https://purl.fdlp.gov/GPO/LPS93946>
283. National Human Genome Research Institute. (2024, April 5). *Phenotype*. <https://www.genome.gov/genetics-glossary/Phenotype>
284. Nawroth, J. C., Barrile, R., Conegliano, D., van Riet, S., Hiemstra, P. S., & Villenave, R. (2019). Stem cell-based Lung-on-Chips: The best of both worlds? *Advanced Drug Delivery Reviews*, 140, 12–32. <https://doi.org/10.1016/j.addr.2018.07.005>
285. Neilson, L., Mankus, C., Thorne, D., Jackson, G., DeBay, J., & Meredith, C. (2015). Development of an in vitro cytotoxicity model for aerosol exposure using 3D reconstructed

- human airway tissue; application for assessment of e-cigarette aerosol. *Toxicology in Vitro*, 29(7), 1952–1962. <https://doi.org/10.1016/j.tiv.2015.05.018>
286. Nelson, C. P., Rainbow, R. D., Brignell, J. L., Perry, M. D., Willets, J. M., Davies, N. W., Standen, N. B., & Challiss, R. A. J. (2011). Principal role of adenylyl cyclase 6 in K⁺ channel regulation and vasodilator signalling in vascular smooth muscle cells. *Cardiovascular Research*, 91(4), 694–702. <https://doi.org/10.1093/cvr/cvr137>
287. Newman, S. P. (2017). Drug delivery to the lungs: Challenges and opportunities. *Therapeutic Delivery*, 8(8), 647–661. <https://doi.org/10.4155/tde-2017-0037>
288. Nguyen, L. T. H., Muktabar, A., Tang, J., Wong, Y. S., Thaxton, C. S., Venkatraman, S. S., & Ng, K. W. (2018). The Potential of Fluocinolone Acetonide to Mitigate Inflammation and Lipid Accumulation in 2D and 3D Foam Cell Cultures. *BioMed Research International*, 2018, 3739251. <https://doi.org/10.1155/2018/3739251>
289. Nianzhen Li, Schwartz, M., & Ionescu-Zanetti, C. (2009). PDMS compound adsorption in context. *Journal of Biomolecular Screening*, 14(2), 194–202. <https://doi.org/10.1177/1087057108327326>
290. Nichols, J. E., Niles, J., Riddle, M., Vargas, G., Schilagard, T., Ma, L., Edward, K., La Francesca, S., Sakamoto, J., Vega, S., Ogadegbe, M., Mlcak, R., Deyo, D., Woodson, L., Mcquitty, C., Lick, S., Beckles, D., Melo, E., & Cortiella, J. (2013). Production and assessment of decellularized pig and human lung scaffolds. *Tissue Engineering - Part A*, 19(17–18), 2045–2062. <https://doi.org/10.1089/ten.tea.2012.0250>
291. Nickel, S., Clerkin, C. G., Selo, M. A., & Ehrhardt, C. (2016). Transport mechanisms at the pulmonary mucosa: Implications for drug delivery. *Expert Opinion on Drug Delivery*, 13(5), 667–690. <https://doi.org/10.1517/17425247.2016.1140144>
292. Niisato, N., Hasegawa, I., Tokuda, S., Taruno, A., Nakajima, K., Miyazaki, H., Iwasaki, Y., & Marunaka, Y. (2007). Action of nelfinavir on anion secretion in human airway epithelia. *Biochemical and Biophysical Research Communications*, 356(4), 1050–1055. <https://doi.org/10.1016/j.bbrc.2007.03.095>

293. O'Brien, L. E., Zegers, M. M. P., & Mostov, K. E. (2002). Building epithelial architecture: Insights from three-dimensional culture models. *Nature Reviews Molecular Cell Biology*, 3(7), 531–537. <https://doi.org/10.1038/nrm859>
294. Odell, I. D., & Cook, D. (2013). Immunofluorescence Techniques. *Journal of Investigative Dermatology*, 133(1), 1–4. <https://doi.org/10.1038/jid.2012.455>
295. Ogi, C., & Aruga, A. (2013). Immunological monitoring of anticancer vaccines in clinical trials. *Oncot Immunology*, 2(8), e26012. <https://doi.org/10.4161/onci.26012>
296. O'Neill, J. D., Anfang, R., Anandappa, A., Costa, J., Javidfar, J., Wobma, H. M., Singh, G., Freytes, D. O., Bacchetta, M. D., Sonett, J. R., & Vunjak-Novakovic, G. (2013). Decellularization of human and porcine lung tissues for pulmonary tissue engineering. *Annals of Thoracic Surgery*, 96(3), 1046–1056. <https://doi.org/10.1016/j.athoracsur.2013.04.022>
297. O'Sullivan, M. J., Gabriel, E., Panariti, A., Park, C. Y., Ijpma, G., Fredberg, J. J., Lauzon, A.-M., & Martin, J. G. (2017). Epithelial Cells Induce a Cyclo-Oxygenase-1-Dependent Endogenous Reduction in Airway Smooth Muscle Contractile Phenotype. *American Journal of Respiratory Cell and Molecular Biology*, 57(6), 683–691. <https://doi.org/10.1165/rcmb.2016-0427OC>
298. Pammolli, F., Righetto, L., Abrignani, S., Pani, L., Pelicci, P. G., & Rabosio, E. (2020). The endless frontier? The recent increase of R&D productivity in pharmaceuticals. *Journal of Translational Medicine*, 18, 162. <https://doi.org/10.1186/s12967-020-02313-z>
299. Pampaloni, F., Reynaud, E. G., & Stelzer, E. H. K. (2007). The third dimension bridges the gap between cell culture and live tissue. *Nature Reviews Molecular Cell Biology*, 8(10), 839–845. <https://doi.org/10.1038/nrm2236>
300. Papritz, M., Pohl, C., Wübbeke, C., Moisch, M., Hofmann, H., Hermanns, M. I., Thiermann, H., Kirkpatrick, C. J., & Kehe, K. (2010). Side-specific effects by cadmium exposure: Apical and basolateral treatment in a coculture model of the blood-air barrier. *Toxicology and Applied Pharmacology*, 245(3), 361–369. <https://doi.org/10.1016/j.taap.2010.04.002>

301. Pascoe, C. D., Swyngedouw, N. E., Seow, C. Y., & Paré, P. D. (2015). Gene expression in asthmatic airway smooth muscle: A mixed bag. *Canadian Journal of Physiology and Pharmacology*, 93(2), 137–143. <https://doi.org/10.1139/cjpp-2014-0390>
302. Pasman, T., Baptista, D., Riet, S. van, Truckenmüller, R. K., Hiemstra, P. S., Rottier, R. J., Hamelmann, N. M., Paulusse, J. M. J., Stamatialis, D., & Poot, A. A. (2021). Development of an In Vitro Airway Epithelial–Endothelial Cell Culture Model on a Flexible Porous Poly(Trimethylene Carbonate) Membrane Based on Calu-3 Airway Epithelial Cells and Lung Microvascular Endothelial Cells. *Membranes* 2021, Vol. 11, Page 197, 11(3), 197. <https://doi.org/10.3390/MEMBRANES11030197>
303. Pepe, C., Foley, S., Shannon, J., Lemiere, C., Olivenstein, R., Ernst, P., Ludwig, M. S., Martin, J. G., & Hamid, Q. (2005). Differences in airway remodeling between subjects with severe and moderate asthma. *The Journal of Allergy and Clinical Immunology*, 116(3), 544–549. <https://doi.org/10.1016/j.jaci.2005.06.011>
304. Pezzulo, A. A., Starner, T. D., Scheetz, T. E., Traver, G. L., Tilley, A. E., Harvey, B.-G., Crystal, R. G., McCray, P. B., & Zabner, J. (2011). The air-liquid interface and use of primary cell cultures are important to recapitulate the transcriptional profile of in vivo airway epithelia. *American Journal of Physiology-Lung Cellular and Molecular Physiology*, 300(1), L25–L31. <https://doi.org/10.1152/ajplung.00256.2010>
305. Phan, T. H., Shi, H., Denes, C. E., Cole, A. J., Wang, Y., Cheng, Y. Y., Hesselson, D., Roelofs, S. H., Neely, G. G., Jang, J.-H., & Chrzanowski, W. (2023). Advanced pathophysiology mimicking lung models for accelerated drug discovery. *Biomaterials Research*, 27, 35. <https://doi.org/10.1186/s40824-023-00366-x>
306. PhRMA. (2014). *PERCENTAGE OF SALES THAT WENT TO R&D IN 2013*.
307. Pilcer, G., & Amighi, K. (2010). Formulation strategy and use of excipients in pulmonary drug delivery. *International Journal of Pharmaceutics*, 392(1–2), 1–19. <https://doi.org/10.1016/j.ijpharm.2010.03.017>
308. Pognan, F., Beilmann, M., Boonen, H. C. M., Czich, A., Dear, G., Hewitt, P., Mow, T., Oinonen, T., Roth, A., Steger-Hartmann, T., Valentin, J.-P., Van Goethem, F., Weaver, R.

- J., & Newham, P. (2023). The evolving role of investigative toxicology in the pharmaceutical industry. *Nature Reviews Drug Discovery*, 22(4), 317–335. <https://doi.org/10.1038/s41573-022-00633-x>
309. Polini, A., Prodanov, L., Bhise, N. S., Manoharan, V., Dokmeci, M. R., & Khademhosseini, A. (2014). Organs-on-a-chip: A new tool for drug discovery. *Expert Opinion on Drug Discovery*, 9(4), 335–352. <https://doi.org/10.1517/17460441.2014.886562>
310. Polson, C., Sarkar, P., Incledon, B., Raguvaran, V., & Grant, R. (2003). Optimization of protein precipitation based upon effectiveness of protein removal and ionization effect in liquid chromatography–tandem mass spectrometry. *Journal of Chromatography B*, 785(2), 263–275. [https://doi.org/10.1016/S1570-0232\(02\)00914-5](https://doi.org/10.1016/S1570-0232(02)00914-5)
311. *Primary Bronchial/Tracheal Smooth Muscle Cells; Normal, Human—PCS-130-011* | ATCC. (2024). ATCC. <https://www.atcc.org/products/pcs-130-011>
312. Purandare, A. V. (2021). Understanding Drug Development: A Primer on the Food and Drug Administration. *Journal of the Pediatric Infectious Diseases Society*, piab023. <https://doi.org/10.1093/jpids/piab023>
313. Qing, F., Rahman, S. U., Rhodes, C. G., Hayes, M. J., Sriskandan, S., Ind, P. W., Jones, T., & Hughes, J. M. (1997). Pulmonary and cardiac beta-adrenoceptor density in vivo in asthmatic subjects. *American Journal of Respiratory and Critical Care Medicine*, 155(3), 1130–1134. <https://doi.org/10.1164/ajrccm.155.3.9116998>
314. Raeburn, D., & Webber, S. E. (1994). Proinflammatory potential of the airway epithelium in bronchial asthma. *The European Respiratory Journal*, 7(12), 2226–2233. <https://doi.org/10.1183/09031936.94.07122226>
315. Raherison, C., & Girodet, P.-O. (2009). Epidemiology of COPD. *European Respiratory Review*, 18(114), 213–221. <https://doi.org/10.1183/09059180.00003609>
316. Ramme, A. P., Koenig, L., Hasenberg, T., Schwenk, C., Magauer, C., Faust, D., Lorenz, A. K., Krebs, A.-C., Drewell, C., Schirrmann, K., Vladetic, A., Lin, G.-C., Pabinger, S., Neuhaus, W., Bois, F., Lauster, R., Marx, U., & Dehne, E.-M. (2019). Autologous

- induced pluripotent stem cell-derived four-organ-chip. *Future Science OA*, 5(8), FSO413. <https://doi.org/10.2144/fsoa-2019-0065>
317. Ramos-Vara, J. (2010). *Principles and Methods of Histology*.
318. Rasmussen, K., Pedersen-Bjergaard, S., Hansen, S. H., & Hansen, S. H. (2011). *Introduction to Pharmaceutical Chemical Analysis*. John Wiley & Sons, Incorporated. <http://ebookcentral.proquest.com/lib/herts/detail.action?docID=822569>
319. Reddel, R. R., Ke, Y., Gerwin, B. I., McMenamin, M. G., Lechner, J. F., Su, R. T., Brash, D. E., Park, J.-B., Rhim, J. S., & Harris, C. C. (1988). Transformation of Human Bronchial Epithelial Cells by Infection with SV40 or Adenovirus-12 SV40 Hybrid Virus, or Transfection via Strontium Phosphate Coprecipitation with a Plasmid Containing SV40 Early Region Genes. *Cancer Research*, 48(7), 1904–1909. Scopus.
320. Ricard-Blum, S. (2011). The Collagen Family. *Cold Spring Harbor Perspectives in Biology*, 3(1), a004978. <https://doi.org/10.1101/cshperspect.a004978>
321. Riess, A., Wiggs, B., Verburgt, L., Wright, J. L., Hogg, J. C., & Paré, P. D. (1996). Morphologic determinants of airway responsiveness in chronic smokers. *American Journal of Respiratory and Critical Care Medicine*, 154(5), 1444–1449. Scopus. <https://doi.org/10.1164/ajrccm.154.5.8912762>
322. Rock, J. R., Onaitis, M. W., Rawlins, E. L., Lu, Y., Clark, C. P., Xue, Y., Randell, S. H., & Hogan, B. L. M. (2009). Basal cells as stem cells of the mouse trachea and human airway epithelium. *Proceedings of the National Academy of Sciences of the United States of America*, 106(31), 12771–12775. <https://doi.org/10.1073/pnas.0906850106>
323. Rotoli, B. M., Barilli, A., Visigalli, R., Ferrari, F., Frati, C., Lagrasta, C. A., Di Lascia, M., Riccardi, B., Puccini, P., & Dall'Asta, V. (2020). Characterization of ABC Transporters in EpiAirway™, a Cellular Model of Normal Human Bronchial Epithelium. *International Journal of Molecular Sciences*, 21(9), 3190. <https://doi.org/10.3390/ijms21093190>
324. Rotoli, B. M., Visigalli, R., Barilli, A., Ferrari, F., Bianchi, M. G., Di Lascia, M., Riccardi, B., Puccini, P., & Dall'Asta, V. (2020). Functional analysis of OCTN2 and ATB0,+ in normal

- human airway epithelial cells. *PLoS ONE*, 15(2), e0228568. <https://doi.org/10.1371/journal.pone.0228568>
325. Ryan, J. A. (2008). *Introduction to Animal Cell Culture*. Technical Bulletin Corning.
326. Sachs, L. A., Finkbeiner, W. E., & Widdicombe, J. H. (2003). Effects of media on differentiation of cultured human tracheal epithelium. *In Vitro Cellular and Developmental Biology - Animal*, 39(1–2), 56–62. Scopus. [https://doi.org/10.1290/1543-706X\(2003\)039<0056:EOMODO>2.0.CO;2](https://doi.org/10.1290/1543-706X(2003)039<0056:EOMODO>2.0.CO;2)
327. Sadaria, M. R., Smith, P. D., Fullerton, D. A., Justison, G. A., Lee, J. H., Puskas, F., Grover, F. L., Cleveland, J. C., Reece, T. B., & Weyant, M. J. (2011). Cytokine expression profile in human lungs undergoing normothermic ex-vivo lung perfusion. *Annals of Thoracic Surgery*, 92(2), 478–484. <https://doi.org/10.1016/j.athoracsur.2011.04.027>
328. Sahiner, N. (2013). Soft and flexible hydrogel templates of different sizes and various functionalities for metal nanoparticle preparation and their use in catalysis. *Progress in Polymer Science*, 38(9), 1329–1356. <https://doi.org/10.1016/j.progpolymsci.2013.06.004>
329. Sakagami, M. (2006). In vivo, in vitro and ex vivo models to assess pulmonary absorption and disposition of inhaled therapeutics for systemic delivery. *Advanced Drug Delivery Reviews*, 58(9–10), 1030–1060. <https://doi.org/10.1016/j.addr.2006.07.012>
330. Sakamoto, A., Matsumaru, T., Yamamura, N., Suzuki, S., Uchida, Y., Tachikawa, M., & Terasaki, T. (2015). Drug Transporter Protein Quantification of Immortalized Human Lung Cell Lines Derived from Tracheobronchial Epithelial Cells (Calu-3 and BEAS2-B), Bronchiolar-Alveolar Cells (NCI-H292 and NCI-H441), and Alveolar Type II-like Cells (A549) by Liquid Chromatography-Tandem Mass Spectrometry. *Journal of Pharmaceutical Sciences*, 104(9), 3029–3038. <https://doi.org/10.1002/JPS.24381>
331. Sakamoto, S., Putalun, W., Vimolmangkang, S., Phoolcharoen, W., Shoyama, Y., Tanaka, H., & Morimoto, S. (2018). Enzyme-linked immunosorbent assay for the quantitative/qualitative analysis of plant secondary metabolites. *Journal of Natural Medicines*, 72(1), 32–42. <https://doi.org/10.1007/s11418-017-1144-z>

332. Salomon, J. J., Endter, S., Tachon, G., Falson, F., Buckley, S. T., & Ehrhardt, C. (2012). Transport of the fluorescent organic cation 4-(4-(dimethylamino)styryl)-N-methylpyridinium iodide (ASP+) in human respiratory epithelial cells. *European Journal of Pharmaceutics and Biopharmaceutics*, 81(2), 351–359. <https://doi.org/10.1016/J.EJPB.2012.03.001>
333. Salvi, S. S., & Barnes, P. J. (2009). Chronic obstructive pulmonary disease in non-smokers. *Lancet (London, England)*, 374(9691), 733–743. [https://doi.org/10.1016/S0140-6736\(09\)61303-9](https://doi.org/10.1016/S0140-6736(09)61303-9)
334. Sampaziotis, F., de Brito, M. C., Geti, I., Bertero, A., Hannan, N. R., & Vallier, L. (2017). Directed differentiation of human induced pluripotent stem cells into functional cholangiocyte-like cells. *Nature Protocols*, 12(4), 814–827. <https://doi.org/10.1038/nprot.2017.011>
335. Sanyal, S., & Kosovsky, M. (2017). Materials and assay systems used for three-dimensional cell culture. In *Technology Platforms for 3D Cell Culture* (pp. 143–172). John Wiley & Sons, Ltd. <https://doi.org/10.1002/9781118851647.ch7>
336. Sato, M., Shay, J. W., & Minna, J. D. (2020). Immortalized normal human lung epithelial cell models for studying lung cancer biology. *Respiratory Investigation*, 58(5), 344–354. <https://doi.org/10.1016/j.resinv.2020.04.005>
337. Scheerlinck, J.-P. Y., Snibson, K. J., Bowles, V. M., & Sutton, P. (2008). Biomedical applications of sheep models: From asthma to vaccines. *Trends in Biotechnology*, 26(5), 259–266. <https://doi.org/10.1016/j.tibtech.2008.02.002>
338. Schimek, K., Frentzel, S., Luettich, K., Bovard, D., Rüttschle, I., Boden, L., Rambo, F., Erfurth, H., Dehne, E. M., Winter, A., Marx, U., & Hoeng, J. (2020). Human multi-organ chip co-culture of bronchial lung culture and liver spheroids for substance exposure studies. *Scientific Reports*, 10(1), 1–13. <https://doi.org/10.1038/s41598-020-64219-6>
339. Schlender, M., Hernandez-Villafuerte, K., Cheng, C.-Y., Mestre-Ferrandiz, J., & Baumann, M. (2021). How Much Does It Cost to Research and Develop a New Drug? A

- Systematic Review and Assessment. *Pharmacoeconomics*, 39(11), 1243–1269.
<https://doi.org/10.1007/s40273-021-01065-y>
340. Schmeichel, K. L., & Bissell, M. J. (2003). Modelling tissue-specific signaling and organ function in three dimensions. *Journal of Cell Science*, 116(12), 2377–2388.
<https://doi.org/10.1242/jcs.00503>
341. Schroeder, J. A., Ruta, J. D., Gordon, J. S., Rodrigues, A. S., & Foote, C. C. (2012). The phosphodiesterase inhibitor isobutylmethylxanthine attenuates behavioral sensitization to cocaine. *Behavioural Pharmacology*, 23(3), 310–314.
<https://doi.org/10.1097/FBP.0b013e3283536d04>
342. Sécher, T., Bodier-Montagutelli, E., Guillon, A., & Heuzé-Vourc'h, N. (2020). Correlation and clinical relevance of animal models for inhaled pharmaceuticals and biopharmaceuticals. *Advanced Drug Delivery Reviews*, 167, 148–169.
<https://doi.org/10.1016/j.addr.2020.06.029>
343. Sécher, T., Dalonneau, E., Ferreira, M., Parent, C., Azzopardi, N., Paintaud, G., Si-Tahar, M., & Heuzé-Vourc'h, N. (2019). In a murine model of acute lung infection, airway administration of a therapeutic antibody confers greater protection than parenteral administration. *Journal of Controlled Release*, 303, 24–33.
<https://doi.org/10.1016/j.jconrel.2019.04.005>
344. Sécher, T., Mayor, A., & Heuzé-Vourc'h, N. (2019). Inhalation of Immuno-Therapeutics/-Prophylactics to Fight Respiratory Tract Infections: An Appropriate Drug at the Right Place! *Frontiers in Immunology*, 10, 2760.
<https://doi.org/10.3389/fimmu.2019.02760>
345. Secondo, L. E., Liu, N. J., & Lewinski, N. A. (2017). Methodological considerations when conducting *in vitro*, air–liquid interface exposures to engineered nanoparticle aerosols. *Critical Reviews in Toxicology*, 47(3), 225–262.
<https://doi.org/10.1080/10408444.2016.1223015>
346. Sedláková, V., Kloučková, M., Garlíková, Z., Vašíčková, K., Jaroš, J., Kandra, M., Kotasová, H., & Hampl, A. (2019). Options for modeling the respiratory system: Inserts,

- scaffolds and microfluidic chips. *Drug Discovery Today*, 24(4), 971–982. <https://doi.org/10.1016/j.drudis.2019.03.006>
347. Sellers, J. R., Spudich, J. A., & Sheetz, M. P. (1985). Light chain phosphorylation regulates the movement of smooth muscle myosin on actin filaments. *The Journal of Cell Biology*, 101(5 Pt 1), 1897–1902. <https://doi.org/10.1083/jcb.101.5.1897>
348. Sellers, S., Horodnik, W., House, A., Wylie, J., Mauser, P., Garber, N., Pu, Y. E., Berry, J., & Donovan, B. (2015). The in vitro and in vivo investigation of inhaled migraine therapies using a novel aerosol delivery system consisting of an air pressurized capsule device (APCD) in combination with a pMDI spacer for endotracheal dosing into beagle dogs. *Drug Development and Industrial Pharmacy*, 41(12), 1989–1996. <https://doi.org/10.3109/03639045.2015.1029936>
349. Selo, M. A., Sake, J. A., Kim, K.-J., & Ehrhardt, C. (2021). In vitro and ex vivo models in inhalation biopharmaceutical research—Advances, challenges and future perspectives. *Advanced Drug Delivery Reviews*, 177, 113862. <https://doi.org/10.1016/j.addr.2021.113862>
350. Shah, P., Fritz, J. V., Glaab, E., Desai, M. S., Greenhalgh, K., Frachet, A., Niegowska, M., Estes, M., Jäger, C., Seguin-Devaux, C., Zenhausem, F., & Wilmes, P. (2016). A microfluidics-based in vitro model of the gastrointestinal human-microbe interface. *Nature Communications*, 7(1), 1–15. <https://doi.org/10.1038/ncomms11535>
351. Shapland, C., Hsuan, J. J., Totty, N. F., & Lawson, D. (1993). Purification and properties of transgelin: A transformation and shape change sensitive actin-gelling protein. *The Journal of Cell Biology*, 121(5), 1065–1073. <https://doi.org/10.1083/jcb.121.5.1065>
352. Sharma, K. (2024, January 18). *UV-Vis Spectrophotometer: Principle, Components, Uses*. <https://scienceinfo.com/uv-vis-spectrophotometer-principle/>
353. Sheffield, S. (2017, November 13). *Bronchioles: Function and diagram*. GetBodySmart. <https://www.getbodysmart.com/lungs/bronchiole-wall/>
354. Si, L., Bai, H., Rodas, M., Cao, W., Oh, C. Y., Jiang, A., Moller, R., Hoagland, D., Oishi, K., Horiuchi, S., Uhl, S., Blanco-Melo, D., Albrecht, R. A., Liu, W.-C., Jordan, T., Nilsson-

- Payant, B. E., Logue, J., Haupt, R., McGrath, M., ... Ingber, D. E. (2020). *Human organ chip-enabled pipeline to rapidly repurpose therapeutics during viral pandemics* (p. 2020.04.13.039917). bioRxiv. <https://doi.org/10.1101/2020.04.13.039917>
355. Sibinovska, N., Žakelj, S., Roškar, R., & Kristan, K. (2020). Suitability and functional characterization of two Calu-3 cell models for prediction of drug permeability across the airway epithelial barrier. *International Journal of Pharmaceutics*, 585. Scopus. <https://doi.org/10.1016/j.ijpharm.2020.119484>
356. Sichletidis, L., Daskalopoulou, E., Kyriazis, G., Kosmidou, I., Koupidou, S., Pechlivanidis, T., & Chloros, D. (1993). Comparative efficacy of salbutamol and salmeterol in exercise-induced asthma. *The Journal of International Medical Research*, 21(2), 81–88. <https://doi.org/10.1177/030006059302100203>
357. Sieck, G. C., & Gransee, H. (2012). *Respiratory Muscles: Structure, Function and Regulation*. Morgan & Claypool Life Science Publishers. <http://ebookcentral.proquest.com/lib/herts/detail.action?docID=919690>
358. Sims, A. C., Burkett, S. E., Yount, B., & Pickles, R. J. (2008). SARS-CoV replication and pathogenesis in an in vitro model of the human conducting airway epithelium. *Virus Research*, 133(1), 33–44. <https://doi.org/10.1016/j.virusres.2007.03.013>
359. Snider, G. L. (1985). Distinguishing Among Asthma, Chronic Bronchitis, and Emphysema. *Chest*, 87(1, Supplement), 35S–39S. <https://doi.org/10.1378/chest.87.1.35S>
360. Sontheimer-Phelps, A., Chou, D. B., Tovaglieri, A., Ferrante, T. C., Duckworth, T., Fadel, C., Frimantas, V., Sutherland, A. D., Jalili-Firoozinezhad, S., Kasendra, M., Stas, E., Weaver, J. C., Richmond, C. A., Levy, O., Prantil-Baun, R., Breault, D. T., & Ingber, D. E. (2020). Human Colon-on-a-Chip Enables Continuous In Vitro Analysis of Colon Mucus Layer Accumulation and Physiology. *Cellular and Molecular Gastroenterology and Hepatology*, 9(3), 507–526. <https://doi.org/10.1016/j.jcmgh.2019.11.008>
361. Sood, B. G., Shen, Y., Latif, Z., Chen, X., Sharp, J., Neelavalli, J., Joshi, A., Slovis, T. L., & Haacke, E. M. (2008). Aerosol delivery in ventilated newborn pigs: An MRI evaluation. *Pediatric Research*, 64(2), 159–164. <https://doi.org/10.1203/PDR.0b013e3181761841>

362. Spring, J., Clague, J., & Ind, P. W. (1992). A comparison of the effect of salmeterol and salbutamol in normal subjects. *British Journal of Clinical Pharmacology*, 33(2), 139–141. <https://doi.org/10.1111/j.1365-2125.1992.tb04015.x>
363. Srinivasan, B., Kolli, A. R., Esch, M. B., Abaci, H. E., Shuler, M. L., & Hickman, J. J. (2015). TEER measurement techniques for in vitro barrier model systems. *Journal of Laboratory Automation*, 20(2), 107–126. <https://doi.org/10.1177/2211068214561025>
364. Srivastava, S. K., Foo, G. W., Aggarwal, N., & Chang, M. W. (2024). Organ-on-chip technology: Opportunities and challenges. *Biotechnology Notes*, 5, 8–12. <https://doi.org/10.1016/j.biotno.2024.01.001>
365. Stanfield, C. L. (2016). *Principles of Human Physiology* (Sixth Edition). Pearson Education.
366. Stewart, C. E., Torr, E. E., Mohd Jamili, N. H., Bosquillon, C., & Sayers, I. (2012a). Evaluation of Differentiated Human Bronchial Epithelial Cell Culture Systems for Asthma Research. *Journal of Allergy*, 2012, e943982. <https://doi.org/10.1155/2012/943982>
367. Stewart, C. E., Torr, E. E., Mohd Jamili, N. H., Bosquillon, C., & Sayers, I. (2012b). Evaluation of Differentiated Human Bronchial Epithelial Cell Culture Systems for Asthma Research. *Journal of Allergy*, 2012, 1–11. <https://doi.org/10.1155/2012/943982>
368. Stoker, A. W., Streuli, C. H., Martins-Green, M., & Bissell, M. J. (1990). Designer microenvironments for the analysis of cell and tissue function. *Current Opinion in Cell Biology*, 2(5), 864–874. [https://doi.org/10.1016/0955-0674\(90\)90085-S](https://doi.org/10.1016/0955-0674(90)90085-S)
369. Straus, D. S. (1981). Effects of insulin on cellular growth and proliferation. *Life Sciences*, 29(21), 2131–2139. [https://doi.org/10.1016/0024-3205\(81\)90482-3](https://doi.org/10.1016/0024-3205(81)90482-3)
370. Stresser, D. M., Kopec, A. K., Hewitt, P., Hardwick, R. N., Van Vleet, T. R., Mahalingaiah, P. K. S., O'Connell, D., Jenkins, G. J., David, R., Graham, J., Lee, D., Ekert, J., Fullerton, A., Villenave, R., Bajaj, P., Gosset, J. R., Ralston, S. L., Guha, M., Amador-Arjona, A., ... Homan, K. A. (2023). Towards in vitro models for reducing or replacing the use of animals in drug testing. *Nature Biomedical Engineering*, 1–6. <https://doi.org/10.1038/s41551-023-01154-7>

371. Stucki, A. O., Stucki, J. D., Hall, S. R. R., Felder, M., Mermoud, Y., Schmid, R. A., Geiser, T., & Guenat, O. T. (2015). A lung-on-a-chip array with an integrated bio-inspired respiration mechanism. *Lab on a Chip*, 15(5), 1302–1310. <https://doi.org/10.1039/C4LC01252F>
372. Stucki, J. D., Hobi, N., Galimov, A., Stucki, A. O., Schneider-Daum, N., Lehr, C.-M., Huwer, H., Frick, M., Funke-Chambour, M., Geiser, T., & Guenat, O. T. (2018). Medium throughput breathing human primary cell alveolus-on-chip model. *Scientific Reports*, 8(1), 14359. <https://doi.org/10.1038/s41598-018-32523-x>
373. Stuetz, H., Reihs, E. I., Neuhaus, W., Pflüger, M., Hundsberger, H., Ertl, P., Resch, C., Bauer, G., Povoden, G., & Rothbauer, M. (2023). The Cultivation Modality and Barrier Maturity Modulate the Toxicity of Industrial Zinc Oxide and Titanium Dioxide Nanoparticles on Nasal, Buccal, Bronchial, and Alveolar Mucosa Cell-Derived Barrier Models. *International Journal of Molecular Sciences*, 24(6), 5634. <https://doi.org/10.3390/ijms24065634>
374. Sugawara, E., & Nikaido, H. (2014). Properties of AdeABC and AdeIJK efflux systems of *Acinetobacter baumannii* compared with those of the AcrAB-TolC system of *Escherichia coli*. *Antimicrobial Agents and Chemotherapy*, 58(12), 7250–7257. <https://doi.org/10.1128/AAC.03728-14>
375. Sui, C., & Lee, W. (2023). Role of interleukin 6 and its soluble receptor on the diffusion barrier dysfunction of alveolar tissue. *Biomedical Microdevices*, 25(4), 40. <https://doi.org/10.1007/s10544-023-00680-0>
376. Sun, D., Gao, W., Hu, H., & Zhou, S. (2022). Why 90% of clinical drug development fails and how to improve it? *Acta Pharmaceutica Sinica B*, 12(7), 3049–3062. <https://doi.org/10.1016/j.apsb.2022.02.002>
377. Sun, H., Zhu, Y., Pan, H., Chen, X., Balestrini, J. L., Lam, T. T., Kanyo, J. E., Eichmann, A., Gulati, M., Fares, W. H., Bai, H., Feghali-Bostwick, C. A., Gan, Y., Peng, X., Moore, M. W., White, E. S., Sava, P., Gonzalez, A. L., Cheng, Y., ... Herzog, E. L. (2016). Netrin-1 Regulates Fibrocyte Accumulation in the Decellularized Fibrotic Sclerodermatous Lung

- Microenvironment and in Bleomycin-Induced Pulmonary Fibrosis. *Arthritis and Rheumatology*, 68(5), 1251–1261. <https://doi.org/10.1002/art.39575>
378. Sun, S., Schiller, J. H., & Gazdar, A. F. (2007). Lung cancer in never smokers—A different disease. *Nature Reviews. Cancer*, 7(10), 778–790. <https://doi.org/10.1038/nrc2190>
379. Suresh, K., & Shimoda, L. A. (2016). Lung Circulation. *Comprehensive Physiology*, 6(2), 897–943. <https://doi.org/10.1002/cphy.c140049>
380. Suresh, M. V., Wagner, M. C., Rosania, G. R., Stringer, K. A., Min, K. A., Risler, L., Shen, D. D., Georges, G. E., Reddy, A. T., Parkkinen, J., & Reddy, R. C. (2012). Pulmonary Administration of a Water-Soluble Curcumin Complex Reduces Severity of Acute Lung Injury. *American Journal of Respiratory Cell and Molecular Biology*, 47(3), 280–287. <https://doi.org/10.1165/rcmb.2011-0175OC>
381. T0493 | Immortalized Human Bronchial Smooth Muscle Cells—Academic. (2024). Clinisciences.Com. <https://www.clinisciences.com/es/-186/immortalized-human-bronchial-smooth-55432740.html>
382. Tapia, R., Kralicek, S. E., & Hecht, G. A. (2017). Modulation of epithelial cell polarity by bacterial pathogens. *Annals of the New York Academy of Sciences*, 1405(1), 16–24. <https://doi.org/10.1111/nyas.13388>
383. Tata, P. R., Mou, H., Pardo-Saganta, A., Zhao, R., Prabhu, M., Law, B. M., Vinarsky, V., Cho, J. L., Breton, S., Sahay, A., Medoff, B. D., & Rajagopal, J. (2013). Dedifferentiation of committed epithelial cells into stem cells in vivo. *Nature*, 503(7475), 218–223. <https://doi.org/10.1038/nature12777>
384. Taylor, P. J. (2005). Matrix effects: The Achilles heel of quantitative high-performance liquid chromatography–electrospray–tandem mass spectrometry. *Clinical Biochemistry*, 38(4), 328–334. <https://doi.org/10.1016/j.clinbiochem.2004.11.007>
385. Technavio. (2023). *Respiratory Drugs Market by Distribution Channel, Type and Geography—Forecast and Analysis 2023-2027*. <https://www.technavio.com/report/global-respiratory-drugs-market-analysis-share?tnplus>

386. Tefferi, A., Kantarjian, H., Rajkumar, S. V., Baker, L. H., Abkowitz, J. L., Adamson, J. W., Advani, R. H., Allison, J., Antman, K. H., Bast, R. C., Bennett, J. M., Benz, E. J., Berliner, N., Bertino, J., Bhatia, R., Bhatia, S., Bhojwani, D., Blanke, C. D., Bloomfield, C. D., ... LeMaistre, C. A. (2015). In Support of a Patient-Driven Initiative and Petition to Lower the High Price of Cancer Drugs. *Mayo Clinic Proceedings*, 90(8), 996–1000. <https://doi.org/10.1016/j.mayocp.2015.06.001>
387. *The Basics of Fetal Bovine Serum Use—UK*. (2024). <https://www.thermofisher.com/uk/en/home/references/gibco-cell-culture-basics/cell-culture-environment/culture-media/fbs-basics.html>
388. The Lancet. (2018). GBD 2017: A fragile world. *The Lancet*, 392(10159), 1683. [https://doi.org/10.1016/S0140-6736\(18\)32858-7](https://doi.org/10.1016/S0140-6736(18)32858-7)
389. Thiel-Demby, V. E., Humphreys, J. E., St. John Williams, L. A., Ellens, H. M., Shah, N., Ayrton, A. D., & Polli, J. W. (2009). Biopharmaceutics Classification System: Validation and Learnings of an in Vitro Permeability Assay. *Molecular Pharmaceutics*, 6(1), 11–18. <https://doi.org/10.1021/mp800122b>
390. Thompson, C. L., Fu, S., Heywood, H. K., Knight, M. M., & Thorpe, S. D. (2020a). Mechanical Stimulation: A Crucial Element of Organ-on-Chip Models. *Frontiers in Bioengineering and Biotechnology*, 8, 602646. <https://doi.org/10.3389/fbioe.2020.602646>
391. Thompson, C. L., Fu, S., Heywood, H. K., Knight, M. M., & Thorpe, S. D. (2020b). Mechanical Stimulation: A Crucial Element of Organ-on-Chip Models. *Frontiers in Bioengineering and Biotechnology*, 8, 602646. <https://doi.org/10.3389/FBIOE.2020.602646>
392. Toepke, M. W., & Beebe, D. J. (2006). PDMS absorption of small molecules and consequences in microfluidic applications. *Lab on a Chip*, 6(12), 1484–1486. <https://doi.org/10.1039/b612140c>
393. Travaglini, K. J., Nabhan, A. N., Penland, L., Sinha, R., Gillich, A., Sit, R. V., Chang, S., Conley, S. D., Mori, Y., Seita, J., Berry, G. J., Shrager, J. B., Metzger, R. J., Kuo, C. S., Neff, N., Weissman, I. L., Quake, S. R., & Krasnow, M. A. (2020). A molecular cell atlas

- of the human lung from single-cell RNA sequencing. *Nature*, 587(7835), 619–625.
<https://doi.org/10.1038/s41586-020-2922-4>
394. Trieu, D., Waddell, T. K., & McGuigan, A. P. (2014). A microfluidic device to apply shear stresses to polarizing ciliated airway epithelium using air flow. *Biomicrofluidics*, 8(6), 064104. <https://doi.org/10.1063/1.4901930>
395. Tschumperlin, D. J., & Drazen, J. M. (2001). Mechanical Stimuli to Airway Remodeling. *American Journal of Respiratory and Critical Care Medicine*, 164(supplement_2), S90–S94. https://doi.org/10.1164/ajrccm.164.supplement_2.2106060
396. Tsukita, S., & Furuse, M. (1999). Occludin and claudins in tight-junction strands: Leading or supporting players? *Trends in Cell Biology*, 9(7), 268–273. [https://doi.org/10.1016/s0962-8924\(99\)01578-0](https://doi.org/10.1016/s0962-8924(99)01578-0)
397. Turner, D. A., Baillie-Johnson, P., & Martinez Arias, A. (2016). Organoids and the genetically encoded self-assembly of embryonic stem cells. *Bioessays*, 38(2), 181–191. <https://doi.org/10.1002/bies.201500111>
398. Uhl, F. E., Vierkotten, S., Wagner, D. E., Burgstaller, G., Costa, R., Koch, I., Lindner, M., Meiners, S., Eickelberg, O., & Königshoff, M. (2015). Preclinical validation and imaging of Wnt-induced repair in human 3D lung tissue cultures. *European Respiratory Journal*, 46(4), 1150–1166. <https://doi.org/10.1183/09031936.00183214>
399. Underwood, S. L., & Raeburn, D. (1996). Methods of Drug Administration to the Lung in Animals. In D. Raeburn & M. A. Giembycz (Eds.), *Airways Smooth Muscle: Modelling the Asthmatic Response In Vivo* (pp. 27–50). Birkhäuser. https://doi.org/10.1007/978-3-0348-9000-7_2
400. University of Nebraska: Medical Center. (2020, September). *Pros and Cons | Stem Cells | University of Nebraska Medical Center*. <https://www.unmc.edu/stemcells/educational-resources/prosandcons.html>
401. Uwagboe, I., Adcock, I. M., Lo Bello, F., Caramori, G., & Mumby, S. (2022). New drugs under development for COPD. *Minerva Medica*, 113(3), 471–496. <https://doi.org/10.23736/S0026-4806.22.08024-7>

402. van der Deen, M., de Vries, E. G. E., Timens, W., Scheper, R. J., Timmer-Bosscha, H., & Postma, D. S. (2005). ATP-binding cassette (ABC) transporters in normal and pathological lung. *Respiratory Research*, 6(1), 59. <https://doi.org/10.1186/1465-9921-6-59>
403. Van Der Sanden, B., Dhobb, M., Berger, F., & Wion, D. (2010). Optimizing stem cell culture. *Journal of Cellular Biochemistry*, 111(4), 801–807. <https://doi.org/10.1002/jcb.22847>
404. van der Worp, H. B., Howells, D. W., Sena, E. S., Porritt, M. J., Rewell, S., O'Collins, V., & Macleod, M. R. (2010). Can Animal Models of Disease Reliably Inform Human Studies? *PLoS Medicine*, 7(3), e1000245. <https://doi.org/10.1371/journal.pmed.1000245>
405. van Schilfgaarde, M., van Alphen, L., Eijk, P., Everts, V., & Dankert, J. (1995). Paracytosis of *Haemophilus influenzae* through cell layers of NCI-H292 lung epithelial cells. *Infection and Immunity*, 63(12), 4729–4737. <https://doi.org/10.1128/iai.63.12.4729-4737.1995>
406. Vis, M. A. M., Ito, K., & Hofmann, S. (2020). Impact of Culture Medium on Cellular Interactions in in vitro Co-culture Systems. *Frontiers in Bioengineering and Biotechnology*, 8, 911. <https://doi.org/10.3389/fbioe.2020.00911>
407. Vogelmeier, C., Aquino, T. O., O'Brien, C. D., Perrett, J., & Gunawardena, K. A. (2012). A Randomised, Placebo-Controlled, Dose-Finding Study Of AZD9668, An Oral Inhibitor of Neutrophil Elastase, in Patients with Chronic Obstructive Pulmonary Disease Treated with Tiotropium. *COPD: Journal of Chronic Obstructive Pulmonary Disease*, 9(2), 111–120. <https://doi.org/10.3109/15412555.2011.641803>
408. Wages, J. M. (2004). Polymerase Chain Reaction. In *Encyclopedia of Analytical Science: Second Edition* (pp. 243–250). Elsevier Inc. <https://doi.org/10.1016/B0-12-369397-7/00475-1>
409. Wagner, D. E., Bonenfant, N. R., Parsons, C. S., Sokocevic, D., Brooks, E. M., Borg, Z. D., Lathrop, M. J., Wallis, J. D., Daly, A. B., Lam, Y. W., Deng, B., DeSarno, M. J., Ashikaga, T., Loi, R., & Weiss, D. J. (2014). Comparative decellularization and

- recellularization of normal versus emphysematous human lungs. *Biomaterials*, 35(10), 3281–3297. <https://doi.org/10.1016/j.biomaterials.2013.12.103>
410. Wagner, D. E., Bonenfant, N. R., Sokocevic, D., DeSarno, M. J., Borg, Z. D., Parsons, C. S., Brooks, E. M., Platz, J. J., Khalpey, Z. I., Hoganson, D. M., Deng, B., Lam, Y. W., Oldinski, R. A., Ashikaga, T., & Weiss, D. J. (2014). Three-dimensional scaffolds of acellular human and porcine lungs for high throughput studies of lung disease and regeneration. *Biomaterials*, 35(9), 2664–2679. <https://doi.org/10.1016/j.biomaterials.2013.11.078>
411. Walker, G. M., Zeringue, H. C., & Beebe, D. J. (2004). Microenvironment design considerations for cellular scale studies. *Lab on a Chip*, 4(2), 91–97. <https://doi.org/10.1039/B311214D>
412. Walters, E. H., Walters, J. A., & Gibson, P. G. (2002). Regular treatment with long acting beta agonists versus daily regular treatment with short acting beta agonists in adults and children with stable asthma. *The Cochrane Database of Systematic Reviews*, 2002(3), CD003901. <https://doi.org/10.1002/14651858.CD003901>
413. Walters, M. S., Gomi, K., Ashbridge, B., Moore, M. A. S., Arbelaez, V., Heldrich, J., Ding, B. S., Rafii, S., Staudt, M. R., & Crystal, R. G. (2013). Generation of a human airway epithelium derived basal cell line with multipotent differentiation capacity. *Respiratory Research*, 14(1), 135. <https://doi.org/10.1186/1465-9921-14-135>
414. Wang, J. D., Douville, N. J., Takayama, S., & Elsayed, M. (2012). Quantitative analysis of molecular absorption into PDMS microfluidic channels. *Annals of Biomedical Engineering*, 40(9), 1862–1873. <https://doi.org/10.1007/s10439-012-0562-z>
415. Wang, Y. I., Carmona, C., Hickman, J. J., & Shuler, M. L. (2018). Multiorgan Microphysiological Systems for Drug Development: Strategies, Advances, and Challenges. *Advanced Healthcare Materials*, 7(2), 1–29. <https://doi.org/10.1002/adhm.201701000>
416. Wang, Y., Tang, Z., Huang, H., Li, J., Wang, Z., Yu, Y., Zhang, C., Li, J., Dai, H., Wang, F., Cai, T., & Tang, N. (2018). Pulmonary alveolar type I cell population consists of two

- distinct subtypes that differ in cell fate. *Proceedings of the National Academy of Sciences of the United States of America*, 115(10), 2407–2412. <https://doi.org/10.1073/pnas.1719474115>
417. Ward, J.P.T., Ward, J. and Leach, R. M. (2010). The Respiratory System at a Glance. In *The Respiratory System at a Glance* (pp. 34–35). <https://www.wiley.com/en-ie/The+Respiratory+System+at+a+Glance%2C+4th+Edition-p-9781118761076>
418. Waters, C. M., Roan, E., & Navajas, D. (2012). Mechanobiology in lung epithelial cells: Measurements, perturbations, and responses. *Comprehensive Physiology*, 2(1), 1–29. <https://doi.org/10.1002/cphy.c100090>
419. Webb, R. C. (2003). Smooth muscle contraction and relaxation. *Advances in Physiology Education*, 27(4), 201–206. <https://doi.org/10.1152/advan.00025.2003>
420. Weibel, E. R. (2011). Lung Cell Biology. In *Comprehensive Physiology*. John Wiley & Sons, Incorporated. 10.1002/cphy.cp030102
421. Wemyss-Holden, S. A., Porter, K. J., Baxter, P., Rudkin, G. E., & Maddern, G. J. (1999). The laryngeal mask airway in experimental pig anaesthesia. *Laboratory Animals*, 33(1), 30–34. <https://doi.org/10.1258/002367799780578480>
422. Whitcutt, M. J., Adler, K. B., & Wu, R. (1988). A biphasic chamber system for maintaining polarity of differentiation of culture respiratory tract epithelial cells. *In Vitro Cellular & Developmental Biology*, 24(5), 420–428. <https://doi.org/10.1007/BF02628493>
423. White, E. S. (2015). Lung Extracellular Matrix and Fibroblast Function. *Annals of the American Thoracic Society*, 12(Suppl 1), S30–S33. <https://doi.org/10.1513/AnnalsATS.201406-240MG>
424. WHO. (2020a, December 9). *The top 10 causes of death*. The Top 10 Causes of Death. <https://www.who.int/news-room/fact-sheets/detail/the-top-10-causes-of-death>
425. WHO. (2020b, December 9). *The top 10 causes of death*. <https://www.who.int/news-room/fact-sheets/detail/the-top-10-causes-of-death>
426. Widdicombe, J. H., Sachs, L. A., & Finkbeiner, W. E. (2003). Effects of growth surface on differentiation of cultures of human tracheal epithelium. *In Vitro Cellular &*

- Developmental Biology - Animal*, 39(1), 51–55. [https://doi.org/10.1290/1543-706X\(2003\)039<0051:EOGSOD>2.0.CO;2](https://doi.org/10.1290/1543-706X(2003)039<0051:EOGSOD>2.0.CO;2)
427. Wikswo, J. P., Curtis, E. L., Eagleton, Z. E., Evans, B. C., Kole, A., Hofmeister, L. H., & Matloff, W. J. (2013). Scaling and systems biology for integrating multiple organs-on-a-chip. *Lab on a Chip*, 13(18), 3496–3511. <https://doi.org/10.1039/c3lc50243k>
428. Williams, K., & Roman, J. (2016). Studying human respiratory disease in animals—Role of induced and naturally occurring models. *The Journal of Pathology*, 238(2), 220–232. <https://doi.org/10.1002/path.4658>
429. Woei Ng, K., Speicher, T., Dombrowski, C., Helledie, T., Haupt, L. M., Nurcombe, V., & Cool, S. M. (2007). Osteogenic differentiation of murine embryonic stem cells is mediated by fibroblast growth factor receptors. *Stem Cells and Development*, 16(2), 305–318. <https://doi.org/10.1089/scd.2006.0044>
430. Wood, A. J. j., & Barnes, P. J. (1995). Inhaled glucocorticoids for asthma. *New England Journal of Medicine*, 332(13), 868–875. <https://doi.org/10.1056/NEJM199503303321307>
431. World Cancer Research Fund International. (2022, March 23). Lung cancer statistics | World Cancer Research Fund International. *WCRF International*. <https://www.wcrf.org/cancer-trends/lung-cancer-statistics/>
432. Wright, J. L., Cosio, M., & Churg, A. (2008). Animal models of chronic obstructive pulmonary disease. *American Journal of Physiology - Lung Cellular and Molecular Physiology*, 295(1), L1. <https://doi.org/10.1152/ajplung.90200.2008>
433. Wu, M. H., Huang, S. B., & Lee, G. B. (2010). Microfluidic cell culture systems for drug research. *Lab on a Chip*, 10(8), 939–956. <https://doi.org/10.1039/b921695b>
434. Yaddanapudi, K., Mitchell, R. A., & Eaton, J. W. (2013). Cancer vaccines: Looking to the future. *Oncolmmunology*, 2(3). <https://doi.org/10.4161/onci.23403>
435. Yamaya, M., Finkbeiner, W. E., Chun, S. Y., & Widdicombe, J. H. (1992). Differentiated structure and function of cultures from human tracheal epithelium. *American Journal of Physiology - Lung Cellular and Molecular Physiology*, 262(6 6-6). <https://doi.org/10.1152/ajplung.1992.262.6.l713>

436. Yan, F., Gao, H., Zhao, H., Bhatia, M., & Zeng, Y. (2018). Roles of airway smooth muscle dysfunction in chronic obstructive pulmonary disease. *Journal of Translational Medicine*, 16(1), 262. <https://doi.org/10.1186/s12967-018-1635-z>
437. Yin, X., Mead, B. E., Safaee, H., Langer, R., Karp, J. M., & Levy, O. (2016). Stem Cell Organoid Engineering. *Cell Stem Cell*, 18(1), 25–38. <https://doi.org/10.1016/j.stem.2015.12.005>
438. Yoshisue, H., Puddicombe, S. M., Wilson, S. J., Haitchi, H. M., Powell, R. M., Wilson, D. I., Pandit, A., Berger, A. E., Davies, D. E., Holgate, S. T., & Holloway, J. W. (2004). Characterization of ciliated bronchial epithelium 1, a ciliated cell-associated gene induced during mucociliary differentiation. *American Journal of Respiratory Cell and Molecular Biology*, 31(5), 491–500. Scopus. <https://doi.org/10.1165/rcmb.2004-0050OC>
439. Yu, Y., Yuk, H., Parada, G. A., Wu, Y., Liu, X., Nabzdyk, C. S., Youcef-Toumi, K., Zang, J., & Zhao, X. (2019). Multifunctional “Hydrogel Skins” on Diverse Polymers with Arbitrary Shapes. *Advanced Materials*, 31(7), 1807101. <https://doi.org/10.1002/adma.201807101>
440. Yu, Z., Jang, M., Sabo-Attwood, T., Robinson, S. E., & Jiang, H. (2017). Prediction of delivery of organic aerosols onto air-liquid interface cells *in vitro* using an electrostatic precipitator. *Toxicology in Vitro*, 42, 319–328. <https://doi.org/10.1016/j.tiv.2017.05.011>
441. Yun, Y.-R., Won, J. E., Jeon, E., Lee, S., Kang, W., Jo, H., Jang, J.-H., Shin, U. S., & Kim, H.-W. (2010). Fibroblast Growth Factors: Biology, Function, and Application for Tissue Regeneration. *Journal of Tissue Engineering*, 2010, 218142. <https://doi.org/10.4061/2010/218142>
442. Zabner, J., Karp, P., Seiler, M., Phillips, S. L., Mitchell, C. J., Saavedra, M., Welsh, M., & Klingelutz, A. J. (2003). Development of cystic fibrosis and noncystic fibrosis airway cell lines. *https://doi.org/10.1152/Ajplung.00355.2002*, 284(5 28-5), 844–854. <https://doi.org/10.1152/AJPLUNG.00355.2002>
443. Zandoni, M., Piccinini, F., Arienti, C., Zamagni, A., Santi, S., Polico, R., Bevilacqua, A., & Tesei, A. (2016). 3D tumor spheroid models for in vitro therapeutic screening: A

- systematic approach to enhance the biological relevance of data obtained. *Scientific Reports*, 6. <https://doi.org/10.1038/srep19103>
444. Zeller, P., Legendre, A., Jacques, S., Fleury, M. J., Gilard, F., Tcherkez, G., & Leclerc, E. (2017). Hepatocytes cocultured with Sertoli cells in bioreactor favors Sertoli barrier tightness in rat. *Journal of Applied Toxicology*, 37(3), 287–295. <https://doi.org/10.1002/jat.3360>
445. Zepp, J. A., Zacharias, W. J., Frank, D. B., Cavanaugh, C. A., Zhou, S., Morley, M. P., & Morrissey, E. E. (2017). Distinct Mesenchymal Lineages and Niches Promote Epithelial Self-Renewal and Myofibrogenesis in the Lung. *Cell*, 170(6), 1134–1148.e10. <https://doi.org/10.1016/j.cell.2017.07.034>
446. Zhang, L. J., Xing, B., Wu, J., Xu, B., & Fang, X. L. (2008). Biodistribution in mice and severity of damage in rat lungs following pulmonary delivery of 9-nitrocamptothecin liposomes. *Pulmonary Pharmacology and Therapeutics*, 21(1), 239–246. <https://doi.org/10.1016/j.pupt.2007.04.002>
447. Zhang, L., Prietsch, S. O. M., & Ducharme, F. M. (2014). Inhaled corticosteroids in children with persistent asthma: Effects on growth. *The Cochrane Database of Systematic Reviews*, 2014(7), CD009471. <https://doi.org/10.1002/14651858.CD009471.pub2>
448. Zhou, Q., Zhang, L., Sun, Y., Xie, M., & Lin, J. (2020). Clinical value of N-acetylcysteine combined with terbutaline sulfate in elderly patients with chronic obstructive pulmonary disease and its effect on apoptosis/anti-apoptosis mechanism. *Annals of Palliative Medicine*, 9(5), 3393–3401. <https://doi.org/10.21037/apm-20-1605>
449. Zhou, Y., Horowitz, J. C., Naba, A., Ambalavanan, N., Atabai, K., Balestrini, J., Bitterman, P. B., Corley, R. A., Ding, B.-S., Engler, A. J., Hansen, K. C., Hagood, J. S., Kheradmand, F., Lin, Q. S., Neptune, E., Niklason, L., Ortiz, L. A., Parks, W. C., Tschumperlin, D. J., ... Thannickal, V. J. (2018). Extracellular Matrix in Lung Development, Homeostasis and Disease. *Matrix Biology: Journal of the International Society for Matrix Biology*, 73, 77–104. <https://doi.org/10.1016/j.matbio.2018.03.005>

450. Zscheppang, K., Berg, J., Hedtrich, S., Verheyen, L., Wagner, D. E., Suttorp, N., Hippenstiel, S., & Hocke, A. C. (2018). Human Pulmonary 3D Models For Translational Research. *Biotechnology Journal*, 13(1), 1700341. <https://doi.org/10.1002/biot.201700341>
451. Zucco, F. (2005). *An Inter-laboratory Study to Evaluate the Effects of Medium Composition on the Differentiation and Barrier Function of Caco-2 Cell Lines*. 33(6). <https://doi.org/10.1177/02611929050330061>